Characterizing a novel role for the cytokinesis scaffolding protein Anillin
in regulating cell-cell junctions

By

Ciara Reyes

A dissertation submitted in partial fulfillment
of the requirements for the degree of
Doctor of Philosophy
(Cellular and Molecular Biology)
in the University of Michigan
2016

Doctoral Committee:
Assistant Professor Ann L. Miller, Chair
Professor David A. Antonetti
Professor Benjamin L. Margolis
Professor Asma Nusrat

Dedication

To my family, my parents Bernard and Becky Reyes and my sister Jazmine Reyes

Acknowledgements

I am most grateful to have had the opportunity to complete the thesis work presented in this dissertation, in the lab of Dr. Ann Miller, an incredible scientist and mentor. She has tirelessly invested time and effort into my training as a scientist, supported my professional development, and encouraged me throughout my graduate school journey. Thank you for being such a great mentor, and for welcoming me into your lab and life.

Thank you to my thesis committee members Dr. Ann Miller, Dr. Ben Margolis, Dr. David Antonetti, Dr. Asma Nusrat and Dr. Sivaraj Sivaramakrishnan for all of their helpful experimental feedback, direction and advice, and for their support during my recent search for post-graduate fellowships and opportunities.

Thank you to my colleagues, fellow graduate students Elaina Breznau, Rachel Stephenson and Torey Arnold and Post-doctoral fellow Tomohito Higashi who collectively have challenged me to be a better scientist. Whether by training me on specialized techniques, sharing reagents or offering experimental advice, they created a productive and fun environment to do science. Thanks to the undergraduate researchers in lab who are joyful company: Kayla Dinshaw, Farah Huq and Brandon Coy and Nisha Gopal. A special thank you to two talented and hardworking undergraduate researchers whom I have had the pleasure to work with for the past few years, Rhogelyn Espino and Nisha Gopal. It was great to work with you Rhogelyn; your persistence and hard-work are much appreciated. It has been great working with you Nisha to pioneer an altogether new project in our lab which has become your senior thesis – while it has presented us with our share our experimental challenges, it has been a rewarding journey of discovery and learning, and I'm happy to have experienced it together with you.

I'd also like to thank the Program in Cellular and Molecular Biology (CMB), especially CMB Director Dr. Bob Fuller and CMB Administrator Margarita Biekeras, and previous CMB Director and Administrator Dr. Jessica Schwartz and Cathy Mitchell, respectively, for all of their help and support. Thanks to the Molecular, Cellular and Developmental Biology (MCDB) Department, especially Mary Carr, Diane Durfy and Jacqueline Glebe for their assistance whenever I needed help.

My dear friends in Intervarsity International Christian Fellowship, H20 Campus Church, Reading Group, CMB and MCDB you've made my time in Ann Arbor and graduate school a joyous one – whether we've shared a meal together at a local restaurant, had a good conversation over coffee or lived life in community, I've delighted in your company and will cherish our friendship and memories. To my mentors Dr. Odelet Nance and Nancy Senabulya, thank you for your encouragement along the way.

To my beloved family, my parents Bernard and Becky Reyes and my sister Jazmine Reyes, thank you for your love, encouragement and support – this wouldn't have been possible without you – I love you! My best friend and sister Jazmine, you've always been there for me, especially when I needed you most – thank you! My grandparents, aunts, uncles, cousins and loved ones, thank you for your prayers, love and support.

And in everything, all circumstances, I will give thanks to God for his goodness and grace throughout this journey and the journeys to come.

Ciara C. Reyes

Table of Contents

List of Figures:

Introduction:

Chapter 1:

Chapter 1 Supplemental Figures:

Abstract

Cytokinesis, the division of one cell into two, is a fundamental biological process that drives development and renews and replenishes populations of cells throughout life. Anillin is a highly conserved scaffolding protein required for successful cytokinesis in multiple biological organisms, from flies to human. During cytokinesis, Anillin helps to crosslink and stabilize a number of cytoskeletal, motor, and regulatory proteins including F-actin, Myosin II, Septins, the small GTPase RhoA, and its activity regulators MgcRacGAP and Ect2. Anillin scaffolds this network of proteins into a ring-like structure called the contractile ring just beneath the cell membrane at the cleavage furrow of dividing cells. The contractile ring provides the force to pinch one cell into two. Anillin's localization has been well characterized in isolated cells where it is found in the nucleus of interphase cells, around the cell cortex during metaphase, at the equatorial cortex during anaphase, and at the cleavage furrow and midbody of dividing cells. Using the intact epithelium of *Xenopus laevis* embryos as a model system, my lab identified a population of Anillin localized at cell-cell junctions throughout the cell cycle.

Characterizing the function of this novel junctional population of Anillin was the primary focus of this dissertation. Here, I show that Anillin is required for proper distribution of active RhoA at cell-cell junctions and for maintenance of a robust apical actomyosin belt, which is required for cell-cell junction integrity. I also characterize how Anillin is targeted to cell-cell junctions. I show that the Anillin Homology Domain (AHD) and Pleckstrin Homology (PH) Domain – regions of Anillin which mediate key interactions with RhoA, its activity regulators, lipids and septins – work cooperatively to target Anillin to junctions. Further, I investigate the importance and interdependence of an Anillin-Septin interaction for junctional recruitment of Anillin. Here, I show that Septins 2 and 7 are at cell-cell junctions, where Septin 2 closely co-localizes with Anillin. Additionally, I show that Septins have an important role in maintaining junction integrity, and may

contribute to robust Anillin localization to cell-cell junctions. Taken together, this work characterizes a novel extra-mitotic role at cell-cell junctions for Anillin, which had previously been characterized only for its role in cytokinesis. Further, it provides mechanistic insight into which domains of Anillin are responsible for its association with cell-cell junctions. Importantly, about 85% of human cancers are derived from epithelial tissues, and defects that perturb a cell's ability to adhere to its neighbors may lead to invasion or metastasis of cancers cells; thus, understanding the basic biology of how junctions are regulated and maintained is relevant to understanding human disease. Anillin and Septin are overexpressed in multiple human cancers, and their increased expression correlates with increased metastatic potential. Therefore, gaining a better understanding of Anillin's role in cell-cell junction regulation is relevant to cancer biology.

Introduction

Contributions to this work are as follows:

Reyes, C.R.: wrote the Introduction and prepared Table 1 and Figure 5.

Miller, A.L.: prepared Figures 1-4 and 6.

1.1. Cytokinesis, an elegant biological process essential throughout development and life.

The human body is composed of about 37.2 trillion cells (Bianconi et al., 2013). That's more than the estimated 100 billion stars in the Milky Way galaxy (Masetti, 2015). All of the trillions of cells in the human body began from a single cell – a fertilized egg, called a zygote. Each time an egg is fertilized, its development from a single cell to a multicellular organism is driven by the process of cytokinesis – the division of one cell into two. Even before an egg is fertilized, it undergoes a modified form of cytokinesis called polar body emission to establish the proper amount of maternal DNA that will ultimately combine with the paternal DNA from the sperm (X. J. Liu, 2012).

The newly fertilized egg initially undergoes several rounds of divisions, which increase the number of cells inside the embryo, while maintaining the same volume ("Human Embryonic Development | HHMI's BioInteractive," n.d.). The number of cells within the embryo doubles with each division until a transition period of relaxed asynchronous division where groups of cells begin to develop their own independent identities. Developmental signals promote cell differentiation into functionally specialized cell types like heart muscle cells (cardiomyocytes), liver cells (hepatocytes) and skin color pigment cells (melanocytes). Developmental cues during this time also direct large-scale cell migrations, as groups of specialized cells begin to move to the locations where they will

1

achieve their final fate as part of an organ or tissue and ultimately the organism itself. Even after an organism has completed development and reached adulthood, the process of cytokinesis replenishes populations of cells that are constantly in need of renewal and replacement (Li & Clevers, 2010). Ensuring the fidelity of cytokinesis is essential, as cytokinesis failure produces aneuploid cells (cells with an improper number of chromosomes), which have been linked to miscarriage, birth defects and cancer (Fujiwara et al., 2005; Lacroix and Maddox, 2012; Storchova & Pellman, 2004).

1.2. Rethinking Cytokinesis: from a single cellular view to a multicellular view.

Cytokinesis has largely been studied at the level of the single cell in isolated cultured cells that do not form contacts with their neighbors and grow in two dimensions on a glass or plastic surface (Figure 1). However, the cells within our bodies divide in the context of intact tissues and organs, where they grow in three-dimensions, and form contacts with their neighbors called cell-cell junctions (Figure 1). Cell-Cell junctions are specialized regions that allow polarized epithelial cells to adhere to one another, form protective barriers, be mechanically integrated in epithelial sheets, and influence each other through signaling and mechanical forces. A cell undergoing cytokinesis in the context of an epithelium experiences dramatic shape changes and increased local tension as it constricts, and both the dividing cell and its neighbors respond dynamically to each other (Herszterg, Leibfried, Bosveld, Martin, & Bellaiche, 2013). However, a cell dividing in isolation does not encounter the challenge of balancing the intrinsic forces of constriction at the cleavage furrow with the extrinsic forces of adhesion to and integration with other cells, which are required to maintain tissue integrity (Bourdages & Maddox, 2013).

Emerging evidence suggests that epithelial cytokinesis is more of a multicellular than a single cellular process (Herszterg, Pinheiro, & Bellaïche, 2014). Individual cells that make up an epithelial tissue dynamically sense and respond to the tension and signaling from each other (Gjorevski, S. Piotrowski, Varner, & Nelson, 2015; Guillot &

Lecuit, 2013b; Takeichi, 2014). With an emerging multicellular view of cytokinesis, it is intriguing that key cytokinesis proteins have recently been discovered to have indispensible functions at regions where an individual dividing cell would need to maintain contact and communication with its multiple neighbors (Breznau, Semack, Higashi, & Miller, 2015; Ratheesh et al., 2012; Reyes et al., 2014).
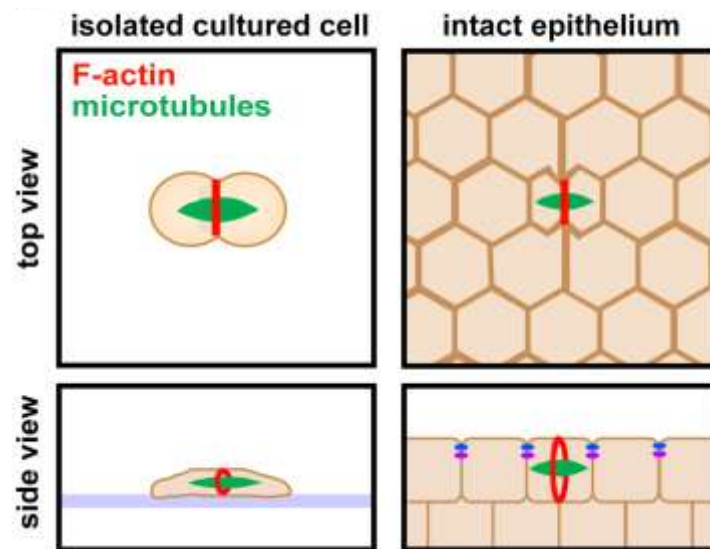
Figure 1. Single cell vs. multicellular view of cytokinesis. (Left) Cells dividing in isolation do not form contacts with neighbors and grow in two dimensions on a flat surface making strong cell-substrate adhesions. (Right) Cells dividing in the context of an intact epithelium are polarized, grow in three dimensions, and must maintain cell-cell junctions with their neighbors during cytokinesis.

1.3. Anillin is a key component of the cytokinetic contractile ring.

Cytokinesis is a highly conserved and fundamental process involving an intricate network of proteins, which must act at the right time and place to coordinate successful cell division. Proper cytokinesis is essential because failure can lead to a binucleate (tetraploid) cell with twice the DNA content of a normal cell, and subsequent divisions can produce polyploidy or aneuploid cells, both of which have been linked to cancer (Fujiwara et al., 2005; Storchova & Pellman, 2004). One key regulator of cytokinesis is Anillin, a multi-domain scaffolding protein that organizes and stabilizes the actomyosin

contractile ring, a structure that forms at the equatorial cortex of a dividing cell, and like a belt, pinches the cell into two (Figure 2).

Figure 2. Cytokinesis. Cytokinesis is driven by a zone of active (GTP-bound) Rho at the equatorial cortex of a dividing cell. Coordination of specific GEFs and GAPs restrict the Rho activity zone to this region of the cell. Active Rho interacts with downstream effector proteins, which promote formation of the actomyosin contractile ring. Anillin can interact with Rho, F-actin and Myosin-2, and Anillin's recruitment to the contractile ring is dependent on active Rho.

Anillin is known to interact with many proteins (Table 1) and major components of the contractile ring including F-actin (K. G. Miller, Field, & Alberts, 1989; Oegema, Savoian, Mitchison, & Field, 2000), which provides the filamentous structural framework of the ring, the motor protein Myosin-2 (Straight, Field, & Mitchison, 2005), which generates contractility, and the small GTPase RhoA (Piekny & Glotzer, 2008), which is the signal that promotes F-actin and Myosin-2's functional output at the division site in addition to recruiting Anillin there (Hickson & O'Farrell, 2008). Two key RhoA activity regulators are Guanine Nucleotide Exchange Factors (GEFs), which promote the exchange of GDP for GTP (activation) and GTPase Activating Proteins (GAPs), which promote the intrinsic hydrolysis of GTP to GDP (inactivation). GEFs and GAPs work together to promote the discrete activation of Rho (A. Hall, 1998; A. L. Miller & Bement, 2009) (Figure 3). In its active GTP-bound form, RhoA can engage with its downstream effectors Rho-associated Kinase (ROCK) or Citron Kinase, to promote the phosphorylation of the regulatory light chain of Myosin-II, which is necessary for contractility (Madaule et al., 1998; N. Watanabe, 1997) (Figure 4). Rho-GTP also promotes the local polymerization of F-actin through the formin mDia (N. Watanabe, 1997) (Figure 4).

4

AH Domain (AHD)

Anillin (ANLN): Formin | myosin | actin | RBD | C2 | PH
1 91 150 250 420 712 801 986 1124

Binding Partner	Function	Region		System	References
APC/ Cyclosome	E3 ubiquitin ligase, promotes cell-cycle dependent degradation of Anillin		1-45	Human (HeLa S3 cells)	Zhao & Fang, 2005
mDia	Formin, promotes F-actin polymerization		1-91	Human (HeLa/HEK-293 cells)	Watanabe et al, 2010
CD2AP	Cytoskeletal adaptor protein		1-155	Human	Monzo et al., 2005
			1-328	Drosophila	Huglund et al, 2010
			930-1239		
Myosin-II	Non-muscle Myosin, promotes contractility		142-254	X. laevis	Straight et al. 2005
Actin	F-actin, binds and bundles		127-371	Drosophila	Field et al., 1996
			231-454	Human	Oegema et al., 2000
			255-418	X. laevis	Kinoshita et al., 2002
		Full-Length		Drosophila	Gregory et al., 2008
MgcRacGAP	GTPase Activating Protein (GAP) that down regulates Rho and Rac; component of Centralspindlin		517-1212	Drosophila	Gregory et al., 2008
			930-1239	Drosophila	D'Avino et al., 2008
RhoA	Binds active GTP bound RhoA		645-980	Human (HeLa/HEK-293 cells)	Piekny & Glotzer, 2008
			712-801	Human	Sun et al., 2015
RhoG			759-1159	C. elegans	Tian et al., 2105
p190RhoGAP	GAP that down regulates Rho		608-1087	Human (HeLa cells)	Manukyan et al., 2015
Ect2	Guanine Nucleotide Exchange Factor (GEF)		608-940	Human (HeLa/HEK-293 cells)	Frenette et al., 2012
Importin α/β	Regulates nuclear localization		815-1201	Drosophila	Silverman-Gavrila et al., 2008
			57-151	Human (HeLa cells)	Chen et al., 2015
Septin	GTP-binding proteins which form intricate structures (rings, rods and filaments)		928-1124	Human (BHK cells)	Oegema et al., 2000
			815-1201	Drosophila	Silverman-Gavrila et al., 2008
		Full-Length		Drosophila	D'Avino et al., 2008
			748-1116	Human	Kinoshita et al., 2002
Phospho- lipids (PIP₂)	PIP₂ is enriched at the cleavage furrow of dividing cells	*T991 and Q996 sufficient for PIP₂ binding	982-1124	Human (HeLa cells)	Liu et al., 2012
			801-986	Human	Sun et al., 2015
Microtubules	Major cytoskeletal component	Full-Length		Drosophila	Sisson et al., 2000
		Motif within AHD		Human (HeLa cells)	Triplet et al., 2014

Table 1. Anillin Domain Diagram and Binding partners. Table showing Anillin and its binding partners, updated from (Piekny & Maddox, 2010). See text for details.

5

Figure 3. The Rho GTPase Cycle. The small GTPase RhoA is regulated by GEFs and GAPs, which promote its localized activation at discrete regions of the cell. GEFs promote the exchange of GDP for GTP, thereby facilitating activation of Rho, while GAPs promote the intrinsic hydrolysis of GTP to GDP, thereby facilitating inactivation of Rho. Rho effector proteins can bind specifically to GTP-bound RhoA to promote assembly of structures including the actomyosin contractile ring during cytokinesis and the apical actomyosin belt at cell-cell junctions.

Anillin has an essential role in cytokinesis in many organisms (Piekny & Maddox, 2010). Anillin is thought to tether the contractile ring to the plasma membrane, which is evidenced by the fact that when Anillin is perturbed, actin and myosin are no longer constrained to the cell equator but instead they, along with the cleavage furrow, dramatically oscillate back and forth, and the cell ultimately fails cytokinesis (Straight et al., 2005). As a scaffolding protein with 13 currently known binding partners, most of which are regulators of the cytoskeleton (Table 1), it is not surprising that Anillin has a fundamental role regulating actomyosin contractile arrays. In addition to interacting with Myosin-2, F-actin, and Rho directly, Anillin also interacts with key regulators of the contractile ring including: 1) the Formin mDia (S. Watanabe et al., 2010), which promotes growth of F-actin filaments, 2) the GEF Ect2 (Frenette et al., 2012), 3) the GAP MgcRacGAP (D'Avino et al., 2008; Gregory et al., 2008), 4) the GAP p190RhoGAP (Manukyan, Ludwig, Sanchez-Manchinelly, Parsons, & Stukenberg, 2015), 5) the cytoskeletal adaptor protein CD2AP (Haglund et al., 2010), and 6) microtubules (MTs), which form the mitotic spindle during cell division (Triplet, Garcia, Bik, Beaudet, & Piekny, 2014). Through its C-terminal PH domain, Anillin also interacts with phospholipids especially PIP_2, which is enriched at the cleavage furrow (J. Liu,

Fairn, Ceccarelli, Sicheri, & Wilde, 2012), and a special class of GTP-binding proteins called Septins, which form diffusion barriers and provide general stability to the plasma membrane (Kinoshita, Field, Coughlin, Straight, & Mitchison, 2002; Mostowy & Cossart, 2012). Anillin also interacts with importins, which mediate its shuttling in and out of the nucleus (Chen, Akhshi, Lavoie, & Wilde, 2015) and the APC/C which promotes its cell-cycle dependent degradation (Zhao & Fang, 2005).
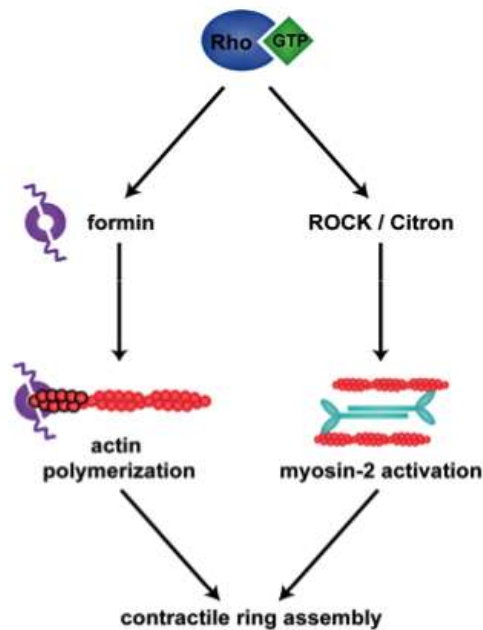
Figure 4. Downstream effectors of active (GTP-bound) RhoA. In its active GTP-bound form, the small GTPase RhoA promotes the local activation of F-actin polymerization and Myosin-2 contractility, through its downstream effectors: the formin mDia, ROCK, and Citron kinase.

1.4. Anillin scaffolds actomyosin contractile arrays in modified forms of cytokinesis.

Anillin helps organize and scaffold transient actomyosin contractile arrays in a myriad of contexts, from the cytokinetic contractile ring of mitotic cells, to the contractile ring that forms during polar body emission in meiotic cells to the furrow canals in *Drosophila* embryos undergoing cellularization (Figure 5). Polar body emission is a highly

asymmetric form of cytokinesis, which occurs in germ cells to establish proper ploidy. Anillin is essential for polar body emission, as when it is perturbed, the polar body collapses and a polyploid cell results (Dorn & Zhang, 2010). Anillin also plays an important role in organizing and scaffolding the actomyosin contractile arrays essential for cellularization, the process whereby individual nuclei within the developing fly become compartmentalized into distinct cells by invaginations of the plasma membrane (Christine M. Field, Coughlin, Doberstein, Marty, & Sullivan, 2005; K. G. Miller et al., 1989). When Anillin is perturbed in this context, disorganized cellular architecture and developmental defects are observed. Anillin is therefore an important component of actomyosin contractile arrays in several contexts, suggesting that it could play a role in regulating other transient contractile arrays.
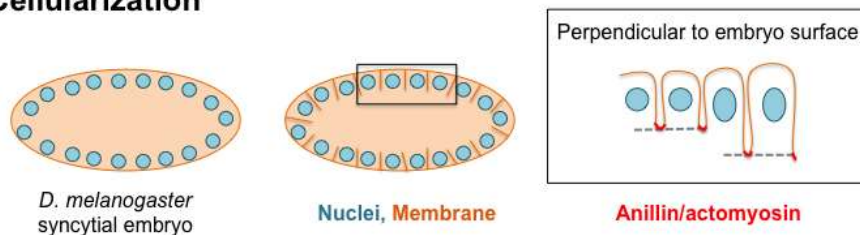
Figure 5. Anillin's Role in Modified Forms of Cytokinesis. Anillin helps organize and scaffold the actomyosin contractile array that forms during a modified form of cytokinesis called polar body emission. In a meiotic cell (in this example the *C. elegans* oocyte) Anillin helps organize a tube-like series of actomyosin rings to facilitate polar body extrusion. Anillin also helps organize the actomyosin contractile array at the front of furrow canals during cellularization in the *D. melanogaster* embryo. The boxed regions are enlarged on the right for each example. This figure is modified from Piekny & Maddox, 2010.

1.5. Extra-mitotic roles for cytokinesis proteins.

In polarized epithelial cells, an apical actomyosin belt, which resembles the cytokinetic contractile ring, connects to cell-cell junctions, mechanically linking cells to each other (Figure 6). This actomyosin belt is regulated by active RhoA in order to to maintain the proper balance of junctional tension and cell-cell adhesion. The two major classes of cell-cell junctions that engage with this apical actomyosin belt are the tight junctions (TJs) and adherens junctions (AJs). At the apical surface of the cell, TJs regulate permeability of small ions and solutes between cells, and function much like a dam, regulating flow in and out of a tissue. Located throughout the basolateral membrane, but clustered in an adhesion belt just basal to the TJs, AJs function much like Velcro, helping cells adhere to each other. The proper function of both TJs and AJs is essential for epithelial tissues during development and disease. For example, compromised barrier function of TJs the intestine can cause irritation of the intestinal lining and trigger diseases like inflammatory bowel disease (Edelblum & Turner, 2009). Further, metastatic cancer cells that travel from one tissue to invade another have lost their adhesive integrity, which is associated with down-regulation of adherens junction proteins (Ohtani et al., 2009; Zheng et al., 1999).

Recently, populations of several cytokinesis proteins have been found at the cell-cell junctions of interphase cells; further, a large-scale proteomic study suggests that some well-characterized cytokinesis proteins may interact with the major AJ component E-cadherin (Guo et al., 2014; Toret, D'Ambrosio, Vale, Simon, & Nelson, 2014). For example, centralspindlin, a heterotetrameric complex consisting of two molecules of the plus end directed motor protein MKLP1 and two molecules of MgcRacGAP, has a well-characterized role at the cytokinetic furrow. Upon anaphase onset, centralspindlin accumulates on and bundles the plus ends of central spindle MTs and through an association with the GEF Ect2, locally activates RhoA at the cell equator, which promotes formation and contractility of the actomyosin contractile ring (A. L. Miller & Bement, 2009; Nishimura & Yonemura, 2006; Yuce, Piekny, & Glotzer, 2005). A population of centralspindlin, as well as Ect2, was recently found to localize to apical

cell-cell junctions through an interaction with the cadherin associated protein α-catenin (Ratheesh et al., 2012). Once at junctions, MgcRacGAP recruits the GEF Ect2 to activate Rho (Guillemot et al., 2014), thus locally regulating the apical actomyosin belt and junction structure (Breznau et al., 2015). Given that almost half of Anillin's known binding partners are present at junctions - MgcRacGAP, Ect2, RhoA, F-actin, Myosin II, formins - it begs the question of whether Anillin itself, a central player in organizing contractile arrays, is there as well.
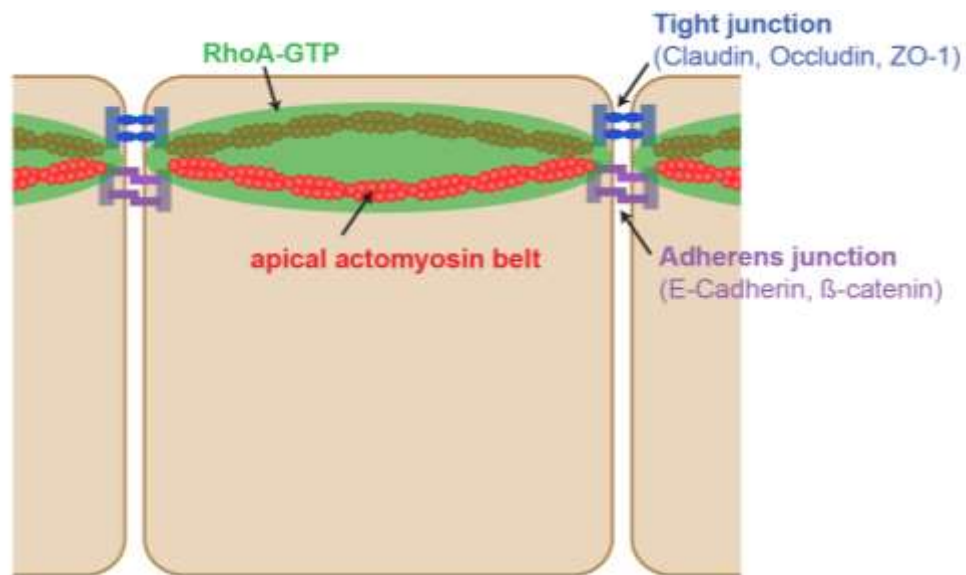
Figure 6. Cell-Cell Junction Structure. Epithelial cell-cell junctions are characterized by two major classes of junctions, tight junctions (TJs) which are apical and regulate influx of small solutes in and out of the epithelial layer, and adherens junctions (AJs) which are basal to tight junctions and maintain adhesion between cells. Both TJs and AJs are connected to an apical actomyosin belt, which resembles the cytokinetic contractile ring, and is similarly regulated by the small GTPase RhoA.

1.6. A case for Anillin at junctions.

Anillin was first discovered in *Drosophila* as an actin-binding and bundling protein (K. G. Miller et al., 1989). In early fly development, Anillin was found to localize at furrow canals, the leading edge of membrane invaginations that compartmentalize nuclei into

distinct cells during cellularization (K. G. Miller et al., 1989) (Figure 5). In the gastrulating fly embryo and isolated human cultured cells, Anillin was reported to be in the nucleus of non-dividing interphase cells, at the cortex of metaphase cells, at the contractile ring of dividing cells and finally at the intercellular bridge during abscission (C. M. Field & Alberts, 1995; Oegema et al., 2000). Upon further inspection, we note that in some of the earliest confocal immunofluorescence imaging of Anillin in the gastrulating fly embryo, there are examples of Anillin appearing weakly present at cell-cell junctions throughout the cell cycle (C. M. Field & Alberts, 1995). However, this population remained unreported and uncharacterized, possibly in large part because many studies that followed were conducted in isolated cultured cells, which do not form junctions with their neighbors.

Over the years, several clues emerged supporting the case for Anillin playing a role at cell-cell junctions. One clue came from isolated cultured cells undergoing cytokinesis where Anillin is perturbed; these cell membranes are characterized by excessive blebbing as a result of Myosin-2 mislocalization (Straight et al., 2005). This finding highlights a key role for Anillin in spatiotemporally regulating contractility, which when misregulated may promote ectopic and detrimental deformation of the cell membrane; in the context of an intact epithelium, deformation of the cell membrane could disrupt cell-cell junctions. Another clue came from the fact that Anillin is known to be overexpressed in human carcinomas (cancers of epithelial origin) such as lung and pancreas, and increased Anillin expression correlates with increased migratory capabilities (P. A. Hall et al., 2005; Olakowski et al., 2009; Ronkainen, Hirvikoski, Kauppila, & Vaarala, 2011; Zhou et al., 2014). Indeed, junction disassembly and disruption could explain these enhanced migratory capabilities. Furthermore, perturbation of Anillin expression via lentivirus in human breast cancer cells (Zhou et al., 2014) or via a translation blocking microRNA (miR-497/tumor suppressor) in naso-pharyngeal carcinomas (Wang et al., 2015) suppressed cell growth and migration. A third clue came when Anillin was implicated in Focal segmental glomerulosclerosis (FSGS), a disease that compromises kidney function and can lead to kidney failure. Overexpression of Anillin in podocytes (cells in the kidney) led to enhanced motility, while Anillin knock down in zebrafish led to

a loss of glomerular filtration barrier (Gbadegesin et al., 2014). These examples suggest that maintaining a proper balance of Anillin-mediated contractility is essential: too much Anillin leads to increased migratory capabilities of carcinomas, which can be reduced by knockdown of Anillin, while too little or complete abolishment of Anillin disrupts the cell membrane of dividing cells and compromises barrier function in intact organs such as the zebrafish kidney.

Perhaps the most striking indication that Anillin may have important structural roles at cell-cell junctions, was a study characterizing Anillin mutants with point mutations in the Anillin homology domain and PH domain, which disrupted Anillin's interaction with Septins (Christine M. Field et al., 2005). Compared to the tightly apposed cell membranes of control cells in fly embryos undergoing cellularization, the cell membranes of these Anillin mutants were malformed, peppered with regions of un-paired plasma membrane, and exhibited vesicularization, an indication of decreased membrane stability. Further, in the gastrulating fly embryo, in addition to large binucleate cells caused by cytokinesis failure, cells were apparently more rounded and sometimes surrounded by spaces suggesting physical separation, compared to polygonal and tightly apposed control cells.

An additional intriguing case exists in the nematode *C. elegans* which has three homologs of Anillin (ANI-1, ANI-2, ANI-3) with non-redundant roles in the developing worm (Maddox, Habermann, Desai, & Oegema, 2005). ANI-1 was shown to have an important role in actomyosin cortical ruffling and psuedocleavage events at the 1-cell stage, yet a non-essential role for cytokinesis (Maddox et al., 2005). However, ANI-2 was found to have an important role in maintaining proper organization and structure of the adult worm gonad (Maddox et al., 2005). When ANI-2 was perturbed, the rachis, an open compartment which shares cytoplasm with maturing oocytes in the gonad, was found to have either fragmented, disordered or absent membrane partitions separating nuclei. ANI-3 has no known function and has not been characterized. Together, these studies in *C. elegans* and *Drosophila* suggested a role for Anillin in maintaining the

proper actomyosin organization required for membrane stability and proper membrane apposition at cell junctions.

Evidence more directly linking Anillin to junction assembly and possible interactions with junction proteins also exists in the literature. In the intact epithelium of *Drosophila* embryos, when cells divide new junctions must be formed at the contact site between the two new daughter cells. Here, formation of AJs is characterized by E-cadherin disengagement (break) and then re-engagement (repair) (Guillot & Lecuit, 2013). Recently, it was found that when Anillin or Septins are perturbed in dividing cells, the contractile ring constricts at a slower rate thereby slowing down junction assembly, suggesting an indirect role for Anillin in AJ assembly through organization of the contractile ring (Founounou, Loyer, & Le Borgne, 2013; Guillot & Lecuit, 2013a; Herszterg et al., 2013). Further, a screen for novel proteins associated with the AJ protein E-cadherin, identified Anillin and some of its binding partners, Septin2/7/9 and CD2AP as being in close proximity with E-cadherin in the cell (Guo et al., 2014). *Drosophila* Anillin also has SH3 binding domains upstream of the Actin binding domain (C. M. Field & Alberts, 1995), which are known to mediate protein-protein interactions in junctional proteins like ZO-1 (González-Mariscal, Betanzos, & Ávila-Flores, 2000), but it is unknown how conserved these sites are in other species, and future work is necessary to address whether indeed Anillin directly interacts with junctional proteins. These data made a strong case for a potential role for Anillin at junctions in epithelial tissues. Anillin is therefore emerging as a multi-tasking protein within epithelia, where it organizes the cytokinetic furrow of dividing cells, and may link and couple the contractile ring to new junction formation and help reinforce cell adhesive integrity.

1.7. Organization of the dissertation.

Key questions remain regarding Anillin's potential role in epithelia. Is a population of Anillin at cell-cell junctions where many of its binding partners also reside? If so, does

Anillin help organize and scaffold the apical actomyosin belt that links to cell-cell junctions, and how is Anillin targeted to cell-cell junctions?

Using the intact epithelium of *Xenopus laevis* (African clawed frog) embryos as a model system, my lab identified a population of Anillin localized at cell-cell junctions throughout the cell cycle (Reyes et al., 2014). Characterizing the function of this novel junctional population of Anillin and addressing the three major questions above has been the primary focus of this dissertation. This dissertation contains three data chapters followed by a Conclusions chapter. The content of each data chapter is briefly outlined below.

Chapter 1: Here, I show that a population of Anillin is identified at cell-cell junctions and that this population is important for proper TJ and AJ structure. Further, Anillin is required for proper RhoA-GTP distribution at cell-cell junctions and for maintenance of a robust apical actomyosin belt, which is required for cell-cell junction integrity. (published)

Chapter 2: Here, I characterize which junctions Anillin associates with and how Anillin is targeted to cell-cell junctions. I show that Anillin associates with the TJ protein ZO-1 and partially overlaps with the AJ protein E-cadherin. Further, I show that Anillin Homology Domain (AHD) and Plekstrin Homology Domain (PH), which mediate important interactions with RhoA, RhoA activity regulators, lipids and Septins, are sufficient to target Anillin to junctions. (unpublished)

Chapter 3: Here, I interrogate a key binding partner of Anillin, Septins, which interact with Anillin via Anillin's AHD and PH domains, to determine its contribution to Anillin's localization to junctions. My undergraduate mentee and I show that Septins 2 and 7 are indeed present at cell-cell junctions where Septin 2 specifically co-localizes with Anillin. Further, we show that while Septins have an important role in maintaining junction integrity, and may contribute to robust Anillin localization to cell-cell junctions. (unpublished)

References:

Bianconi, E., Piovesan, A., Facchin, F., Beraudi, A., Casadei, R., Frabetti, F., … Canaider, S. (2013). An estimation of the number of cells in the human body. *Annals of Human Biology*, *40*(6), 463–471. http://doi.org/10.3109/03014460.2013.807878

Bourdages, K. G., & Maddox, A. S. (2013). Dividing in Epithelia: Cells Let Loose during Cytokinesis. *Developmental Cell*, *24*(4), 336–338. http://doi.org/10.1016/j.devcel.2013.02.006

Breznau, E. B., Semack, A. C., Higashi, T., & Miller, A. L. (2015). MgcRacGAP restricts active RhoA at the cytokinetic furrow and both RhoA and Rac1 at cell-cell junctions in epithelial cells. *Molecular Biology of the Cell*, *doi: 10.1091/mbc. E14-11-1553.*

Chen, A., Akhshi, T. K., Lavoie, B. D., & Wilde, A. (2015). Importin β2 Mediates the Spatio-temporal Regulation of Anillin through a Noncanonical Nuclear Localization Signal. *Journal of Biological Chemistry*, *290*(21), 13500–13509. http://doi.org/10.1074/jbc.M115.649160

D'Avino, P. P., Takeda, T., Capalbo, L., Zhang, W., Lilley, K. S., Laue, E. D., & Glover, D. M. (2008). Interaction between Anillin and RacGAP50C connects the actomyosin contractile ring with spindle microtubules at the cell division site. *Journal of Cell Science*, *121*(8), 1151–1158. http://doi.org/10.1242/jcs.026716

Dorn, J. F., & Zhang, L. (2010). Actomyosin Tube Formation in Polar Body Cytokinesis Requires Anillin in C. elegans. *Current Biology*, *20*(22), 2046–2051.

Edelblum, K. L., & Turner, J. R. (2009). The Tight Junction in Inflammatory Disease: Communication Breakdown. *Current Opinion in Pharmacology*, *9*(6), 715–720. http://doi.org/10.1016/j.coph.2009.06.022

Field, C. M., & Alberts, B. M. (1995). Anillin, a contractile ring protein that cycles from the nucleus to the cell cortex. *The Journal of Cell Biology*, *131*(1), 165–178. http://doi.org/10.1083/jcb.131.1.165

Field, C. M., Coughlin, M., Doberstein, S., Marty, T., & Sullivan, W. (2005). Characterization of anillin mutants reveals essential roles in septin localization and plasma membrane integrity. *Development*, *132*(12), 2849–2860. http://doi.org/10.1242/dev.01843

Founounou, N., Loyer, N., & Le Borgne, R. (2013). Septins Regulate the Contractility of the Actomyosin Ring to Enable Adherens Junction Remodeling during

Cytokinesis of Epithelial Cells. *Developmental Cell*, *24*(3), 242–255. http://doi.org/10.1016/j.devcel.2013.01.008

Frenette, P., Haines, E., Loloyan, M., Kinal, M., Pakarian, P., & Piekny, A. (2012). An Anillin-Ect2 Complex Stabilizes Central Spindle Microtubules at the Cortex during Cytokinesis. *PLoS ONE, 7*(4), e34888. http://doi.org/10.1371/journal.pone.0034888

Fujiwara, T., Bandi, M., Nitta, M., Ivanova, E. V., Bronson, R. T., & Pellman, D. (2005). Cytokinesis failure generating tetraploids promotes tumorigenesis in p53-null cells. *Nature*, *437*(7061), 1043–1047. http://doi.org/10.1038/nature04217

Gbadegesin, R. A., Hall, G., Adeyemo, A., Hanke, N., Tossidou, I., Burchette, J., … Winn, M. P. (2014). Mutations in the gene that encodes the F-actin binding protein anillin cause FSGS. *Journal of the American Society of Nephrology: JASN*, *25*(9), 1991–2002. http://doi.org/10.1681/ASN.2013090976

Gjorevski, N., S. Piotrowski, A., Varner, V. D., & Nelson, C. M. (2015). Dynamic tensile forces drive collective cell migration through three-dimensional extracellular matrices. *Scientific Reports*, *5*, 11458. http://doi.org/10.1038/srep11458

González-Mariscal, L., Betanzos, A., & Ávila-Flores, A. (2000). MAGUK proteins: structure and role in the tight junction. *Seminars in Cell & Developmental Biology*, *11*(4), 315–324. http://doi.org/10.1006/scdb.2000.0178

Gregory, S. L., Ebrahimi, S., Milverton, J., Jones, W. M., Bejsovec, A., & Saint, R. (2008). Cell Division Requires a Direct Link between Microtubule-Bound RacGAP and Anillin in the Contractile Ring. *Current Biology*, *18*(1), 25–29. http://doi.org/10.1016/j.cub.2007.11.050

Guillemot, L., Guerrera, D., Spadaro, D., Tapia, R., Jond, L., & Citi, S. (2014). MgcRacGAP interacts with cingulin and paracingulin to regulate Rac1 activation and development of the tight junction barrier during epithelial junction assembly. *Molecular Biology of the Cell*, *25*(13), 1995–2005. http://doi.org/10.1091/mbc.E13-11-0680

Guillot, C., & Lecuit, T. (2013a). Adhesion Disengagement Uncouples Intrinsic and Extrinsic Forces to Drive Cytokinesis in Epithelial Tissues. *Developmental Cell*, *24*(3), 227–241. http://doi.org/10.1016/j.devcel.2013.01.010

Guillot, C., & Lecuit, T. (2013b). Mechanics of Epithelial Tissue Homeostasis and Morphogenesis. *Science*, *340*(6137), 1185–1189. http://doi.org/10.1126/science.1235249

Guo, Z., Neilson, L. J., Zhong, H., Murray, P. S., Zanivan, S., & Zaidel-Bar, R. (2014). E-cadherin interactome complexity and robustness resolved by quantitative proteomics | Science Signaling. *Science Signaling*, *7*(354), rs7.

Haglund, K., Nezis, I. P., Lemus, D., Grabbe, C., Wesche, J., Liestol, K., … Stenmark, H. (2010). Cindr Interacts with Anillin to Control Cytokinesis in Drosophila melanogaster. *Current Biology*, *20*(10), 944–950.

Hall, A. (1998). Rho GTPases and the Actin Cytoskeleton. *Science*, *279*(5350), 509–514. http://doi.org/10.1126/science.279.5350.509

Hall, P. A., Todd, C. B., Hyland, P. L., McDade, S. S., Grabsch, H., Dattani, M., … Russell, S. E. H. (2005). The Septin-Binding Protein Anillin Is Overexpressed in Diverse Human Tumors. *Clinical Cancer Research*, *11*(19), 6780–6786. http://doi.org/10.1158/1078-0432.CCR-05-0997

Herszterg, S., Leibfried, A., Bosveld, F., Martin, C., & Bellaiche, Y. (2013). Interplay between the Dividing Cell and Its Neighbors Regulates Adherens Junction Formation during Cytokinesis in Epithelial Tissue. *Developmental Cell*, *24*(3), 256–270. http://doi.org/10.1016/j.devcel.2012.11.019

Herszterg, S., Pinheiro, D., & Bellaïche, Y. (2014). A multicellular view of cytokinesis in epithelial tissue. *Trends in Cell Biology*, *24*(5), 285–293. http://doi.org/10.1016/j.tcb.2013.11.009

Hickson, G. R. X., & O'Farrell, P. H. (2008). Rho-dependent control of anillin behavior during cytokinesis. *The Journal of Cell Biology*, *180*(2), 285–294. http://doi.org/10.1083/jcb.200709005

Human Embryonic Development | HHMI's BioInteractive. (n.d.). Retrieved January 26, 2016, from http://www.hhmi.org/biointeractive/human-embryonic-development.

Kimura, K., Ito, M., Amano, M., Chihara, K., Fukata, Y., Nakafuku, M., … Kaibuchi, K. (1996). Regulation of Myosin Phosphatase by Rho and Rho-Associated Kinase (Rho-Kinase). *Science*, *273*(5272), 245–248. http://doi.org/10.1126/science.273.5272.245

Kinoshita, M., Field, C. M., Coughlin, M. L., Straight, A. F., & Mitchison, T. J. (2002). Self- and Actin-Templated Assembly of Mammalian Septins. *Developmental Cell*, *3*(6), 791–802. http://doi.org/10.1016/S1534-5807(02)00366-0

Lacroix, B., Maddox, A.S. (2012) Cytokinesis, ploidy, and aneuploidy. The Journal of Pathology, 226(2): 338-351. http://dx.doi.org/10.1002/path.3013

Li, L., & Clevers, H. (2010). Coexistence of Quiescent and Active Adult Stem Cells in Mammals. *Science*, *327*(5965), 542–545. http://doi.org/10.1126/science.1180794

Liu, J., Fairn, G. D., Ceccarelli, D. F., Sicheri, F., & Wilde, A. (2012). Cleavage Furrow Organization Requires PIP2-Mediated Recruitment of Anillin. *Current Biology*, *22*(1), 64–69. http://doi.org/10.1016/j.cub.2011.11.040

Liu, X. J. (2012). Polar body emission. *Cytoskeleton*, *69*(10), 670–685. http://doi.org/10.1002/cm.21041

Madaule, P., Eda, M., Watanabe, N., Fujisawa, K., Matsuoka, T., Bito, H., … Narumiya, S. (1998). Role of citron kinase as a target of the small GTPase Rho in cytokinesis. *Nature*, *394*(6692), 491–494. http://doi.org/10.1038/28873

Maddox, A. S., Habermann, B., Desai, A., & Oegema, K. (2005). Distinct roles for two C. elegans anillins in the gonad and early embryo. *Development*, *132*(12), 2837–2848. http://doi.org/10.1242/dev.01828

Manukyan, A., Ludwig, K., Sanchez-Manchinelly, S., Parsons, S. J., & Stukenberg, P. T. (2015). A complex of p190RhoGAP-A and anillin modulates RhoA-GTP and the cytokinetic furrow in human cells. *J Cell Sci*, *128*(1), 50–60. http://doi.org/10.1242/jcs.151647

Masetti, M. (2015, July 22). How Many Stars in the Milky Way? Retrieved January 26, 2016, from http://asd.gsfc.nasa.gov/blueshift/index.php/2015/07/22/how-many-stars-in-the-milky-way/

Miller, A. L., & Bement, W. M. (2009). Regulation of cytokinesis by Rho GTPase flux. *Nature Cell Biology*, *11*(1), 71–77. http://doi.org/10.1038/ncb1814

Miller, K. G., Field, C. M., & Alberts, B. M. (1989). Actin-binding proteins from Drosophila embryos: a complex network of interacting proteins detected by F-actin affinity chromatography. *The Journal of Cell Biology*, *109*(6), 2963–2975. http://doi.org/10.1083/jcb.109.6.2963

Mostowy, S., & Cossart, P. (2012). Septins: the fourth component of the cytoskeleton. *Nature Reviews Molecular Cell Biology*, *13*(3), 183–194. http://doi.org/10.1038/nrm3284

Nishimura, Y., & Yonemura, S. (2006). Centralspindlin regulates ECT2 and RhoA accumulation at the equatorial cortex during cytokinesis. *Journal of Cell Science*, *119*(1), 104–114. http://doi.org/10.1242/jcs.02737

Oegema, K., Savoian, M. S., Mitchison, T. J., & Field, C. M. (2000). Functional Analysis of a Human Homologue of the Drosophila Actin Binding Protein Anillin Suggests a Role in Cytokinesis. *The Journal of Cell Biology*, *150*(3), 539–552. http://doi.org/10.1083/jcb.150.3.539

Ohtani, S., Terashima, M., Satoh, J., Soeta, N., Saze, Z., Kashimura, S., … Gotoh, M. (2009). Expression of tight-junction-associated proteins in human gastric cancer: downregulation of claudin-4 correlates with tumor aggressiveness and survival. *Gastric Cancer*, *12*(1), 43–51. http://doi.org/10.1007/s10120-008-0497-0

Olakowski, M., Tyszkiewicz, T., Jarzab, M., Król, R., Oczko-Wojciechowska, M., Kowalska, M., … Jarzab, B. (2009). NBL1 and anillin (ANLN) genes over-expression in pancreatic carcinoma. *Folia Histochemica Et Cytobiologica / Polish Academy of Sciences, Polish Histochemical and Cytochemical Society*, *47*(2), 249–255. http://doi.org/10.2478/v10042-009-0031-1

Piekny, A. J., & Glotzer, M. (2008). Anillin Is a Scaffold Protein That Links RhoA, Actin, and Myosin during Cytokinesis. *Current Biology*, *18*(1), 30–36.

Piekny, A. J., & Maddox, A. S. (2010). The myriad roles of Anillin during cytokinesis. *Seminars in Cell & Developmental Biology*, *21*(9), 881–891. http://doi.org/10.1016/j.semcdb.2010.08.002

Ratheesh, A., Gomez, G. A., Priya, R., Verma, S., Kovacs, E. M., Jiang, K., ⋯ Yap, A. S. (2012). Centralspindlin and α-catenin regulate Rho signalling at the epithelial zonula adherens. *Nature Cell Biology*, *14*(8), 818–828. http://doi.org/10.1038/ncb2532

Reyes, C. C., Jin, M., Breznau, E. B., Espino, R., Delgado-Gonzalo, R., Goryachev, A. B., & Miller, A. L. (2014). Anillin Regulates Cell-Cell Junction Integrity by Organizing Junctional Accumulation of Rho-GTP and Actomyosin. *Current Biology*, *24*(11), 1263–1270.

Ronkainen, H., Hirvikoski, P., Kauppila, S., & Vaarala, M. H. (2011). Anillin expression is a marker of favourable prognosis in patients with renal cell carcinoma. *Oncology Reports*, *25*(1), 129–133.

Storchova, Z., & Pellman, D. (2004). From polyploidy to aneuploidy, genome instability and cancer. *Nature Reviews Molecular Cell Biology*, *5*(1), 45–54. http://doi.org/10.1038/nrm1276

Straight, A. F., Field, C. M., & Mitchison, T. J. (2005). Anillin Binds Nonmuscle Myosin II and Regulates the Contractile Ring. *Molecular Biology of the Cell*, *16*(1), 193–201. http://doi.org/10.1091/mbc.E04-08-0758

Takeichi, M. (2014). Dynamic contacts: rearranging adherens junctions to drive epithelial remodelling. *Nature Reviews Molecular Cell Biology*, *15*(6), 397–410. http://doi.org/10.1038/nrm3802

Toret, C. P., D'Ambrosio, M. V., Vale, R. D., Simon, M. A., & Nelson, W. J. (2014). A genome-wide screen identifies conserved protein hubs required for cadherin-

mediated cell–cell adhesion. *The Journal of Cell Biology*, *204*(2), 265–279. http://doi.org/10.1083/jcb.201306082

Triplet, C. van O., Garcia, M. J., Bik, H. H., Beaudet, D., & Piekny, A. (2014). Anillin interacts with microtubules and is part of the astral pathway that defines cortical domains. *J Cell Sci*, *127*(17), 3699–3710. http://doi.org/10.1242/jcs.147504

Wang, S., Mo, Y., Midorikawa, K., Zhang, Z., Huang, G., Ma, N., … Murata, M. (2015). The potent tumor suppressor miR-497 inhibits cancer phenotypes in nasopharyngeal carcinoma by targeting ANLN and HSPA4L. *Oncotarget*. http://doi.org/10.18632/oncotarget.5651

Watanabe, N. (1997). p140mDia, a mammalian homolog of Drosophila diaphanous, is a target protein for Rho small GTPase and is a ligand for profilin. *The EMBO Journal*, *16*(11), 3044–3056. http://doi.org/10.1093/emboj/16.11.3044

Watanabe, S., Okawa, K., Miki, T., Sakamoto, S., Morinaga, T., Segawa, K., … Narumiya, S. (2010). Rho and Anillin-dependent Control of mDia2 Localization and Function in Cytokinesis. *Molecular Biology of the Cell*, *21*(18), 3193–3204. http://doi.org/10.1091/mbc.E10-04-0324

Yuce, O., Piekny, A., & Glotzer, M. (2005). An ECT2–centralspindlin complex regulates the localization and function of RhoA. *The Journal of Cell Biology*, *170*(4), 571–582. http://doi.org/10.1083/jcb.200501097

Zhao, W., & Fang, G. (2005). Anillin Is a Substrate of Anaphase-promoting Complex/Cyclosome (APC/C) That Controls Spatial Contractility of Myosin during Late Cytokinesis. *Journal of Biological Chemistry*, *280*(39), 33516–33524. http://doi.org/10.1074/jbc.M504657200

Zheng, Z., Pan, J., Chu, B., Wong, Y.-C., Cheung, A. L.-M., & Tsao, S.-W. (1999). Downregulation and abnormal expression of E-cadherin and β-catenin in nasopharyngeal carcinoma: Close association with advanced disease stage and lymph node metastasis. *Human Pathology*, *30*(4), 458–466. http://doi.org/10.1016/S0046-8177(99)90123-5

Zhou, W., Wang, Z., Shen, N., Pi, W., Jiang, W., Huang, J., … Sun, L. (2014). Knockdown of ANLN by lentivirus inhibits cell growth and migration in human breast cancer - Springer. *Molecular and Cellular Biochemistry*, *398*(1), 11–19.

Chapter 1: Anillin Regulates Cell-Cell Junctions Integrity by Organizing Junctional Accumulation of Rho-GTP and Actomyosin

This chapter describes work that was published in *Current Biology*.

Reyes, C.C., Jin, M., Breznau, E.B., Espino, R, Delgado-Gonzalo, R., Goryachev, A.B., **Miller, A.L.** (2014) Anillin Regulates Cell-Cell Junction Integrity by Organizing Junctional Accumulation of Rho-GTP and Actomyosin. *Current Biology*. 24:1263-1270.

Reyes, C.R.: contributed intellectually and to experimental design, executed experiment and data analysis in Figure 1.2 B-G, Figure 1.3 A-C, Figure 1.4 G-I, Figure S1.2 C-G, Figure S1.3 F, G and assisted in completing replicate experiments for endogenous Anillin staining in Figure 1.1 B and F-actin staining in Anillin KD embryos in Figure 1.4 F, and wrote methods.

Jin, M.: contributed intellectually and to experimental design, executed experiments in Figure 1.1A, Figure 1.2A, Figure S1.1 C, C', C", E and Figure S1.3 E, assisted in completing replicate experiments for endogenous Anillin staining in Figure 1.1 B.

Breznau, E.B.: executed western blot experiments in Figure S1.2 B and live-imaging of 3xGFP alone in Figure S1.1 B.

Espino, R.: executed experiments for F-actin fixed staining in Anillin KD embryos in Figure 1.4F.

Delgado-Gonzalo, R.: implemented the Kymographer ImageJ plugin used for quantification of Rho flares in Figure 1.4 B-E and S1.3 D.

Goryachev, A.: contributed intellectually and conceived and piloted the Kymographer analysis approach used for quantification of Rho flares in Figure 1.4B-E and S1.3 D, and advised R. Delgado-Gonzalo.

Miller, A.L.: contributed intellectually and to experimental design and data analysis, executed experiments in Figure 1.4 A-B, Figure S1.1 D-I, Figure S1.3 A-C', completed replicate experiments for endogenous Anillin staining in Figure 1.1 B, 4A-B and preliminary experiments for junction staining (ZO-1/β-cat), performed quantification in Figure 1.1A, C and D and Figure 1.4 C-E, made schematic in 1.4 J, wrote manuscript, advised Reyes, Jin, Breznau, and Espino, and provided lab space and funding for project.

Abstract:

Anillin is a scaffolding protein that organizes and stabilizes actomyosin contractile rings and was previously thought to function primarily in cytokinesis (D'Avino et al., 2008; Christine M. Field, Coughlin, Doberstein, Marty, & Sullivan, 2005; C. M. Field & Alberts, 1995; Frenette et al., 2012; Gregory et al., 2008; J. Liu, Fairn, Ceccarelli, Sicheri, & Wilde, 2012; K. G. Miller & Alberts, 1989; Oegema, Savoian, Mitchison, & Field, 2000; Piekny & Glotzer, 2008; Straight, Field, & Mitchison, 2005). Using *Xenopus laevis* embryos as a model system to examine Anillin's role in the intact vertebrate epithelium, we find that a population of Anillin surprisingly localizes to epithelial cell-cell junctions throughout the cell cycle, whereas it was previously thought to be nuclear during interphase (D'Avino, 2009; Oegema et al., 2000). Further, we show that Anillin plays a critical role in regulating cell-cell junction integrity. Both tight junctions and adherens junctions are disrupted when Anillin is knocked down, leading to altered cell shape and increased intercellular spaces. Anillin interacts with Rho, F-actin, and Myosin II (K. G. Miller & Alberts, 1989; Piekny & Glotzer, 2008; Straight et al., 2005), all of which regulate cell-cell junction structure and function. When Anillin is knocked down, active Rho (Rho-GTP), F-actin, and Myosin II are misregulated at junctions. Indeed, increased dynamic "flares" of Rho-GTP are observed at cell-cell junctions, while overall junctional F-actin and Myosin II accumulation is reduced when Anillin is depleted. We propose that Anillin is required for proper Rho-GTP distribution at cell-cell junctions and for maintenance of a robust apical actomyosin belt, which is required for cell-cell junction integrity. These results reveal a novel role for Anillin in regulating epithelial cell-cell junctions.

Results and Discussion:

Anillin localizes to cell-cell junctions in epithelial cells
The role of vertebrate Anillin has been characterized in isolated cultured cells, where it promotes stable cleavage furrow positioning during cytokinesis (D'Avino, 2009; Goldbach et al., 2010; Piekny & Maddox, 2010; Straight et al., 2005). Anillin is also

enriched in the actomyosin-rich structures required for modified forms of cytokinesis including cellularization and polar body emission (Dorn & Zhang, 2010; Christine M. Field et al., 2005; C. M. Field & Alberts, 1995). However, almost nothing is known about Anillin's function during cytokinesis in vertebrate organisms *in vivo*, and potential roles outside cytokinesis are completely uncharacterized. Thus, we examined Anillin's localization in gastrula-stage *Xenopus laevis* embryos where a polarized epithelium with functional cell-cell junctions has formed (Figure S1.1A) (Merzdorf, Chen, & Goodenough, 1998). We first expressed tagged Anillin (Anillin-3XGFP) in embryos where endogenous Anillin was depleted with a morpholino oligonucleotide (MO) (Figures 1.1A and S1.1B-D). Consistent with work from isolated cultured cells (D'Avino, 2009; C. M. Field & Alberts, 1995; Oegema et al., 2000; Straight et al., 2005), Anillin-3XGFP was primarily nuclear during interphase and strongly accumulated at the contractile ring during cytokinesis (Figures 1.1A and S1.1C-D). Surprisingly, however, an additional population of Anillin-3XGFP was observed at cell-cell boundaries in both mitotic and interphase cells and was focused toward the apical surface (Figure 1.1A and S1.1C-D).

Immunostaining with antibodies against *Xenopus* Anillin confirmed that endogenous Anillin localized to cell-cell junctions in both interphase and mitotic cells, and was clearly focused apically at cell-cell junctions (Figures 1.1B and S1.1E-F). Upon Anillin MO injection, Anillin protein levels were reduced to 42% ± 8% of control levels (Figure S1.1H-I). Anillin KD also led to cytokinesis defects, consistent with previous reports (Figure S1.1G) (Straight et al., 2005). Furthermore, endogenous Anillin signal was sharply reduced at cell-cell junctions and in the nucleus when Anillin was knocked down, confirming that the MO targets Anillin (Figures 1.1B-D). Taken together, these results demonstrate that a pool of endogenous Anillin is localized at cell-cell junctions in epithelial cells.

Anillin is required for proper adherens junction and tight junction structure
The surprising observation that Anillin localizes at cell-cell junctions led us to examine whether Anillin is functionally regulating the apical junctional complex (Figure S1.2A).

Anillin KD produced several striking junctional phenotypes. First, while the apical cell membranes were closely apposed in control cells, Anillin depleted cells often exhibited intercellular spaces (Figure 1.2A). Second, control cells were polygonal and came to a point at tricellular junctions (the sites where three cells come together), but Anillin KD cells exhibited a rounded shape (Figure 1.2A), suggesting that Anillin may be important for junctional tension. Third, β-catenin, an adherens junction (AJ) plaque protein was apically enriched at the zonula adherens in controls (Figures 1.2B and F). However, in Anillin KD embryos, basolateral localization of β-catenin was retained, but the increased apical concentration was lost (Figures 1.2B and F). Importantly, when Anillin mRNA was re-expressed in cells where endogenous Anillin was depleted, the effect on β-catenin was partially rescued (Figures S1.2B-C). Fourth, when Anillin was depleted, staining for E-Cadherin, an AJ transmembrane protein, showed strongly reduced signal as well as reduced apical concentration (Figure 1.2C).

To determine whether Anillin likewise participates in tight junction (TJ) structure, the TJ proteins ZO-1 and Claudin were analyzed. In control cells, staining for the TJ plaque protein ZO-1 was sharp and linear at cell-cell junctions, present at the apical surface of each cell-cell junction, and enriched at tricellular TJs relative to bicellular TJs (Figures 1.2D and S1.2D). In contrast, in Anillin KD cells, ZO-1 accumulation was discontinuous and wavy (Figures 1.2D and S1.2D), suggesting that Anillin depletion may result in decreased apicolateral tension (Smutny et al., 2010). In Anillin KD cells, concentrated ZO-1 was not observed at the apical surface of each cell-cell junction, and was sometimes buried basally (Figure 1.2D). Additionally, ZO-1 was not strongly enriched at tricellular TJs in Anillin KD cells (Figures S1.2D). Staining for Claudin, a TJ transmembrane protein, showed that the relative intensity of Claudin at TJs was significantly decreased in Anillin KD embryos (Figures 1.2E and G). Taken together, these findings demonstrate that Anillin is required for proper organization of both AJ and TJ structure in epithelial cells.

Anillin is required for junctional integrity

Because the apical junctional complex forms adhesive contacts between cells and limits the passage of molecules across the epithelium, we tested how the defects in AJs and TJs in Anillin KD embryos affect passage of a low molecular weight (3 kD) fluorescent dextran between cells (Figure S2.1E) (Benais-Pont et al., 2003; Merzdorf et al., 1998). In control embryos, dextran was restricted above the surface of the epithelium; however, in Anillin KD embryos, dextran penetrated into intercellular spaces around the perimeter of the cells, particularly at tricellular junctions (Figure 1.3A). A similar increase in dextran penetration was observed in embryos treated with EGTA to disrupt junctions by depleting calcium (Figure S1.1F) (K. C. Liu & Cheney, 2012; Palmer & Slack, 1970). Both the average percentage of junctions breached by dextran and the average depth of dextran penetration into the intercellular spaces were significantly increased in Anillin depleted embryos (Figures 1.3B and C). The increased dextran penetration in Anillin KD embryos likely reflects both increased permeability, as we observed cases where the 3 kD fluorescent dextran penetrated deeply between the cells as a thread-like protrusion (Figure S1.2G), as well as the apically domed cell shape observed in Anillin KD embryos (see z views of Anillin KD cells in Figures 1.1-3). Taken together, these results suggest that junctional integrity is compromised when Anillin is depleted.

Anillin is necessary for proper distribution of Rho-GTP at cell-cell junctions

We next examined the mechanism by which Anillin regulates cell-cell junctions. The interaction between Anillin and Rho involves a positive feedback loop: Anillin's localization to the cleavage furrow is dependent on active Rho (Hickson & O'Farrell, 2008; Piekny & Glotzer, 2008; Straight et al., 2005), and Anillin, in turn, promotes active Rho accumulation and stability at the cleavage furrow (Piekny & Glotzer, 2008; Wang et al., 2015). Therefore, we reasoned that junctional Rho activity might be altered when Anillin is perturbed. Using a fluorescent probe that binds specifically to Rho-GTP (GFP-rGBD)(Benink & Bement, 2005), we observed that in control cells, Rho-GTP was present at cell-cell junctions and at the cleavage furrow throughout cytokinesis (Figures S1.3A and C). Additionally, dividing cells pulled neighboring cells along with the

constricting cleavage furrow (Figure S1.3B). In contrast, active Rho was not restricted to the cleavage furrow during cytokinesis in Anillin KD embryos. Instead, intense "flares" of active Rho appeared at ectopic positions around the perimeter of the dividing cell as well as in neighboring cells (Figures S1.3A and C), indicating that tension asymmetries in Anillin KD cells may be mechanically integrated among multiple cells (Clark et al., 2009; Fernandez-Gonzalez, Simoes, Röper, Eaton, & Zallen, 2009). Furthermore, junctions were often not properly maintained during cell division in Anillin KD embryos, and the dividing cell separated from its neighboring cells (Figure S1.3B).

Because Anillin depletion disrupted cell-cell junctions in both dividing and non-dividing cells, we examined the effect of Anillin KD on active Rho localization at junctions in non-dividing regions of the epithelium. In control cells, occasional fluctuations in junctional Rho-GTP were observed (Figure 1.4A); however, in Anillin KD cells, a pronounced increase in flares of Rho-GTP was observed around cell-cell junctions, particularly at tricellular junctions (Figure 1.4A). Kymographs generated from time-lapse movies allowed us to quantify the frequency, lifetime, intensity, and breadth of the Rho-GTP flares over time (Figures 1.4B and S3D), revealing a statistically significant increase in the frequency and a reduction in the lifetime of Rho-GTP flares when Anillin is knocked down (Figures 1.4C-D). Although a significant change in Rho-GTP flare intensity was not observed (data not shown), the breadth of flares was increased in Anillin KD embryos (Figure 1.4E). Notably, the Rho-GTP flares were rapidly followed by strong F-actin accumulation (Figure 1.4B), indicating that Rho-GTP flares may be sites of local mechanical perturbation in the epithelia. Together, these results suggest that Anillin is important for proper distribution of junctional Rho-GTP in both mitotic and interphase cells.

Anillin scaffolds the apical actomyosin belt in epithelial cells
Rho signaling can drive junction assembly and disassembly by regulating the tension in the apical actomyosin belt that connects to AJs and TJs (Figure S1.2A) (Rodgers & Fanning, 2011; S. Terry, Nie, Matter, & Balda, 2010). Because Anillin is required for proper accumulation of Rho-GTP at junctions (Figures 1.4A-E), and Anillin can bind

directly to F-actin and Myosin II (C. M. Field & Alberts, 1995; Straight et al., 2005), we hypothesized that loss of proper apical junctional structure and function in Anillin KD embryos could be due to disruption of the apical actomyosin belt. To test this idea, we first stained control, Anillin KD, and Anillin overexpressing (OE) embryos for F-actin. F-actin accumulated in a strong apical band in controls, but Anillin depletion decreased the intensity and breadth of F-actin accumulation at cell-cell junctions (Figures 1.4F, 1.4H, and S1.3F). Moreover, Anillin OE increased the intensity of F-actin at cell-cell junctions and led to intense, spiky contractile rings in dividing cells (Figures 1.4F and S1.3E-F), suggesting that Anillin is hyperactive in its role as a scaffolding protein when OE.

Phosphorylation of the regulatory light chain of Myosin II (P-MLC) promotes the ATPase activity of Myosin II, which is necessary for generating actomyosin contraction (Vicente-Manzanares, Ma, Adelstein, & Horwitz, 2009). Therefore, increased P-MLC staining can be used as a readout for increased tension. In control embryos, P-MLC localized along bicellular junctions and was intensely localized at tricellular junctions (Figure 1.4G); however, P-MLC intensity was significantly reduced in Anillin KD embryos (Figures 1.4G and I). Further, when Anillin was OE, P-MLC accumulated strongly at junctions and the apical cell cortex, and cells appeared hypercontractile (Figures 1.4G and S1.3G). These results support the idea that Anillin scaffolds the apical actomyosin belt. We propose that Anillin is necessary to stabilize and properly distribute tension in the apical actomyosin belt (Figure 1.4J).

Conclusions:

Our results demonstrate that Anillin, which was previously thought to be nuclear during interphase and function solely in cytokinesis (D'Avino, 2009; Piekny & Maddox, 2010), plays a critical role in interphase and dividing epithelial cells where it regulates cell-cell junctions. While previous research on Anillin was generally conducted in isolated cells, our work in an intact vertebrate epithelium revealed this novel function for Anillin. Clues to Anillin's localization at junctions were observed previously, including the cortical

localization of Anillin in blastula-stage *Xenopus* embryos (Page, Chartrain, Badouel, & Tassan, 2011) and the apparent localization of Anillin to junctions in interphase epithelial cells of gastrulating *Drosophila* embryos (C. M. Field & Alberts, 1995). However, other studies in the *Drosophila* epithelia did not reveal junctional localization for Anillin (Haglund et al., 2010). We show here that a pool of Anillin localizes to cell-cell junctions in interphase and mitotic cells and regulates apical junctional structure and function in epithelial cells of the gastrulating *Xenopus* embryo. We predict that Anillin's role in regulating cell-cell junctions is likely conserved among higher vertebrates, as Anillin and the other key players are highly conserved.

The defects reported in AJ and TJ structure in Anillin depleted cells were observed in both dividing and non-dividing cells. Importantly, these defects were observed in mononucleate cells, demonstrating that the effects on cell-cell junctions are not secondary to the cytokinesis defect. We have not yet examined how cell division failure elsewhere in the epithelium may perturb tension homeostasis or affect cell-cell junctions at a distance, but this will be an interesting question for future studies.

We propose that Anillin regulates cell-cell junction integrity by controlling the distribution of junctional Rho-GTP and stabilizing the apical actomyosin belt (Figure 1.4J). We show that Anillin is required for proper distribution of Rho-GTP at apical junctions. Our live imaging of junctional Rho-GTP dynamics extends previous fixed imaging studies showing that a localized zone of Rho-GTP forms at cell-cell junctions (Ratheesh et al., 2012; Ratheesh & Yap, 2012; S. J. Terry et al., 2011; S. Terry et al., 2010). We show that when Anillin is depleted, the sustained junctional Rho activation observed in controls is replaced by frequent, dynamic flares of Rho-GTP followed rapidly by increased F-actin accumulation. We propose that the pronounced Rho-GTP flares in Anillin KD embryos may represent sites of junction disassembly or repair. While the mechanisms that control localized formation and dynamics of the junctional Rho-GTP zone are not well understood, emerging evidence implicates a number of proteins known to regulate Rho activity during cytokinesis including MgcRacGAP, Ect2, p190RhoGAP, and GEF-H1 (Benais-Pont et al., 2003; X.-F. Liu, Ishida, Raziuddin, &

Miki, 2004; Ratheesh et al., 2012; Wildenberg et al., 2006). Interestingly, Anillin binds MgcRacGAP (D'Avino, 2009; Gregory et al., 2008) and Ect2 (Frenette et al., 2012) and could serve as a scaffold to recruit and/or retain them at cell-cell junctions. Thus, Anillin may be involved in regulating the distribution of junctional Rho-GTP directly through its ability to bind Rho or indirectly through its interactions with Ect2 and MgcRacGAP. Additionally, Ect2 can regulate function of the Par6/Par3/aPKC polarity complex through Cdc42, thus playing a role in epithelial junction assembly and cell polarity (X.-F. Liu et al., 2004); therefore, it would be interesting to test whether Anillin depletion also affects Cdc42 activation at cell-cell junctions.

Anillin is a strong candidate to scaffold and organize the apical actomyosin belt at cell-cell junctions given its interactions with F-actin, Myosin II, and the formin mDia2 (C. M. Field & Alberts, 1995; K. G. Miller & Alberts, 1989; Straight et al., 2005; Watanabe et al., 2010). We show here that Anillin regulates the proper accumulation of F-actin and P-MLC at cell-cell junctions. The cell rounding and apical doming phenotypes observed when Anillin is perturbed likely result from changes in tension of the apical actomyosin belt, as apical doming has been observed in other situations where apical tension is altered (Fanning, Itallie, & Anderson, 2012; Yonemura, Wada, Watanabe, Nagafuchi, & Shibata, 2010). Our data suggests that Anillin is required for properly distributing Rho-GTP and scaffolding the apical actomyosin belt (Figure 1.4J). However, Anillin could potentially make direct connections with a TJ and/or AJ component or use its pleckstrin homology domain to directly couple the apical actomyosin belt to the plasma membrane (Figure 1.4J); these will be important avenues for future research. Finally, Anillin is OE 2-6 fold in diverse human tumors, and higher expression levels correlate with increased metastatic potential (Hall et al., 2005; Suzuki et al., 2005). Therefore, misregulation of cell-cell junctions represents a novel mechanism by which Anillin may contribute to cancer progression.

Figures & Legends:
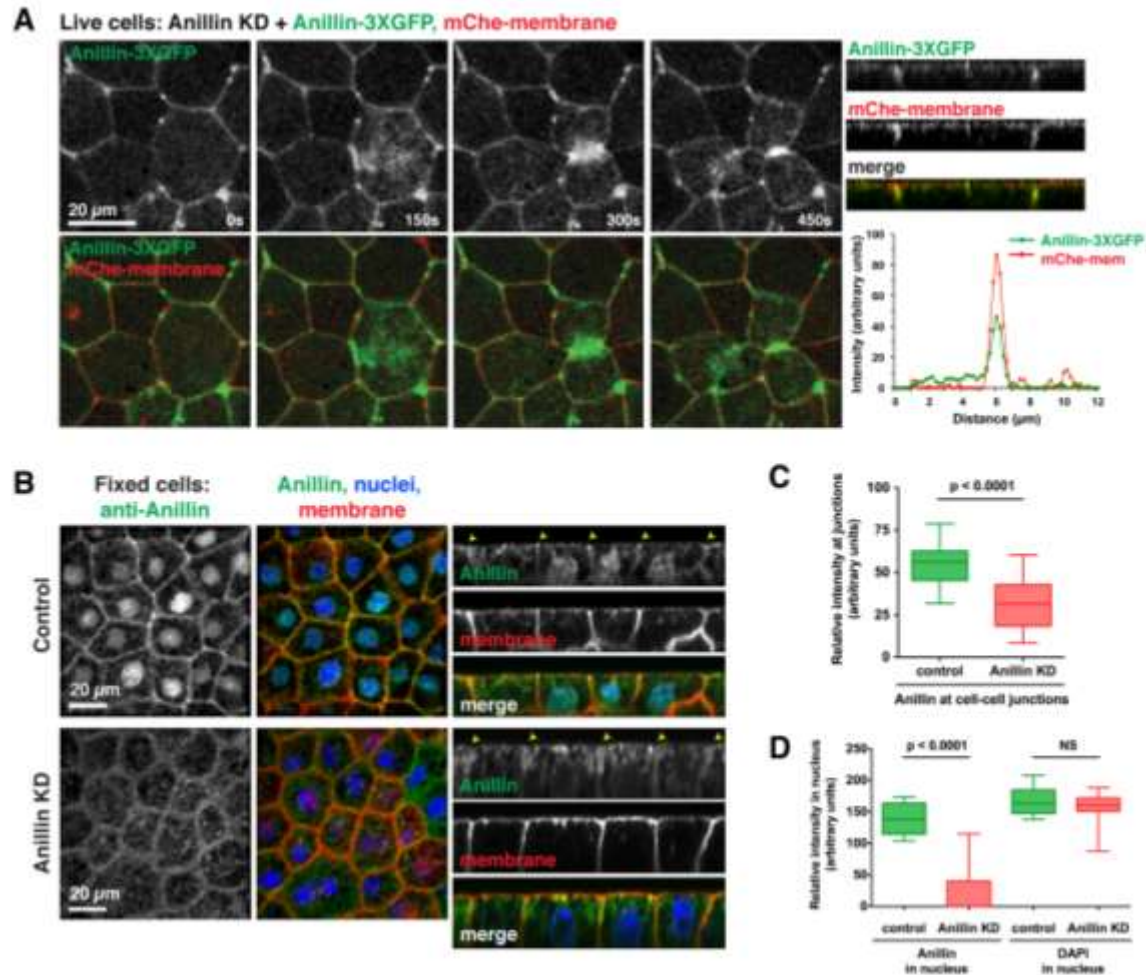
Figure 1.1 Anillin localizes at cell-cell junctions in interphase and mitotic epithelial cells. (A) Live imaging of Anillin-3XGFP in gastrula stage embryos where endogenous Anillin was depleted. mChe-membrane labels the plasma membrane. Images are brightest point projections of 17 apical z planes. Nuclear Anillin is not visible because only apical planes were captured. (Right) z view show that Anillin-3XGFP is apically focused. Graph shows an average of five line scans drawn perpendicular to junctions, indicating that the peak intensities of Anillin-3XGFP and mChe-mem overlap. (B) Embryos were injected with a GFP-mem injection marker with or without the Anillin MO. Gastrula-stage embryos were fixed and stained with an anti-Anillin antibody (pseudocolored green), anti-GFP to view the membrane (pseudocolored red), and DAPI (blue). Z views show that apically focused Anillin accumulation at cell-cell junctions is reduced when Anillin is depleted (yellow arrowheads). (C) Quantification of the average intensity of endogenous Anillin at cell-cell junctions in control and Anillin KD cells (see Experimental Procedures for details). Data is from three separate experiments, n = 18 embryos for control, n = 19 embryos for Anillin KD, graphed as box

31

and whiskers plots with the whiskers representing the 1-99 percentile, p < 0.0001. (D) Quantification of the average endogenous Anillin and DAPI intensity in the nucleus in control and Anillin KD cells (see Experimental Procedures for details). Data is from three independent experiments, n = 18 embryos for control, n = 19 embryos for Anillin KD, graphed as box and whiskers plot wth the whiskers representing the 1-99 percentile, p < 0.0001 for control vs. Anillin KD for nuclear Anillin signal, p = 0.16 for control vs. Anillin KD for DAPI signal. See also Figure S1.

Figure 2

A Control — Anillin KD (GFP-membrane)

B ß-catenin (AJ plaque)

C E-Cadherin (AJ transmembrane)

D ZO-1 (TJ plaque)

E Claudin (TJ transmembrane)

F

Relative intensity of β-catenin along basolateral domain (arbitrary units)

Position - apical to basal (µm)

Control / Anillin KD

G

p < 0.0001

Relative intensity of Claudin at junctions (arbitrary units)

Length of line scan (µm)
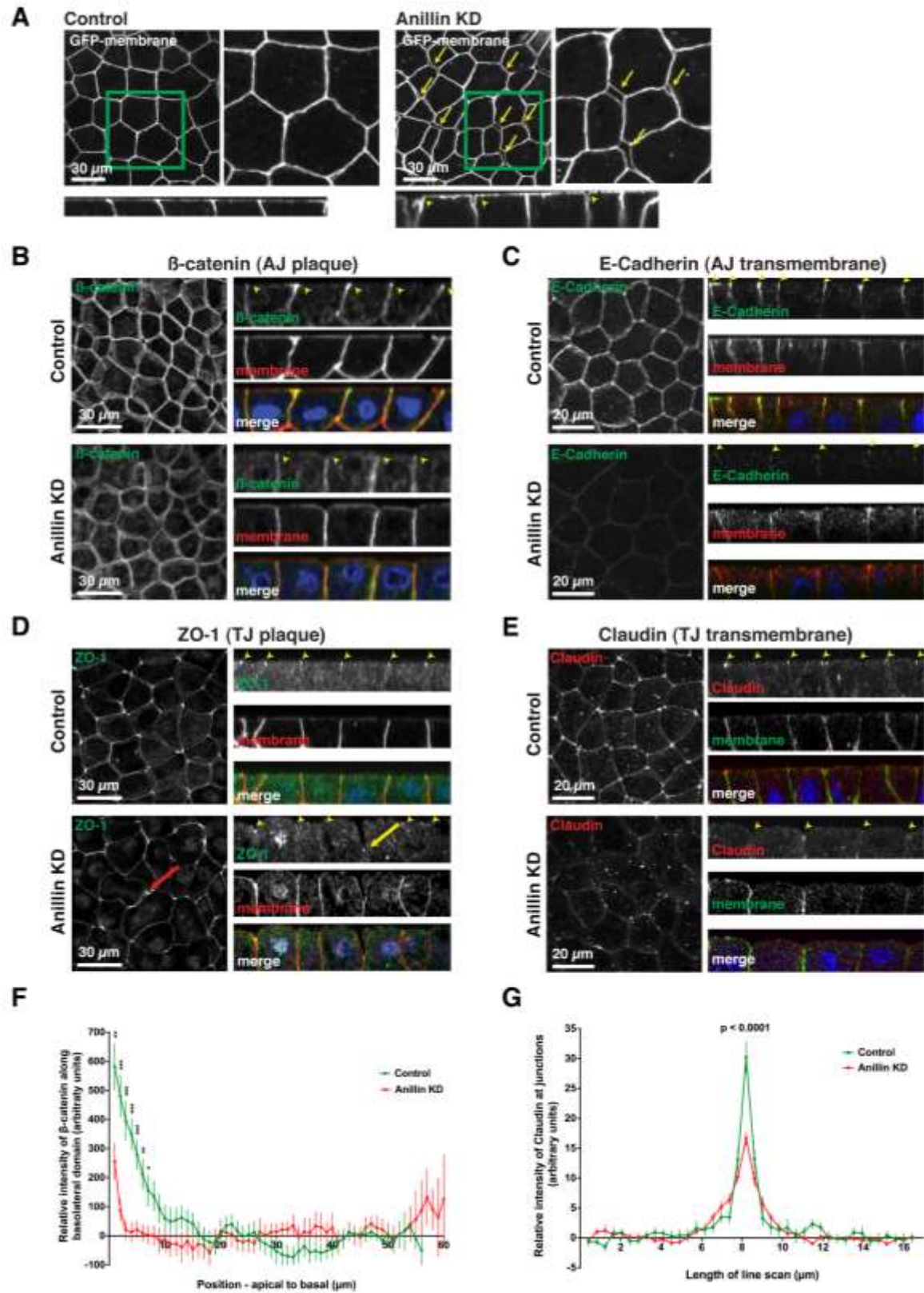
Control / Anillin KD

Figure 1.2. **Adherens junctions and tight junctions are disrupted when Anillin is knocked down.** **(**A) Single intermediate plane views (top) and z views (bottom) of GFP-membrane in control and Anillin KD embryos reveal increased intercellular spaces in Anillin KD embryos (yellow arrows and arrowheads). B-E. Fixed staining of control and Anillin KD embryos for β-catenin (B), E-Cadherin (C), ZO-1 (D), and Claudin (E). GFP-mem or mChe-mem was used as a MO injection marker, and DAPI labels DNA. Z views show the normal localization of the cell-cell junction proteins in control cells as well as the disrupted localization in Anillin KD cells (see yellow arrowheads). The x-y tight junction protein images on the left in D and E are maximal intensity projections of serial z sections. The red arrow in D highlights an intercellular space between a dividing cell and its neighbor, while the yellow arrow indicates a ZO-1 concentration that is buried basally. (F) Quantification of β-catenin polarization in control and Anillin KD cells from line scans along the basolateral surface. The β-catenin signal at the 10 most basal points was normalized to zero so that data from multiple embryos could be averaged (see Experimental Procedures for details). Data is from two independent experiments, n = 26 embryos for control, n = 18 embryos for Anillin KD, graphed as mean +/- SEM, * indicates $p \leq 0.05$, ** indicates $p \leq 0.01$, *** indicates $p \leq 0.001$. (G) Quantification of the relative intensity of Claudin at cell-cell junctions by generating line scans perpendicular to junctions (see Experimental Procedures for details). Data is from two independent experiments, n = 10 embryos for control, n = 12 for Anillin KD, graphed as mean +/- SEM, $p < 0.0001$. See also Figure S2.
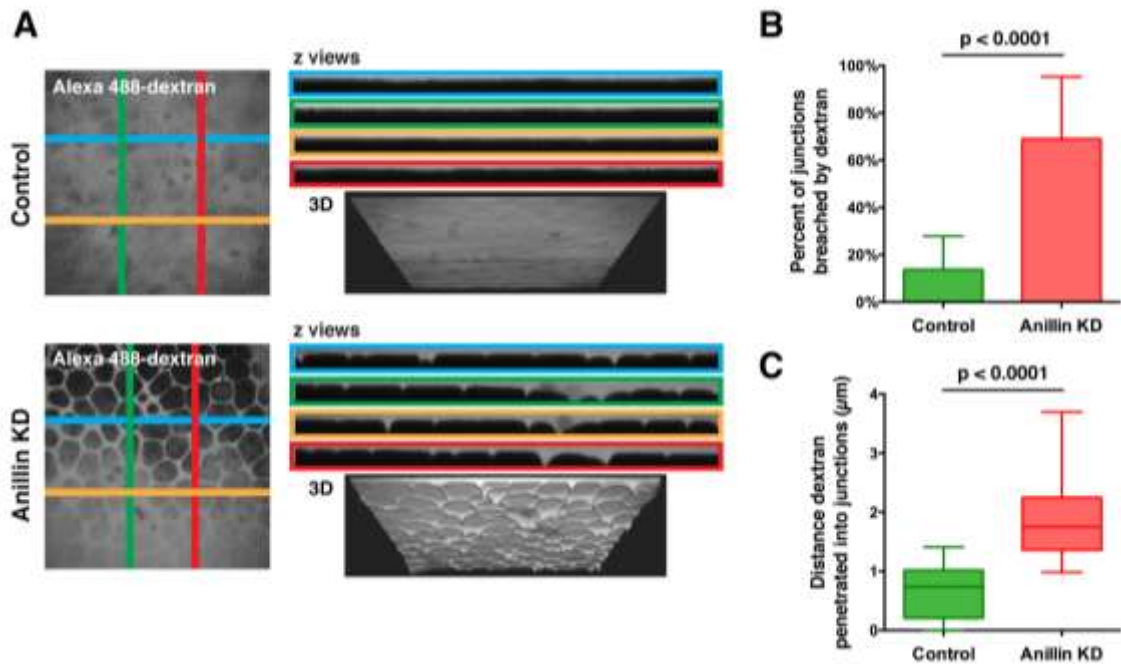
Figure 1.3. Junctional integrity is compromised when Anillin is knocked down.
(A) Live control or Anillin KD embryos were mounted in 3,000 MW Alexa 488-Dextran. (Left) x-y views show that dextran can penetrate between rounded cells in Anillin KD embryos. (Right) z views generated along the indicated lines(top) and 3D views (bottom) show that while dextran remains at the surface in control embryos, it can penetrate between cells in Anillin KD embryos. (B) Quantification of the average percentage of junctions where dextran penetrated into the intercellular space in control and Anillin KD embryos. Data is from three independent experiments, n = 13 embryos for controls, n = 17 embryos for Anillin KD, graphed as mean + SEM, p < 0.0001. (C) Quantification of the average depth of dextran penetration for control and Anillin KD embryos. Data is from three independent experiments, n = 13 embryos for controls, n = 17 embryos for Anillin KD, graphed as box and whiskers plot with the whiskers representing the 1-99 percentile, p < 0.0001. See also Figure S2.
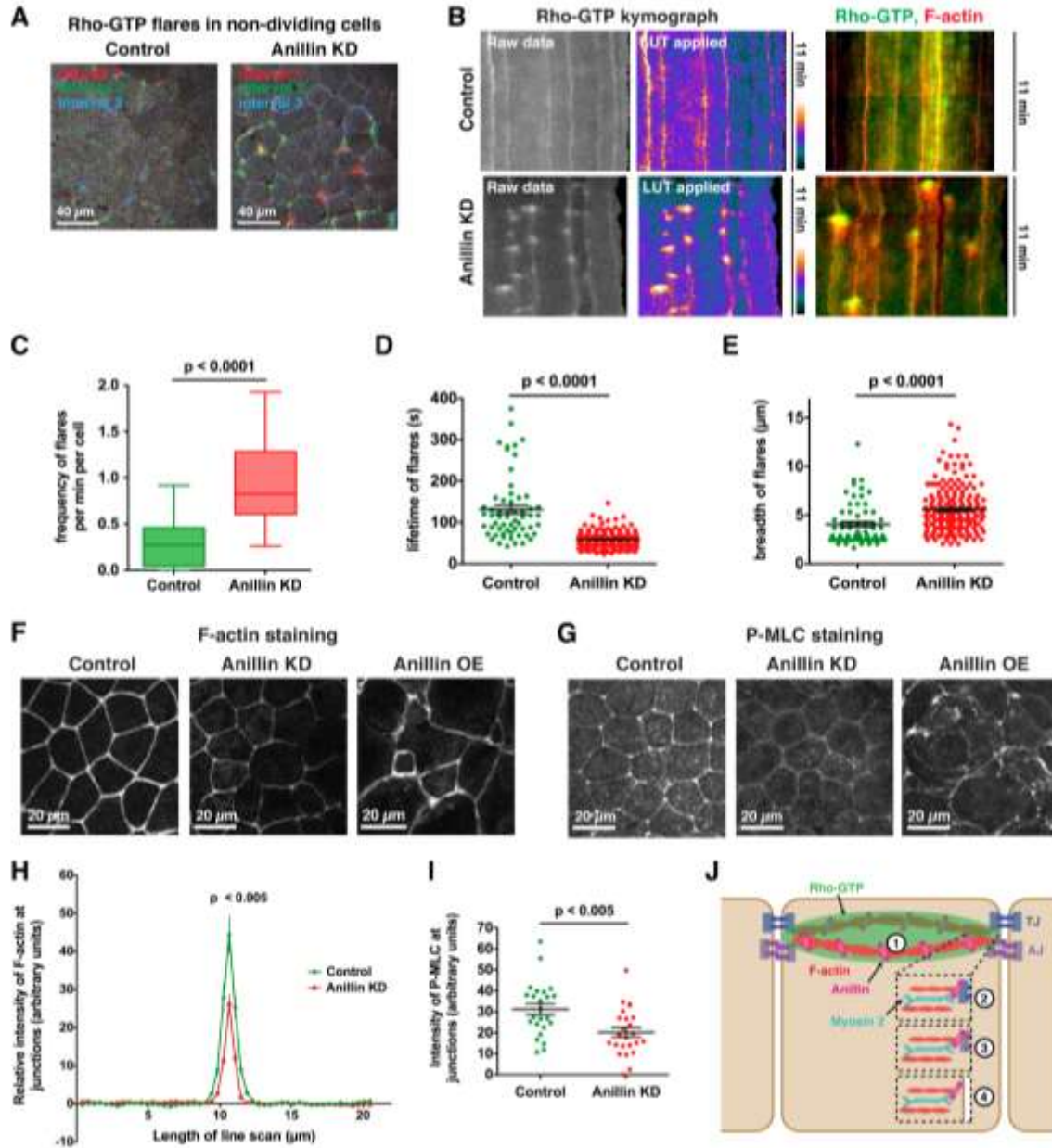
Figure 1.4. Anillin regulates the distribution of Rho-GTP, F-actin, and Phospho-Myosin II at cell-cell junctions. (A) Embryos were injected with GFP-rGBD (Rho binding domain of Rhotekin) as a probe for active Rho. Brightest point projections of Rho-GTP flares over three time intervals in non-dividing control and Anillin KD cells (see Experimental Procedures). Red = flare during minutes 0-2.5, green = flare during minutes 2.5-5, blue = flare during minutes 5-7.5, white = overlap of Rho-GTP flares. (B) Rho-GTP kymographs for non-dividing control and Anillin KD cells. (Left) raw data and LUT kymographs (see Experimental Procedures) show increased Rho-GTP flares in Anillin KD cells, which occur more frequently along tricellular junctions (vertical lines in kymographs). (Right) kymographs with Rho-GTP (green) and F-actin (red) overlaid. (C) Quantification of frequency of Rho-GTP (flares per minute per cell) for control and Anillin KD embryos. Data is from three independent experiments, n = 21 kymographs

36

for controls, n = 21 kymographs for Anillin KD, graphed as box and whiskers plot with the whiskers representing the 1-99 percentile, p < 0.0001. (D) Quantification of the lifetime of Rho-GTP flares for control and Anillin KD embryos. Data is from two independent experiments, n = 59 flares from 16 kymographs for controls, n = 177 flares from 16 kymographs for Anillin KD, graphed as a scatter dot plot with mean +/- SEM indicated, p < 0.0001. (E) Quantification of breadth of Rho-GTP flares for control and Anillin KD embryos. Data is from two independent experiments, n = 62 flares from 16 kymographs for controls, n = 190 flares from 16 kymographs for Anillin KD, graphed as a scatter dot plot with mean +/- SEM indicated, p < 0.0001. (F) Fixed staining for F-actin in control, Anillin KD, and Anillin OE embryos. In Anillin KD embryos, junctional accumulation of F-actin is reduced, whereas in Anillin OE embryos, it is more intense at cell-cell junctions and the cell cortex, and cell shapes are abnormal. (G) Fixed staining for Phospho-Myosin Light Chain 2 (P-MLC) in control, Anillin KD, and Anillin OE embryos. In Anillin KD embryos, junctional accumulation of P-MLC is reduced, whereas in Anillin OE embryos, P-MLC is strongly accumulated at junctions and the cell cortex. (H) Quantification of the relative intensity of F-actin at cell-cell junctions. Line scans from control and Anillin KD embryos were acquired and normalized (see Experimental Procedures). Data is from three independent experiments, n = 24 embryos for control and n = 23 embryos for Anillin KD, graphed as mean +/- SEM, p < 0.005. (I) Quantification of the intensity of P-MLC at cell-cell junctions. Data is from four independent experiments, n = 24 embryos for control and n = 24 embryos for Anillin KD, graphed as a scatter dot plot with mean +/- SEM indicated, p < 0.005. (J) Model showing possible mechanisms by which Anillin may regulate cell-cell junctions. While our results suggest Anillin regulates cell-cell junction integrity by controlling the distribution of junctional Rho-GTP and stabilizing the apical actomyosin belt (1), it is also possible that Anillin may directly interact with a TJ component (2), AJ component (3), or link the apical actomyosin belt with the plasma membrane (4). See also Figure S3.

Supplemental Material:

Figure S1. Reyes et al.

A

1-cell egg — ~2 hours → 4-cell embryo — ~24 hours at 17°C → gastrula (stage 10-11)

Microinject blastomeres with:
Anillin MO, fluorescent probes

Make lysates, Western blot
Fix and stain
Live imaging

B Live imaging of 3XGFP tag alone

3XGFP / mChe-membrane
20 µm / 20 µm — 0s
200s
350s
500s

C

Anillin MO: + − + + +
Anillin-3XGFP: − − 10 12.5 16 ng/µl (needle conc.)

250 —
150 —
Anillin-3XGFP
endogenous Anillin

tubulin

C'

Anillin OE / control / Anillin KD

250 —
150 —
cross-reacting band at ~250 kD
Anillin

C'' Fixed cells: Anillin KD + Anillin-3XGFP

anti-GFP / anti-Anillin / merge

D Live cells:
Anillin KD + Anillin-3XGFP / microtubules
internal plane / surface plane
20 µm

E Fixed cells: Control, gastrulation
Anillin / Anillin, nuclei
20 µm

F Fixed cells: Control, neurulation
Anillin / Anillin, nuclei
20 µm

G Fixed cells: F-actin / nuclei
Control / Anillin KD
100 µm / 100 µm

H

Anillin OE / control / Anillin KD

Anillin

tubulin

I

Anillin expression at gastrula stage (% of control)

120%
100%
80%
60%
40%
20%
0%

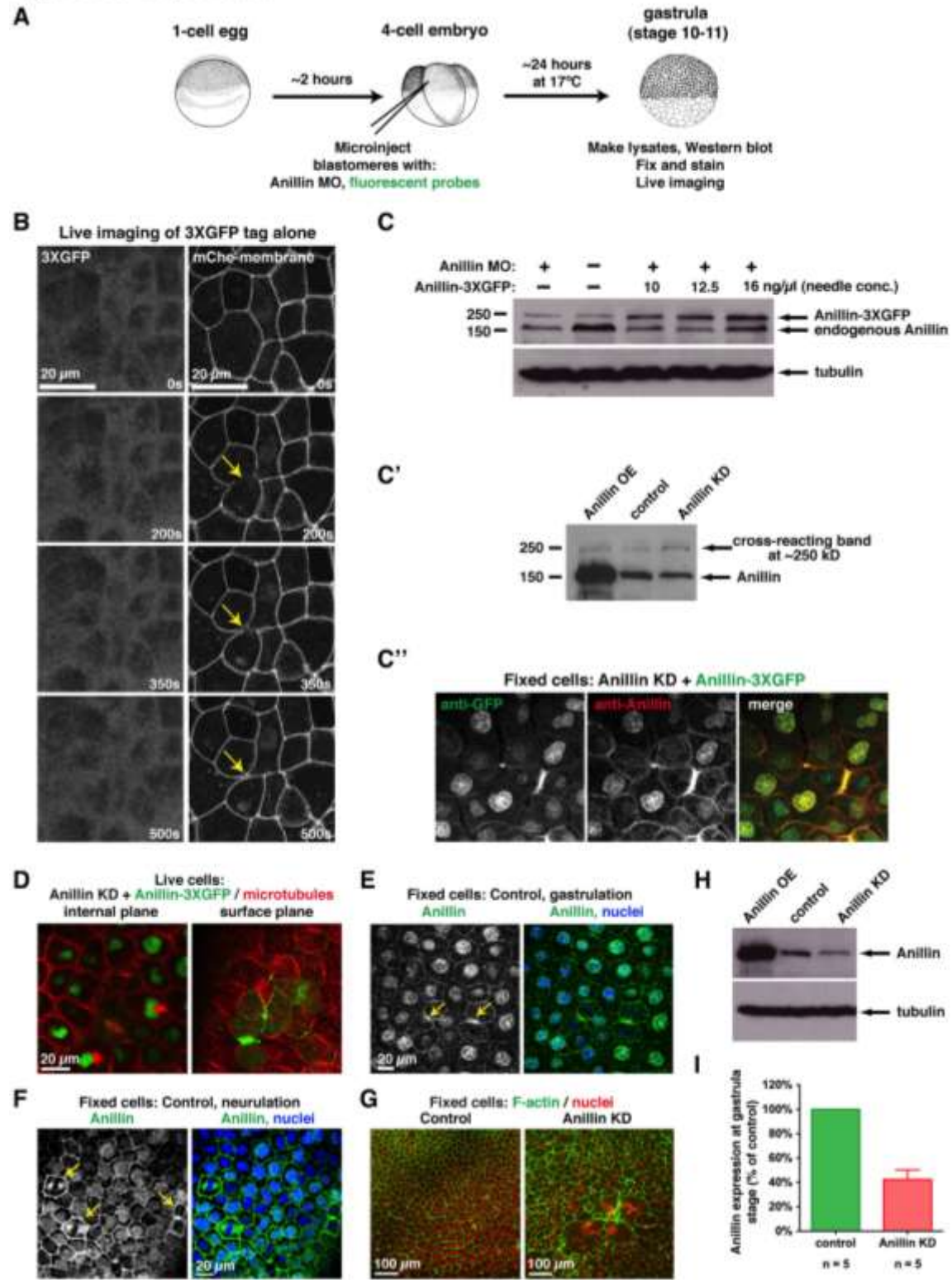control   Anillin KD
n = 5   n = 5

38

Figure S1.1. Anillin localizes at cell-cell junctions in interphase and mitotic epithelial cells, and Anillin protein levels are knocked down by the Anillin MO, Related to Figure 1. (A) Cartoon of injection scheme and timing. *Xenopus* embryos were injected at the 2-cell or 4-cell stage with the Anillin MO and/or mRNAs for fluorescent probes. Embryos were used for live imaging, fixation, or lysates at gastrulation (stage 10-11) for all experiments unless otherwise indicated. (B) Live co-imaging of 3XGFP alone (left) and mChe-membrane (right). Images are brightest point projections of 14 apical z planes. The 3XGFP tag alone exhibits non- specific cytoplasmic localization. (C) Western blot showing KD of endogenous Anillin and expression levels for three replacement concentrations of Anillin-3XGFP. Bottom panel shows the same blot stripped and re-probed for tubulin as a loading control. (C') Western blot showing that a cross-reactive band of the same size as Anillin-3XGFP is present in embryos that were not injected with Anillin-3XGFP. C". Cells were injected with the Anillin MO and Anillin-3XGFP then fixed and stained with anti-GFP (mouse, green) and anti-Anillin (rabbit, red) antibodies. The population of Anillin detected by each antibody is overlapping and highlights Anillin's localization to the contractile ring, nuclei, and cell-cell junctions. (D) Internal and surface views of epithelial cells in a gastrula stage *Xenopus* embryo injected with Anillin MO, Anillin-3XGFP (green), and 2XmChe-EMTB (red) to visualize microtubules. (E) Control gastrula stage embryos were fixed and stained with anti-Anillin antibodies for endogenous Anillin (green) and with DAPI (blue). Endogenous Anillin is localized at the cell-cell junctions, nuclei, and contractile rings of dividing cells (yellow arrows). (F) Same as Figure S1E but embryos were fixed at neurulation (stage 14). Endogenous Anillin strongly accumulates at the cell-cell junctions of dividing cells (marked by yellow arrows). (G) Control and Anillin KD gastrula stage embryos were fixed and stained for F-actin (phalloidin, green) and nuclei (DAPI, pseudocolored red). Anillin KD embryos exhibit large, multinucleate cells, which result from cytokinesis failure. (H) Western blot showing Anillin protein levels when Anillin was OE or KD as compared to control embryos. *Xenopus* embryo lysates were collected at gastrulation (stage 10- 11). The top panel shows the immunoblot probed with an anti-Anillin antibody, and the bottom panel shows the immunoblot probed with an anti-α-tubulin antibody as a loading control. (I) Quantification of average Anillin KD efficiency expressed as a percentage of control levels. Control levels were normalized to 100%, and results from five independent experiments were averaged and graphed as mean + SEM.

Figure S2. Reyes et al.

A

tight junction (TJ)
adherens junction (AJ)
apical actomyosin belt

B

Anillin MO: −   +   +   +
WT Anillin: −   −   0.4   0.8 ng/µl (needle conc.)

← Anillin

← tubulin

C

merge | ß-catenin | enlargement

GFP-mem

ß-catenin
GFP-mem
nuclei

30 µm

GFP-mem + Anillin MO

ß-catenin
GFP-mem
nuclei

30 µm

GFP-mem + Anillin MO + rescue

ß-catenin
GFP-mem
nuclei

30 µm

ß-cat: control
ß-cat: GFP-mem

ß-cat: control
ß-cat: Anillin MO

ß-cat: control
ß-cat: Anillin MO + rescue

D

Control

ZO-1

20 µm

Anillin KD

ZO-1

20 µm

E Live embryos mounted in: Alexa 488-dextran. 3,000 MW

junction intact

junction disrupted

F control embryo treated with EGTA
mounted in Alexa 488-dextran 3,000 MW

mCry-membrane

20 µm

G Anillin KD embryos
mounted in Alexa 488-dextran 3,000 MW

Three examples of dextran penetrating deeply into Anillin KD cell-cell junctions
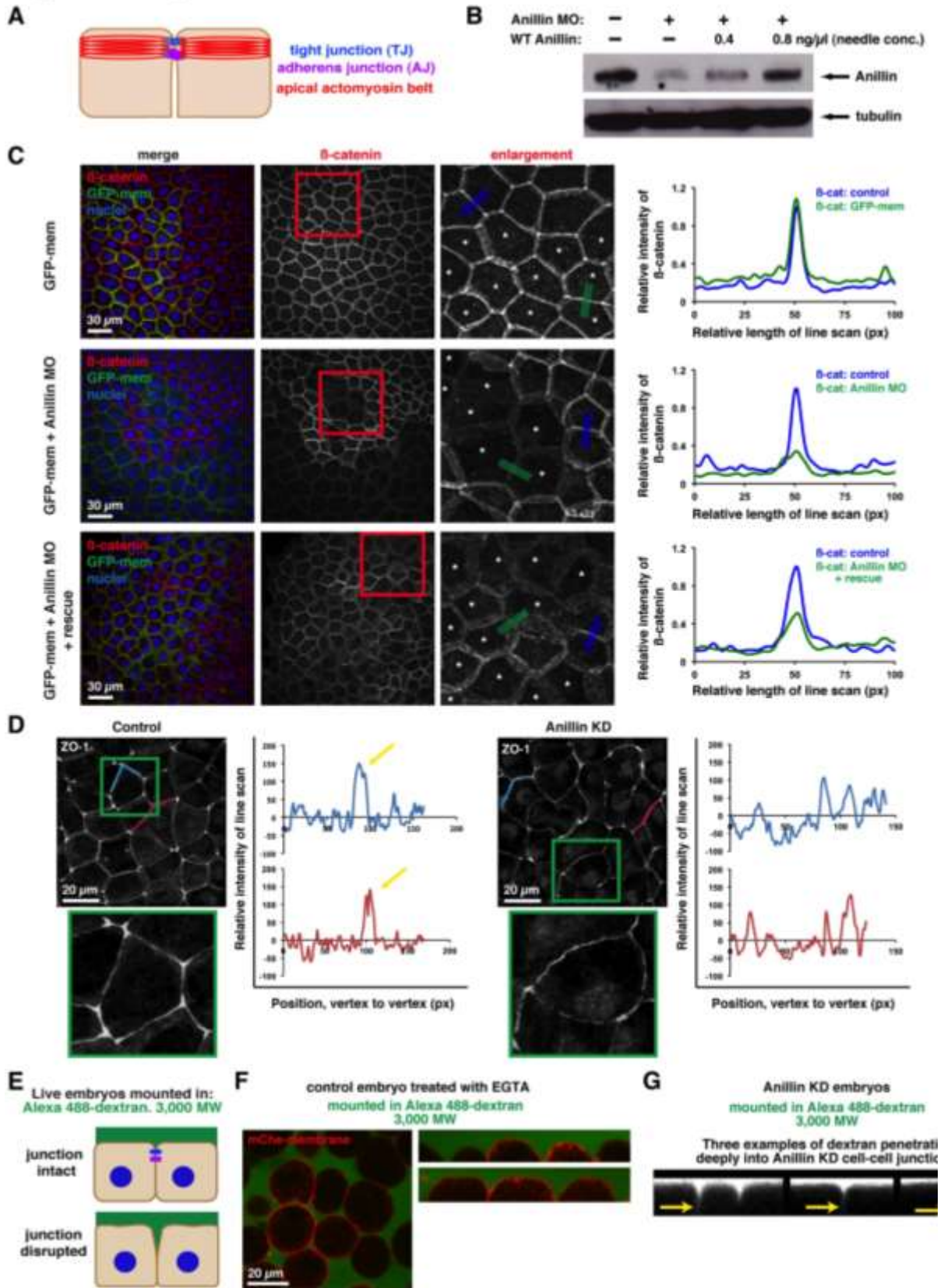
40

Figure S1.2. Anillin knock down leads to defects in adherens junctions, which can be partially rescued by Anillin re-expression, as well as disrupted tight junctions and defects in junctional integrity, Related to Figures 2 and 3. (A) Cartoon of the apical junctional complex showing the position of TJs and AJs in polarized epithelia. Both AJs and TJs are connected to the apical actomyosin belt. (B) Western blot showing Anillin KD and rescue. Embryos were injected at the 4-cell stage with either 4 mM Anillin MO alone or 4 mM Anillin MO + 0.4 or 0.8 ng/µl needle concentration of WT Anillin mRNA. Cell lysates were collected from gastrula stage embryos, and the blot was probed with anti-Anillin antibodies. Bottom panel shows the same blot stripped and re-probed for tubulin as a loading control. (C) Embryos were injected with GFP-mem alone, GFP-mem + Anillin MO, or GFP-mem + Anillin MO + Anillin mRNA (1.25 ng/µl) at the 4- or 8-cell stage. Embryos were fixed and stained for AJ component β-catenin (red), GFP-mem as a MO injection marker (green) and DAPI (blue). Each embryo expresses GFP-mem (and the Anillin MO and rescue construct, when present) in a mosaic pattern. β-catenin images show that in controls where just GFP-mem was injected, the β-catenin intensity appears consistent throughout the field of view, whereas when Anillin MO was co-injected with GFP-mem, β-catenin signal is strongly reduced in GFP-expressing cells (marked by asterisks in enlargement). In contrast, when both Anillin MO and Anillin mRNA were co-injected with GFP-mem, β- catenin signal is only mildly reduced in GFP-expressing cells compared to the internal control cells, demonstrating that Anillin mRNA can partially rescue the effect of Anillin depletion on β-catenin. (Right) line scans highlight the differences in β-catenin intensity at cell-cell junctions in internal control cells vs. cells expressing GFP-mem (and the Anillin MO and rescue construct, when present). (D) Line scans of ZO-1 signal along cell-cell junctions in control and Anillin KD embryos reveal that in control cells, ZO-1 signal is enriched at tTJs relative to bicellular TJs, whereas in Anillin KD embryos, ZO-1 signal is minimally increased at tTJs. Enlargements boxed in green show that ZO-1 signal is sharp and linear in controls but wavy and discontinuous in Anillin KD embryos. (E) Cartoon shows experimental plan where embryos are mounted in 3,000 MW Alexa 488-Dextran. If junctions are intact, the dextran will not be able to penetrate the intercellular space, but if junctional integrity is breached, the dextran will penetrate the intercellular space. (F) Control embryos were incubated with 3 mM EGTA in 0.1X MMR for 15 minutes to chelate calcium and disrupt cell-cell junctions, mounted, and images were taken 45 minutes post incubation. Dextran was able to penetrate into the increased intercellular spaces created between cells after EGTA treatment. G. Anillin KD gastrula stage embryos were mounted in 3,000 MW Alexa 488-dextran. Z views show that the Alexa 488-Dextran could penetrate deeply into the spaces between cell-cell junctions (yellow arrows).

Figure S3. Reyes et al.

A Rho-GTP flares in dividing cells

Control — Rho-GTP — 20 μm — 0s / 144s / 304s / 464s / 672s

Anillin KD — RhoA-GTP — 20 μm — 0s / 81s / 103s / 247s / 328s

B F-actin

Control — 20 μm — 672s

Anillin KD — 20 μm — 653s

C Rho-GTP flares in dividing cells

red = flare during min 0-2.5
green = flare during min 2.5-5
blue = flare during min 5-7.5

Control / Anillin KD / Anillin KD — 20 μm

C' Anillin KD Rho-GTP flares

time (2.7s intervals) → 0s ... 81s

1 / 2 / 3 / 4

D outline cell → linearize outline → Rho-GTP kymograph: align linearized outline for each timepoint below the previous

1 2 3 4 5 6

time — Control / Anillin KD
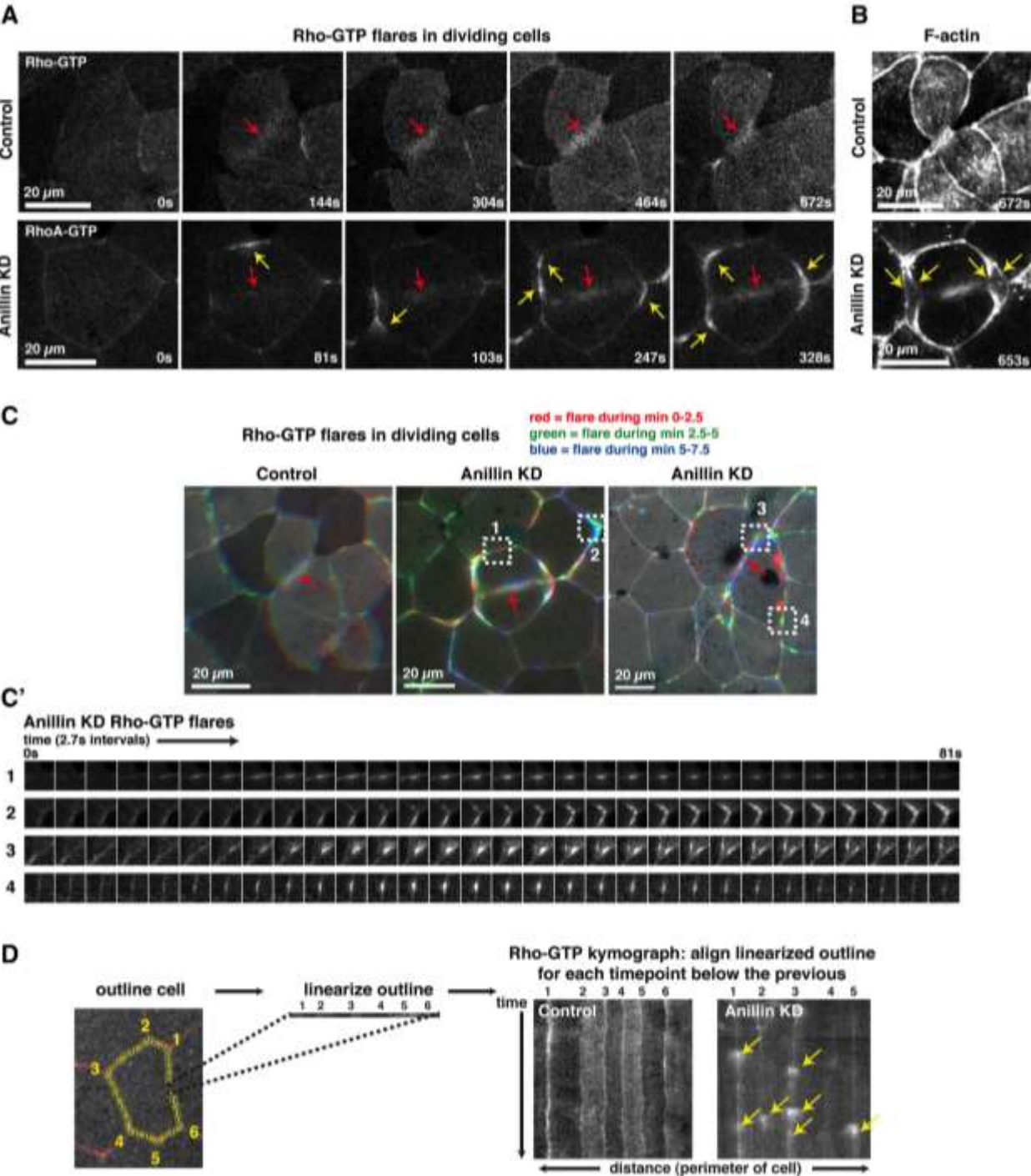
distance (perimeter of cell)
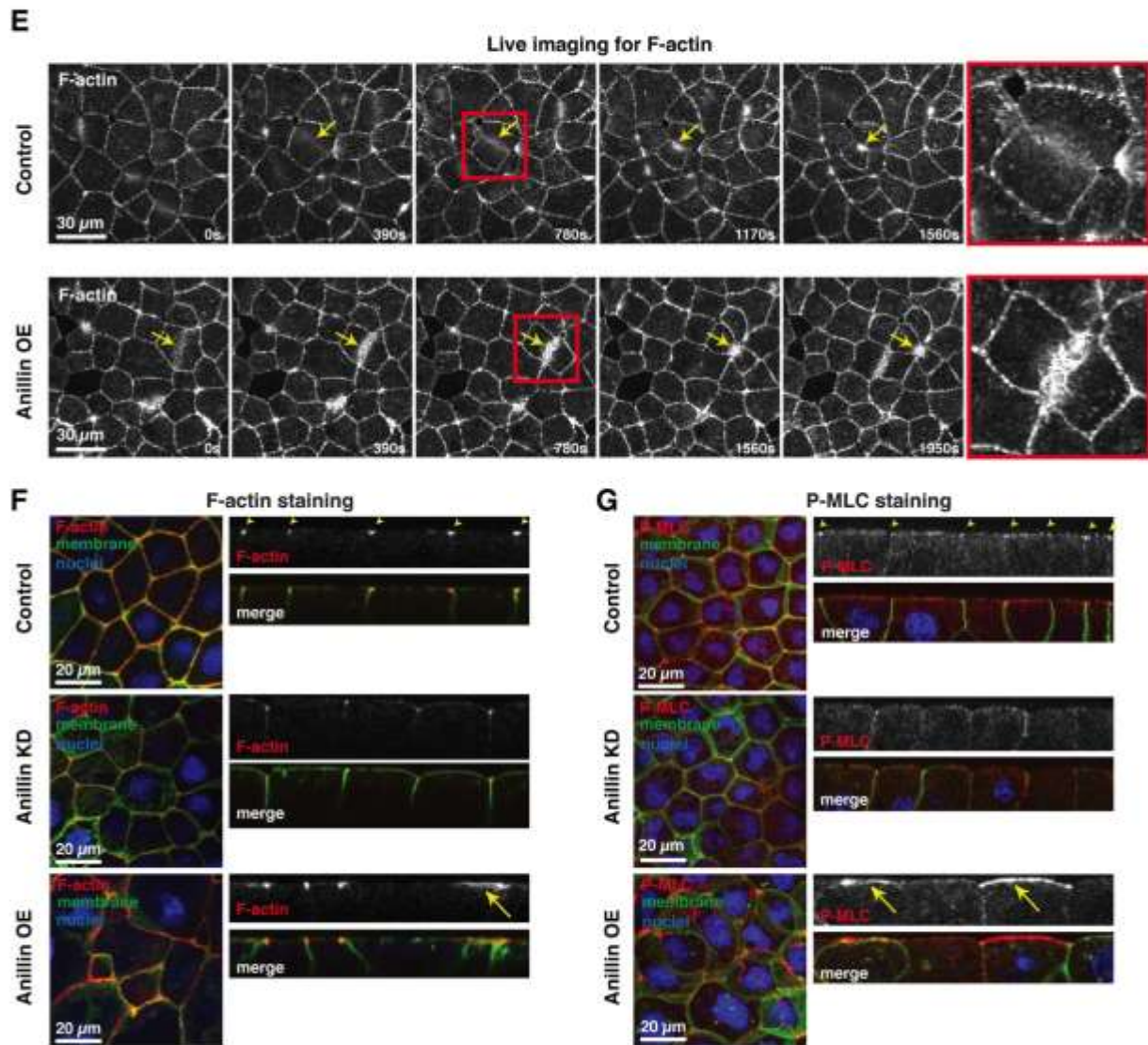
42

Figure S3. Reyes et al. (continued)

Figure S1.3. Anillin regulates the distribution of Rho-GTP, F-actin, and P-MLC, Related to Figure 4. (A) Frames from live confocal imaging of Rho-GTP dynamics in dividing control and Anillin KD embryos. Embryos were injected with GFP-rGBD (Rho binding domain of Rhotekin) as a probe for active Rho. In control embryos, Rho-GTP is present around cell-cell junctions and remains focused at the equatorial cortex (red arrow) throughout cytokinesis. When Anillin is knocked down, active Rho is not restricted to the equatorial cortex (red arrow). Flares of Rho-GTP appear at cell-cell junctions around the perimeter of the cell (yellow arrows). (B) F-actin (mChe-UtrCH) images corresponding to late cytokinesis in the control and Anillin KD cells in Figure S3A showing that the dividing Anillin KD cell is separating from its neighboring cells (yellow arrows), whereas the control cell maintains adhesion with its neighbors. (C) Brightest point projections of Rho-GTP flares over three time intervals in dividing control and Anillin KD cells (division site marked by red arrow). Red = flare during minutes 0-

43

2.5, green = flare during minutes 2.5-5, blue = flare during minutes 5-7.5, white = overlap of Rho-GTP flares through the time intervals. Boxed regions are enlarged in Figure S3C'. (C') Montage of frames from time lapse movies corresponding to the dashed boxes marked in the Anillin KD images in Figure S3C highlighting the lifetime of the Rho-GTP flares. (D) Scheme showing how kymographs were generated for analysis of junctional Rho- GTP over time (see Experimental Procedures). Tricellular junctions where three cells come together are numbered above the resulting kymographs and are marked by vertical lines in the kymographs. (E) Frames from live confocal movies of F-actin in control and Anillin OE embryos. Embryos were injected with 20 ng/µl Anillin mRNA and imaged by live confocal microscopy at late blastula (stage 9). Embryos were co-injected with a probe for F-actin (mChe-UtrCH). Yellow arrows highlight dividing cells, and the red-boxed regions are enlarged on the right. When Anillin is OE, the F-actin in the contractile ring is intense and spiky, and the cells divide more slowly. (F) (Left) merged images that correspond to those in Figure 4F of F-actin (red), GFP- mem (green), and nuclei (blue) for control, Anillin KD, and Anillin OE embryos. For OE, embryos were injected with 40 ng/µl Anillin mRNA. (Right) z views of F-actin staining for
control, Anillin KD, and Anillin OE embryos. F-actin is concentrated at the apical surface of each junction in controls (yellow arrowheads). However, F-actin accumulation is reduced in apically domed Anillin KD cells. In Anillin OE embryos, F-actin is more strongly accumulated at junctions and the apical cell cortex (yellow arrow) compared with controls. (G) (Left) merged images that correspond to those in Figure 4G of P-MLC (red), GFP- mem (green), and nuclei (blue) for control, Anillin KD, and Anillin OE embryos. For OE, embryos were injected with 40 ng/µl Anillin mRNA. (Right) z views of P-MLC for control, Anillin KD, and Anillin OE embryos. P-MLC is accumulated at the apical surface of each junction in controls (yellow arrowheads). However, P-MLC accumulation is reduced or lacking in Anillin KD cells. The remaining P-MLC signal in Anillin KD cells often is more broadly distributed compared with the focused apical signal in controls. In Anillin OE embryos, P-MLC is more strongly accumulated at junctions and the apical cell cortex (yellow arrows) compared with controls, and the apical cell surface is sometimes contracted (left yellow arrow).

Materials & Methods:

DNA constructs, mRNA preparation, and Anillin morpholino. pCS2+/*Xenopus laevis* Anillin and Anillin-3XGFP were generated using a GFP-*Xenopus* Anillin vector generously provided by Aaron Straight, Stanford University, as the template. Anillin was amplified by PCR and cloned into the pCS2+ or pCS2+/C-3XGFP vector using ClaI and XhoI restriction sites. The pCS2+/GFP-rGBD probe for active Rho was described previously (Benink & Bement, 2005). The pCS2+/mChe-UtrCH probe for F-actin was described previously (Burkel, von Dassow, & Bement, 2007). pCS2+/2XmChe-EMTB, a probe for microtubules, was described previously (Dassow, Verbrugghe, Miller, Sider, & Bement, 2009). pCS2+/mChe-mem and pCS2+/GFP-mem probes for the plasma membrane were generated by PCR amplifying the C-terminal sequence from human Ras, which is farnesylated, and ligating it into the BglII and XbaI sites of pCS2+/N-mChe or pCS2+/N- GFP. pCS2+/mChe-H2B was generated by using PCR to amplify human H2B and cloning it into the BspEI and XhoI sites of pCS2+/N-mChe. mRNAs were transcribed *in vitro* from pCS2+-based vectors using the mMessage mMachine SP6 kit (Ambion) (Woolner, Miller, & Bement, 2010). An antisense MO (Gene Tools) was generated to target the 5´UTR of *Xenopus laevis* Anillin with the sequence 5' – TGGCTAGTAACTCGATCCTCAGACT – 3'.

Antibodies. An antibody to *Xenopus* Anillin ABD was generously provided by Aaron Straight, Stanford University (Straight et al., 2005). A *Xenopus*-specific polyclonal Anillin antibody was generated (Primm) by immunizing rabbits with a protein fragment corresponding to amino acids 731-887 of *Xenopus* Anillin, and the antibodies were affinity purified. Other antibodies used were anti-GFP (clone JL-8, Clontech no. 632381), anti-mCherry (abcam, no. Ab167453), anti-α-tubulin (DM1A, Sigma no. T9026), anti-β-catenin (abcam, no. Ab2365), anti-ZO-1 (Invitrogen, no. 61-7300), anti-E-Cadherin (DSHB, no. 5D3-c), anti-Claudin-5 (Abcam, no. Ab53765; note that the anti-Claudin-5 antibody may cross- react with other Claudins so we have referred to it simply at "anti-Claudin" in the text and figures), and anti-P-MLC (Cell Signaling Technologies, no. 3671). Secondary antibodies for Western blotting were HRP-conjugated anti-rabbit

or anti-mouse (Promega). Secondary antibodies for immunofluorescence were Alexa 488 or Alexa 568-conjugated anti-mouse or anti-rabbit (Invitrogen).

***Xenopus* embryos and microinjections.** All studies with *Xenopus laevis* embryos were conducted in compliance with the US Department of Health and Human Services Guide for the Care and Use of Laboratory Animals and were approved by the University Committee on Use and Care of Animals at the University of Michigan. *Xenopus laevis* embryos were collected, fertilized, and dejellied as described previously (A. L. Miller & Bement, 2009; Woolner et al., 2010). Embryos were stored at 15° C or 17° C in 0.1X MMR (1X MMR = 100 mM NaCl, 2 mM KCl, 2 mM CaCl2, 1 mM MgCl2, 5 mM Hepes, pH 7.4). Embryos were microinjected using a Microinject-1000 microinjector (BTX/Harvard Apparatus) with embryos in a mesh bottom dish filled with 0.1X MMR with 5% ficoll. Embryos at the 2- or 4-cell stage were microinjected with 5 nl of MO at a needle concentration of 4-5 mM. mRNAs were injected at the 2- or 4-cell stage with needle concentrations as follows: Anillin, 0.4-40 ng/µl; Anillin-3XGFP, 16 ng/µl; GFP-rGBD, 20 ng/µl; mChe-UtrCH, 20 ng/µl; 2XmChe- EMTB, 12.5 ng/µl; mChe-mem, 10-20 ng/µl; GFP-mem, 10-20 ng/µl; mChe-H2B, 10- 12.5 ng/µl.

Embryo lysates and immunoblotting. Gastrula stage embryos (stage 10-11) were lysed in 5 µl ice cold PHEME lysis buffer per embryo (60 mM K-PIPES, 25 mM Hepes, 10 mM EGTA, 2 mM MgCl2, pH 7.0) supplemented immediately before use with 0.5% NP40, protease inhibitor cocktail (Thermo Scientific Halt Protease Inhibitor + EDTA, no. 78410), and phosphatase inhibitor cocktail (Thermo Scientific Halt Phosphatase Inhibitor, no. 1862495). Embryos were manually lysed in a 1.5 ml eppindorf tube with a pestle. Samples were transferred to a 3/16 x 25/32 Ultra-Clear tube (Beckman, no. 344718). Samples were centrifuged at 16,000*g* for 5 min at 4°C to stratify the lysates. The cytoplasmic layer was removed by puncturing the side of the tube with at 27 G 1/2 needle (BD PrecisionGlide, no. 305109) attached to a 1 ml syringe. The cytoplasmic extract was mixed with 6X LSB and boiled for 10 min. Samples were separated on 8% SDS-PAGE gels and transferred to nitrocellulose membranes. Membranes were probed with anti-*Xenopus* Anillin (Primm, 1:2000), anti-GFP (1:1000), or anti-α-tubulin

(1:30,000) antibodies overnight at 4°C and were then incubated with the appropriate HRP- conjugated secondary antibodies (1:5000 (1:20,000 for anti-α-tubulin)) for 1.5 h at room temperature. Membranes were developed using an ECL detection kit (Pierce, no. 32209). Western blot bands were quantified using FIJI.

Immunofluorescence staining. For fixed staining for Anillin, albino embryos were injected with Anillin MO + GFP-mem as an injection marker or GFP-mem alone. Embryos at gastrula stage (stage 10-11) were fixed and stained according to the protocol from Le Page et al. (Page et al., 2011). In one case (Fig. S1E), we show embryos fixed at neurulation (stage 14). Briefly, embryos were washed in PBS then fixed with 2% TCA in PBS for 2 h at room temperature. Embryos were bisected keeping the animal hemisphere, transferred to 0.6 ml eppindorf tubes, and permeabilized in PBS + 1% Triton-X-100 for 20 min at room temperature followed by PBS + 0.1% Triton-X-100 (PBST) for 20 min at room temperature. Embryos were then blocked with PBST + 5% fetal bovine serum (Invitrogen, no. 10082-139) for 1 h at room temperature. Embryos were incubated with primary antibodies in blocking solution overnight at 4-10° C with gentle shaking (anti-Anillin (Straight), 1:1000; anti-GFP, 1:150-1:300), washed with blocking solution (5 min, 15 min, 2 h, overnight at 4-10° C), incubated with secondary antibodies in blocking solution overnight at 4-10° C (Alexa 568-anti-rabbit for Anillin, 1:200; and Alexa 488-anti-mouse for GFP, 1:200), and washed with PBST (5 min, 15 min, 2 h, overnight at 4-10° C). Embryos were then stained with 10 µg/ml DAPI (Invitrogen, no. D1306) in PBST for 30 min at room temperature, and mounted in Vectashield mounting medium (Vector Laboratories, no. H-1000).

For fixed staining for E-Cadherin, the TCA fixation procedure described above was followed with the following exceptions: embryos were fixed for 1.5 h at room temperature, and embryos were blocked overnight at 4° C. The anti-E-Cadherin antibody was used at 1:200, and the anti-mCherry antibody was used at 1:500.

For fixed staining for β-catenin, ZO-1, Claudin, or P-MLC, albino or pigmented embryos were injected with Anillin MO (+/- Anillin mRNA for rescue experiments) + GFP-mem as

an injection marker or GFP-mem alone. Gastrula stage embryos (stage 10-11) were washed two times with PBS then fixed overnight at room temperature in 3.7% formaldehyde, 0.25% glutaraldehyde, 0.2% Triton-X-100 in buffer containing 80 mM K-PIPES, 5 mM EGTA and 1 mM MgCl2, pH 6.8. Embryos were quenched for 1 h at room temperature in PBS containing 100 mM sodium borohydride, rinsed once in PBS, bisected keeping the animal hemisphere, and transferred to 0.6 ml eppindorf tubes. Pigmented embryos were bleached for 1 h on a light box in 10% H2O2 in PBS. Embryos were blocked with TBS + 10% FBS, 5% DMSO, and 0.1% NP40 for 4 h at 4° C, changing the solution 2-3 times during blocking. A volume of 450 μl of the appropriate solution was added to the tubes for this and all subsequent steps. Embryos were incubated with primary antibodies in blocking solution overnight at 4° C on a nutator (anti-β-catenin, 1:200; anti-ZO-1, 1:200; anti-Claudin, 1:50; anti-P-MLC, 1:100; anti-GFP, 1:200), washed with blocking solution (5 min, 15 min, 2 h, overnight at 4° C), incubated with secondary antibodies in blocking solution overnight at 4° C (Alexa 568-anti-rabbit for β- catenin, ZO-1, and P-MLC, 1:200; and Alexa 488-anti-mouse for GFP, 1:200), and washed with blocking solution (5 min, 15 min, 2 h, overnight at 4° C). Embryos were washed with TBSN (TBS + 0.1% NP40) then stained with 10 μg/ml DAPI diluted in TBSN for 30 min at room temperature. Embryos were then dehydrated using a dilution series of TBSN:MeOH (two 5 min washes of each: TBSN:MeOH 4:1, 1:1, 1:4, then 100% MeOH), cleared with Murray's Clear (1:2 mixture of Benzyl Alcohol:Benzyl Benzoate), and mounted.

For phalloidin staining, embryos were fixed as above, but 66 nM Alexa 568-phalloidin (Molecular Probes, no. A12380) was added to the fixation buffer, and embryos were again stained with 66 nM Alexa 568-phalloidin along with DAPI. Embryos were not dehydrated or cleared prior to imaging, as this compromised the phalloidin signal.

Live and fixed confocal microscopy. Images were collected on an Olympus Fluoview 1000 confocal microscope with FV10-ASW software equipped with a 60X supercorrected PLAPON 60XOSC objective (NA = 1.4, working distance = 0.12 mm). For live imaging, intact gastrula stage (stage 10-11) embryos were mounted in custom

chambers that consisted of a metal slide ~0.8 mm thick with a ~0.5 cm hole in the center to which a coverslip was affixed with a thin layer of vacuum grease (Dow Corning high vacuum grease). We use 0.17mm glass coverslips, (Warner, 22 x 22 mm), which are of an optimized thickness for the 60X supercorrected objective. Embryos were transferred into the chamber in 0.1XMMR, and a second coverslip was placed over the embryos and gently pressed down and affixed with a thin layer of vacuum grease. The chambers were oriented such that cells in the animal hemisphere were imaged.

For fixed imaging, cleared bisected embryos were transferred in Murray's Clear into a small vacuum grease ring on a glass coverslip with animal hemisphere up, and a coverslip was placed over the embryos and gently pressed down to flatten the bisected embryos. For mounting in Vectashield, a similar approach was used, but the embryos were first transferred into the chamber; then, the PBST was removed and replaced with Vectashield. Images were collected as z-stacks that encompass the entire superficial layer of epithelial cells. All images for each independent experiment were acquired using similar acquisition parameters.

Dextran mounting. Pigmented embryos were injected at the 4-cell stage with Anillin MO + mCherry-H2B as an injection marker or mCherry-H2B alone. Gastrula stage (stage 10-11)**,** embryos were rinsed in 0.1X MMR and then incubated in 0.1 mM Alexa Fluor 488 3,000 MW Dextran (Molecular Probes, no. D34682) at room temperature for 2 minutes while protected from light. For EGTA experiments, cells were treated with 3 mM EGTA in 0.1X MMR. Embryos were then mounted in 0.1 mM Dextran solution and imaged. An average of 15 z stack images was collected for each embryo.

Image processing and quantification. Time-lapse images were processed using Volocity (PerkinElmer) and converted to Quicktime movies; z views (x-z or y-z) were generated using Volocity; still images were processed in Photoshop; graphing was performed using Microsoft Excel and Prism, and statistical analysis was done in Prism. Unpaired Student's *t*-test (2-tailed, 2 sample unequal variance) was used to calculate *P* values.

Quantification of endogenous Anillin accumulation at cell-cell junctions and in the nucleus. 3D data was rendered using the Opacity function in Volocity software, and images were processed with a fine filter to remove noise. Flattened images were then exported and analyzed in FIJI. For quantification of Anillin at cell-cell junctions, a 5 px wide line was drawn along 5 bicellular junctions in each image, and the intensity was measured. The Anillin MO injection marker, GFP-mem was used to confirm that the Anillin MO was present in measured regions, and was further used to detect the position of cell-cell junctions when Anillin was KD. Lines of identical size were drawn in a cytoplasmic region next to the junction, and the measured intensity was used for background subtraction. Five measurements for each embryo imaged were averaged, and that value was considered one data point (n = 1). For quantification of Anillin in the nucleus, the intensity of a 15 x 15 px circular region was determined inside the nucleus and at a background region in the cytoplasm (used for background subtraction) for both Anillin antibody staining signal and DAPI staining. Three measurements were averaged for each embryo imaged, and that value was considered one data point (n = 1).

Quantification of relative intensity of β-catenin accumulation along the basolateral domain. z views were collected for embryos fixed and stained for β-catenin. A line scan of β-catenin signal from apical to basal was captured with the 'Measure Line Profiles' feature in Volocity. Three line scans for each embryo were averaged, and that value was considered one data point (n = 1). The line scans were then normalized so that scans for multiple embryos could be compared. Normalization was carried out by subtracting a constant value (calculated by averaging the 10 most basal points of the line scan) from all points in the line scan.

Quantification of dextran penetration. x-z and y-z views were generated for each image of an embryo mounted in fluorescent dextran. The images were imported into FIJI, a straight line was drawn across the apical surface of the cells, and its position was recorded. The line was then moved to the base of each intercellular space where dextran penetrated, and the difference between the apical surface and base of dextran

penetration was calculated and recorded. The depth of dextran penetration for all junctions in the two z views of each embryo was quantified and averaged. The percent of breached junctions was calculated by dividing the number of intercellular spaces >0 by the number of junctions for each z view.

Brightest point projections of Rho-GTP flares. These three-color images were made in order to illustrate the dynamic Rho-GTP flares in a static image. Maximum intensity projections of frames from successive 2.5 min time windows of a time-lapse movie were made using FIJI. Then, three maximum intensity projections were overlaid by pseudocoloring each projection red, green, or blue. Red regions indicate a Rho-GTP flare in the first 0-2.5 minute interval, green regions highlight a Rho-GTP flare in the 2.5-5 minute time interval, and blue regions identify a Rho-GTP flare in the 5-7.5 minute time interval. White or black regions in the resulting image indicate that Rho activity was unchanging or absent during the 7.5 minute total time interval.

Kymograph analysis of Rho-GTP flares. Kymographs were generated in ImageJ using the beta version of Kymographer, a plugin for ImageJ and Fiji developed by the Biomedical Imaging Group, EPFL. A future paper will describe this method and its applications in detail. Briefly, two-color movies with mChe-UtrCH (F-actin probe) and GFP-rGBD (Rho-GTP probe) were analyzed. Kymographer automatically tracked the changing shape of an epithelial cell over time using mChe-UtrCH signal as the information about the cell outline, and output a kymograph showing dynamic changes in the distribution of junctional F-actin and Rho-GTP in space and time. The raw data kymographs were used for intensity measurements. The intensity was measured for a 4x4 px circle drawn on the flare, and the intensity for a background region of the same size was subtracted. In order to be defined as a Rho-GTP "flare", the increase in intensity had to be >25 arbitrary units over background. For measuring the duration and breadth of Rho-GTP flares, the kymographs were contrast enhanced, and the "cool" lookup table in ImageJ was applied. Duration was measured in the vertical direction using the line tool, and breadth was measured in the horizontal direction.

Line scan analysis of F-actin and Claudin accumulation at junctions. 3D data was rendered using the Extended Focus function in Volocity software. Flattened images were then exported and analyzed in FIJI. Line scans of a fixed length perpendicular to and centered on bicellular junctions were performed. Two line scans were generated and averaged for each embryo. All line scans were normalized to background by averaging the 10 outermost points on each side of the line scan and subtracting the result from each position.

Quantification of P-MLC data. 3D data was rendered using the Extended Focus function in Volocity software. Flattened images were then exported and analyzed in FIJI. The segmented line tool with a width of 2 px was used to trace the outline of a cell, and the mean intensity of P-MLC signal within the outlined perimeter of the cell was measured. Measurements were normalized by background subtraction (background was an 11x11 px circle in the cytoplasm). Dividing cells and cells adjacent to them were not included in the analysis. Five outlines were generated for each embryo and averaged, and that value was considered one data point (n = 1).

Acknowledgments:

References:

Benais-Pont, G., Punn, A., Flores-Maldonado, C., Eckert, J., Raposo, G., Fleming, T. P., … Matter, K. (2003). Identification of a tight junction–associated guanine nucleotide exchange factor that activates Rho and regulates paracellular permeability. *The Journal of Cell Biology*, *160*(5), 729–740. http://doi.org/10.1083/jcb.200211047

Benink, H. A., & Bement, W. M. (2005). Concentric zones of active RhoA and Cdc42 around single cell wounds. *The Journal of Cell Biology*, *168*(3), 429–439. http://doi.org/10.1083/jcb.200411109

Burkel, B. M., von Dassow, G., & Bement, W. M. (2007). Versatile fluorescent probes for actin filaments based on the actin-binding domain of utrophin. *Cell Motility and the Cytoskeleton*, *64*(11), 822–832. http://doi.org/10.1002/cm.20226

Clark, A. G., Miller, A. L., Vaughan, E., Yu, H.-Y. E., Penkert, R., & Bement, W. M. (2009). Integration of Single and Multicellular Wound Responses. *Current Biology*, *19*(16), 1389–1395. http://doi.org/10.1016/j.cub.2009.06.044

Dassow, G. von, Verbrugghe, K. J. C., Miller, A. L., Sider, J. R., & Bement, W. M. (2009). Action at a distance during cytokinesis. *The Journal of Cell Biology*, *187*(6), 831–845. http://doi.org/10.1083/jcb.200907090

D'Avino, P. P. (2009). How to scaffold the contractile ring for a safe cytokinesis – lessons from Anillin-related proteins | Journal of Cell Science. *Journal of Cell Science*, *122*(8), 1071–1079.

D'Avino, P. P., Takeda, T., Capalbo, L., Zhang, W., Lilley, K. S., Laue, E. D., & Glover, D. M. (2008). Interaction between Anillin and RacGAP50C connects the actomyosin contractile ring with spindle microtubules at the cell division site. *Journal of Cell Science*, *121*(8), 1151–1158. http://doi.org/10.1242/jcs.026716

Dorn, J. F., & Zhang, L. (2010). Actomyosin Tube Formation in Polar Body Cytokinesis Requires Anillin in C. elegans. *Current Biology*, *20*(22), 2046–2051.

Fanning, A. S., Itallie, C. M. V., & Anderson, J. M. (2012). Zonula occludens-1 and -2 regulate apical cell structure and the zonula adherens cytoskeleton in polarized epithelia. *Molecular Biology of the Cell*, *23*(4), 577–590. http://doi.org/10.1091/mbc.E11-09-0791

Fernandez-Gonzalez, R., Simoes, S. de M., Röper, J.-C., Eaton, S., & Zallen, J. A. (2009). Myosin II Dynamics Are Regulated by Tension in Intercalating Cells. *Developmental Cell*, *17*(5), 736–743. http://doi.org/10.1016/j.devcel.2009.09.003

Field, C. M., & Alberts, B. M. (1995). Anillin, a contractile ring protein that cycles from the nucleus to the cell cortex. *The Journal of Cell Biology*, *131*(1), 165–178. http://doi.org/10.1083/jcb.131.1.165

Field, C. M., Coughlin, M., Doberstein, S., Marty, T., & Sullivan, W. (2005). Characterization of anillin mutants reveals essential roles in septin localization and plasma membrane integrity. *Development*, *132*(12), 2849–2860. http://doi.org/10.1242/dev.01843

Frenette, P., Haines, E., Loloyan, M., Kinal, M., Pakarian, P., & Piekny, A. (2012). An Anillin-Ect2 Complex Stabilizes Central Spindle Microtubules at the Cortex during Cytokinesis. *PLoS ONE*, *7*(4), e34888. http://doi.org/10.1371/journal.pone.0034888

Goldbach, P., Wong, R., Beise, N., Sarpal, R., Trimble, W. S., & Brill, J. A. (2010). Stabilization of the Actomyosin Ring Enables Spermatocyte Cytokinesis in Drosophila. *Molecular Biology of the Cell*, *21*(9), 1482–1493. http://doi.org/10.1091/mbc.E09-08-0714

Gregory, S. L., Ebrahimi, S., Milverton, J., Jones, W. M., Bejsovec, A., & Saint, R. (2008). Cell Division Requires a Direct Link between Microtubule-Bound RacGAP and Anillin in the Contractile Ring. *Current Biology*, *18*(1), 25–29. http://doi.org/10.1016/j.cub.2007.11.050

Haglund, K., Nezis, I. P., Lemus, D., Grabbe, C., Wesche, J., Liestol, K., … Stenmark, H. (2010). Cindr Interacts with Anillin to Control Cytokinesis in Drosophila melanogaster. *Current Biology*, *20*(10), 944–950.

Hall, P. A., Todd, C. B., Hyland, P. L., McDade, S. S., Grabsch, H., Dattani, M., … Russell, S. E. H. (2005). The Septin-Binding Protein Anillin Is Overexpressed in Diverse Human Tumors. *Clinical Cancer Research*, *11*(19), 6780–6786. http://doi.org/10.1158/1078-0432.CCR-05-0997

Hickson, G. R. X., & O'Farrell, P. H. (2008). Rho-dependent control of anillin behavior during cytokinesis. *The Journal of Cell Biology*, *180*(2), 285–294. http://doi.org/10.1083/jcb.200709005

Liu, J., Fairn, G. D., Ceccarelli, D. F., Sicheri, F., & Wilde, A. (2012). Cleavage Furrow Organization Requires PIP2-Mediated Recruitment of Anillin. *Current Biology*, *22*(1), 64–69. http://doi.org/10.1016/j.cub.2011.11.040

Liu, K. C., & Cheney, R. E. (2012). Myosins in cell junctions. *BioArchitecture*, *2*(5), 158–170. http://doi.org/10.4161/bioa.21791

Liu, X.-F., Ishida, H., Raziuddin, R., & Miki, T. (2004). Nucleotide Exchange Factor ECT2 Interacts with the Polarity Protein Complex Par6/Par3/Protein Kinase Cζ

(PKCζ) and Regulates PKCζ Activity. *Molecular and Cellular Biology*, *24*(15), 6665–6675. http://doi.org/10.1128/MCB.24.15.6665-6675.2004

Merzdorf, C. S., Chen, Y. H., & Goodenough, D. A. (1998). Formation of functional tight junctions in Xenopus embryos. *Developmental Biology*, *195*(2), 187–203. http://doi.org/10.1006/dbio.1997.8846

Miller, A. L., & Bement, W. M. (2009). Regulation of cytokinesis by Rho GTPase flux. *Nature Cell Biology*, *11*(1), 71–77. http://doi.org/10.1038/ncb1814

Miller, K. G., & Alberts, B. M. (1989). F-actin affinity chromatography: technique for isolating previously unidentified actin-binding proteins. *Proceedings of the National Academy of Sciences*, *86*(13), 4808–4812.

Oegema, K., Savoian, M. S., Mitchison, T. J., & Field, C. M. (2000). Functional Analysis of a Human Homologue of the Drosophila Actin Binding Protein Anillin Suggests a Role in Cytokinesis. *The Journal of Cell Biology*, *150*(3), 539–552. http://doi.org/10.1083/jcb.150.3.539

Page, Y. L., Chartrain, I., Badouel, C., & Tassan, J.-P. (2011). A functional analysis of MELK in cell division reveals a transition in the mode of cytokinesis during Xenopus development. *J Cell Sci*, *124*(6), 958–968. http://doi.org/10.1242/jcs.069567

Palmer, J. F., & Slack, C. (1970). Some bio-electric parameters of early Xenopus embryos. *Development*, *24*(3), 535–553.

Piekny, A. J., & Glotzer, M. (2008). Anillin Is a Scaffold Protein That Links RhoA, Actin, and Myosin during Cytokinesis. *Current Biology*, *18*(1), 30–36.

Piekny, A. J., & Maddox, A. S. (2010). The myriad roles of Anillin during cytokinesis. *Seminars in Cell & Developmental Biology*, *21*(9), 881–891. http://doi.org/10.1016/j.semcdb.2010.08.002

Ratheesh, A., Gomez, G. A., Priya, R., Verma, S., Kovacs, E. M., Jiang, K., … Yap, A. S. (2012). Centralspindlin and α-catenin regulate Rho signalling at the epithelial zonula adherens. *Nature Cell Biology*, *14*(8), 818–828. http://doi.org/10.1038/ncb2532

Ratheesh, A., & Yap, A. S. (2012). A bigger picture: classical cadherins and the dynamic actin cytoskeleton. *Nature Reviews Molecular Cell Biology*, *13*(10), 673–679. http://doi.org/10.1038/nrm3431

Rodgers, L. S., & Fanning, A. S. (2011). Regulation of epithelial permeability by the actin cytoskeleton. *Cytoskeleton*, *68*(12), 653–660. http://doi.org/10.1002/cm.20547

Smutny, M., Cox, H. L., Leerberg, J. M., Kovacs, E. M., Conti, M. A., Ferguson, C., … Yap, A. S. (2010). Myosin II isoforms identify distinct functional modules that support integrity of the epithelial zonula adherens. *Nature Cell Biology*, *12*(7), 696–702. http://doi.org/10.1038/ncb2072

Straight, A. F., Field, C. M., & Mitchison, T. J. (2005). Anillin Binds Nonmuscle Myosin II and Regulates the Contractile Ring. *Molecular Biology of the Cell*, *16*(1), 193–201. http://doi.org/10.1091/mbc.E04-08-0758

Suzuki, C., Daigo, Y., Ishikawa, N., Kato, T., Hayama, S., Ito, T., … Nakamura, Y. (2005). ANLN Plays a Critical Role in Human Lung Carcinogenesis through the Activation of RHOA and by Involvement in the Phosphoinositide 3-Kinase/AKT Pathway. *Cancer Research*, *65*(24), 11314–11325. http://doi.org/10.1158/0008-5472.CAN-05-1507

Terry, S. J., Zihni, C., Elbediwy, A., Vitiello, E., Leefa Chong San, I. V., Balda, M. S., & Matter, K. (2011). Spatially restricted activation of RhoA signalling at epithelial junctions by p114RhoGEF drives junction formation and morphogenesis. *Nature Cell Biology*, *13*(2), 159–166. http://doi.org/10.1038/ncb2156

Terry, S., Nie, M., Matter, K., & Balda, M. S. (2010). Rho Signaling and Tight Junction Functions. *Physiology*, *25*(1), 16–26. http://doi.org/10.1152/physiol.00034.2009

Vicente-Manzanares, M., Ma, X., Adelstein, R. S., & Horwitz, A. R. (2009). Non-muscle myosin II takes centre stage in cell adhesion and migration. *Nature Reviews Molecular Cell Biology*, *10*(11), 778–790. http://doi.org/10.1038/nrm2786

Wang, S., Mo, Y., Midorikawa, K., Zhang, Z., Huang, G., Ma, N., … Murata, M. (2015). The potent tumor suppressor miR-497 inhibits cancer phenotypes in nasopharyngeal carcinoma by targeting ANLN and HSPA4L. *Oncotarget*. http://doi.org/10.18632/oncotarget.5651

Watanabe, S., Okawa, K., Miki, T., Sakamoto, S., Morinaga, T., Segawa, K., … Narumiya, S. (2010). Rho and Anillin-dependent Control of mDia2 Localization and Function in Cytokinesis. *Molecular Biology of the Cell*, *21*(18), 3193–3204. http://doi.org/10.1091/mbc.E10-04-0324

Wildenberg, G. A., Dohn, M. R., Carnahan, R. H., Davis, M. A., Lobdell, N. A., Settleman, J., & Reynolds, A. B. (2006). p120-Catenin and p190RhoGAP Regulate Cell-Cell Adhesion by Coordinating Antagonism between Rac and Rho. *Cell*, *127*(5), 1027–1039. http://doi.org/10.1016/j.cell.2006.09.046

Woolner, S., Miller, A., & Bement, W. (2010). Imaging the Cytoskeleton in Live Xenopus laevis Embryos. In R. H. Gavin (Ed.), *Cytoskeleton Methods and Protocols* (pp. 23–39). Humana Press. Retrieved from http://dx.doi.org/10.1007/978-1-60761-376-3_2

Yonemura, S., Wada, Y., Watanabe, T., Nagafuchi, A., & Shibata, M. (2010). α-Catenin as a tension transducer that induces adherens junction development. *Nature Cell Biology*, *12*(6), 533–542. http://doi.org/10.1038/ncb2055

Chapter 2: Anillin's AHD and PH Domains are Sufficient for its Localization at Cell-Cell Junctions

Contributions to this work are as follows:

Reyes, C.R.: contributed intellectually and to experimental design, the writing of this Chapter, and executed all experiments and data analysis except Figure 2.2.

Higashi, T.: contributed to Figure 2.2, performing the live imaging experiment co-imaging for 3xGFP-Anillin and ZO-1 and E-cadherin.

Miller, A.L.: contributed intellectually and to experimental design and data analysis, as well as provided lab space and funding for project.

Abstract

Anillin is a scaffolding protein that organizes and stabilizes actomyosin contractile arrays and was previously thought to function primarily in cytokinesis. Using *Xenopus laevis* embryos as a model system to examine Anillin's role in the intact vertebrate epithelium, we previously identified a novel role for Anillin in regulating epithelial cell-cell junctions. However, it remained unclear where Anillin localizes with respect to tight junctions and adherens junctions and how Anillin is targeted to cell-cell junctions. To address these questions, we first performed live co-imaging of Anillin and the tight junction component ZO-1 or the adherens junction component E-cadherin. We found that Anillin strongly co-localizes with the tight junction and partially overlaps with the adherens junction. In work-in-progress, we are also testing the proximity of endogenous Anillin to ZO-1 or E-cadherin via a proximity ligation assay. To determine how Anillin is targeted to junctions, we generated a series of 3xGFP-tagged fragments

of Anillin's major functional domains, expressed them in *Xenopus laevis* embryos, and quantified the extent of junctional co-localization with a membrane marker or tagged junctional protein. 3xGFP-tagged Anillin fragments include the Myosin-2 binding domain, the F-actin binding domain, the Anillin homology domain (AHD, which contains the C2 and GBD domains and mediates interactions with RhoA and a Rho GEF and GAP), and the pleckstrin homology domain (PH, which interacts with Septins and lipids in the plasma membrane). Analysis of the 3xGFP-tagged Anillin fragments revealed that an AHDPH fragment exhibits narrow, apical localization at cell-cell junctions, which is similar to full length Anillin, indicating that these domains are sufficient for Anillin's recruitment to junctions. These findings demonstrate an important role for Anillin's AHD and PH domains in its localization to cell-cell junctions, and suggest that proteins which bind Anillin via the AHD and PH domains are important for its recruitment to cell-cell junctions.

Introduction:

Anillin is a cytokinesis scaffolding protein whose best-characterized role is to help crosslink a number of cytoskeletal, motor and regulatory proteins and stabilize them at the cleavage furrow of dividing cells. It does so by scaffolding this network into a ring-like structure called the contractile ring that is linked to the plasma membrane and provides the underlying force to separate one cell into two. Anillin also organizes and scaffolds actomyosin contractile arrays during polar body extrusion (Dorn & Zhang, 2010), a highly asymmetric form of cytokinesis in meiotic cells, and cellularization, a stage in fly embryo development where the membrane compartmentalizes nuclei into distinct cells (Christine M. Field, Coughlin, Doberstein, Marty, & Sullivan, 2005; K. G. Miller, Field, & Alberts, 1989). Anillin is well suited for these roles as its multi-domain structure allows it to crosslink many of the proteins involved in actomyosin contractile array formation. These domains include binding sites for F-actin (K. G. Miller et al., 1989; Oegema, Savoian, Mitchison, & Field, 2000), Myosin-2 (Straight, Field, & Mitchison, 2005), Septins (Kinoshita, Field, Coughlin, Straight, & Mitchison, 2002; Mostowy & Cossart, 2012), the small GTPase RhoA (Kimura et al., 1996; Piekny &

Glotzer, 2008) and the Rho activity regulators Ect2 (Frenette et al., 2012), MgcRacGAP (D'Avino et al., 2008; Gregory et al., 2008) and p190RhoGAP (Manukyan, Ludwig, Sanchez-Manchinelly, Parsons, & Stukenberg, 2015).

Using the intact epithelium of *Xenopus laevis* embryos as a model system, we previously identified a population of Anillin present at cell-cell junctions throughout the cell cycle (see Chapter 1 of this Dissertation; (Reyes et al., 2014)). This was unexpected, as Anillin was thought to be sequestered in the nucleus of non-dividing interphase cells and only at the cleavage furrow of dividing cells (C. M. Field & Alberts, 1995). We showed that Anillin has an important role in regulating the proper accumulation of junctional RhoA-GTP, F-actin and Myosin-2, as well as maintaining the structure and function of cell-cell junctions (Reyes et al., 2014). However, key questions remained including: how is Anillin recruited to cell-cell junctions? And which of Anillin's binding interactions are required for its function at junctions?

Anillin's recruitment to the cleavage furrow of dividing cells has been characterized and may be instructive to understand how it is recruited to junctions. The contractile ring is assembled in response to local activation of F-actin and Myosin-2 by an equatorial zone of RhoA activity (Bement, Benink, & Dassow, 2005; Nishimura & Yonemura, 2006). The Rho zone is regulated by a number of proteins – most prominently Ect2, a guanine nucleotide exchange factor (GEF) that activates RhoA and MgcRacGAP, a GTPase activating protein (GAP) that can inactivate RhoA and promote discrete activation of a zone of active Rho (Lee, Kamijo, Ohara, Kitamura, & Miki, 2004; A. L. Miller & Bement, 2009; Prokopenko et al., 1999; Tatsumoto, Xie, Blumenthal, Okamoto, & Miki, 1999). Importantly, the equatorial Rho zone has been shown to serve as the signal that recruits Anillin to the contractile ring (Hickson & O'Farrell, 2008; Piekny & Glotzer, 2008; Straight et al., 2005). Indeed, Cytokinesis initiates upon anaphase onset (Glotzer, 2001), and Anillin is one of the first proteins recruited, even before the accumulation of F-actin and Myosin-2 and before the cleavage furrow begins to ingress. When Rho signaling is perturbed via knockdown of the Rho GEF Ect2, Anillin is no longer recruited to the cleavage furrow, demonstrating Rho-dependent control of Anillin localization

during cytokinesis (Hickson & O'Farrell, 2008). Experiments characterizing which domains and interacting partners of Anillin are required for its ability to localize to the cleavage furrow of dividing cells have demonstrated that Anillin's N-terminal Formin-, Myosin- and Actin-binding domains are important primarily for its *function* to scaffold actomyosin contractile arrays. The C-terminal AHD and PH domains, which mediate interactions with RhoA and its GEF and GAPs, Septins and lipids, are important for Anillin *targeting* (Figure 2.1).

Deletion of Anillin's N-terminus does not affect its ability to localize to the cleavage furrow, but does result in failed cytokinesis. As Anillin's primary role is to scaffold actomyosin contractile arrays, it is not surprising that its N-terminal myosin- and actin-binding domains, while dispensable for targeting, are required for this function. Depletion of formin by RNAi or deletion of Anillin's formin-binding domain does not prevent Anillin from reaching the cleavage furrow (Hickson & O'Farrell, 2008; Piekny & Glotzer, 2008). Disruption of Anillin's interaction with Myosin-2 whether by deletion of the Myosin binding domain or treatment of the cells with the Myosin-2 inhibitor blebbistatin, also do not perturb Anillin localization to the furrow (Piekny & Glotzer, 2008; Straight et al., 2003). While perturbation of F-actin with the actin depolymerizing drug Latrunculin A causes patchy and filamentous distribution of Anillin, it still reaches the cleavage furrow, and deletion of the actin-binding domain does not affect Anillin's recruitment (Hickson & O'Farrell, 2008; Piekny & Glotzer, 2008). Additionally, an Anillin mutant where both the Myosin- and Actin-binding domains were deleted was still able to target to the cleavage furrow, but exhibited a high rate of cytokinesis failure (Kechad, Jananji, Ruella, & Hickson, 2012a; Piekny & Glotzer, 2008). Finally, the linker region that connects Anillin's N-terminal domains with its C-terminal domains has no known function and is not sufficient for Anillin's localization at the cleavage furrow (Oegema et al., 2000; Piekny & Glotzer, 2008).

When Anillin's C-terminal domains are perturbed, Anillin's robust localization at the cleavage furrow is lost. When the AHD domain, which mediates interactions with Rho, Ect2, MgcRacGAP and p190RhoGAP is deleted, Anillin reaches the equatorial cortex

but does not persist there (Piekny & Glotzer, 2008). Instead of remaining equatorial, it moves to the polar regions of the cell, showing that the AHD is required for Anillin's stable contractile ring localization. Expression of a GFP-tagged AHD domain shows weak furrow localization, demonstrating that this region is sufficient for targeting (Piekny & Glotzer, 2008). Finally, perturbation of the PH domain, which mediates interactions with Septins and lipids (particularly PIP$_2$) reduces robust furrow accumulation and in some cases abolishes it. Deletion of the PH domain results in cytoplasmic distribution and weak accumulation at the equatorial cortex (Oegema et al., 2000). Furthermore, while a fragment containing the AHD and PH domains is sufficient to robustly localize to the furrow (Kechad, Jananji, Ruella, & Hickson, 2012b; Oegema et al., 2000; Piekny & Glotzer, 2008), introducing point mutations in this fragment that disrupt its ability to interact with lipids results in complete abolishment of furrow localization (J. Liu, Fairn, Ceccarelli, Sicheri, & Wilde, 2012).

Additional mechanisms that regulate Anillin recruitment exist outside of metazoans. For example in fission yeast, the Anillin-like proteins Mid1 and Mid2 are phospho-regulated by polo-like kinase (Plo1) and the dYRK kinase Pom1. Plo1 phosphorylates Mid1 during mitosis to induce export of Anillin from the nucleus to the cytoplasm, and Pom1 phosphorylates Anillin to maintain its proper spatiotemporal localization (Almonacid et al., 2011; Celton-Morizur, Racine, Sibarita, & Paoletti, 2006; Padte, Martin, Howard, & Chang, 2006; Rincon & Paoletti, 2012). However, to date, similar mechanisms of Anillin phospho-regulation have not been identified in metazoans.

Here, we examined where Anillin localizes with respect to tight junctions (TJs) and adherens junctions (AJs) and characterized which domains of Anillin are sufficient for its ability to target to cell-cell junctions. Based on what's know about how Anillin is recruited to the contractile ring during cytokinesis, we hypothesized that Anillin's C-terminal AHD and PH domains would be important for its ability to target to cell-cell junctions throughout the cell-cycle. Our approach was to generate 3xGFP-tagged fragments of Anillin's major binding domains, including the Formin, Myosin, Actin, AHD and PH domains and examine their ability to target to cell-cell junctions. These fragments were

expressed in *Xenopus laevis* embryos, and their localization and behavior compared to that of full length Anillin, which exhibits a narrow and apical junctional distribution (Reyes et al., 2014). We found that while the N-terminal Myosin- and Actin-binding domains were not sufficient for junctional localization, the C-terminal AHD and PH domains were. A combined fragment with the AHD and PH domain most closely recapitulated full length Anillin's narrow and apical distribution, suggesting that these domains may work cooperatively in Anillin localization. These findings provide important mechanistic insight into Anillin's localization at cell-cell junctions.

Results

Anillin co-localizes with the tight junction protein ZO-1 and partially overlaps with the adherens junction protein E-cadherin

Previously, we showed that a population of Anillin is localized at cell-cell junctions throughout the cell-cycle, exhibits a narrow distribution and is apically enriched (Reyes et al., 2014). We also showed that when Anillin is knocked down, both TJs and AJs are disrupted, demonstrating that it has a role in regulating both types of junctions (Reyes et al., 2014). However, we did not extensively characterize where Anillin localizes with respect to TJs or AJs. To address this, we knocked down endogenous Anillin and expressed 3xGFP-tagged Anillin (Anillin-3xGFP) at near endogenous levels, along with a tagged TJ protein (mRFP-ZO-1) or AJ protein (E-cadherin-3xmcherry). We then examined Anillin's co-localization with ZO-1 or E-cadherin in gastrula stage (stage 10.5) *Xenopus laevis* embryos using confocal microscopy (Figure 2.2). 3xGFP-tagged Anillin accumulated at the cleavage furrow of dividing cells, midbody of recently divided cells and was present at cell-cell junctions in both dividing and non-dividing cells where it co-localized with both ZO-1 and E-cadherin. Anillin appeared to co-localize more strongly with ZO-1 in *en face* views, as evidenced by the more prominent yellow signal. Side views confirmed this, showing that Anillin closely overlapped with ZO-1 and only partially overlapped with E-cadherin. Fixed staining for endogenous Anillin along with endogenous ZO-1 or E-cadherin confirmed this pattern of localization: close association of Anillin with ZO-1 and partial overlap with E-cadherin (Figure S2.1).

In polarized epithelial cells, TJs and AJs are spatially distinct. TJ proteins are located most apically, while AJ proteins can be detected throughout the basolateral membrane but are concentrated at the zonula adherens (ZA). At the ZA, located just basal to the TJ, E-cadherin clusters into a ring-like structure encircling each epithelial cell, and adhesion is coordinated with contractile forces from the underlying actomyosin belt (Hoffman & Yap, 2015). Given that the tight junction protein ZO-1, while spatially distinct from the adherens junction protein E-cadherin, may be in close proximity with E-cadherin clusters in the ZA, we wondered whether the partial overlap observed between Anillin and E-cadherin was due to the limited z-resolution of confocal microscopy. Indeed, fixed co-staining for ZO-1 and E-cadherin showed that their distinct patterns of localization were difficult to differentiate with confocal microscopy (Figure S2.2); thus, we wished to use an approach with higher sensitivity and resolution.

Proximity Ligation Assay (PLA) to test whether Anillin interacts with the tight junction protein ZO-1 and/or the adherens junction protein E-cadherin

Proximity ligation assay (PLA) is a simple and sensitive way of detecting endogenous protein-protein interactions <40 nm apart. The PLA technique involves using two primary antibodies raised in different species that detect a specific region or epitope of their targeted proteins, in this case Anillin (rabbit antibody) and a TJ protein (mouse antibody) or Anillin (rabbit antibody) and an AJ protein (mouse antibody). Species-specific secondary antibodies with complementary tails of oligonucleotide sequence (synthetic DNA) attached to them, bind to their respective primary antibody. If Anillin and ZO-1, for example, are in close proximity in the cell, the complementary tails of nucleotide sequences will hybridize. Upon addition of an polymerase, these hybridized tails are amplified via rolling circle amplification, and their signal detected through immunofluorescence microscopy, where sites of interaction appear as punctate structures (Figure S2.3).

PLA is often used for cultured cells, which are ~20 μm in diameter and are plated on coverslips, but a single *Xenopus laevis* embryo is ~1.2 mm in diameter, so using the

PLA reagents at this scale would be cost prohibitive. To optimize PLA for our system, I performed microsurgeries on *Xenopus* gastrula stage embryos to isolate animal cap explants (Figure S2.4). These explants were allowed to adhere to fibronectin-coated coverslips, flattened, fixed and PLA was performed. The explant retains epithelial polarity like the intact embryo, as the tight junction protein ZO-1 and the adherens junction protein E-cadherin are localized appropriately (Figure S2.4). A PLA using two different species-specific antibodies for ZO-1 (mouse and rabbit) as a positive control showed multiple distinct puncta around the perimeter of the cells, almost perfectly tracing their polygonal outline (Figure 2.3). The negative control, antibodies for ZO-1 (rabbit) and E-cadherin (mouse), showed only non-specific occasional puncta that did not encircle the perimeter of the cells (Figure 2.3). In preliminary experiments, PLA for Anillin and ZO-1 detected sporadic puncta around the perimeter of cells, while Anillin and E-cadherin did not detect continuous patterns around the perimeter of cells - only sometimes sparse puncta like the negative control (Figure 2.3). Continued work is necessary, however, to repeat and optimize the PLA protocol for detection and quantification.

Anillin and fragment localization at the cleavage furrow of dividing cells
Anillin's recruitment to the cleavage furrow of dividing cells is dependent on active GTP-bound RhoA (Hickson & O'Farrell, 2008). Given that RhoA and its activity regulators Ect2, MgcRacGAP, and p190RhoGAP are also present at cell-cell junctions (X.-F. Liu, Ishida, Raziuddin, & Miki, 2004; Ratheesh et al., 2012; Wildenberg et al., 2006), we speculated that a RhoA-dependent mechanism might also be important for Anillin's recruitment to junctions. Thus, we hypothesized that the AHD region of Anillin, which mediates interactions with RhoA and Rho activity regulators including Ect2, MgcRacGAP and p190RhoGAP, might be sufficient for targeting it to cell-cell junctions. Before examining the localization of the 3xGFP-tagged fragments at cell-cell junctions, we first confirmed that the fragments are localized as expected at the cleavage furrow of dividing cells. We generated N-terminally 3xGFP-tagged fragments of Anillin's major binding domains including the Myosin-2, F-actin, AHD and PH domains, in addition to a combined Formin and Myosin-2 fragment and an AHDPH fragment. mRNA for each

fragment was injected, and the embryos were allowed to develop to the gastrula stage (Figure 2.4). Western blotting for 3xGFP-tagged Anillin and fragments shows that each fragment is at the expected molecular weight; however, the western blots must be stained for tubulin to allow quantification and confirmation of similar levels of expression (Figure S2.5). Further, N- or C- terminally 3xGFP-tagged full length Anillin behaved similarly, as we detected it at both the junctions and at the cleavage furrow of dividing cells; thus, we used them interchangeably for this study (Figure S2.6).

Full length Anillin was recruited to the cleavage furrow early in cytokinesis, and as the cell ingressed it became more enriched at the furrow and later at the midbody (Figure 5). N-terminal Myosin-2 and F-actin fragments were not observed at the cleavage furrow either before or after ingression (Figure 2.5). A combined FBD and Myosin-2 fragment was detected at the cleavage furrow after ingression had initiated. Consistent with previous reports, the C-terminal AHD and combined AHDPH fragments were enriched at the furrow (Figure 2.5). However, the PH domain fragment alone was not generally enriched at the furrow; in some examples it did localize in puncta at near the ingressing furrow (Figure S2.7).

As our goal was to compare the recruitment of each of the fragments to full length Anillin, which localizes to the cleavage furrow early in cytokinesis, we quantified the mean intensity of each of the fragments at the equator at 20% ingression and graphed the ratio of signal at the equator over the poles (Figure S2.8). Full length Anillin and its C-terminal AHD and AHDPH domains were recruited to the furrow at 20% ingression (Figure 2.6), although the PH domain by itself was not (Figure 2.6). The N-terminal FBDMyosin, Myosin-2 and Actin domains were not enriched at the furrow at 20% ingression (Figure 2.6)

Anillin's C-terminal AHDPH domains recapitulate Anillin's narrow distribution at the plasma membrane
Next, we examined the localization of each of the 3xGFP-tagged fragments at the cell membrane and compared their distribution to that of full length Anillin by live imaging in

gastrula stage embryos. We co-injected each of the 3xGFP-tagged fragments with a membrane marker (mcherry-farnesyl). Full length Anillin exhibits a narrow, focused distribution at the membrane throughout the cell-cycle (Figure 2.7). The FBDMyo fragment was present at the membrane in a cell-cycle dependent manner; during interphase it was sequestered in the nucleus, at metaphase it was present at the membrane, and in dividing cells it was present at the cleavage furrow (Figure S2.9). The Myosin-2 fragment alone did not localize to the membrane and resembled the distribution of the 3xGFP negative control (Figure 2.7). The Actin domain exhibited a wide distribution at the membrane compared with full length Anillin's focused distribution (Figure 2.7). The AHD was at the membrane, but there was also cytoplasmic background (Figure 2.7). The AHDPH decorated the membrane in a focused, but discontinuous stud-like pattern (we have also observed this type of pattern with full length Anillin in some cells), and the PH domain exhibited regions of strong continuous signal at the membrane and regions of weaker signal that was punctate as well as vesicular signal (Figure 2.7).

Quantification using Full-Width-Half-Max (FWHM) analysis of line scans drawn across bicellular junctions confirmed that Anillin has a narrow distribution at the membrane, and that the AHDPH most closely resembled this distribution (Figure S2.10, S2.11 & Figure 2.8). The AHDPH had a FWHM 1.04 µm, which most closely resembled full length Anillin's FWHM of 1.09 µm. The PH and Actin domains were noticeably wider, with FWHMs of 1.78 µm and 3.17 µm, respectively (Figure 2.8). As the PH fragment exhibited regions of strong and weak signal, line scans were performed from this data set on both populations to capture the representative value. FWHM analysis was performed on the AHD fragment, but the Gaussian curve fit had a low R^2 value of 0.31 as opposed to the higher R^2 values ranging from 0.87-0.64 for full length Anillin and the Actin, PH and AHDPH fragments. The weak R^2 value is likely due to the fact that the AHD fragment exhibited higher background in the cytoplasm. As the Myosin binding domain was not at the membrane, and the FBDMyosin was only at the membrane in a cell-cycle dependent manner, they were not included in the FWHM analysis.

Examining the co-localization of Anillin fragments with the TJ protein ZO-1 and characterizing their apico-lateral distribution

It was difficult to determine the extent of apical enrichment for each of the Anillin fragments from live imaging movies due to the limited number of z-planes that could be acquired during live imaging (~7 z-planes, 0.75 µm each; Figure S2.12). Furthermore, for the live imaging approach we co-imaged each of the 3xGFP-tagged fragments with a membrane marker (mcherry-farnesyl) that indiscriminantly labeled the membrane as opposed to a junctional protein with specific localization. Thus, we next used a fixed staining approach in order to acquire more z-planes (~20 z-planes, 0.41 µm each) and to probe for the 3xGFP-tagged Anillin fragments along with the apically enriched endogenous ZO-1 protein. Because the combined AHDPH fragment most closely resembled full length Anillin's narrow distribution, we focused our efforts on characterizing the apicobasal polarity of the C-terminal AHD, AHDPH and PH domains.

Fixed staining confirmed the junctional presence of the AHD, AHDPH and PH domains that we had observed in live imaging (Figure 2.9). *En face* views showed that the AHD was at junctions, and also present in the cytoplasm (Figure 2.9). The AHDPH domain studded junctions with little to no background in the cytoplasm, while the PH domain had junctional signal and intermediate background in the cytoplasm (Figure 2.9). Side views showed that the AHD varied in its distribution, ranging from regions of weak apical enrichment to localization throughout the lateral membrane (Figure 2.9). The PH domain indiscriminantly labeled the lateral membrane, while the AHDPH was tightly apically focused (Figure 2.9). Further, while the AHD and PH only partially overlapped with ZO-1, the AHDPH colocalized with ZO-1, most closely resembling full length Anillin (Figure 2.9). Using line scans drawn across the apical to basal membrane (line scans started from the point where ZO-1 signal begins and ended slightly below that point) we normalized to background and plotted the distribution of each of the fragments, comparing them to full length Anillin and ZO-1. The analysis showed that the AHDPH may also closely recapitulate full length Anillin's apical distribution. However, in this analysis the intensity of the line scans was not normalized to 1 and the line sans were not aligned based on ZO-1 peak intensity. Using an alternative quantification for these

data where line scan intensity was normalized to 1 and all line scans for Anillin and fragments were aligned with the peak intensity of ZO-1, did not show a major resemblance between any of the Fragments and full length Anillin, which closely matched ZO-1 (Figure S2.13). More work is necessary to optimize a method of quantification for these data.

Discussion:

Anillin was reported to be in the nucleus of non-dividing interphase cells and at the division site of dividing cells (D'Avino, 2009; C. M. Field & Alberts, 1995), however, our lab was the first to report a population of Anillin at epithelial cell-cell junctions throughout the cell cycle (Reyes et al., 2014). We identified an important role for this population of Anillin in functionally regulating an apical belt of F-actin and Myosin 2, which is connected to cell-cell junctions. Furthermore, we found that Anillin is important for the proper regulation of key junction proteins including the TJ proteins ZO-1 and Claudin, and the AJ proteins β-catenin and E-cadherin. However, it remained unclear (1) where Anillin localized with respect to TJs and AJs, (2) whether Anillin interacted with junctional proteins, and (3) how Anillin was targeted to cell-cell junctions. Here, we addressed these questions.

To address the first question, we performed live co-imaging of Anillin-3xGFP and the TJ component ZO-1 (mRFP-ZO-1) or the AJ component E-cadherin (E-cad-3xmCherry). We found that Anillin strongly co-localizes with the TJ protein ZO-1 and partially overlaps with the AJ protein E-cadherin. While these data were informative, there were limitations to this approach, which made it challenging to draw further conclusions. First, live imaging of Anillin and junction proteins involves visualizing both proteins by tagging them with fluorescent proteins like GFP or mCherry/mRFP. Proteins in their native environment in the cell do not have large fluorescent tags, and artificial tags can affect protein localization or protein-protein interactions. Second, although Anillin was knocked down and Anillin-3xGFP was expressed at near endogenous levels, the fluorescently-tagged junction proteins were expressed in embryos that also contain

endogenous untagged junction proteins; this overexpression of junctional proteins may also introduce artifacts. Thus, it is most physiologically relevant to study the endogenous proteins as they naturally occur in the cell. Third, live imaging has limitations in the degree of resolution that we are able to obtain, particularly in the z space. The partial overlap of Anillin with E-cad that we are detecting by live imaging may or may not be real. Fixed immunofluorescence staining of embryos for endogenous Anillin and junction proteins did not resolve this issue. In the future, we will continue to pursue the PLA as well as use super-resolution microscopy and/or electron microscopy to better understand where Anillin localizes with respect to TJs and AJs.

We employed the proximity ligation assay (PLA), a simple, sensitive method for assessing endogenous protein-protein co-localization. To our knowledge, PLA had not been used before on gastrula stage *Xenopus* embryos. Therefore, we had to optimize PLA for our model system, which involved: performing microsurgeries to make animal cap explants, finding and characterizing species-specific antibodies that cross-reacted with *Xenopus* proteins, using a humidity chamber to prevent evaporation of the small volume of PLA reagents during incubations, and using a shaker during all reactions to ensure an even distribution of reagents. Once these parameters were optimized, we obtained successful detection of PLA signal for our positive control, anti-mouse ZO-1 and anti-rabbit ZO-1, using PLA. In the positive controls, the characteristic PLA puncta studded the membranes of the explant, uniformly outlining polygonal cell shapes. In the negative control, anti-mouse E-cadherin and anti-rabbit ZO-1, only sparse single or paired PLA dots were detected, which may represent either false positives or indeed a point of interaction, as E-cad and ZO-1 have been observed to co-distribute in granular clusters (Rajasekaran, Hojo, Huima, & Rodriguez-Boulan, 1996).

Preliminary data indicated that the experimental groups (Anillin/ZO-1 and Anillin/E-cadherin) appeared different from the positive control; the PLA puncta detected were fewer than the positive control and more closely resembled the negative control, suggesting that Anillin may not strongly interact with either ZO-1 or E-cadherin. In the future, it will be necessary to repeat this preliminary data. Additionally, we will KD

endogenous Anillin and perform PLA for Anillin/ZO-1 or Anillin/E-cad to determine if the few PLA puncta that decorate the experimental groups may represent real sites of protein-protein interaction that are reduced when Anillin is knocked down. Additionally, it is possible that the epitopes for the anti-ZO-1 and/or the anti-E-cadherin antibodies are such that the distance between these sites and the anti-Anillin antibody are too far apart to be detected by PLA. A study found that different termini of ZO-1 associate with different proteins – the N-terminus most closely associates with integral membrane proteins, while the C-terminus associates with cytoskeletal proteins (van Itallie et al., 2014).

While our preliminary PLA results do not indicate that Anillin interacts with either ZO-1 or E-cadherin, it does not exclude the possibility that Anillin may interact with other junctional proteins. It may be advantageous to perform PLA for Anillin and a transmembrane TJ protein like Claudin. Furthermore, ZO-1 is a large protein (isoforms have a molecular weight around 220kDa (Balda & Anderson, 1993), and the epitope for the mouse anti-ZO-1 antibody used in this experiment is a small region in the N-terminus of the protein (334-634). It may be useful to identify another ZO-1 antibody that recognizes the C-terminus of ZO-1 and test whether the results are the same. It may also be useful to test for an interaction between Anillin and the AJ cytoplasmic plaque protein β-catenin. Previous work from our lab showed that when Anillin is KD, β-catenin's normal apicobasal polarity is disrupted (Reyes et al., 2014). Future work will seek to identify novel interactions between Anillin and junction proteins using immunoprecipitation and mass spectrometry.

The mounting solution for the Duolink PLA kit contained DAPI to stain the nuclei; however, we did not obtain uniform or robust labeling of the nuclei. This made it difficult to clearly distinguish individual cells, especially in the negative controls and experimental groups, and therefore, challenging to quantify the number of PLA puncta per cell. Future work will seek to repeat this experiment and optimize conditions for either the detection of nuclei or cell outlines (via a lipid stain, or microinjection of GFP-farnesyl to label the membrane) to enable quantification.

Analysis of the 3xGFP-tagged Anillin fragments ability to target to the cortex and junctions revealed that a combined AHD-PH fragment mostly closely resembled full length Anillin's narrow and apical localization at cell-cell junctions, indicating that these domains are sufficient for Anillin's recruitment to junctions. It was intriguing that a combined AHD-PH fragment of Anillin most closely recapitulates full length Anillin's junctional localization (narrow and apical junctional distribution) as opposed to either the AHD or PH alone, suggesting some degree of cooperativity. Additionally, the AHD and PH domains have binding partners whose interaction with Anillin spans both domains, such as the GTP-binding proteins Septins. Future work is necessary to differentiate possible unique contributions of the AHD and PH domains to Anillin's localization at junctions. The AHD was recently found to consist of a Rho Binding Domain (RBD) and a C2 domain (Sun et al., 2015). Therefore, it may be of interest to generate an AHDPH fragment with point mutations disrupting RBD binding to Rho or other disrupting interactions with other binding partners within this region. Other approaches may include using Anillin and its fragments for Immunoprecipitation (IP) and mass spec analysis to identify novel binding partners, which may include junction proteins.

Intriguingly, the AHD was the only fragment that was dynamic, as we observed transient "flares" or flashes of its accumulation at the cortex, in addition to more stable populations (data not shown). The flares resembled active Rho, which we previously detected in our system as both stable and dynamic populations of short-lived transient flares in control embryos. Our probe for active Rho contains the Rho-binding domain of the Rho effector protein Rhotekin fused to GFP, thus the AHD, which indeed binds active Rho, may be functioning as a probe for active Rho. Given the dynamic nature of the AHD fragment, a different type of analysis may be required to quantify its distribution at junctions.

The PH domain was static in comparison to the AHD fragment and was detected throughout the membrane both in *en face* and side views. In live imaging, we observed regions of stronger and weaker accumulation of the PH domain – some of which

appeared punctate and linear, while others appeared fuzzy and weak. Further, we observed vesicle-like accumulations of the PH domain in the cytoplasm. In fixed staining for the PH domain, we observed uniform patterns of distribution at junctions and no vesicle-like accumulations. It is possible that the fixation conditions used (TCA) did not preserve these vesicle-like structures or that use of detergent to permeabilize the cells before incubation with antibodies may account for the loss in detection of these structures. It may be helpful to try other fixation conditions in the future.

The PH domain and the Myosin-2- and F-actin-binding domains did not localize specifically at junctions. However, a fragment with the Myosin-2 binding domain and an upstream region known to bind formin (FBD) and contain two nuclear localization sequences (NLS) (C. M. Field & Alberts, 1995; Watanabe et al., 2010), localized to the cortex in a cell cycle dependent manner. During interphase it was sequestered in the nucleus, after nuclear envelope breakdown it became cortical, and in dividing cells was present at the cleavage furrow and cortex. Co-staining of the FBDMyo fragment with the TJ protein ZO-1, however, showed that FDMyo was not apically focused and did not strongly co-localize with ZO-1 (Figure S2.9). While the FBDMyo fragment may not be junctional, it remains an interesting question how it is targeted to the cortex. As the Myosin binding domain alone was not sufficient for junctional or even cortical localization, it suggests that the FBD and interaction with formins may have an important role in its ability to target there. Notably, the FBDMyo fragment was the only fragment that was detected in the nuclei during interphase. A population of full length Anillin is present at cell junctions throughout the cell-cycle, even during interphase when a population of it is sequestered in the nucleus. It will be interesting to test whether the nuclear and junctional populations of Anillin are distinct or exchange and how they might be differentially regulated to target populations to the nucleus and to junctions. Future plans to test Anillin shuttling in and out of nucleus may include using a photoactivatable Anillin to discretely activate a population of Anillin, for example, in the nucleus and look for exchange at the junctions. Investigating possible sites of phosphorylation and their candidate kinases will also be of interest.

This work provides further evidence that Anillin localizes to apical cell-cell junctions and mechanistic insight into which domains of Anillin are responsible for its association with junctions. Anillin is overexpressed in multiple human cancers, and its increased expression correlates with increased metastatic potential (Hall et al., 2005; Olakowski et al., 2009; Ronkainen, Hirvikoski, Kauppila, & Vaarala, 2011; Zhou et al., 2014). With roles in regulating both cytokinesis and cell-cell junction integrity, misregulation of Anillin could potentially contribute both to tumor formation and cancer cell metastasis. Therefore, gaining a better understanding of the Anillin's recruitment to and role in cell-cell junction regulation may be relevant to cancer biology.

Figures and Legends:

Anillin (ANLN)

AH Domain (AHD)

| Formin | myosin | actin | | RBD | C2 | PH |

N-terminal domains organize contractility

Linker (no known function)

C-terminal domains are sufficient for equatorial targeting

Domain Deletion

ΔFormin
ΔMyosin
ΔActin

Anillin at the equatorial cortex.

ΔMyosinΔActin

Anillin reaches the equatorial cortex but shifts as the furrow oscillates

Inhibitors
Blebbistatin

Anillin at the equatorial cortex, but the cell doesn't ingress.

Latrunculin

Anillin has patchy and filamentous accumulation at equator.

RNAi
RNAi mDia
RNAi MRLC

Anillin at the equatorial cortex.

Domain Deletion

ΔLinker

Anillin at the equatorial cortex.

Domain Deletion

ΔAHD

Anillin at the equatorial cortex but doesn't persist moves to poles.

ΔPH

Anillin is weakly at the equatorial cortex and cytoplasmic.

Overexpression of fragments

AHD-GFP

Anillin is weakly at the equatorial cortex or absent.

AHDPH-GFP

Anillin at the equatorial cortex.

Mutations

AHDPH-GFP
T91I, G998E,
A740D, E758,
L3-7KA, ΔL3

Anillin is abolished at equatorial cortex.

Overexpression of fragment

Linker-GFP

Linker is not sufficient for recruitment to furrow.

Figure 2.1 Summary of approaches to characterize Anillin's recruitment to the cleavage furrow of dividing cells. See text for details. (Piekny & Glotzer, 2008; Straight et al. 2005; Zhao et al., 2005; Reyes et al. 2014; Hickson & O'Farrell, 2008; D'Avino et al., 2008; Kechad et al., 2012; Sun et al., 2015; Liu et al., 2012; Lee & Wu, 2012)

76

A

Anillin-3xGFP | mRFP-ZO-1 | merge

Anillin-3xGFP | E-cadherin-3xmcherry | merge

B

Anillin-3xGFP | Anillin-3xGFP

mRFP-ZO-1 | E-cadherin-3xmcherry

merge | merge

Anillin-3xGFP | mRFP-ZO-1 | merge

Anillin-3xGFP | E-cad 3xmche | merge
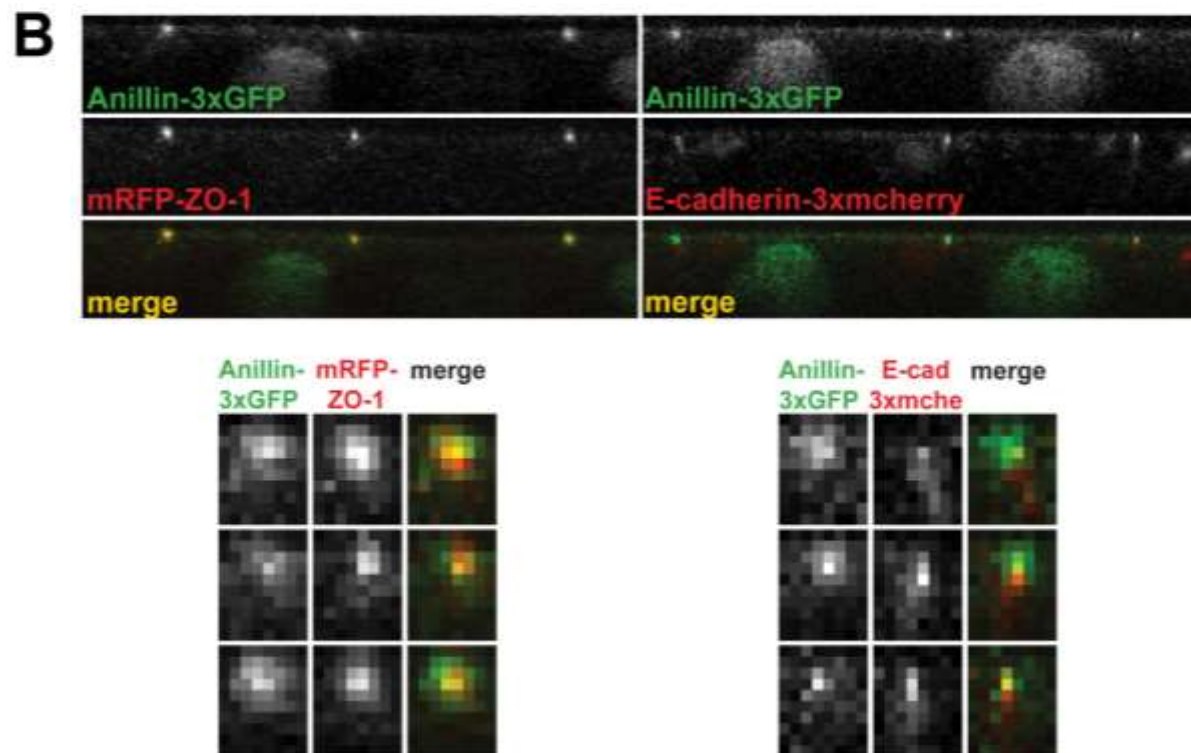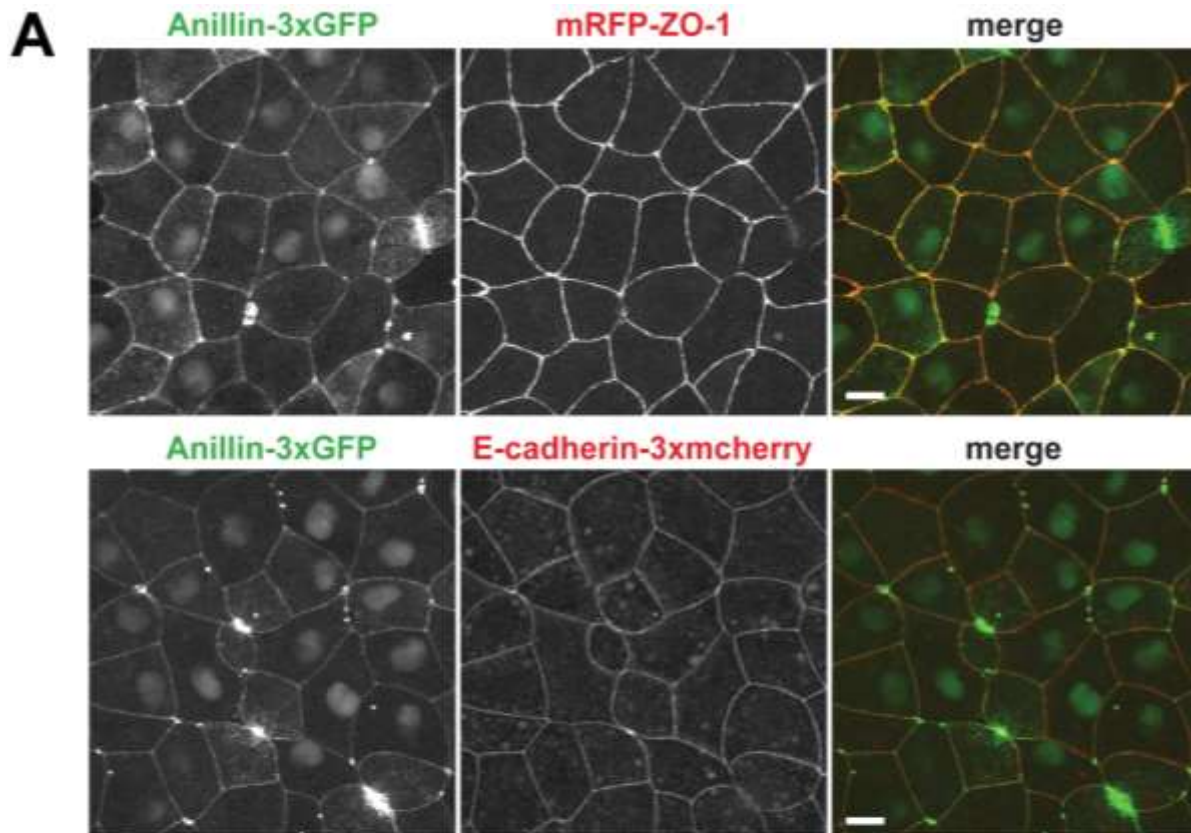
Figure 2.2 Characterization of Anillin-3xGFP localization at cell-cell junctions. (A) *En face* views from a live movie of embryos where endogenous Anillin was knocked down via an antisense morpholino and replaced at near endogenous levels with Anillin-3xGFP and ZO-1 tagged with mRFP or E-cadherin tagged with 3xmcherry. Anillin-3xGFP co-localizes with the tight junction protein ZO-1 and partially overlaps with the adherens junction protein E-cadherin in *en face* views (A) and side views (B). Scale bars are 15 μm. Smaller boxes at the bottom of (B) are zoomed in regions of Anillin and ZO-1 or E-cadherin signal at individual cell junctions. Yellow signal in the merged channel represents colocalization.
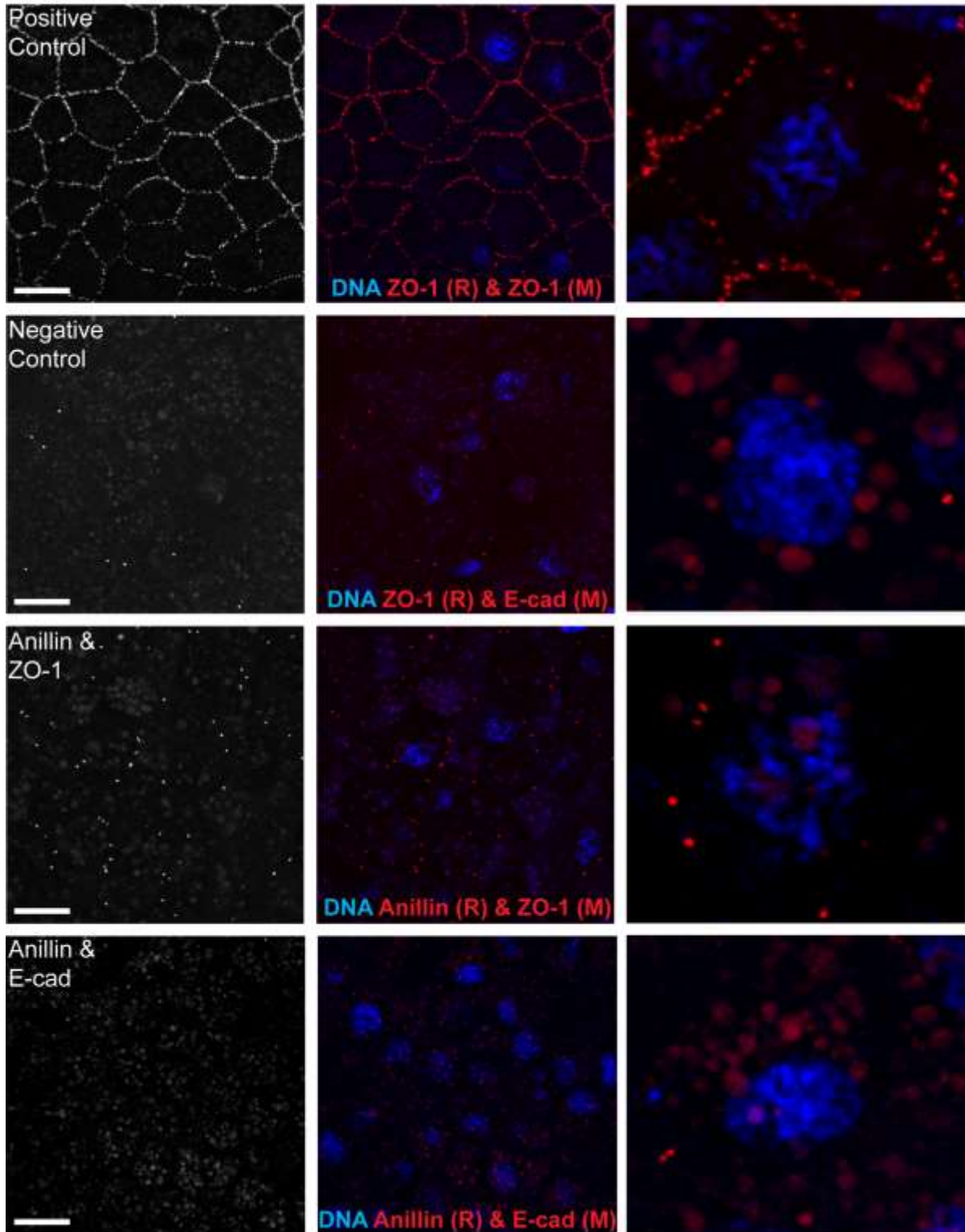
Figure 2.3 Proximity ligation assay for Anillin and ZO-1 or E-cadherin. Representative *en face* images of *Xenopus* explants probed with species-specific antibodies for PLA analysis. Positive controls were probed with anti-mouse and anti-rabbit antibodies for ZO-1, while negative controls were probed with anti-mouse E-

cadherin and anti-rabbit ZO-1 antibodies. Experimental groups were probed with either anti-mouse E-cadherin and anti-rabbit Anillin or anti-mouse ZO-1 and anti-rabbit Anillin. Scale bars are 20 μm.
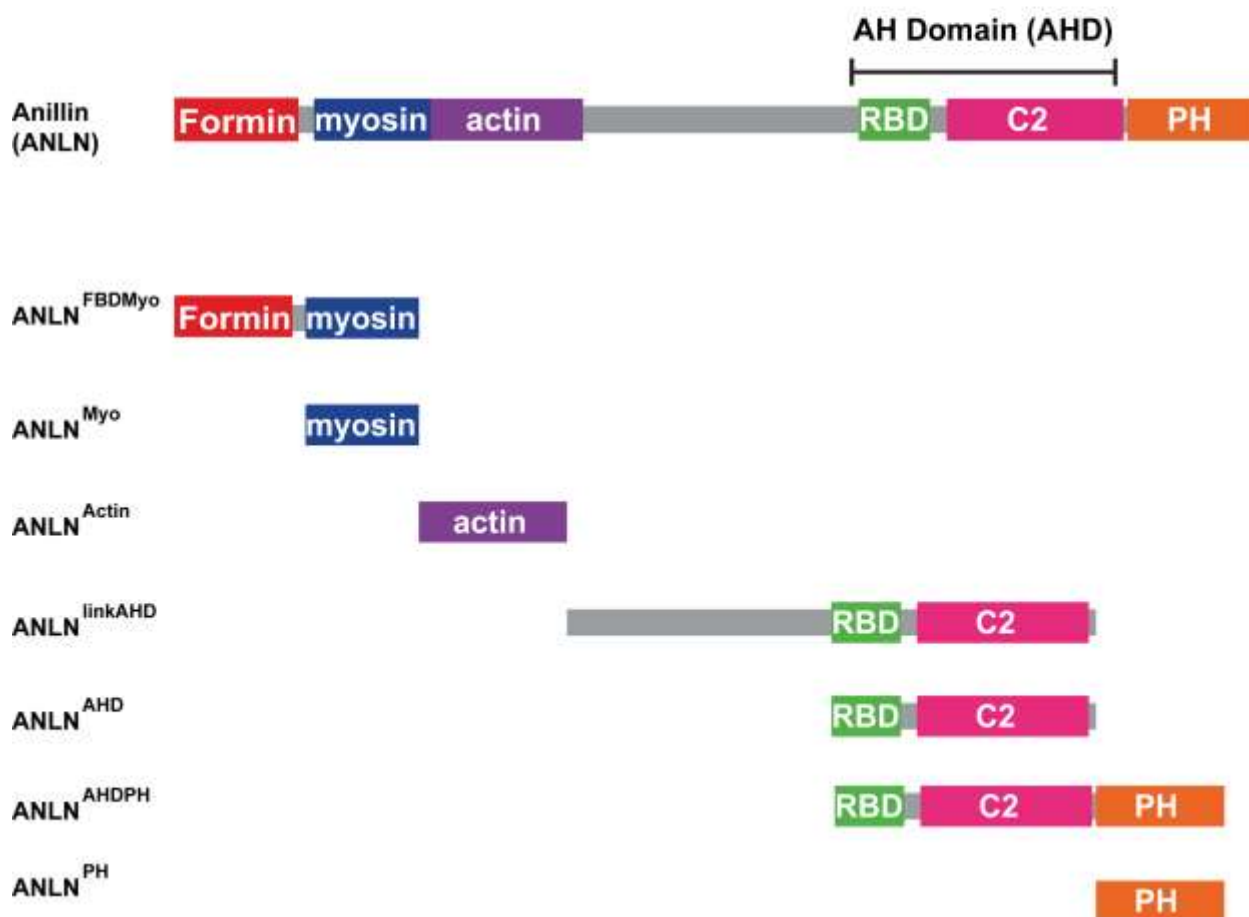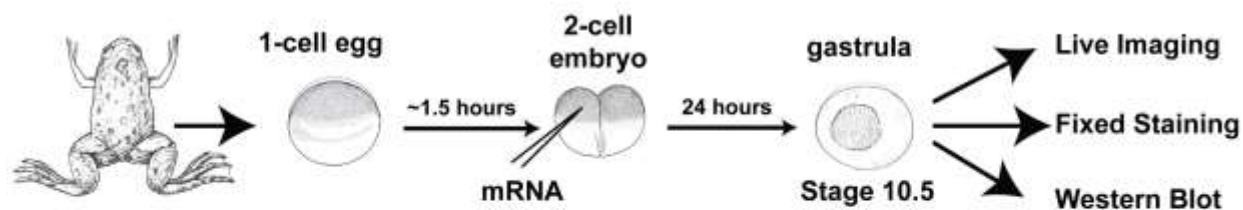
Figure 2.4 Experimental approach. (top) Cartoon showing experimental methods. For all experiments eggs were collected from ovulating adult female frogs, fertilized in vitro, microinjected at the 2-cell stage and live imaging, fixed staining or western blots performed at the gastrula stage (~10.5-11). (bottom) Cartoon diagram of full length Anillin and its major binding domains, which include the Formin binding domain (FBD), Myosin-2 and Actin domains at the N-terminus and the AHD (which consists of the RBD and C2) and PH domains at the C-terminus. N-terminally tagged 3xGFP fragments of Anillin's major binding domains were generated.
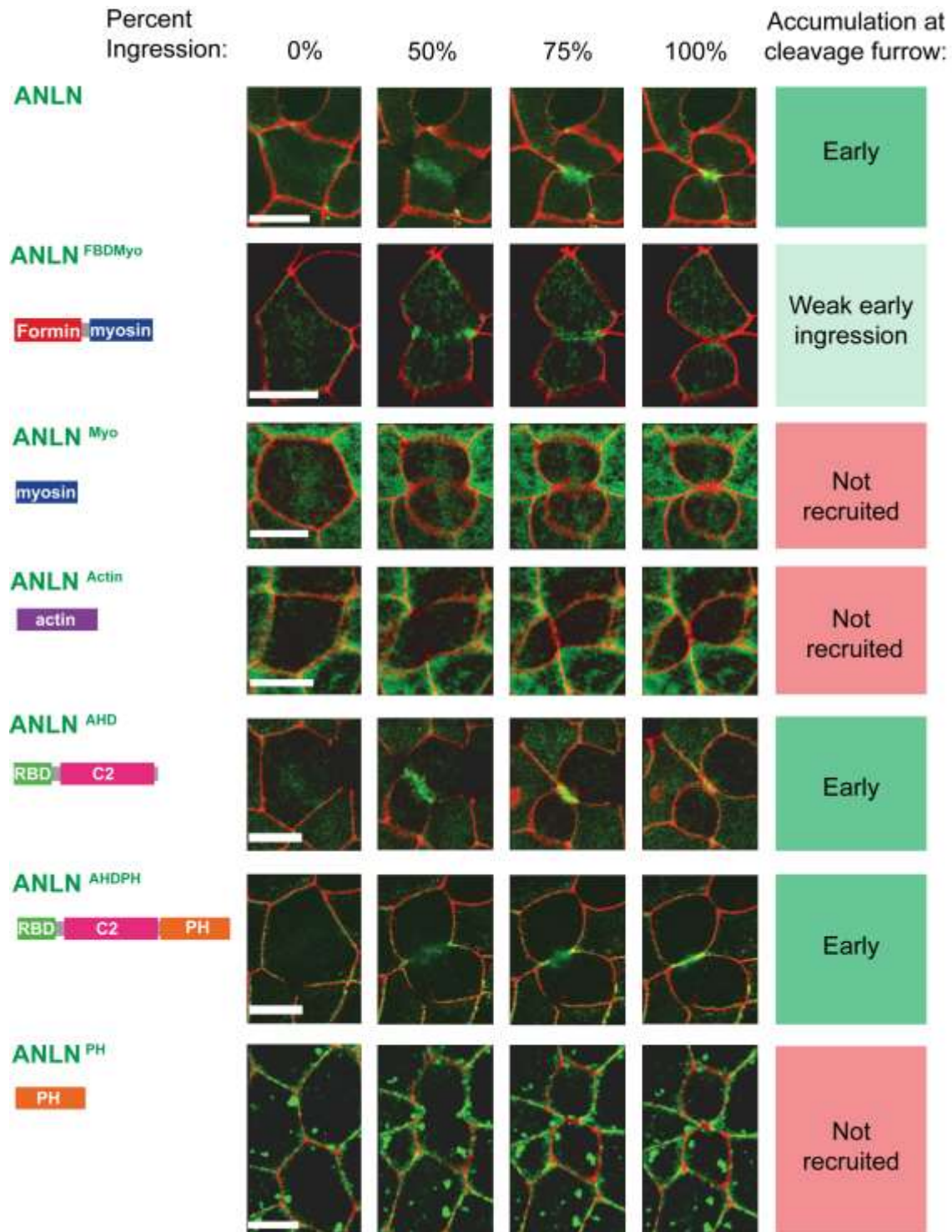
Figure 2.5 Recruitment of Anillin and fragments to the cleavage furrow of dividing cells. Time lapse images of dividing cells expressing full length Anillin (ANLN) tagged with three copies of GFP or fragments of ANLN domains tagged with three copies of GFP (green) and a membrane marker (red). Images show the accumulation of tagged ANLN and fragments before ingression, at 50%, 75% and 100% ingression. Scale bars are 20 μm.
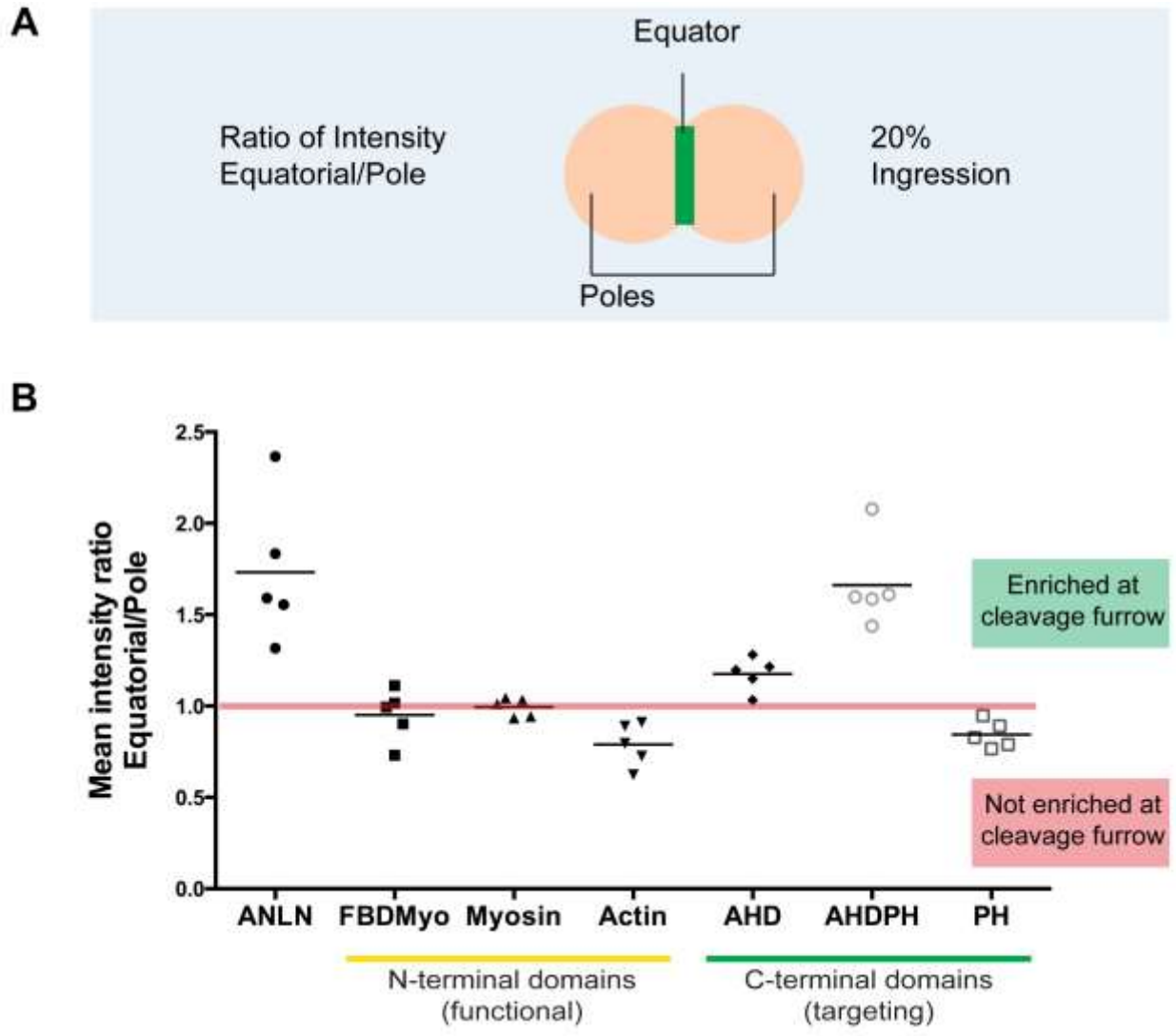
Figure 2.6 Quantification of the recruitment of Anillin and fragments at early ingression. (A) The ratio of signal at the equator over the signal at the poles at 20% ingression was measured with a small ROI, quantified and graphed in B (see methods for details). (B) Graph showing the recruitment of 3xGFP-tagged Anillin and fragments to the equatorial cortex of dividing cells at 20% ingression. n=5 embryos.
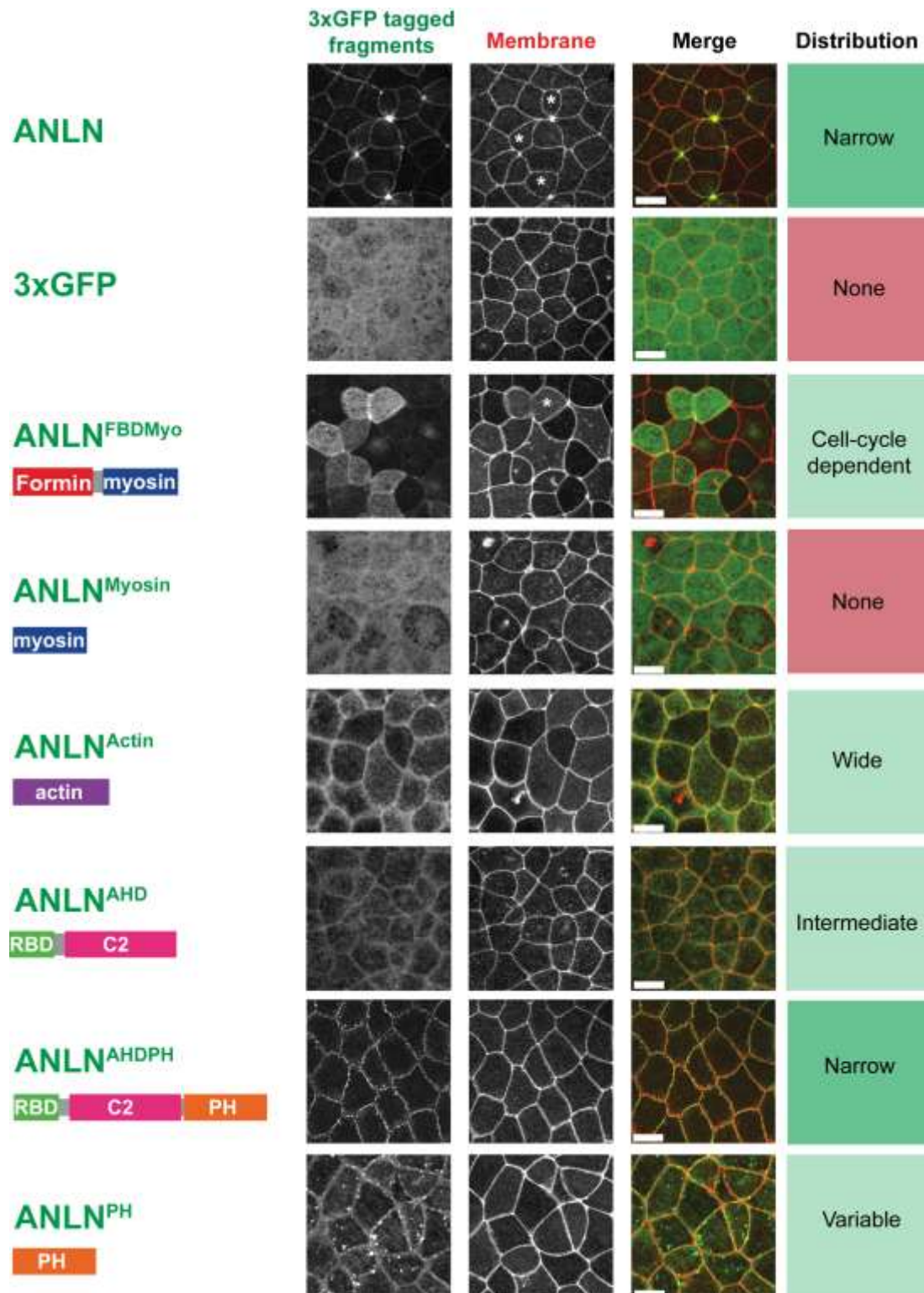
Figure 2.7 Localization of Anillin and fragments at the cortex. *En face* extended focus still images from live movies showing distribution of 3xGFP-tagged Anillin fragments (Green) with membrane marker (Red). Dividing or recently divided cells are marked with asterisks.
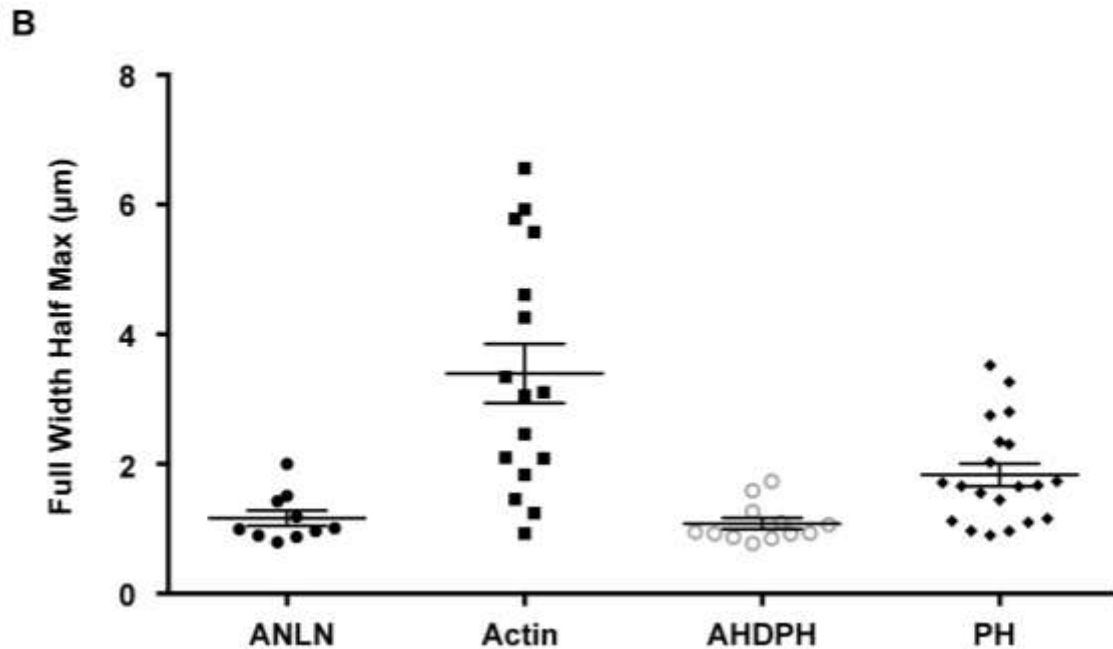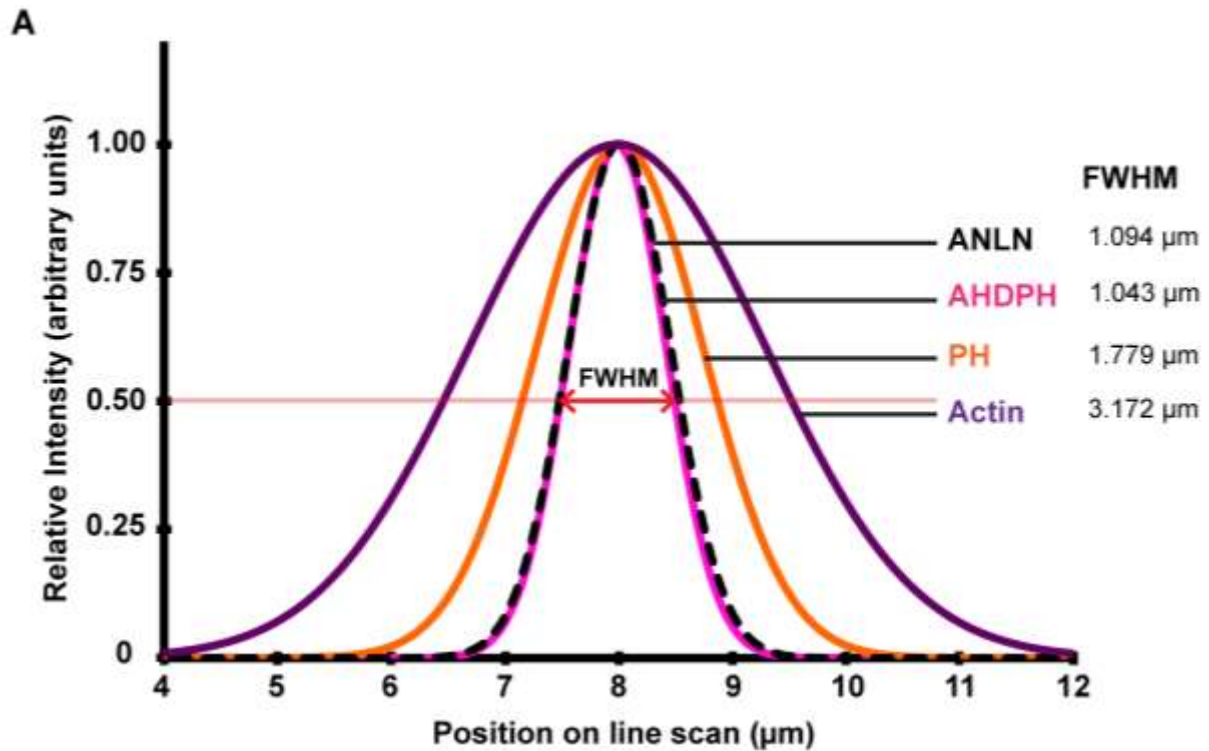
Figure 2.8 Full width half max analysis of the junctional distribution of Anillin and fragments. (A) Graph showing Gaussian curve fit analysis for Anillin and its fragments, where relative intensity from line scans is plotted on the y-axis and relative position on the x-axis. Curves represent the mean distribution of all line scans, and were used to determine the mean FWHM. (B) Graph plotting individual FWHM values for each line scan for Anillin and its fragments. The black line represents the mean FWHM and the whiskers represent the SEM. n=10-20 line scans.
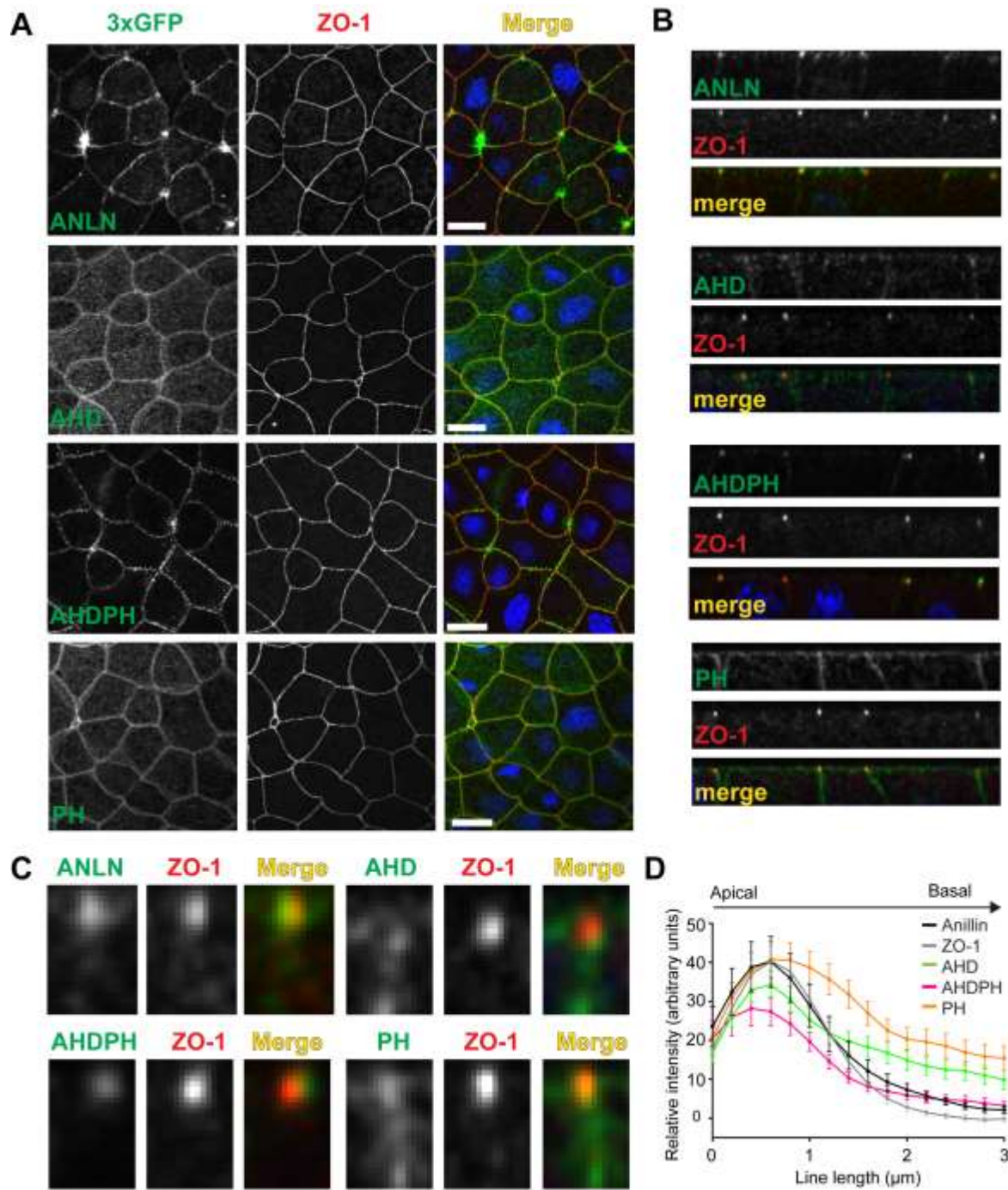
Figure 2.9 Co-staining of Anillin and fragments with the tight junction protein ZO-1. (A) *En face* extended focus images from fixed staining experiments of 3xGFP-fragments and full length Anillin stained with anti-GFP and anti-ZO-1 antibodies. (B) Side views from fixed staining experiments and (C) enlarged views of regions of co-localization of ZO-1 with the fragments. (D) Graph of line scans plotting the relative distribution of ZO-1, Anillin and fragments from the apical to basal lateral region. N=21-30 line scans.
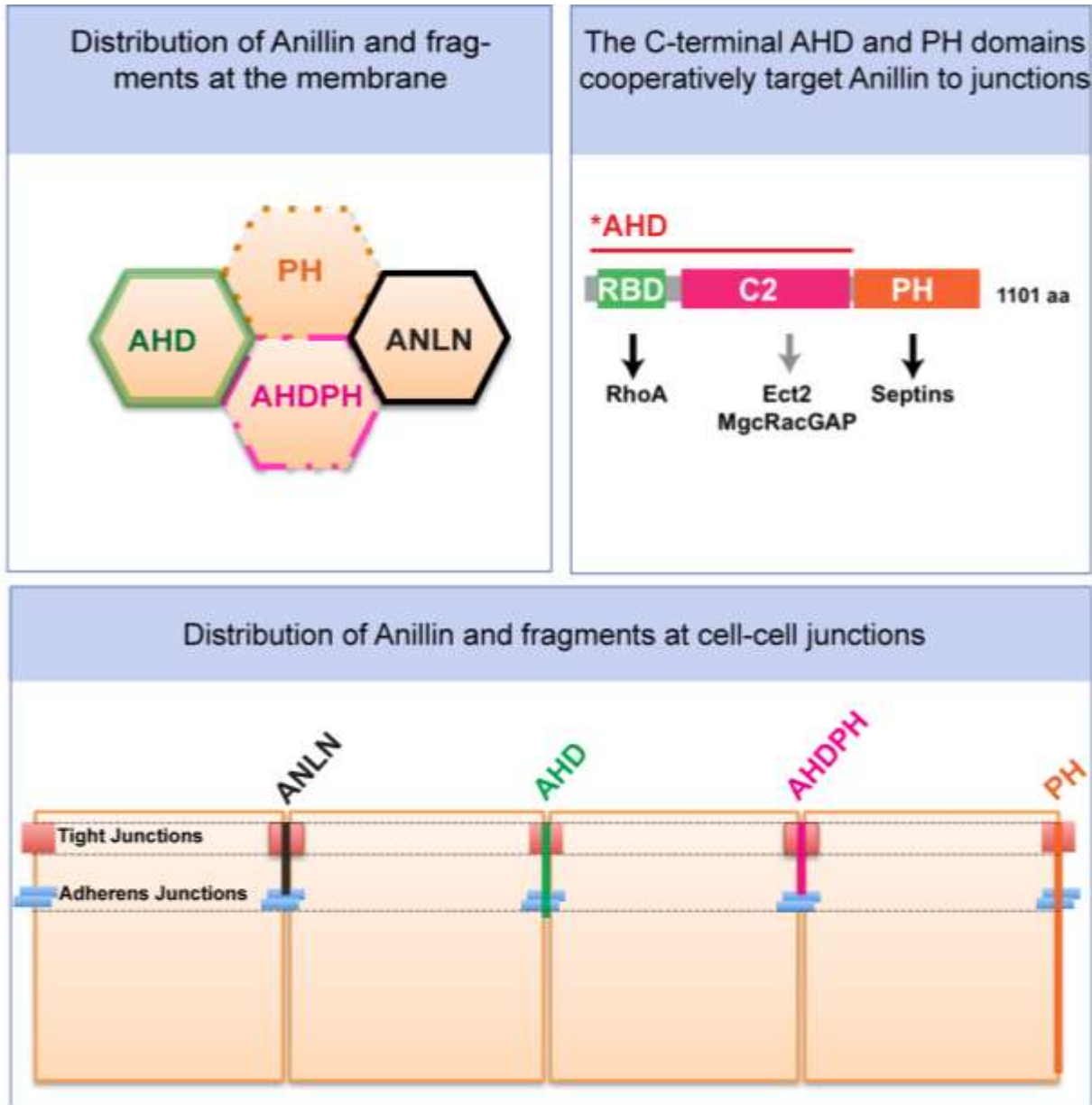
Figure 2.10 Summary of the distribution of Anillin and C-terminal fragments AHD, AHDPH and PH at the cleavage furrow of dividing cells and at cell-cell junctions. The combined AHDPH fragment most closely resembles full length Anillin's narrow and apical localization. This suggests that the AHD and PH domains may work cooperatively to facilitate Anillin's localization at junctions.
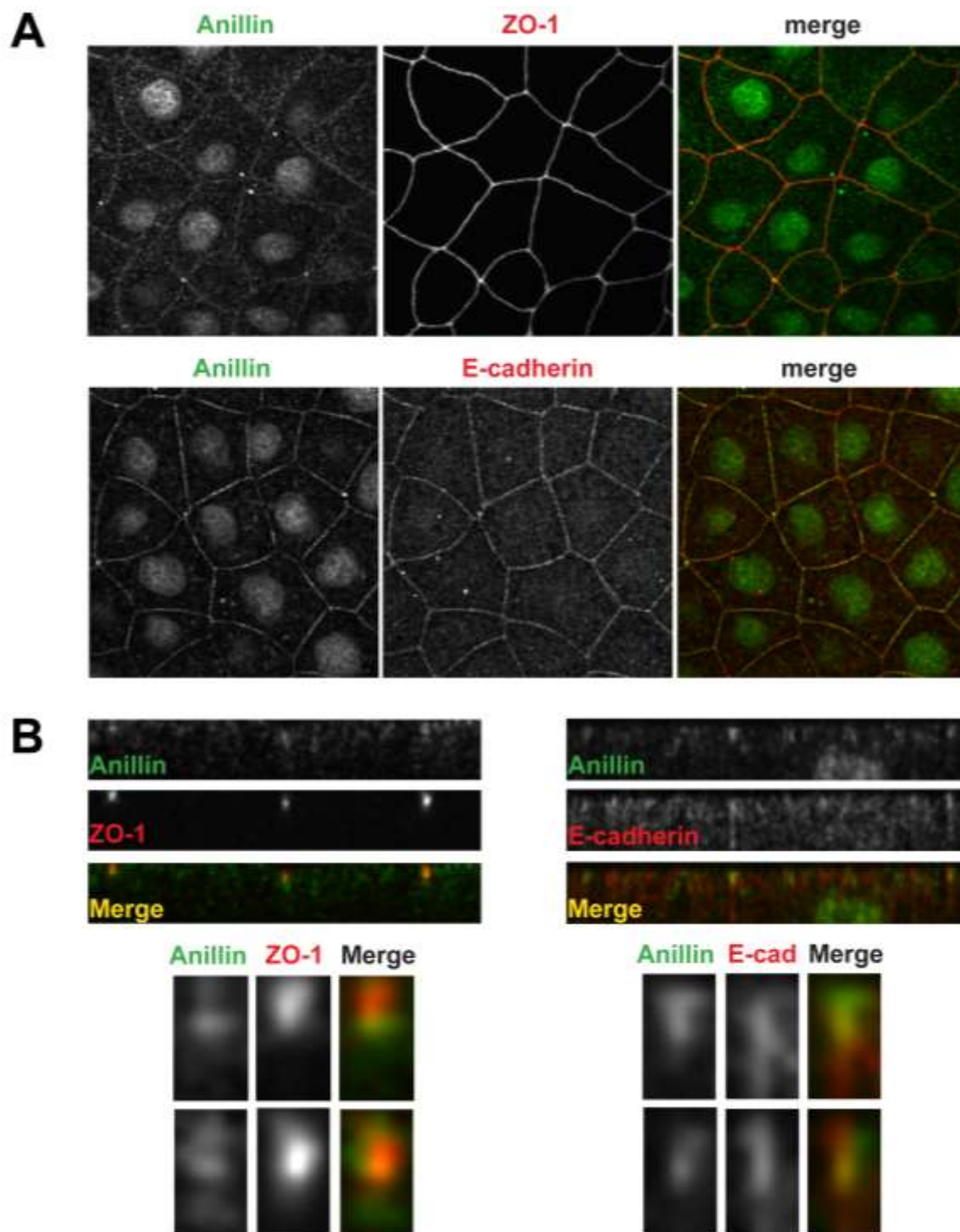
Figure S2.1 Endogenous Anillin and ZO-1 and E-cadherin. *En face* (A) and side views (B) from fixed staining experiment to co-stain for endogenous Anillin along with ZO-1 or E-cadherin.
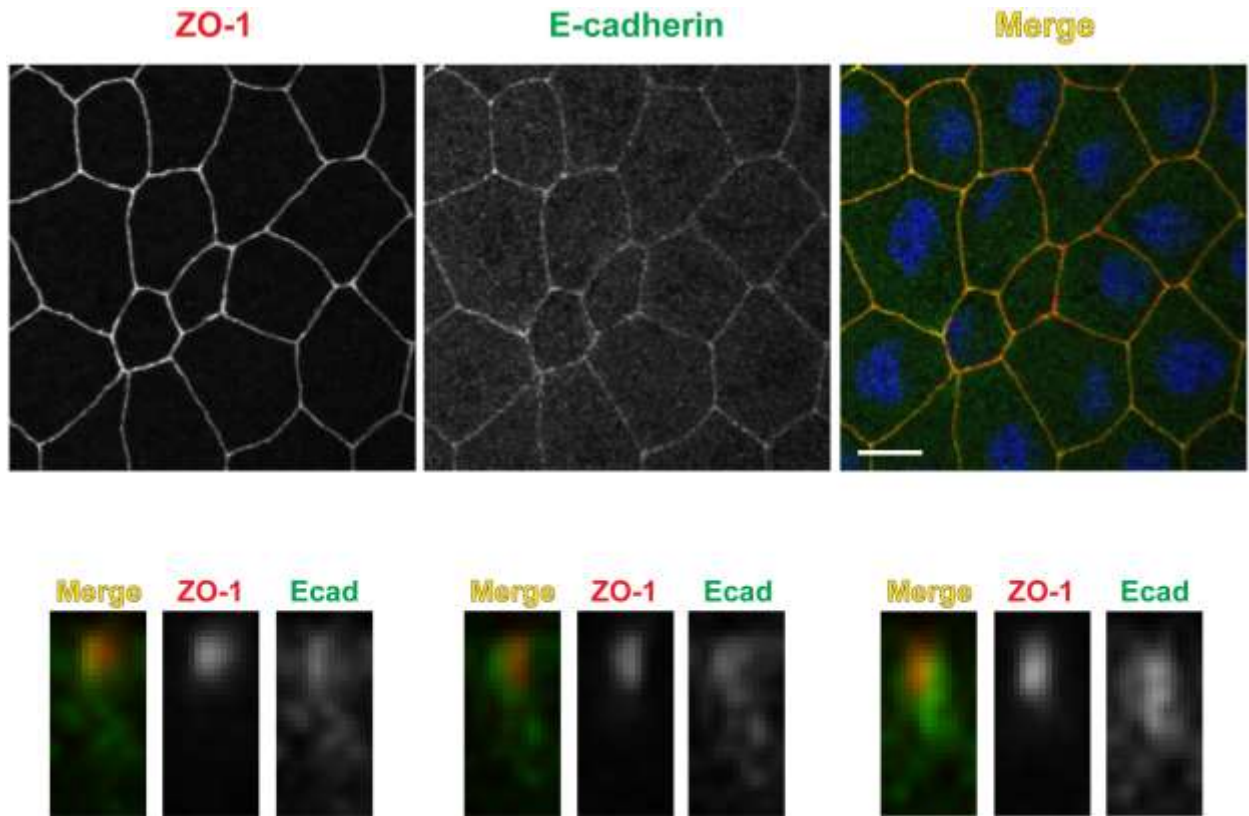
Figure S2.2 Endogenous ZO-1 and E-cadherin. *En face* and side views from fixed staining experiment co-staining for endogenous ZO-1 and E-cadherin.

Protein A ● ● Protein B
Incubate with target antibodies from different species

Add species specific PLA probes PLUS and MINUS

Hybridize connector oligos

Ligation to form a complete DNA circle

Rolling circle amplification

Add fluorescent probes to reveal interaction

En Face

Positive Control

Negative Control

DNA ZO-1 (Mouse) & ZO-1 (Rabbit)

DNA ZO-1 (Rabbit) & E-cad (Mouse)

Side views

90
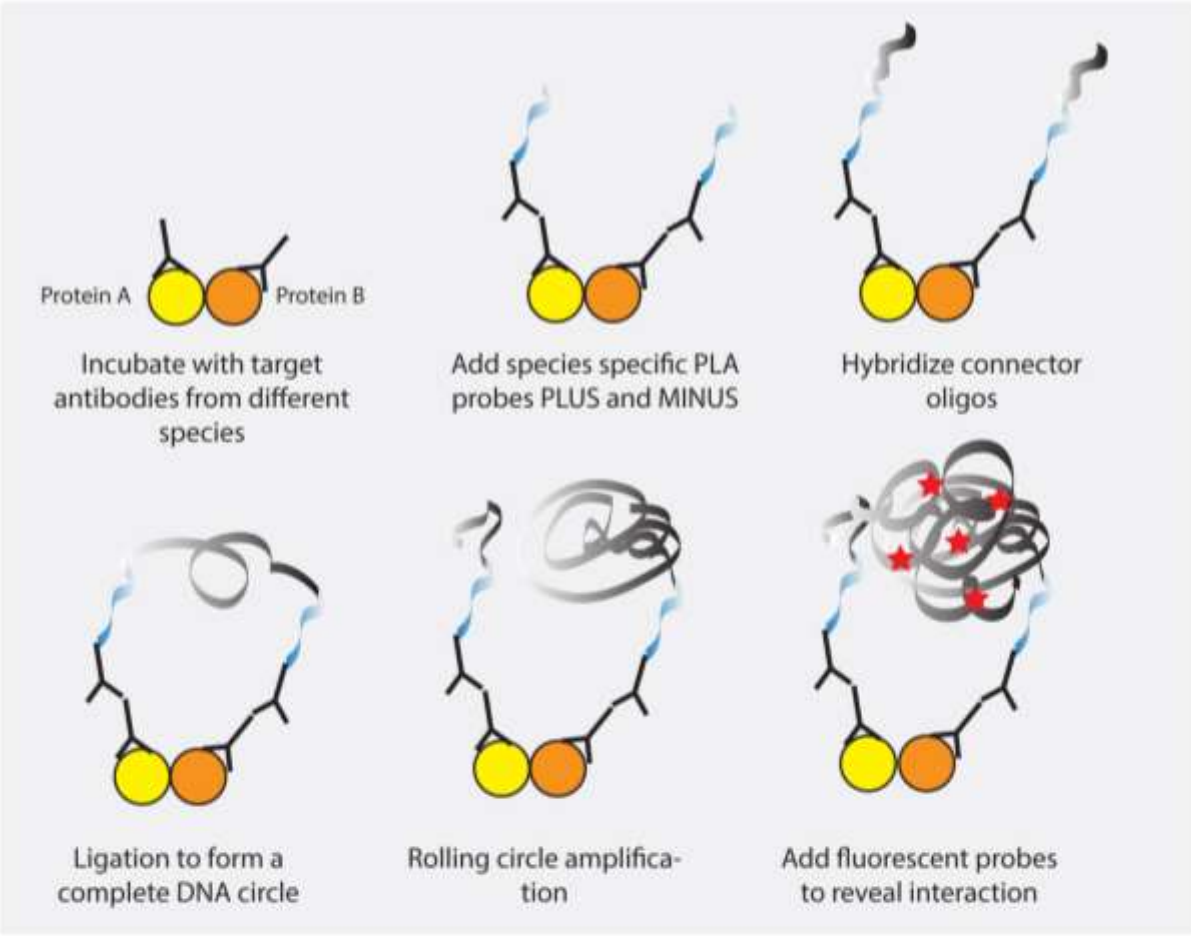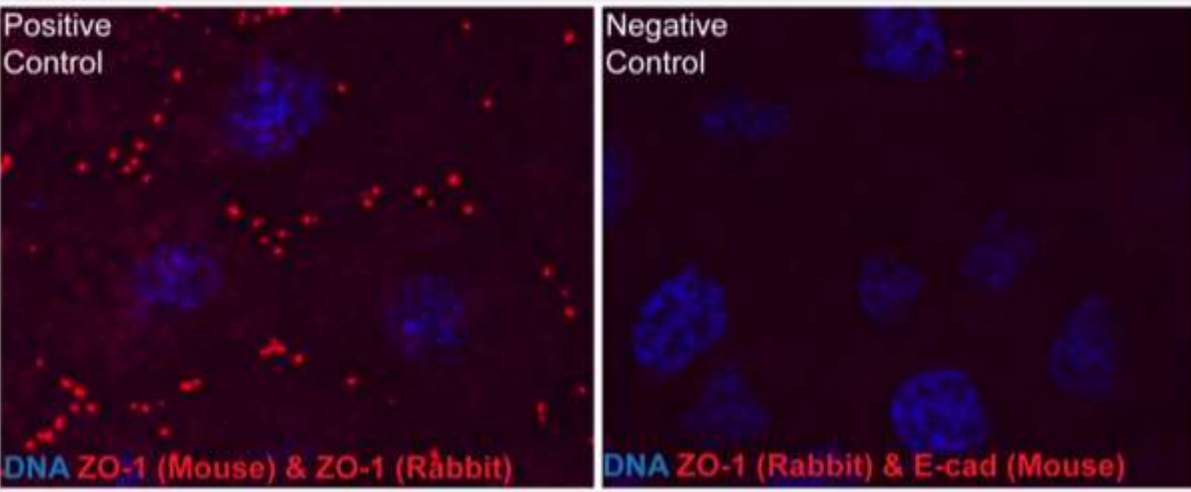
Figure S2.3 Proximity Ligation Assay. (top) *Xenopus* animal cap explants were fixed and probed with primary antibodies and a Proximity ligation assay (PLA) performed (see Figure above for details; cartoon modified from antibodies-online.com). (bottom) *En Face* and side views of positive and negative controls. PLA successfully detected an interaction between two species specific ZO-1 antibodies (positive control) and not between ZO-1 and E-cadherin (negative control).

1. Isolate animal cap from gastrula stage embryo, attach to fibronectin coated coverslip, allow to spread and fix.

Animal
Vegetal

Stage 10.5 Animal Cap Explant Fibronectin Coated Coverslip
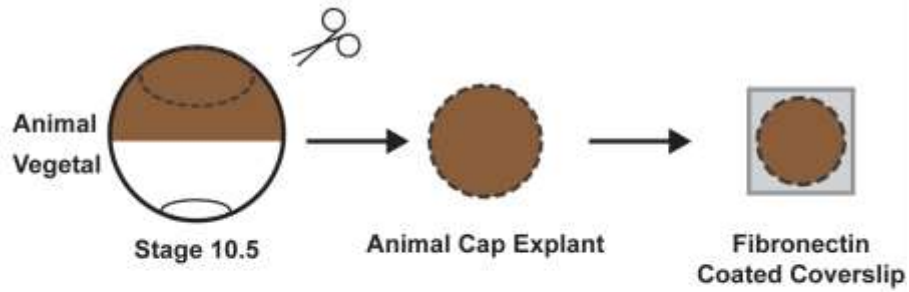
2. Explants are permeabilized, incubated in antibody, rinsed, flattened and imaged with a confocal microscope.

Glass bottom microwell dish
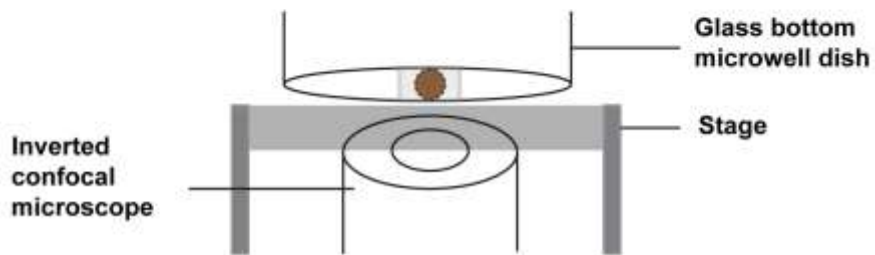Stage
Inverted confocal microscope

En face

ZO-1 ß-catenin Merge

Side views

ZO-1

ß-catenin

Merge
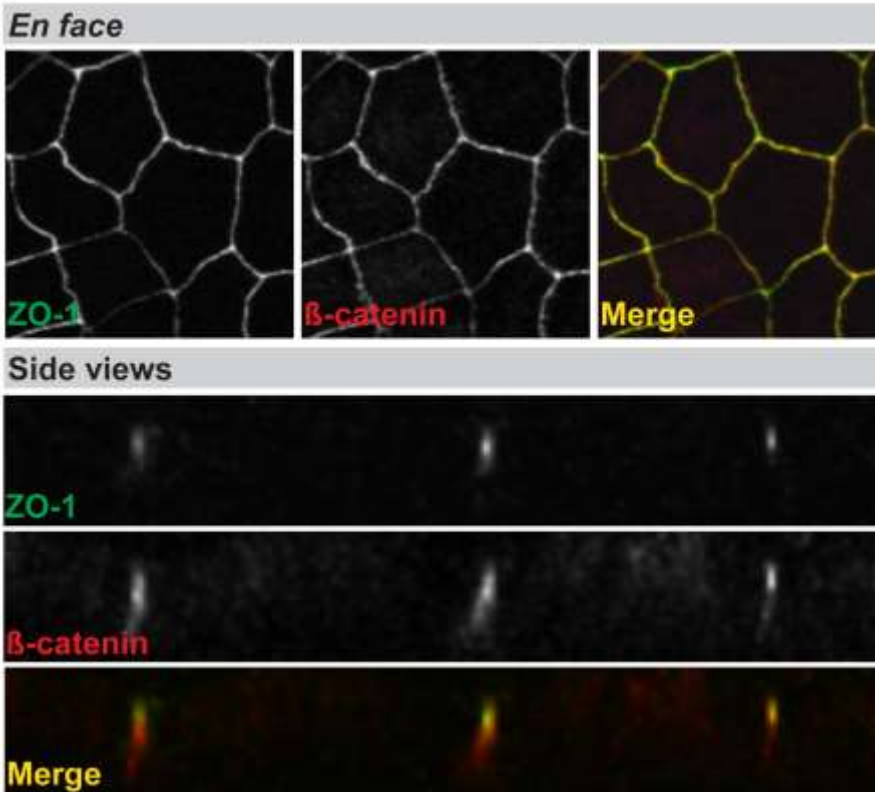
Figure S2.4 *Xenopus* animal cap explants. Animal caps were (1) isolated from stage 10.5 gastrula embryos, plated on fibronectin-coated coverslips, and (2) fixed, stained and imaged as shown in cartoon. Fixed animal cap explants maintain proper tight junction (ZO-1) and adherens junctions (ß-catenin) structure and polarity.
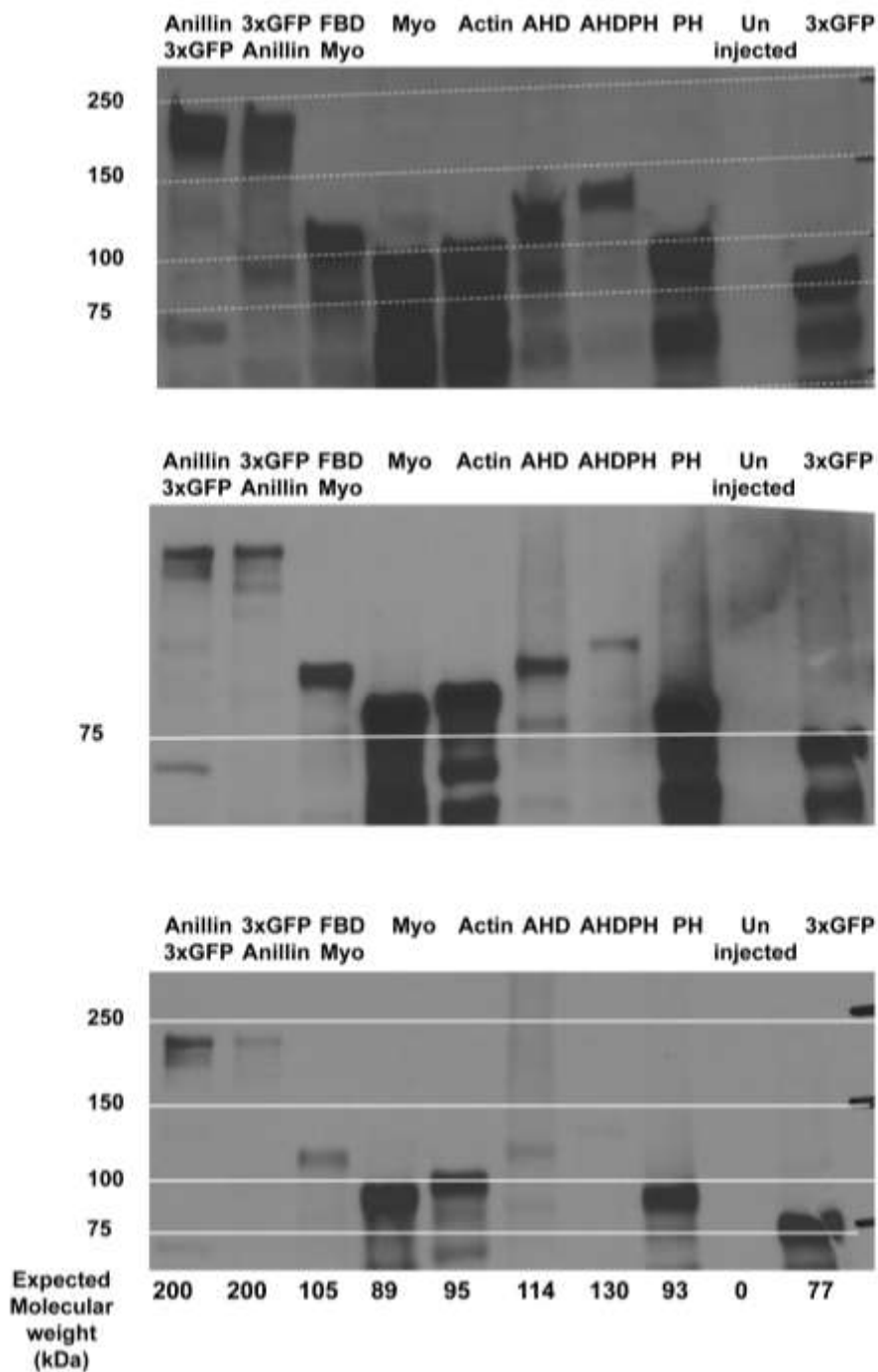
Figure S2.5 Western blot to detect expression of Anillin and fragments. Full length Anillin and fragments were detected at their expected size with western blots using anti-GFP antibodies to probe for their expression. Top blot was loaded with 15 μL of lysates, and had a 1 second exposure, while the bottom two blots were loaded with 5 μL of the same lysate to reduce over saturation and at different exposure times. More western blots will need to be repeated and probed for tubulin.
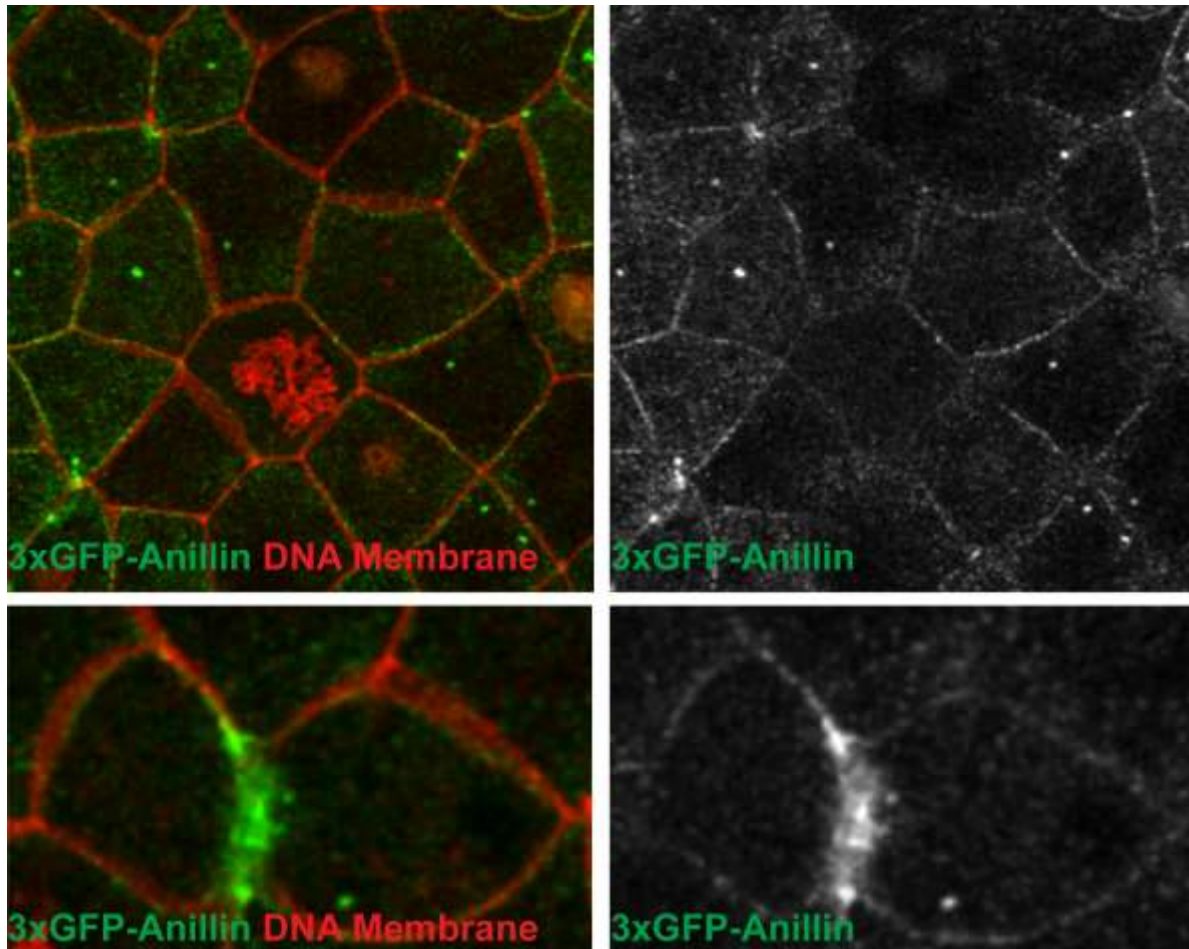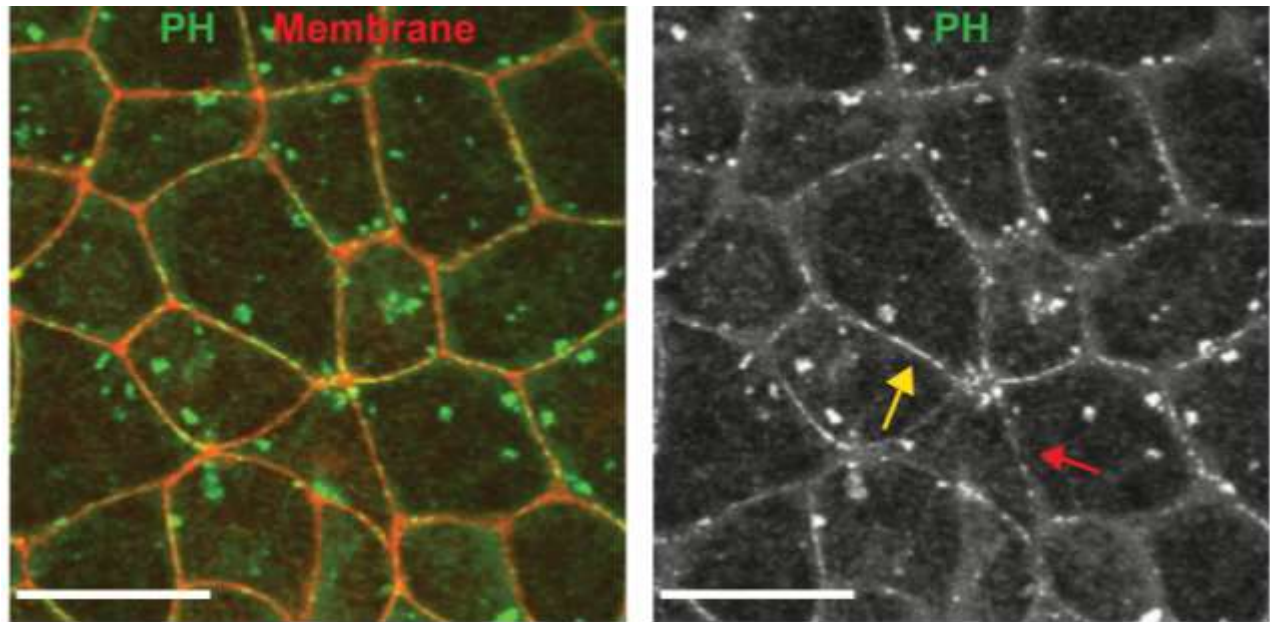
93

Figure S2.6 N-terminally 3xGFP-tagged Anillin localization. 3xGFP-Anillin localizes to cell-cell junctions in dividing and non-dividing cells, in addition to being present at the cleavage furrow of dividing cells. This is indistinguishable from C-terminally tagged Anillin-3xGFP.
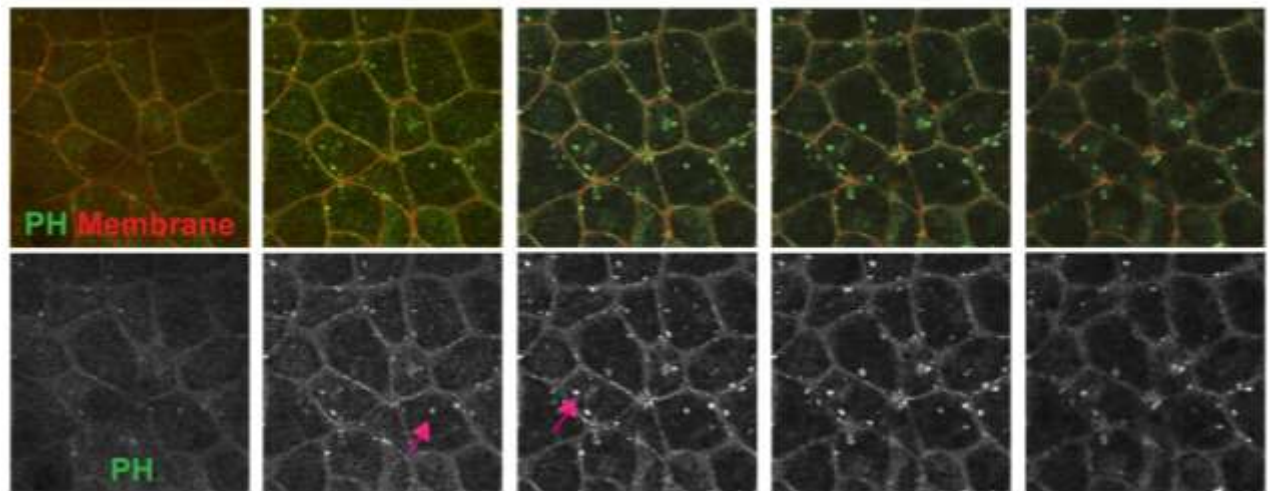
Figure S2.7 Anillin's PH domain exhibits different patterns of distribution. (top) Maximum point projection image of a single frame from a live movie showing Anillin's PH domain N-terminally tagged with 3xGFP in green, and the cell membrane labeled in red. Yellow arrow highlights an example of continuous and strong expression at junctions, while the red arrow highlights an example of weak accumulation of the fragment at junctions. Both examples were represented in the FWHM analysis. (bottom) Individual Z-planes from image on the top. Pink arrows point to unknown vesicle-like structures we observed in the cytoplasm of cells expressing the 3xGFP-PH construct.
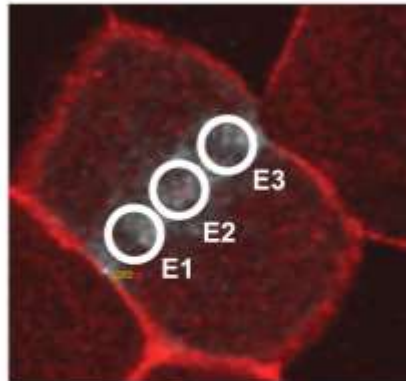
95

1. Determine the cleavage furrow site and measure the length at 0% ingression.
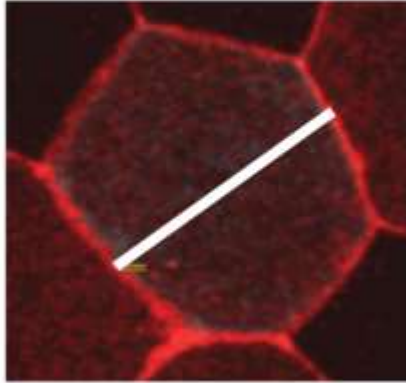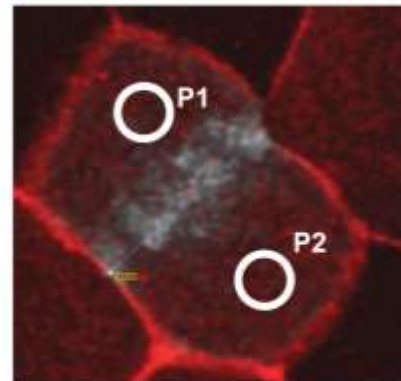
2. Find the point at which the cleavage furrow reaches 20% ingression.
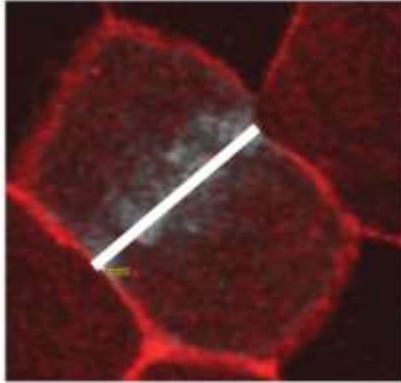
3. Measure relative intensity with ROIs across the cell equator and average intensity.

4. Normalize to the intensity at the poles by calculating the ratio of equatorial/pole.

$$\frac{(E1+E2+E3)/3}{(P1+P2)/2} = \text{Mean intensity ratio Equatorial/Pole}$$

Figure S2.8 Quantification methods for the recruitment of 3xGFP-tagged Anillin and fragments in dividing cells. Dividing cells at 20% ingression were identified and three small circular ROIs were drawn along the equator and averaged. Two small circular ROIs were drawn at the poles of the cells and averaged. The ratio of the mean intensity at the equator and poles was graphed.

96

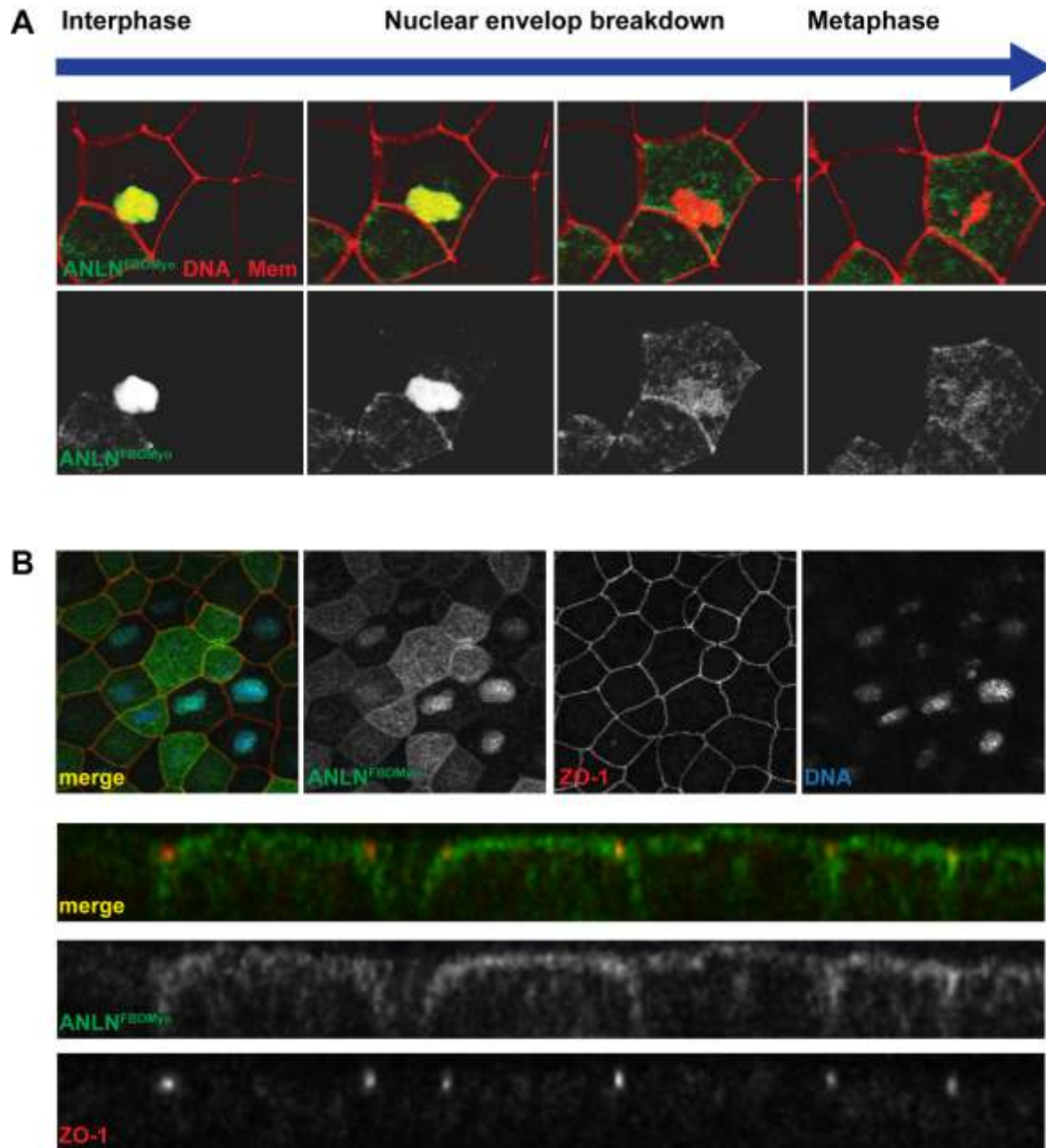**Figure S2.9 FBDMyo localization is cell-cycle dependent.** (A) Time lapse images of embryo expressing 3xGFP-tagged FBDMyo and probes for DNA and the cell membrane. During interphase, FBDMyo is sequestered in the nucleus, however, upon nuclear envelop breakdown it moves to the cytoplasm and cortex. (B) *En face* and sideviews of fixed embryos expressing GFP-tagged FBDMyo, and stained for DNA and ZO-1.
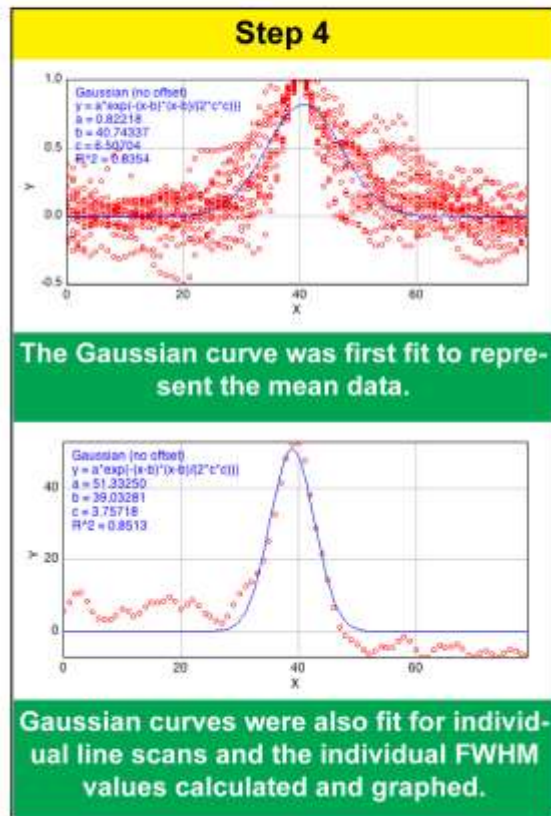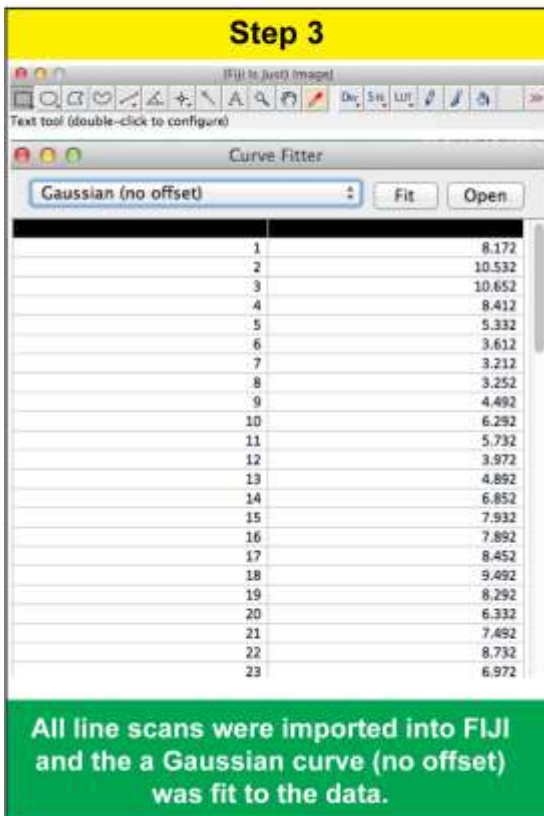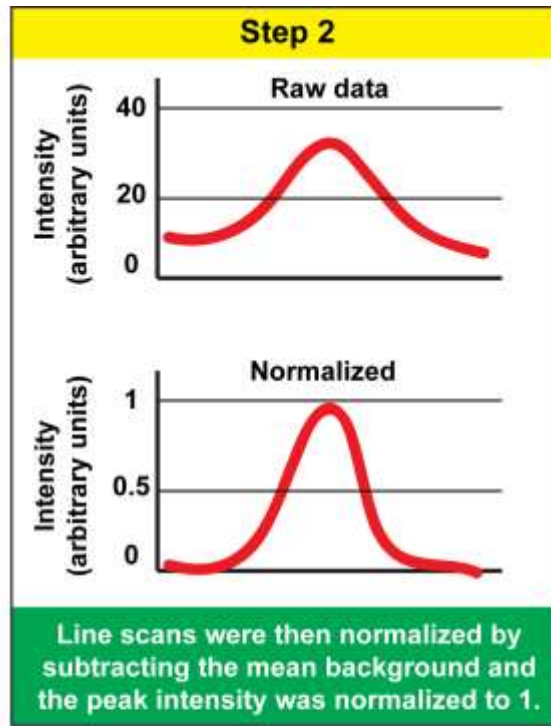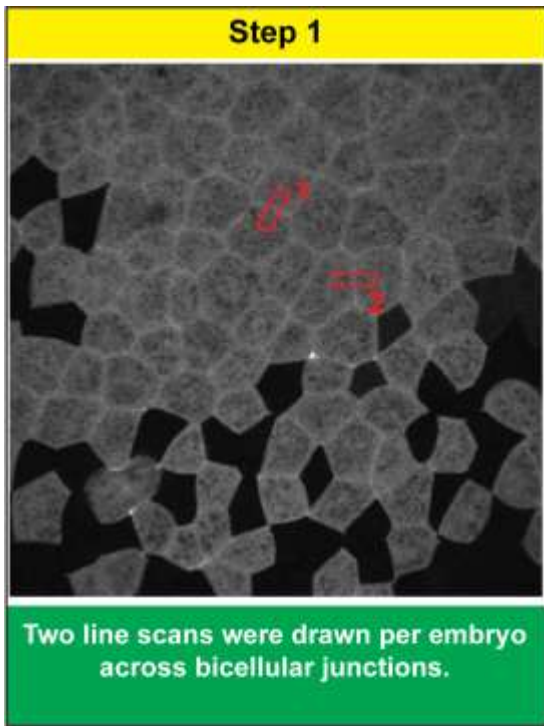
Figure S2.10 Quantification methods for full width half max analysis (FWHM). See figure for overview of analysis and the experimental methods of this chapter for details.

Anillin

Gaussian (no offset)
y = a*exp(-(x-b)*(x-b)/(2*c*c))
a = 0.94392
b = 40.03094
c = 2.24569
R^2 = 0.8524

Actin

Gaussian (no offset)
y = a*exp(-(x-b)*(x-b)/(2*c*c))
a = 0.82218
b = 40.74337
c = 6.50704
R^2 = 0.6354

AHD

Gaussian (no offset)
y = a*exp(-(x-b)*(x-b)/(2*c*c))
a = 0.92841
b = 39.90029
c = 3.65
R^2 = 0.3454

AHDPH

Gaussian (no offset)
y = a*exp(-(x-b)*(x-b)/(2*c*c))
a = 0.94925
b = 39.94562
c = 2.13982
R^2 = 0.8718

PH

Gaussian (no offset)
y = a*exp(-(x-b)*(x-b)/(2*c*c))
a = 0.06880
b = 40.04627
c = 3.65045
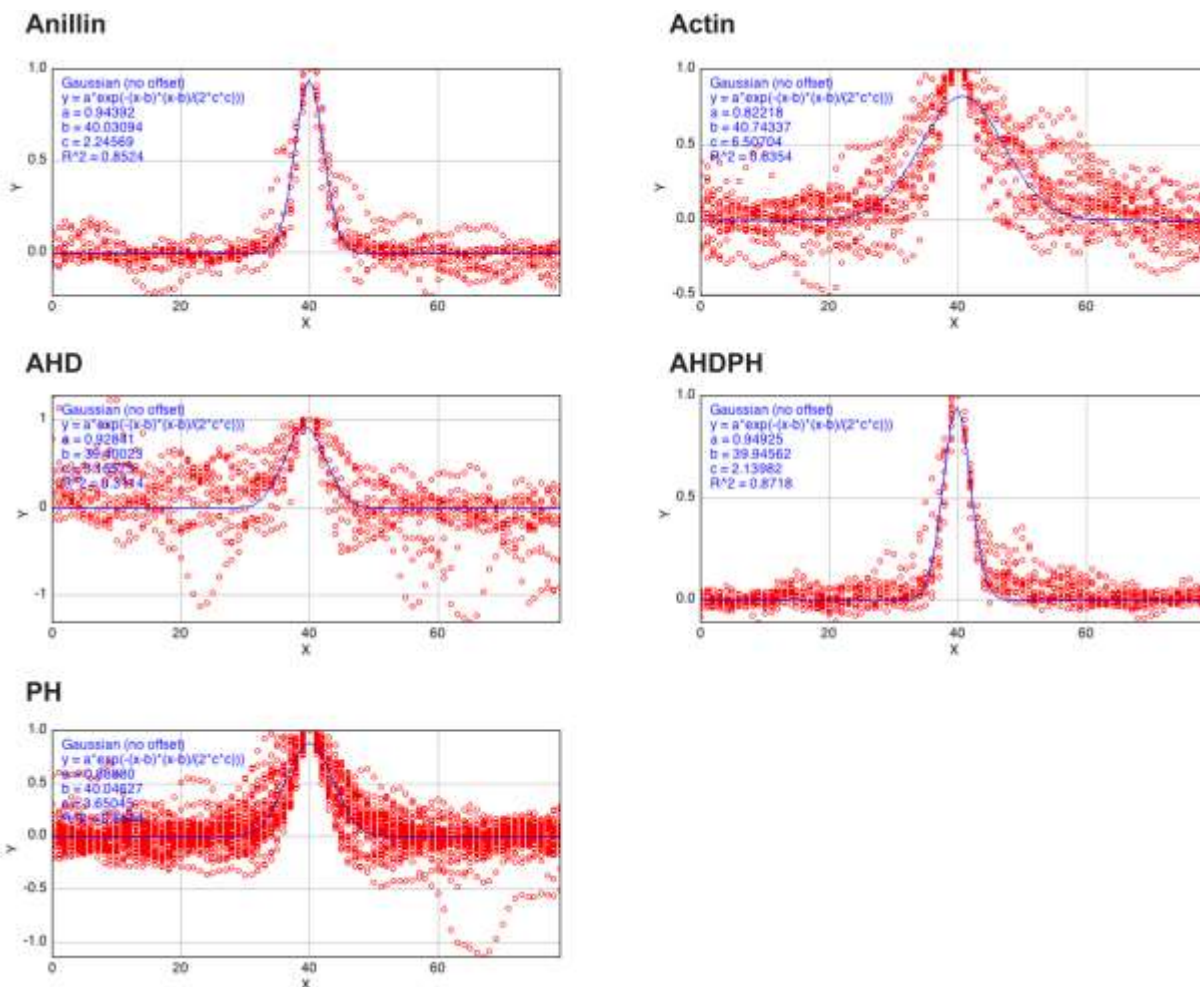
Figure S2.11 Gaussian Curve Fit analysis. Using FIJI, Gaussian curves were fit to all line scans as part of the FWHM analysis. Raw data points are graphed as red dots in each figure for each fragment and the continuous blue curved line is the Gaussian fit for the entire distribution of data points.

99
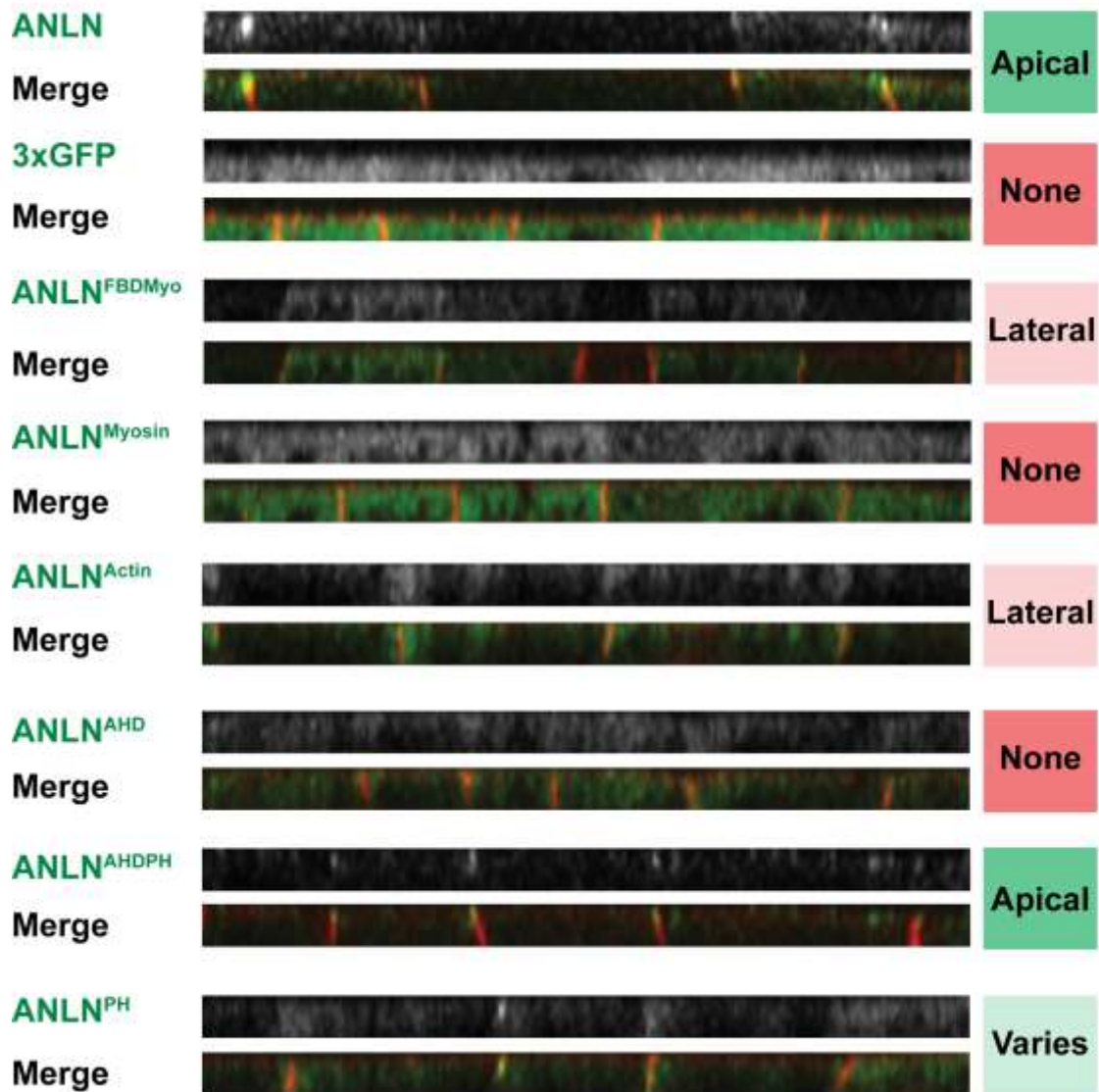
Figure S 2.12 Side views from live imaging of GFP-tagged Anillin and fragments. Side views showing localization and distribution of 3xGFP-tagged Anillin and fragments along with a membrane marker (red), which is present throughout the basal lateral membrane. Each side view is from a live movie and 7 Z-stacks of 0.75 μm each were acquired.

Figure S2.13 Alternative quantification for data in Figure 9D. The apical to basal line scans from Figure 9D were normalized to background and an intensity of 1 and the starting point for all line scans (point zero on the y-axis) aligned based on ZO-1 peak intensity. Relative intensity if plotted on the y-axis, and position in microns on the x-axis. ZO-1 is indicated in grey.

Materials and Methods

DNA constructs, mRNA preparation, and Anillin morpholino. pCS2+/*Xenopus laevis* Anillin and Anillin-3XGFP and 3XGFP-Anillin were generated using a GFP-*Xen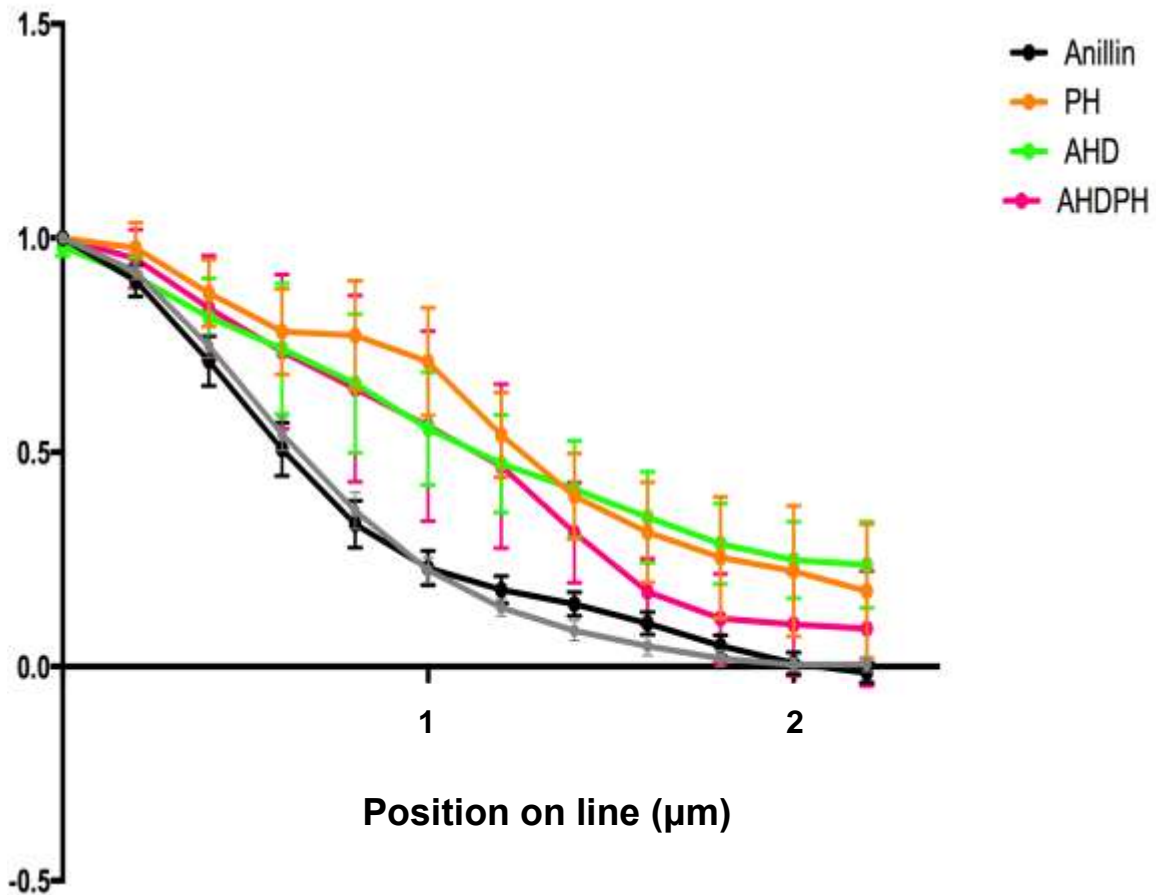opus* Anillin vector generously provided by Aaron Straight, Stanford University, as the template. Anillin was amplified by PCR and cloned into the pCS2+ or pCS2+/C-3XGFP vector using ClaI and XhoI restriction sites. Each domain of Anillin was cloned from the pCS2+/X*enopus laveis* Anillin vector using BspEI and Xho1, and was N-terminally tagged with 3xGFP. pCS2+/mChe-mem and pCS2+/GFP-mem probes for the plasma membrane, and pCS2+/mChe-H2B were generated as previously described (Reyes et al., 2014). mRFP-ZO-1 and Ecad-3xmChe were generated using BspE I/Xma I and Sac I, and Stu I and Xba I respectively (Higashi et al., 2016). mRNAs were transcribed *in vitro* from pCS2+-based vectors using the mMessage mMachine SP6 kit (Ambion). An antisense MO (Gene Tools) was generated to target the 5´UTR of *Xenopus laevis* Anillin with the sequence 5' – TGGCTAGTAACTCGATCCTCAGACT – 3' (Reyes et al., 2014).

***Xenopus* embryos and microinjections.** All studies with *Xenopus laevis* embryos were conducted in compliance with the US Department of Health and Human Services Guide for the Care and Use of Laboratory Animals and were approved by the University of Michigan IACUC. *Xenopus laevis* embryos were collected, fertilized, and dejellied as described previously (A. L. Miller & Bement, 2009; Woolner, Miller, & Bement, 2010). Embryos were stored at 15°C or 17°C in 0.1X MMR (1X MMR = 100 mM NaCl, 2 mM KCl, 2 mM $CaCl_2$, 1 mM $MgCl_2$, 5 mM Hepes, pH 7.4). Embryos were microinjected using a Microinject-1000 microinjector (BTX/Harvard Apparatus) with embryos in a mesh bottom dish filled with 0.1X MMR with 5% ficoll. Embryos at the 2-cell stage were microinjected with mRNAs with needle concentrations as follows: Anillin-3XGFP, 16 ng/µl; All 3xGFP-tagged fragments except the AHDPH, 9.6 ng/µl; 3xGFP-AHDPH, 4.8 ng/µl; mCherry-farnesyl, 10-20 ng/µl; mChe-H2B, 10- 12.5 ng/µl. For the live imaging experiment of Anillin-3XGFP and tagged ZO-1 and E-cadherin, embryos were

microinjected with 5 nl of Anillin MO at a needle concentration of 4.5 mM to KD endogenous Anillin, and 3xGFP-tagged Anillin was introduced at near endogenous levels.

Antibodies. An antibody to *Xenopus* Anillin ABD was generously provided by Aaron Straight from Stanford University and was used for PLA experiments. Other antibodies used were anti-GFP (clone JL-8, Clontech no. 632381), anti-α-tubulin (DM1A, Sigma no. T9026), anti-ZO-1 (Invitrogen, no. 61-7300), and anti-E-Cadherin (DSHB, no. 5D3-c). Secondary antibodies for Western blotting were HRP-conjugated anti-rabbit or anti-mouse (Promega). Secondary antibodies for immunofluorescence were Alexa 488 or Alexa 568-conjugated anti-mouse or anti-rabbit (Invitrogen).

Immunofluorescence Staining. For fixed staining experiments albino/wild-type embryos were injected with 3xGFP-tagged constructs alone or co-injected with mCherry-farnesyl as a lineage tracer. Embryos at gastrula stage (Nieuwkoop and Faber stage 10-11) were fixed and stained according to the protocol from Le Page et al (Le Page, Chartrain, Badouel, & Tassan, 2011). Briefly, embryos were washed in PBS then fixed with 2% TCA in PBS for 2 h at room temperature (RT). Embryos were then bisected keeping the animal hemisphere, permeabilized in PBS + 1% Triton-X-100 for 20 min at RT followed by PBS + 0.1% Triton-X-100 (PBST) for 20 min at RT. Embryos were then blocked with PBST + 5% fetal bovine serum (Invitrogen, no. 10082-139) for 30 mins-1 hr at RT. Embryos were incubated with primary antibodies in blocking solution overnight at 4°C with gentle shaking (anti-GFP, 1:200; anti-ZO-1, 1:200), washed with blocking solution (5 min, 15 min, 2 h, overnight at 4°C), incubated with secondary antibodies in blocking solution overnight at 4°C (Alexa 568-anti-rabbit for ZO-1, 1:200; and Alexa 488-anti-mouse for GFP, 1:200), and washed with PBST (5 min, 15 min, 2 h, overnight at 4C). Embryos were then stained with 10 µg/ml DAPI (Invitrogen, no. D1306) in PBS for 30 min at RT, rinsed and imaged.

Proxomity ligation assay (PLA). For PLA analysis, we used the Sigma Aldrich Duolink In Situ Red Starter Kit Mouse/Rabbit (Catalog number: DUO92101-1KT). Explants (see

below) were first fixed (2% TCA in PBS, 2 hrs at RT), blocked (O/N, 1X PBS + 0.1% Triton-X-100 + 5% FBS at 4°C), stained in primary antibody (4 hrs, RT) and rinsed (O/N, 4°C), and then PLA was performed. Explants were incubated in PLA probes at 37°C in a petri dish and stored in a humidity chamber (Tupperware with damp paper towels) for 60 mins and then rinsed in PLA Wash Buffer A (Sigma kit). Following rinses, the explants were incubated in ligation solution (Sigma kit) for 30 mins at 37°C, rinsed in PLA Wash Buffer A, and incubated with amplification reagents for 100 mins at 37°C inside the humidity chamber. Explants were then rinsed in 1X Wash Buffer B (Sigma kit), 0.01X Wash Buffer B, incubated in the Duolink In Situ Mounting Medium with DAPI for ~15 mins at RT, mounted in a glass bottom microwell dish (MatTek, P35G-1.5-14-C, 35 mm petri dish 14 mm Microwell, No. 1.5 coverglass, (0.16-0.19 mm) and imaged on an inverted confocal microscope. All PLA reactions were performed on a shaker to ensure even distribution of reagents.

Explants. Wild-type *Xenopus laevis* embryos at gastrula stage (stage 10.5) were placed in Danilchik's for Amy explant culture media (DFA; 53 mM $NaCl_2$, 5 mM Na_2CO_3, 4.5 mM Potassium gluconate, 32 mM Sodium gluconate, 1mM $CaCl_2$, 1mM $MgSO_4$; 0.1% BSA, pH 8.3, sterile filtered with a 0.2um filter) with antibiotics and antimyotics (0.8% in media; A5955, Sigma-Aldrich). Embryos were devitellinated using forceps, and the animal caps were isolated using an eyebrow knife and hairloop. Explants were gently placed on top of fibronectin-coated coverslips. Coverslips were cut with a diamond knife into small rectangular fragments, flame sterilized and incubated in 10 µg of fibronectin/1X MMR either O/N at 4°C or 30 minutes at RT the day of the experiment. After the explants were allowed to adhere and spread, another coverslip was placed on top to flatten them. Embryos were then fixed in 2% TCA in PBS, and PLA performed as described above.

Embryo lysates and immunoblotting. 10-15 gastrula stage embryos (stage 10-11) were lysed in 5 µl ice cold PHEME lysis buffer per embryo (60 mM K-PIPES, 25 mM Hepes, 10 mM EGTA, 2 mM MgCl2, pH 7.0) supplemented immediately before use with 0.5% NP40, protease inhibitor cocktail (Thermo Scientific Halt Protease Inhibitor +

EDTA, no. 78410), and phosphatase inhibitor cocktail (Thermo Scientific Halt Phosphatase Inhibitor, no. 1862495), as previously described (Reyes et al., 2014). Embryos were manually lysed in a 1.5 ml eppendorf tube with a pestle. Samples were transferred to a 3/16 x 25/32 Ultra-Clear tube (Beckman, no. 344718). Samples were centrifuged at 16,000g for 5 min at 4°C to stratify the lysates. The cytoplasmic layer was removed by puncturing the side of the tube with at 27 G 1/2 needle (BD PrecisionGlide, no. 305109) attached to a 1 ml syringe. The cytoplasmic extract was mixed with 6X LSB and boiled for 10 min. Samples were separated on a gradient SDS-PAGE gel (BIO-RAD Mini-PROTEAN TGX Gels; no. 456-1086) and transferred to nitrocellulose membranes. Membranes were probed with anti-GFP (1:1000), or anti-α-tubulin (1:20,000) antibodies overnight at 4°C and were then incubated with the appropriate HRP- conjugated secondary antibodies (1:10,000 (1:20,000 for anti-α-tubulin)) for 1 h at RT. Membranes were developed using an ECL detection kit (Pierce, no. 32209).

Live and fixed confocal microscopy. Images were collected on an Olympus Fluoview 1000 confocal microscope with FV10-ASW software equipped with a 60X supercorrected PLAPON 60XOSC objective (NA = 1.4, working distance = 0.12 mm). For live imaging, intact gastrula stage (stage 10-11) embryos were mounted in custom chambers that consisted of a metal slide ~0.8 mm thick with a ~0.5 cm hole in the center to which a coverslip was affixed with a thin layer of vacuum grease (Dow Corning high vacuum grease). We used 0.17mm glass coverslips, (Warner, 22 x 22 mm), which are of an optimized thickness for the 60X supercorrected objective. Embryos were transferred into the chamber in 0.1X MMR, and a second coverslip was placed over the embryos and gently pressed down and affixed with a thin layer of vacuum grease. The chambers were oriented such that cells in the animal hemisphere were imaged.

For fixed imaging, bisected embryos were mounted on a glass coverslip with the animal hemisphere up, and a coverslip was placed over the embryos and gently pressed down to flatten the bisected embryos. For PLA experiments, coverslips with explants attached were placed animal hemisphere downward inside a glass bottom microwell dish and flattened with another coverslip and vacuum grease to stabilize.

Quantification Methods.

Analysis of Anillin accumulation in dividing cells. All live imaging movies acquired from confocal microscopy were imported to Volocity 3D imaging software (Perkin Elmer) for analysis. First, the future cleavage furrow site was identified in live imaging movies, and the length across the presumptive furrow was measured at 0% ingression. This measurement was then used to identify the timeframe at 20% ingression in the live imaging movie. A maximum point projection image at 20% ingression was rendered in Volocity and exported as a TIF for analysis. Using FIJI, we measured the mean intensity at the furrow with three circular ROIs across the cell equator and averaged the intensity. The average equatorial intensity was normalized to the average intensity at the poles, and the ratio of mean equatorial/pole intensity was graphed. A value above 1 would indicate higher signal at the cleavage furrow, while a value below 1 would indicate higher background.

Full width half-max (FWHM) analysis of junctional signal. Using Volocity, a maximum point projection of a single time frame from a time lapse movie was exported as a TIF and imported into FIJI. Two line scans (length 16.56 μm x width 5.175 μm) per embryo were drawn perpendicular to bicellular junctions using the "draw" feature in FIJI. Each line scan was normalized by subtracting the mean background, and the peak intensity was normalized to a value of one. The line scans were then imported into FIJI, and a Gaussian curve (no offset) was fit to the data. Gaussian curves were fit to represent the mean data and also in a separate analysis Gaussian curves were fit to individual line scans and the individual FWHM values calculated and graphed.

Analysis of the apical and basal localization of Anillin and fragments. Side views were isolated from images and line scans (~16 pixels long/~5 pixels wide) were drawn from the apical starting point of ZO-1 to the lateral membrane. Line scans were normalized to background and plotted on a graph in PRISM (Figure 9D). For alternate

analysis in Figure S2.13, line scans started at the peak intensity of ZO-1 signal and were normalized to 1.

Acknowledgements:

References:

Almonacid, M., Celton-Morizur, S., Jakubowski, J. L., Dingli, F., Loew, D., Mayeux, A., … Paoletti, A. (2011). Temporal Control of Contractile Ring Assembly by Plo1 Regulation of Myosin II Recruitment by Mid1/Anillin. *Current Biology*, *21*(6), 473–479. http://doi.org/10.1016/j.cub.2011.02.003

Balda, M. S., & Anderson, J. M. (1993). Two classes of tight junctions are revealed by ZO-1 isoforms. *American Journal of Physiology - Cell Physiology*, *264*(4), C918–C924.

Bement, W. M., Benink, H. A., & Dassow, G. von. (2005). A microtubule-dependent zone of active RhoA during cleavage plane specification. *The Journal of Cell Biology*, *170*(1), 91–101. http://doi.org/10.1083/jcb.200501131

Celton-Morizur, S., Racine, V., Sibarita, J.-B., & Paoletti, A. (2006). Pom1 kinase links division plane position to cell polarity by regulating Mid1p cortical distribution. *J Cell Sci*, *119*(22), 4710–4718. http://doi.org/10.1242/jcs.03261

D'Avino, P. P. (2009). How to scaffold the contractile ring for a safe cytokinesis – lessons from Anillin-related proteins | Journal of Cell Science. *Journal of Cell Science*, *122*(8), 1071–1079.

D'Avino, P. P., Takeda, T., Capalbo, L., Zhang, W., Lilley, K. S., Laue, E. D., & Glover, D. M. (2008). Interaction between Anillin and RacGAP50C connects the actomyosin contractile ring with spindle microtubules at the cell division site. *Journal of Cell Science*, *121*(8), 1151–1158. http://doi.org/10.1242/jcs.026716

Dorn, J. F., & Zhang, L. (2010). Actomyosin Tube Formation in Polar Body Cytokinesis Requires Anillin in C. elegans. *Current Biology*, *20*(22), 2046–2051.

Field, C. M., & Alberts, B. M. (1995). Anillin, a contractile ring protein that cycles from the nucleus to the cell cortex. *The Journal of Cell Biology*, *131*(1), 165–178. http://doi.org/10.1083/jcb.131.1.165

Field, C. M., Coughlin, M., Doberstein, S., Marty, T., & Sullivan, W. (2005). Characterization of anillin mutants reveals essential roles in septin localization and plasma membrane integrity. *Development*, *132*(12), 2849–2860. http://doi.org/10.1242/dev.01843

Frenette, P., Haines, E., Loloyan, M., Kinal, M., Pakarian, P., & Piekny, A. (2012). An Anillin-Ect2 Complex Stabilizes Central Spindle Microtubules at the Cortex during Cytokinesis. *PLoS ONE*, *7*(4), e34888. http://doi.org/10.1371/journal.pone.0034888

Glotzer, M. (2001). Animal Cell Cytokinesis. *Annual Review of Cell and Developmental Biology*, *17*(1), 351–386. http://doi.org/10.1146/annurev.cellbio.17.1.351

Gregory, S. L., Ebrahimi, S., Milverton, J., Jones, W. M., Bejsovec, A., & Saint, R. (2008). Cell Division Requires a Direct Link between Microtubule-Bound RacGAP and Anillin in the Contractile Ring. *Current Biology*, *18*(1), 25–29. http://doi.org/10.1016/j.cub.2007.11.050

Hall, P. A., Todd, C. B., Hyland, P. L., McDade, S. S., Grabsch, H., Dattani, M., … Russell, S. E. H. (2005). The Septin-Binding Protein Anillin Is Overexpressed in Diverse Human Tumors. *Clinical Cancer Research*, *11*(19), 6780–6786. http://doi.org/10.1158/1078-0432.CCR-05-0997

Hickson, G. R. X., & O'Farrell, P. H. (2008). Rho-dependent control of anillin behavior during cytokinesis. *The Journal of Cell Biology*, *180*(2), 285–294. http://doi.org/10.1083/jcb.200709005

Hoffman, B. D., & Yap, A. S. (2015). Towards a Dynamic Understanding of Cadherin-Based Mechanobiology. *Trends in Cell Biology*, *25*(12), 803–814. http://doi.org/10.1016/j.tcb.2015.09.008

Itallie, C. M. V., Tietgens, A. J., Aponte, A., Fredriksson, K., Fanning, A. S., Gucek, M., & Anderson, J. M. (2014). Biotin ligase tagging identifies proteins proximal to E-cadherin, including lipoma preferred partner, a regulator of epithelial cell–cell and cell–substrate adhesion. *J Cell Sci*, *127*(4), 885–895. http://doi.org/10.1242/jcs.140475

Kechad, A., Jananji, S., Ruella, Y., & Hickson, G. R. X. (2012a). Anillin Acts as a Bifunctional Linker Coordinating Midbody Ring Biogenesis during Cytokinesis. *Current Biology*, *22*(3), 197–203.

Kechad, A., Jananji, S., Ruella, Y., & Hickson, G. R. X. (2012b). Anillin Acts as a Bifunctional Linker Coordinating Midbody Ring Biogenesis during Cytokinesis. *Current Biology*, *22*(3), 197–203. http://doi.org/10.1016/j.cub.2011.11.062

Kimura, K., Ito, M., Amano, M., Chihara, K., Fukata, Y., Nakafuku, M., … Kaibuchi, K. (1996). Regulation of Myosin Phosphatase by Rho and Rho-Associated Kinase (Rho-Kinase). *Science*, *273*(5272), 245–248. http://doi.org/10.1126/science.273.5272.245

Kinoshita, M., Field, C. M., Coughlin, M. L., Straight, A. F., & Mitchison, T. J. (2002). Self- and Actin-Templated Assembly of Mammalian Septins. *Developmental Cell*, *3*(6), 791–802. http://doi.org/10.1016/S1534-5807(02)00366-0

Lee, J.-S., Kamijo, K., Ohara, N., Kitamura, T., & Miki, T. (2004). MgcRacGAP regulates cortical activity through RhoA during cytokinesis. *Experimental Cell Research*, *293*(2), 275–282. http://doi.org/10.1016/j.yexcr.2003.10.015

Liu, J., Fairn, G. D., Ceccarelli, D. F., Sicheri, F., & Wilde, A. (2012). Cleavage Furrow Organization Requires PIP2-Mediated Recruitment of Anillin. *Current Biology*, *22*(1), 64–69. http://doi.org/10.1016/j.cub.2011.11.040

Liu, X.-F., Ishida, H., Raziuddin, R., & Miki, T. (2004). Nucleotide Exchange Factor ECT2 Interacts with the Polarity Protein Complex Par6/Par3/Protein Kinase Cζ (PKCζ) and Regulates PKCζ Activity. *Molecular and Cellular Biology*, *24*(15), 6665–6675. http://doi.org/10.1128/MCB.24.15.6665-6675.2004

Manukyan, A., Ludwig, K., Sanchez-Manchinelly, S., Parsons, S. J., & Stukenberg, P. T. (2015). A complex of p190RhoGAP-A and anillin modulates RhoA-GTP and the cytokinetic furrow in human cells. *J Cell Sci*, *128*(1), 50–60. http://doi.org/10.1242/jcs.151647

Miller, A. L., & Bement, W. M. (2009). Regulation of cytokinesis by Rho GTPase flux. *Nature Cell Biology*, *11*(1), 71–77. http://doi.org/10.1038/ncb1814

Miller, K. G., Field, C. M., & Alberts, B. M. (1989). Actin-binding proteins from Drosophila embryos: a complex network of interacting proteins detected by F-actin affinity chromatography. *The Journal of Cell Biology*, *109*(6), 2963–2975. http://doi.org/10.1083/jcb.109.6.2963

Mostowy, S., & Cossart, P. (2012). Septins: the fourth component of the cytoskeleton. *Nature Reviews Molecular Cell Biology*, *13*(3), 183–194. http://doi.org/10.1038/nrm3284

Nishimura, Y., & Yonemura, S. (2006). Centralspindlin regulates ECT2 and RhoA accumulation at the equatorial cortex during cytokinesis. *Journal of Cell Science*, *119*(1), 104–114. http://doi.org/10.1242/jcs.02737

Oegema, K., Savoian, M. S., Mitchison, T. J., & Field, C. M. (2000). Functional Analysis of a Human Homologue of the Drosophila Actin Binding Protein Anillin Suggests a Role in Cytokinesis. *The Journal of Cell Biology*, *150*(3), 539–552. http://doi.org/10.1083/jcb.150.3.539

Olakowski, M., Tyszkiewicz, T., Jarzab, M., Król, R., Oczko-Wojciechowska, M., Kowalska, M., … Jarzab, B. (2009). NBL1 and anillin (ANLN) genes over-expression in pancreatic carcinoma. *Folia Histochemica Et Cytobiologica / Polish Academy of Sciences, Polish Histochemical and Cytochemical Society*, *47*(2), 249–255. http://doi.org/10.2478/v10042-009-0031-1

Padte, N. N., Martin, S. G., Howard, M., & Chang, F. (2006). The Cell-End Factor Pom1p Inhibits Mid1p in Specification of the Cell Division Plane in Fission Yeast. *Current Biology*, *16*(24), 2480–2487. http://doi.org/10.1016/j.cub.2006.11.024

Page, Y. L., Chartrain, I., Badouel, C., & Tassan, J.-P. (2011). A functional analysis of MELK in cell division reveals a transition in the mode of cytokinesis during Xenopus development. *J Cell Sci*, *124*(6), 958–968. http://doi.org/10.1242/jcs.069567

Piekny, A. J., & Glotzer, M. (2008). Anillin Is a Scaffold Protein That Links RhoA, Actin, and Myosin during Cytokinesis. *Current Biology*, *18*(1), 30–36.

Prokopenko, S. N., Brumby, A., O'Keefe, L., Prior, L., He, Y., Saint, R., & Bellen, H. J. (1999). A putative exchange factor for Rho1 GTPase is required for initiation of cytokinesis in Drosophila. *Genes & Development*, *13*(17), 2301–2314.

Rajasekaran, A. K., Hojo, M., Huima, T., & Rodriguez-Boulan, E. (1996). Catenins and zonula occludens-1 form a complex during early stages in the assembly of tight junctions. *The Journal of Cell Biology*, *132*(3), 451–463. http://doi.org/10.1083/jcb.132.3.451

Ratheesh, A., Gomez, G. A., Priya, R., Verma, S., Kovacs, E. M., Jiang, K., … Yap, A. S. (2012). Centralspindlin and α-catenin regulate Rho signalling at the epithelial zonula adherens. *Nature Cell Biology*, *14*(8), 818–828. http://doi.org/10.1038/ncb2532

Reyes, C. C., Jin, M., Breznau, E. B., Espino, R., Delgado-Gonzalo, R., Goryachev, A. B., & Miller, A. L. (2014). Anillin Regulates Cell-Cell Junction Integrity by Organizing Junctional Accumulation of Rho-GTP and Actomyosin. *Current Biology*, *24*(11), 1263–1270.

Rincon, S. A., & Paoletti, A. (2012). Mid1/anillin and the spatial regulation of cytokinesis in fission yeast. *Cytoskeleton*, *69*(10), 764–777. http://doi.org/10.1002/cm.21056

Ronkainen, H., Hirvikoski, P., Kauppila, S., & Vaarala, M. H. (2011). Anillin expression is a marker of favourable prognosis in patients with renal cell carcinoma. *Oncology Reports*, *25*(1), 129–133.

Straight, A. F., Cheung, A., Limouze, J., Chen, I., Westwood, N. J., Sellers, J. R., & Mitchison, T. J. (2003). Dissecting Temporal and Spatial Control of Cytokinesis with a Myosin II Inhibitor. *Science*, *299*(5613), 1743–1747. http://doi.org/10.1126/science.1081412

Straight, A. F., Field, C. M., & Mitchison, T. J. (2005). Anillin Binds Nonmuscle Myosin II and Regulates the Contractile Ring. *Molecular Biology of the Cell*, *16*(1), 193–201. http://doi.org/10.1091/mbc.E04-08-0758

Sun, L., Guan, R., Lee, I.-J., Liu, Y., Chen, M., Wang, J., … Chen, Z. (2015). Mechanistic Insights into the Anchorage of the Contractile Ring by Anillin and Mid1. *Developmental Cell*, *33*(4), 413–426.

Tatsumoto, T., Xie, X., Blumenthal, R., Okamoto, I., & Miki, T. (1999). Human Ect2 Is an Exchange Factor for Rho Gtpases, Phosphorylated in G2/M Phases, and Involved in Cytokinesis. *The Journal of Cell Biology*, *147*(5), 921–928. http://doi.org/10.1083/jcb.147.5.921

Watanabe, S., Okawa, K., Miki, T., Sakamoto, S., Morinaga, T., Segawa, K., … Narumiya, S. (2010). Rho and Anillin-dependent Control of mDia2 Localization and Function in Cytokinesis. *Molecular Biology of the Cell*, *21*(18), 3193–3204. http://doi.org/10.1091/mbc.E10-04-0324

Wildenberg, G. A., Dohn, M. R., Carnahan, R. H., Davis, M. A., Lobdell, N. A., Settleman, J., & Reynolds, A. B. (2006). p120-Catenin and p190RhoGAP Regulate Cell-Cell Adhesion by Coordinating Antagonism between Rac and Rho. *Cell*, *127*(5), 1027–1039. http://doi.org/10.1016/j.cell.2006.09.046

Woolner, S., Miller, A., & Bement, W. (2010). Imaging the Cytoskeleton in Live Xenopus laevis Embryos. In R. H. Gavin (Ed.), *Cytoskeleton Methods and Protocols* (pp. 23–39). Humana Press. Retrieved from http://dx.doi.org/10.1007/978-1-60761-376-3_2

Zhou, W., Wang, Z., Shen, N., Pi, W., Jiang, W., Huang, J., … Sun, L. (2014). Knockdown of ANLN by lentivirus inhibits cell growth and migration in human breast cancer - Springer. *Molecular and Cellular Biochemistry*, *398*(1), 11–19.

Chapter 3: The Role of Septin-Anillin Interactions in the Regulation of Epithelial Cell-Cell Junctions

This chapter describes work that was done in collaboration with an undergraduate researcher in our lab, Nisha Gopal, who I mentored for two years. Nisha also submitted our work as a Biochemistry Honors Thesis.

Contributions to this work are as follows:

Reyes, C.R.: contributed intellectually and to experimental design, executed experiment and data analysis in Figures 3.7 & 3.8, worked together with Nisha on data in Figures 3.9, 3.10, and 3.14, wrote Chapter 3.

Gopal, N.: contributed intellectually and to experimental design, executed experiments in Figures 3.3-6 and 3.11-13, worked together with me on data in Figures 3.9, 3.10, and 3.14.

Miller, A.L.: contributed intellectually and to experimental design and data analysis, as well as provided lab space and funding for project.

Abstract

The actomyosin scaffolding protein Anillin and the GTP-binding Septins have a well-established relationship during cytokinesis, where Anillin is required for Septin's recruitment and retention at the contractile ring (Christine M. Field, Coughlin, Doberstein, Marty, & Sullivan, 2005; Makoto Kinoshita, Field, Coughlin, Straight, & Mitchison, 2002; Oegema, Savoian, Mitchison, & Field, 2000). We have detected a population of Anillin at epithelial cell-cell junctions in the *Xenopus* epithelium (Reyes et

al., 2014), and multiple Anillin binding partners (MgcRacGAP, Ect2, p190RhoGAP) have also recently been reported at junctions (Breznau, Semack, Higashi, & Miller, 2015; X.-F. Liu, Ishida, Raziuddin, & Miki, 2004; Ratheesh et al., 2012). Therefore, we wondered whether Septins might also be localized to junctions, and if so, whether Anillin is important for Septin recruitment. Indeed, A recent study detected a population of Septin 2 at the cortex of epithelial cells (Park et al., 2015) and another large-scale proteomic screen identified Septins as being in close association with the AJ protein E-cadherin (Guo et al., 2014). Perturbation of Septin via knock down or disruption of the Anillin-Septin interaction in intact epithelial tissues in *Xenopus* (Kim et al., 2010) and *Drosophila* (Christine M. Field et al., 2005) results in plasma membrane defects (blebbing, undulating membranes, vesiculation), strengthening the case for a potential role for Septins at junctions. Here, we examined Septin localization in the *Xenopus* epithelium and characterized its localization with respect to Anillin and the tight junctions (TJs) and adherens junctions (AJs) proteins ZO-1 and E-cadherin. We found that Septin 2 co-localizes with Anillin at the cortex in dividing and non-dividing cells, and that Septin 2 and 7 overlap with both the TJ and AJ proteins ZO-1 and E-cadherin. Further, Septin 2 has an important role in maintaining proper junction integrity as knock down results in intercellular spaces at the basolateral interface of cells. Work investigating the interdependency of Anillin and Septin recruitment to junctions suggests that Septin 2 and Anilln may have a role in regulating the localization of each other at junctions. This work has uncovered a novel role for Septins in epithelial cell biology in regulating cell junction architecture, potentially independent of its well-established binding partner, Anillin.

Introduction:

Septins: GTP-binding proteins that form Rods, Rings and Cages

Septins are a fascinating class of GTP-binding proteins that, in their active fully functioning form, oligomerize to form higher-ordered structures like rings, rods and intricate cages, which perform distinct functions in the cell (Mostowy & Cossart, 2012). Contractile actomyosin structures like the actomyosin contractile ring that forms at the cleavage furrow of dividing cells or at the tips of furrow canals in *Drosophila* embryos undergoing cellularization, are important sites of action for Septins. Upon Anillin-mediated recruitment to these sites, Septins promote the proper organization of these actomyosin contractile arrays and provide stability to the plasma membrane. Perturbation of Septin in these contexts, whether directly or indirectly through disruption of the Anillin-Septin interaction, results in defects: dividing cells fail cytokinesis (early and late) (Christine M. Field et al., 2005; Surka, Tsang, & Trimble, 2002), while cells undergoing cellularization exhibit a disorganized actin cytoskeleton at the invaginating front of furrow canals and embryos have large-scale gastrulation defects (Adam, Pringle, & Peifer, 2000). Septins also form rod-like structures that hetero-oligomerize into intricate patchworks of cross-hatched filaments (Aurélie Bertin et al., 2012; Rodal, Kozubowski, Goode, Drubin, & Hartwig, 2005), which are thought to provide general stability to the plasma membrane (Gilden & Krummel, 2010; Tooley et al., 2009), promote curvature (Tanaka-Takiguchi, Kinoshita, & Takiguchi, 2009) and function as diffusion barriers limiting the lateral exchange of proteins in the cell membrane (Takizawa, DeRisi, Wilhelm, & Vale, 2000) (Figure 3.1 & 3.2). This function is underscored in the budding yeast *S. cerevisiae*, where Septins form an hourglass structure at the bud neck (interface of mother and daughter cell) to promote the proper asymmetric distribution of proteins for both the mother and daughter cell (Kozubowski, Larson, & Tatchell, 2005). Finally, Septins have been observed to form cage-like structures around intruding microorganisms, presumably to restrict the spread of infection, but less is known about this process (Mostowy et al., 2010).

Septins: A fourth component of the cytoskeleton

Recently, it has been posited that Septins should join the ranks of actin, microtubules (MTs) and intermediate filaments (IFs), and be considered a fourth component of the cytoskeleton (Mostowy & Cossart, 2012). This is not surprising, nor is it unreasonable given the structural resemblance that Septins bear to the core cytoskeletal elements (filamentous in nature) (Figure 3.1), in addition to their structural role in providing rigidity to plasma membrane architecture – a major role of the cytoskeleton. Electron micrographs of Septins revealed that they are filamentous in appearance (Sirajuddin et al., 2007) and on a scale of size are larger than actin filaments which have a diameter of ~7 nm, yet smaller than MTs which have a diameter of ~25 nm; a single hetero-oligomeric Septin dimer is about ~10 nm in diameter, about the size of IFs (~11 nm). Kinetic studies have also revealed that Septins are not as dynamically regulated as actin or MTs (Hagiwara et al., 2011), and that Septin filaments are not polarized (do not have plus and minus ends with different dynamics) (Aurelie Bertin et al., 2008; John et al., 2007; Sirajuddin et al., 2007). Indeed, Septins most closely resemble the non-polar, yet dynamically regulated IFs.

Attributes that are perhaps unique about Septins as a cytoskeletal component are that they are composed of repeating hetero-oligomeric units (Sirajuddin et al., 2007) and have binding sites that mediate interactions with other cytoskeletal components (MTs and F-Actin) (M. Kinoshita et al., 1997; Nagata et al., 2003; Surka et al., 2002). One of the best characterized Septin hetero-oligomeric units is the Septin 2-6-7 complex, as its crystal structure has been resolved (Sirajuddin et al., 2007). In addition to interacting with other cytoskeletal components, Septins interact with the actyomyosin scaffolding protein Anillin (Makoto Kinoshita et al., 2002; Oegema et al., 2000), Myosin-2 (Straight, Field, & Mitchison, 2005), phospholipids (especially PIP_2) (J. Liu, Fairn, Ceccarelli, Sicheri, & Wilde, 2012) in addition to GTP (C. M. Field et al., 1996; Versele & Thorner, 2004), which is thought to induce Septin filament assembly, and other Septins. The general domain structure of Septins from the N- to C- terminus consists of a variable N-terminus, a polybasic region, which mediates interactions with lipids, a GTP-binding

domain, which includes the SUE (Septin Unique Element) and a coiled coil region, which mediates protein-protein interactions (Mostowy & Cossart, 2012)(Figure 3.2). In their oligomeric form, individual Septins interact with one another through their GTP-binding domain (G-interface) and their N- and C-terminal regions (NC-interface) (Mostowy & Cossart, 2012) (Figure 3.2).

Relationship between Septins and Anillin

Anillin and Septins have a well-characterized relationship, especially in dividing cells and cells undergoing modified forms of cytokinesis such as cellularization. In these contexts, Anillin is required for both recruitment and retention of Septins at the cleavage furrow (Christine M. Field et al., 2005; Surka et al., 2002) and furrow canal (Adam et al., 2000). When Anillin is knocked down (KD), Septins mislocalize (Christine M. Field et al., 2005; Makoto Kinoshita et al., 2002; Oegema et al., 2000), and when Anillin's interaction with Septins is perturbed via point mutations or deletion of its PH domain, which mediates interaction with Septins, this results in severe phenotypes including cytokinesis failure, alteration in the timing and rate of cellularization, and vesiculation of the plasma membrane (indicative of membrane instability) (Christine M. Field et al., 2005). Their relationship may even be more extensive as Anillin and Septin 2 (in addition to other Septins) are both highly expressed in similar tissues including the brain, testes and ovary and have been detected from stage 1 (one cell stage) to stage 60 (tadpole) in *Xenopus*. KD of either Anillin or Septin also phenocopies each other in some respects, as cytokinesis defects, gastrulation defects, and intercellular spaces have been observed in both scenarios. Further, both Anillin and Septin are overexpressed in diverse human tumors and cancers, and their increased expression correlates with increased metastatic potential (Chuang & Ou, 2014; Hall et al., 2005; Kato et al., 2007; Montagna et al., 2003; Olakowski et al., 2009).

Emerging roles for Septins at junctions in intact tissues

Recent work examining Septins in the intact epithelium of *Xenopus* embryos has uncovered important roles for them in the preservation of plasma membrane integrity, in properly maintaining apposition to neighboring cells (Kim et al., 2010; Park, Kim, &

Wallingford, 2015), and in compartmentalizing cortical actomyosin during the cell intercalation movements that guide convergent extension (CE) (Kim et al., 2010; Shindo & Wallingford, 2014). When Septin 2 is KD via an antisense morpholino (MO), intercellular spaces are observed at the basolateral interface between cells (Park et al., 2015), plasma membranes become unstable as evidenced by blebbing and undulation and gastrulation defects occur (enlarged blastopore and reduced CE of mesenchymal cells) (Kim et al., 2010). Septins have also been implicated in the planar cell polarity (PCP) pathway through Wdpcp (formerly known as Fritz), which interacts with Septin and is required for its proper cortical localization (Kim et al., 2010).

A recent study published by Park et al., (2015) detected a population of Septin 2 at the cell cortex in the *Xenopus* epithelium (Park et al., 2015); however, the authors did not characterize whether this population was junctional by examining the co-localization of Septin with a TJ or AJ protein. Additionally, the study did not test whether perturbation of Septin affected junction structure or function. Further, a BioID proteomic screen for novel proteins in close association with E-cadherin, identified Septin and Anillin as being in close proximity to E-cadherin (Guo et al., 2014). Because Anillin was recently found to be present at and regulate cell-cell junctions (Reyes et al., 2014), and Septins have an important role in plasma membrane stability (Kim et al., 2010; Park et al., 2015), we wondered whether Septins might also play a role in regulating junctions. In this study we focused on Septins 2 and 7. Previous work in *Xenopus* embryos analyzing these two Septins made them ideal candidates, as their perturbation via translation blocking MOs resulted in loss of plasma membrane integrity and reagents to KD these Septins and perform immunofluorescence microscopy are available. Here, we found that Anillin and Septin co-localize at the cortex, that Septins 2 and 7 are present at TJ and AJs and help maintain proper junctions structure as KD results in basolateral intercellular spaces. Further, we investigated the importance of Anillin or Septin for recruiting the other to junction and found that Septins and Anillin may have a role in regulating the localization of each other at junctions.

Results:

Septins 2 and 7 are present at cell-cell junctions where they overlap with the TJ and AJ proteins ZO-1 and E-cadherin

Recently a study by Park et al. (2015) showed that GFP-Septin 2 localizes at the cell cortex of the stage 26-27 *Xenopus* muco-ciliary epithelium (Park et al., 2015). However, the authors did not characterize whether this cortical population was junctional. We examined the junctional localization of Septins 2 and 7 using fixed staining to co-stain for Septin along with the TJ protein ZO-1 or the AJ protein E-cadherin. Immuno-staining for Septin 2 and the AJ protein E-cadherin showed that Septin 2 was indeed apically enriched at junctions as *en face* views detected co-localization with E-cadherin in dividing and non-dividing cells (Figure 3.3A, C, D). In addition to being present at junctions, Septin 2 was present at the cleavage furrow of dividing cells and as patchy filaments at the cortex, but these did not co-localize with E-cadherin (Figure 3.3A, C, D). Side views indicated that while Septin 2 is apically enriched, it is also present in the basolateral membrane and it co-localizes with E-cadherin's lateral distribution (Figure 3.3B). Immunostaining for Septin 2 and the TJ protein ZO-1 also showed co-localization at junctions in dividing (early and late) and non-dividing cells (Figure 3.4A, C, D). Side views demonstrated co-localization of apically enriched Septin 2 with ZO-1 (Figure 3.4B).

Fixed staining of Septin 7 detected a filamentous distribution throughout the cortex in dividing and non-dividing interphase cells, in addition to a junctional population that co-localized with ZO-1 and E-cadherin (Figure 3.5A, C, D; Figure 3.6 A,C). Septin 7 was not detected at the cleavage furrow of dividing cells like Septin 2 was, and its filaments were much more dense than the patchy pattern we observed with Septin 2 (Figure 3.5A,C, D; Figure 3.6C). Side views of co-staining for Septin 7 and E-cadherin show that it partially overlaps with E-cadherin (Figure 3.5B). Side views of Septin 7 and ZO-1 also show examples of apical co-localization (Figure 3.6B). Future work will be necessary to confirm the extent of co-localization of Septins 2 and 7 with these junctional proteins.

Septin 2 co-localizes with Anillin at the cortex in dividing and non-dividing cells.

As Anillin is a well-characterized binding partner of Septins and is required for Septin recruitment at the cleavage furrow, we examined Anillin and Septin localization in gastrula stage (stage ~10.5) *Xenopus* embryos. We first expressed 3xGFP-tagged full length Anillin, fixed and co-stained with anti-GFP and anti-Septin 2 antibodies. Anillin and Septin 2 strongly co-localized at the cleavage furrow of dividing cells and midbody as expected, in early, mid and late cytokinesis (Figure 3.7). Notably, we detected a population of Septin 2 that overlapped with Anillin at the cortex in dividing and non-dividing cells (Figure 3.7 & 3.8). Yellow signal was relatively weaker at the cortex than at the cleavage furrow and midbody for co-localization of Anillin and Septin 2 (Figure 3.7 & 3.8). Preliminary analysis using line scans to quantify their patterns of cortical distribution showed that Septin 2 may have a slightly wider distribution than Anillin (Figure 3.8).

Characterization of Septin 2 and Septin 7 morpholinos and confirmation of Septin 2 knock down

Given that Septins 2 and 7 were present at cell-cell junctions throughout the cell cycle, we wanted to characterize their function at junctions. Previously, translation blocking MOs for Septin 2 and 7 were characterized in mesenchymal cells undergoing cell intercalation during convergent extension (CE) (Kim et al., 2010). In this context, several phenotypes were observed including intercellular spaces, membrane blebbing and gastrulation defects. Here, in epithelial cells we first optimized the concentration of MO by examining three different concentrations (Figure 3.9). Septin 2 MO injection resulted in multi-nucleation at the lowest concentration (20 ng), and at higher concentrations (40 ng or 60 ng), we observed intercellular spaces and larger cells with rounded edges compared to their polygonal control counterparts (Figure 3.9).

Septin 7 KD also resulted in multi-nucleation at lower MO concentrations (20 ng and 40ng), and at the highest concentration (60 ng), we observed chromosomal bridging (Figure 3.9). We decided to select a concentration of 40 ng as this resulted in detectable phenotypes but not the most severe phenotypes. Because Septin 2 resulted in more

junctional defects than Septin 7, we focused on characterizing its role at junctions. We first confirmed Septin 2 KD using immunofluorescence microscopy (Figure 3.10). Injections were done with a mosaic approach where we injected 2 cells at the 4-cell stage with Septin 2 MO (Figure 3.10A,B). This approach allows us to image cells that received the MO next to internal control cells that did not receive the MO. We then fixed and stained embryos at the gastrula stage with anti-Septin 2 and anti-GFP antibodies. The relative intensity of Septin 2 at bicellular junctions in controls cells and cells where Septin 2 was depleted was quantified. The data indicates that a partial KD of Septin 2 of about 50% was achieved (Figure 3.10C).

Septin 2 KD results in intercellular spaces at the basolateral interface of cells

During optimization and confirmation of Septin 2 KD we observed junctional defects: intercellular spaces and apical doming. Thus, we wanted to carefully characterize junctional defects upon Septin 2 KD. Septin 2 was KD by injecting Septin 2 MO along with a lineage tracer (mCherry-farnesyl) to identify cells that had received the MO (Figure 3.10). Close inspection of control embryos showed the polygonal shaped cells were tightly apposed to one another at the apical surface and also a several z positions deeper into the tissue (3.75-11.25 µm) (Figure 3.11A, B). In contrast, in Septin 2 KD embryos while cells appeared tightly apposed to one another at the apical surface, there were prominent intercellular spaces deeper into the tissue (11.25 µm) (Figure 3.11C, D). This observation is consistent with recently published work showing that Septin 2 KD results in basolateral intercellular spaces between cells in the stage 26-27 *Xenopus* muco-ciliary epithelium.

Septin 2 KD affects the tight junction protein ZO-1 and the adherens junction protein E-cadherin

We examined the TJ protein ZO-1 and the AJ protein E-cadherin when Septin 2 was KD using live imaging (Figure 3.12 & 3.13). For control embryos, E-cadherin-3xGFP and mCherry-farnesyl were co-injected, whereas Septin 2 KD embryos were co-injected with Septin 2 MO, E-cadherin-3xGFP, and mCherry-farnesyl. Preliminary data showed that

compared to controls, Septin 2 KD embryos exhibited a reduction in the relative intensity of E-cadherin at cell-cell junctions, suggesting a role for Septin 2 in regulating AJs (Figure 3.12). Further, preliminary data showed that ZO-1 signal may also be reduced in Septin 2 KD embryos (Figure 3.13). Additionally, in these live imaging experiments we consistently observed intercellular spaces at cell vertices where three cells come together - tricellular junctions (Figure 3.12C). Taken together, these data suggest a potential role for Septin 2 in regulating basolateral membrane apposition and apical cell junction integrity.

Investigating the interdependecnce of Anillin and Septin 2 for localization at junctions
In cytoskinesis, Anillin is required for Septin recruitment and retention. Given that both Anillin and Septin 2 are present at cell junctions and co-localize, we wanted to interrogate the interdependency of their recruitment and regulation of junctions. Work in Chapter 2 of this dissertation demonstrated that the C-terminal AHDPH domains, which mediate Anillin's interaction with Septin, are sufficient for its targeting to cell junctions; therefore, we hypothesized that Septins may be present and have a role in regulating junctions. We performed mosaic injections where 2 cells at the 4-cell stage were injected with Septin 2 MO or Anillin MO along with a lineage tracer (GFP-farnesyl or mCherry-farnesyl). Embryos were then fixed at the gastrula stage and stained with appropriate antibodies for Septin 2 or Anillin as well as antibodies for the lineage tracers. Quantification of the relative intensity of signal at bicellular junctions revealed that when Septin 2 was KD, Anillin was slightly but significantly perturbed (p=0.0075), and when Anillin was KD, Septin was slightly but significantly perturbed (p=0.012) as we observed a reduction in signal for both (Figure 3.14). These data suggest that there may be an interdependent relationship between Septins and Anillin for their localization at junctions. More work is necessary to confirm if indeed this is the case or if a different mechanism is required, specifically for Septin recruitment at junctions.

Discussion

Investigating potential interactions of Septin with TJ and AJ proteins

Here, we identified a population of the GTP-binding proteins, Septin 2 and Septin 7, at epithelial cell-cell junctions where they co-localize with Anillin, the TJ protein ZO-1 and the AJ protein E-cadherin. However, key questions remain about their precise localization, for example whether Septins directly interact with Anillin and junction proteins at cell-cell junctions. Recent proteomic studies have identified Septins and Anillin as being in close proximity with the AJ protein E-cadherin (Guo et al., 2014), while work in progress from our lab (Chapter 2 of this dissertation) using a proximity ligation assay (PLA) detected a possible interaction between Anillin and the TJ protein ZO-1. Septin 2 could also be closely examined via PLA using species-specific antibodies for Septin 2 and TJ and AJ proteins, as well as Anillin. At present, we currently have only rabbit Anillin and Septin 2 antibodies, thus we will need to first identify and validate mouse anti-Septin 2 antibodies (or other non-rabbit antibodies) to enable PLA analysis. Alternatively, we could perform PLA analysis using 3xGFP-tagged Anillin anti-GFP (mouse) and anti-Septin 2 (rabbit). Another approach to identify junctional binding partners for Septin that we may pursue is tagging and immunoprecipitating Septin followed by mass spec to look for novel binding partners, which may include junction proteins. Further, investigating how widespread Septin's localization at junctions is in other tissues and species, will be an important question for future work

Characterizing how apically enriched Septin 2 regulates basolateral membrane apposition of epithelial cells

It is puzzling that Septin 2 is apically enriched at junctions, yet KD of Septin 2 results in intercellular spaces at the basolateral level. Preliminary work in this chapter demonstrated that the relative accumulation of E-cadherin was reduced upon Septin 2 KD. Given that E-cadherin has an important role in mediating basolateral cell-cell adhesion, it will be important to repeat these experiments, test whether the E-cadherin protein level is reduced via western blot, and investigate other AJ proteins to determine if the defects are specific to E-cadherin. In order to determine whether defects in E-cadherin underlie the basolateral intercellular space defect, it may be helpful to

overexpress E-cadherin in Septin 2 KD cells to see if this partially rescues the basal spaces. Additionally, examining the effect of Septin 2 KD on basolateral junction proteins such as members of the desmosomal family would be beneficial. Because Septins interact with both actin and MTs, is will be important to examine F-actin and MTs by live imaging or immunofluorescence to look for large-scale cytoskeletal rearrangements that could be responsible for the intercellular spaces.

Further Characterization of the interdependence of Anillin and Septin for localization at junctions

We observed a small, but statistically significant reduction of Septin 2 at junctions in cells where Anillin was KD, which suggests Anillin may help recruit and/or retain Septin 2 at junctions like it does at the cleavage furrow; however, due to limited repeats, more work is necessary to confirm this. When we knock down Anillin with a MO in *Xenopus* embryos, only a partial KD of Anillin is achieved; therefore, if Anillin is indeed important for recruitment and retention of Septin 2 at junctions, it is possible that the residual population of Anillin present after KD is sufficient to recruit some Septin 2 there. Another way to test the importance of Anillin-mediated Septin 2 recruitment to junctions, will be experiments that disrupt Anillin's ability to interact with Septin while preserving interactions with other binding partners. Work by Liu et al. examined the contribution of lipids and Septin to Anillin's targeting at the cleavage furrow by generating a chimeric Anillin that lacked the native PH domain (which mediates interactions with PIP_2 and Septins) and replaced it with the PH domain of PLCδ (which interacts with PIP_2 but not Septins) (J. Liu et al., 2012). If Septin is no longer recruited or is redistributed upon KD of endogenous Anillin and replacement with the Anillin-ΔPH-PLCδPH construct, this would suggest that Anillin's role in recruiting Septin is conserved at junctions. Alternatively, it is possible that a different scenario exists at junctions, where Anillin is not required for Septin 2 recruitment. Other factors like Wdpcp, a component of the planar cell polarity (PCP) pathway known to be important for Septin recruitment in mesenchymal cells, may be involved in Septin recruitment to junctions (Park et al., 2015). It will be important to examine the effect of Anillin KD on other Septins to see if

there is a more pronounced reduction – if so, Anillin may only recruit specific Septins to junctions.

Septin 2 KD slightly but significantly affected the population of Anillin at junctions, suggesting that it may have a role in Anillin targeting. However, we were only able to achieve a partial KD of Septin 2 (~50%) with Septin 2 MO injection; thus, it is possible that if Septin 2 is important for Anillin at junctions, residual Septin leftover after KD may be sufficient to maintain Anillin there. This does not exclude the possibility that other Septins may have a more prominent role in Anillin targeting at junctions. Thus, it will also be important here to explore alternative methods of KD such as CRISPR/Cas9 attempt to KD other Septins like Septin 7 and examine Anillin's distribution. Further, as Septins are known to heterooligomerize into rods, it will also be of interest to KD one Septin and examine any changes in distribution or patterning of other Septins – as there may be redundancy at play.

Unpublished work from our lab using FRAP to investigate how Anillin KD affects dynamics and turnover of junction proteins has detected changes in ZO-1 recovery – Anillin KD results in faster turnover whereas Anillin overexpression results in slower turnover, suggesting a role for Anillin in regulating the dynamics of proteins at junctions (Torey Arnold, unpublished). Indeed, it will be intriguing to investigate the dynamics of Septin 2 and 7 at junctions in control and Anillin KD embryos. While Septins are not fundamentally as dynamic as their actin or MT counterparts, they do undergo turnover (Mostowy & Cossart, 2012). FRAP studies would help us gain a better understanding of the relationship between Anillin and Septin at junctions. Characterizing Anillin and Septin dynamics at cell junctions independently and then examining changes in their dynamics upon KD of the other will be informative. At present, we have made 3xGFP-tagged Septin 2 and 7 constructs, which can be optimized for FRAP studies.

Our experiments revealed a population of Septin 2 and Septin 7 at cell-cell junctions in the intact epithelium of *Xenopus laevis* gastrula-stage embryos. Further, we characterized a novel role for Septin 2 in epithelial cell junctions, as we observe

changes in the accumulation of the TJ protein ZO-1 and AJ protein E-cadherin, as well as intercellular spaces at a basolateral position. We also showed preliminary data that suggests Anillin targeting to cell junctions may be dependent on Septin 2, and Anillin-mediated recruitment of Septin 2 may be conserved at junctions. These findings have uncovered a previously unknown and uncharacterized role for Septins in regulating cell junctions in intact epithelia. Additionally, they highlight a potential role for Septins in regulating junctions along with Anillin. Septins are indeed emerging as a force to be reckoned with in epithelial cell biology.
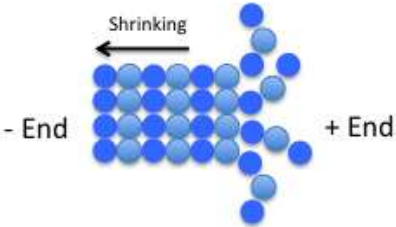
Cytoskeletal Component		Subunits	Diameter	Polar/ Non-Polar
Microtubules (MTs)	– End ← Shrinking + End	α/β tubulin	25 nm	Polar
Actin	– End + End	G-actin	7 nm	Polar
Intermediate Filaments (Ifs)		Tetramer of *ULFs	11 nm	Non-Polar
Septins		Hetero-oligomeric units	10 nm	Non-Polar

Figure 3.1 Cytoskeletal Components. Actin, microtubules (MTs) and intermediate filaments (IFs) are core components of the cytoskeleton and exhibit defining characteristics when it comes to subunit composition, diameter, polarity and dynamics. Septins resemble these major cytoskeletal components in many respects, including their filamentous structure and relative diameter. Figure adapted from (Mostowy & Cossart 2012).
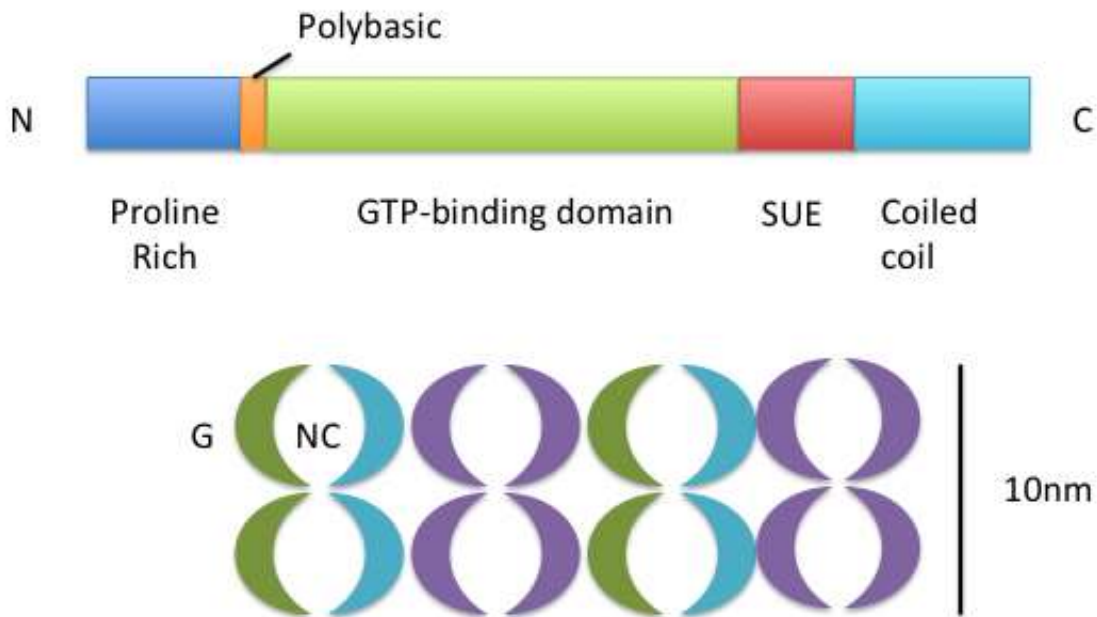
Figure 3.2 Septin Domain Diagram. The structure of Septins includes five major binding domains. An N-terminal variable Proline rich region, a polybasic domain that mediates interactions with lipids, a GTP-binding domain, a Septin Unique Element (SUE) region and a coiled-coil domain that mediates protein-protein interactions. When Septins heterooligomerize into filaments and higher ordered structures, they interact with each other via their G- and NC interfaces. Figure adapted from (Mostowy & Cossart, 2012)
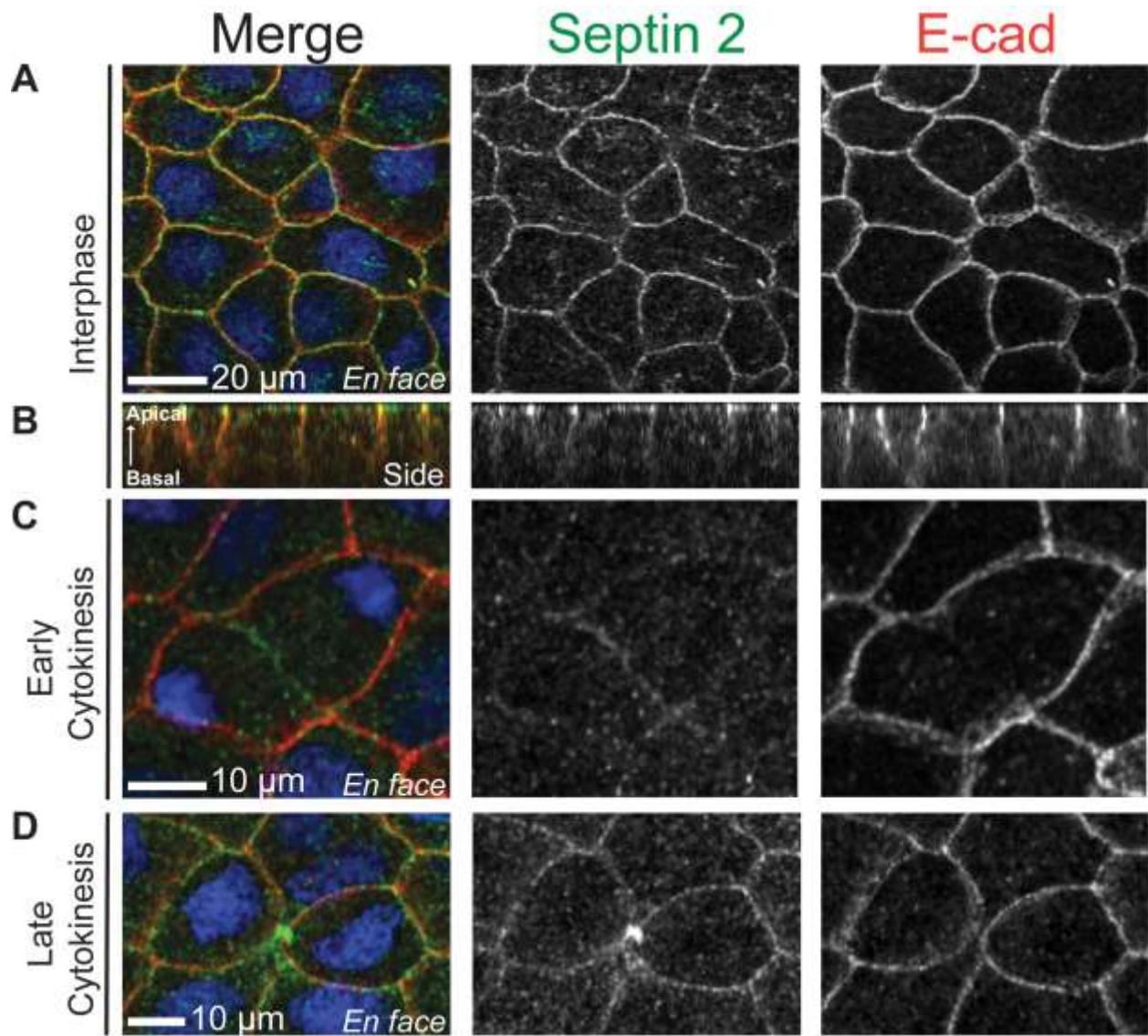
Figure 3.3 Septin 2 co-localizes with the adherens junction protein E-cadherin. (A) *En face* views of non-dividing interphase cells where Septin 2 is in green, E-cadherin red and nuclei in blue. (B) Side views of co-staining for Septin 2 and E-cadherin showing their localization throughout the lateral membrane. *En face* views of Septin 2 and E-cadherin in dividing cells during early (C) and late (D) cytokinesis.
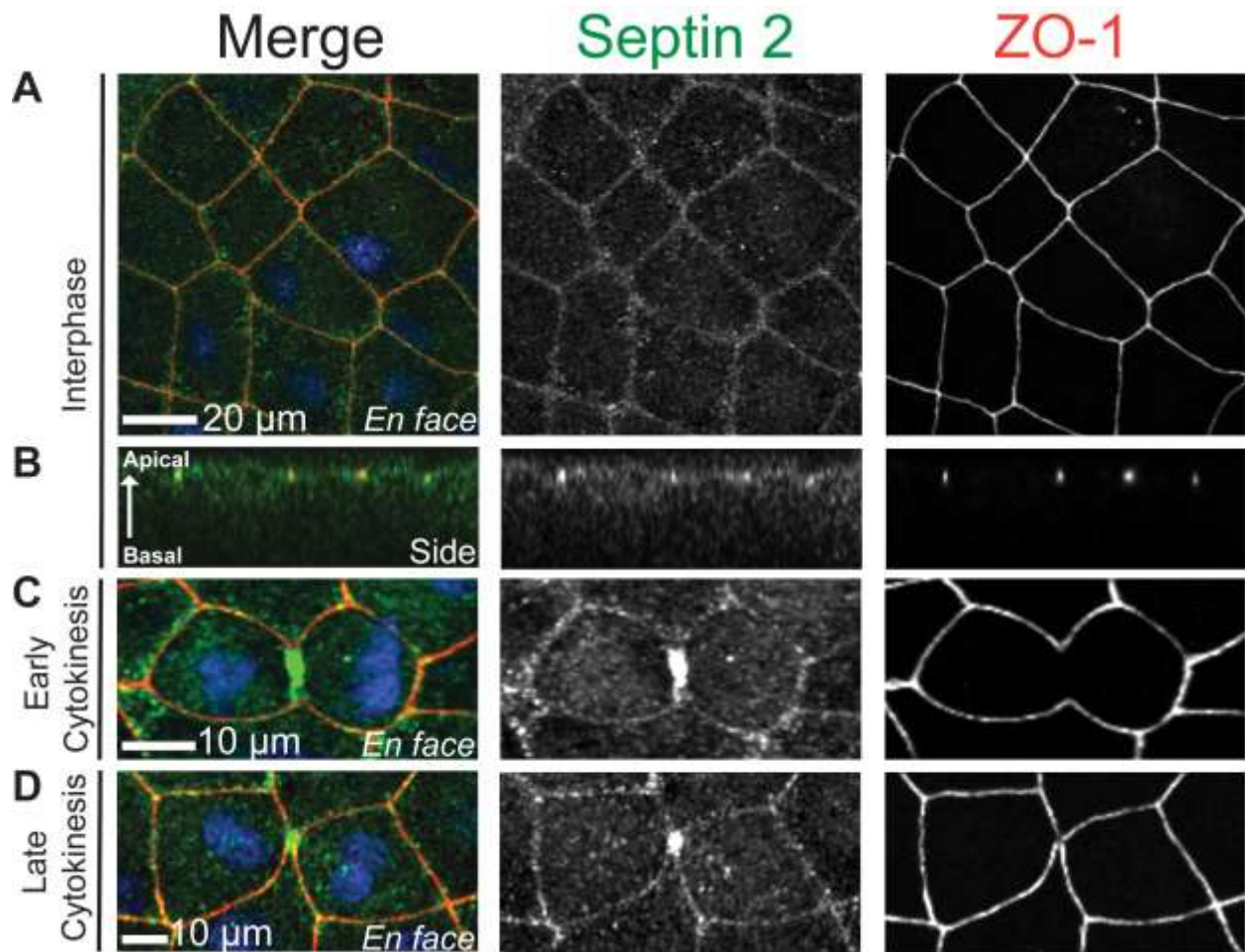
Figure 3.4 Septin 2 co-localizes with the tight junction protein ZO-1. (A) *En face* views of non-dividing interphase cells, (B) side views, and *en face* views of dividing cells during early (C) and late (D) cytokinesis. Embryos were fixed and stained for Septin 2 (green) and the tight junction protein ZO-1 (red), and nuclei are DAPI stained in blue.
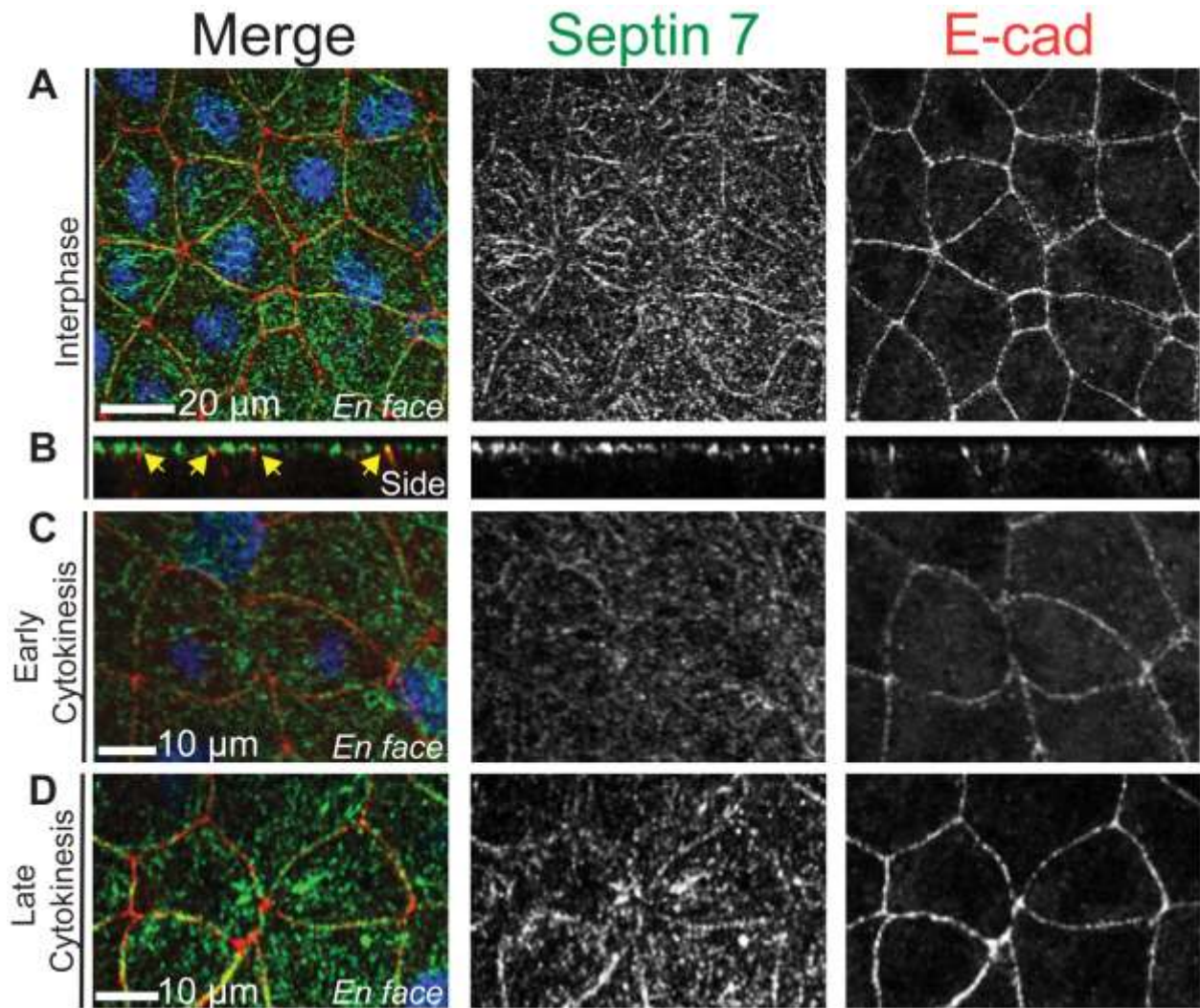
130

Figure 3.5 Septin 7 co-localizes with the adherens junction protein E-cadherin. (A) *En face* and (B) side views of interphase cells fixed and stained for Septin 7 (green), E-cadherin (red) and nuclei (blue). Yellow arrows point to junctions. *En face* views of dividing cells during early (C) and (D) late cytokinesis.

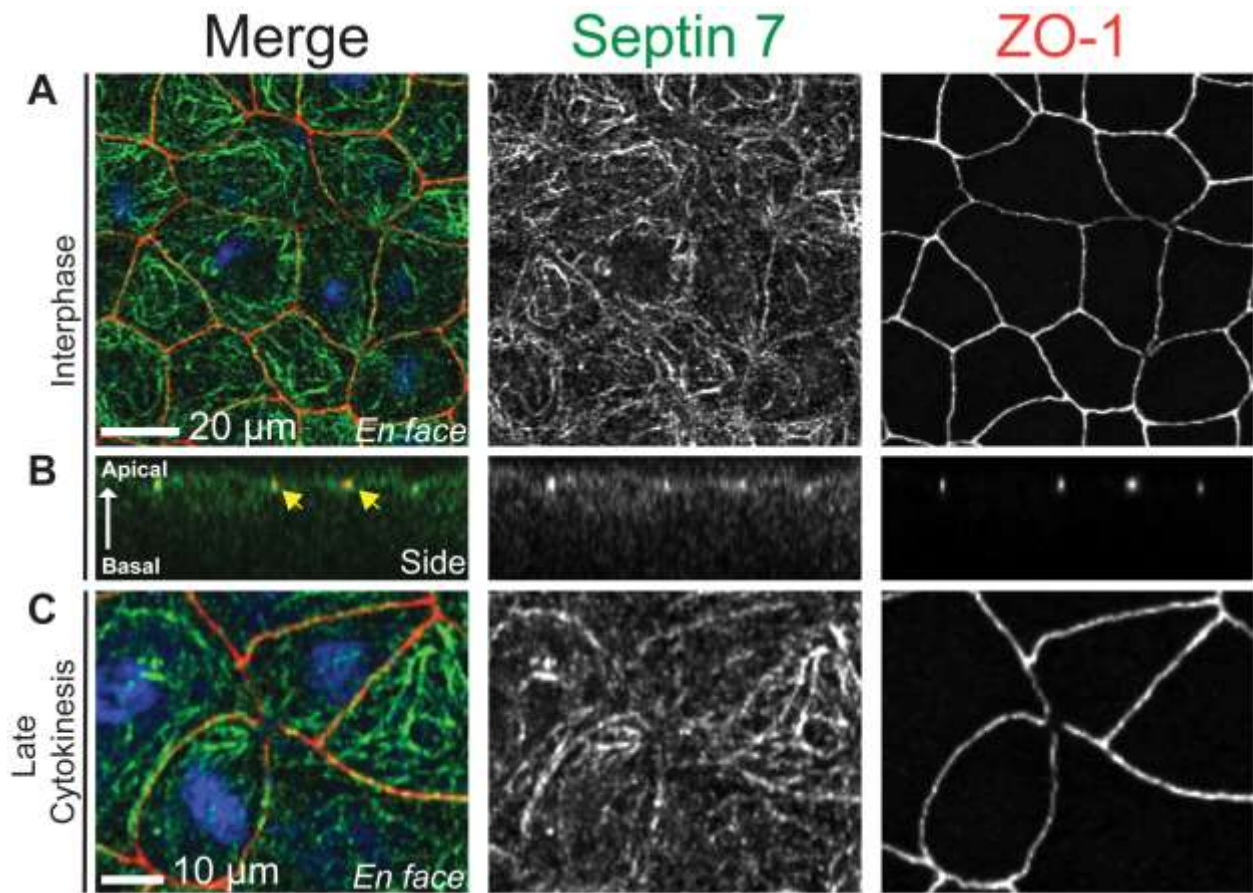131

Figure 3.6 Septin 7 co-localizes with the tight junction protein ZO-1. (A) *En face* view of fixed staining for Septin 7 (green), ZO-1 (red) and nuclei (blue) in non-dividing interphase cells. (B) Side views of Septin 2 and ZO-1 distribution. Yellow arrows point out junctions. (C) An example of a dividing cell during late cytokinesis showing Septin 7 and ZO-1 distribution at junctions.
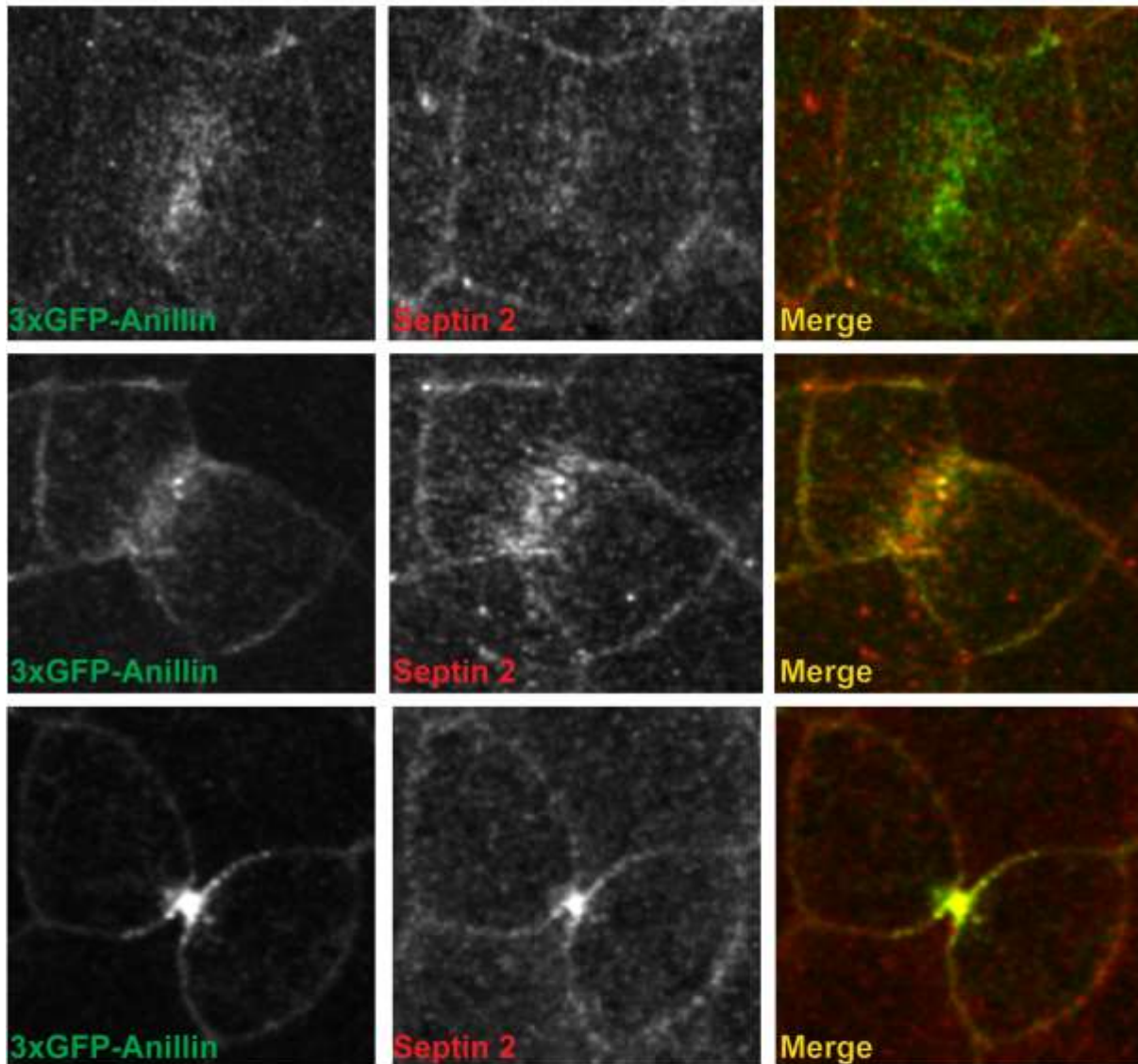
Figure 3.7 Anillin and Septin 2 co-localization in dividing cells. Fixed staining for Anillin-3xGFP (green) and Septin 2 (red) with anti-GFP and anti-Septin 2 antibodies in cells at early, mid and late cytokinesis and at the contractile ring. Regions of yellow signal indicate co-localization.

133
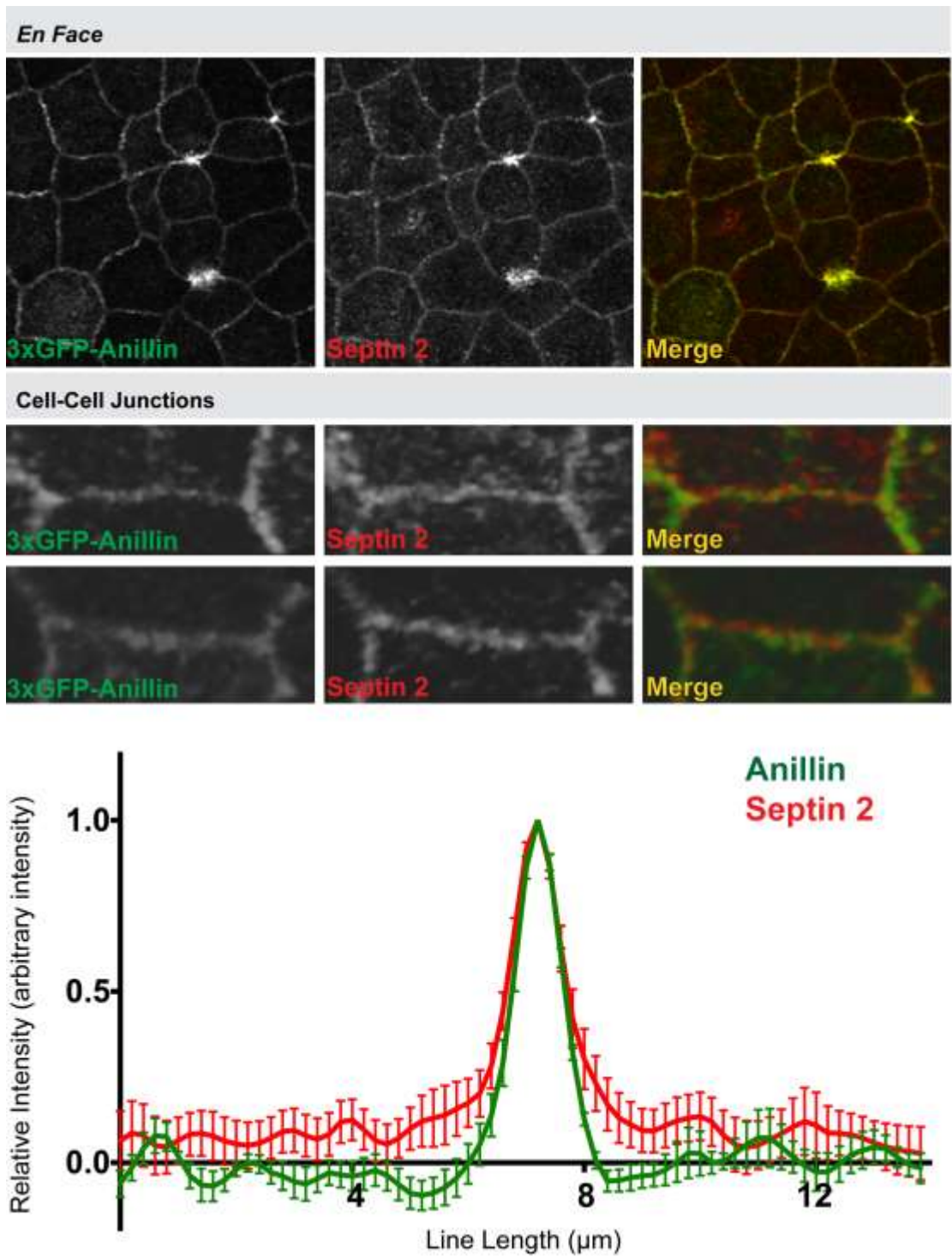
Figure 3.8 Anillin and Septin 2 co-localization at the cortex. Fixed staining for 3xGFP-tagged Anillin (green) and Septin 2 (red) in dividing and non-dividing regions of the epithelium. Images are maximum point projection *en face* views and enlarged close-ups of bicellular junctions. Graph shows quantification using line scans across bicellular junctions for Anillin and Septin 2 distribution at junctions (n=1, 4 embryos, 2 line scans each; 8 analyzed for each).
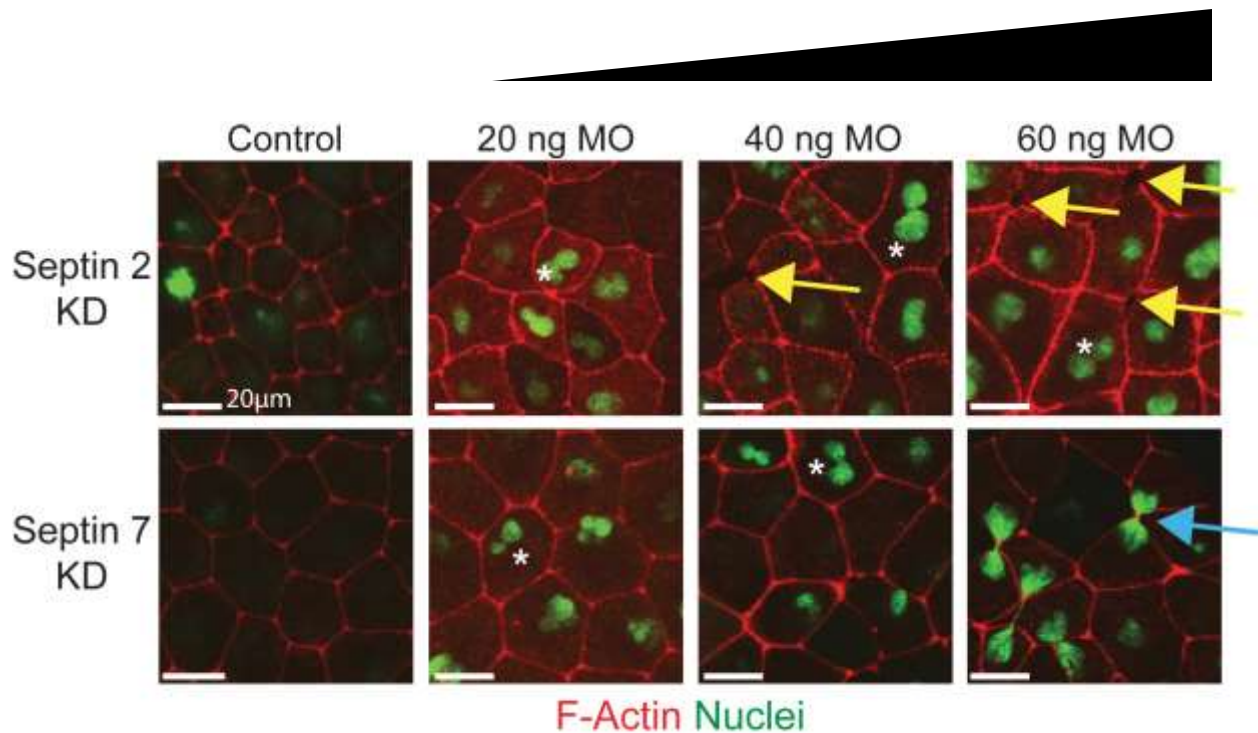
Figure 3.9 Knockdown of Septin 2 and 7 at varying concentrations of morpholino induces cytokinesis and junctional defects. Control embryos were co-injected with probes for F-actin (red) and nuclei (green), while Septin KD embryos were additionally injected with MO at varying concentrations ranging from 20 ng to 60ng. Asterisks indicate examples of multi-nucleation, while yellow arrows indicate intercellular spaces and a blue arrow highlights an example of chromosomal bridging.
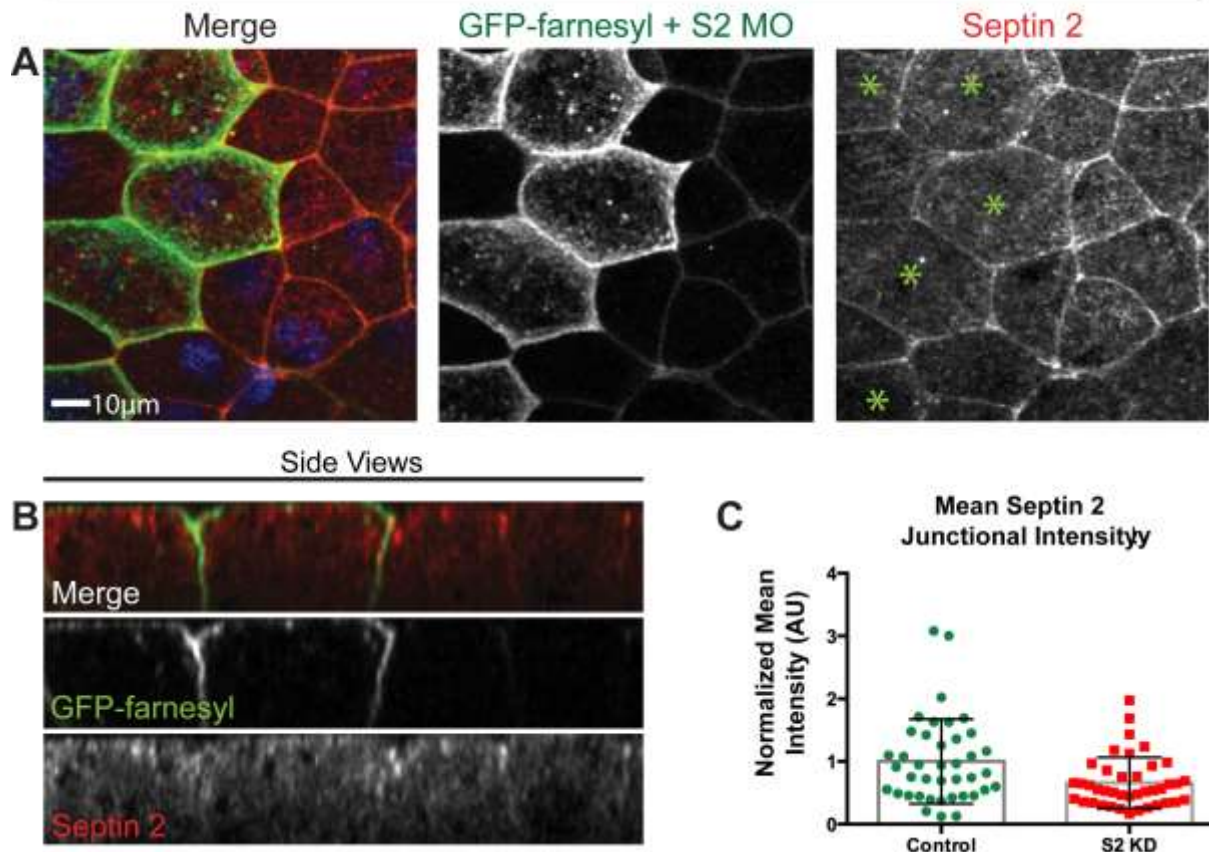
Figure 3.10 Confirmation of Septin 2 Knockdown. (A) *En face* views of embryos mosaically injected with Septin 2 MO to selectively KD Septin 2 in some cells, and not in others (internal control). The Septin 2 MO was coinjected with the lineage tracer (GFP-farnesyl). Green cells have received Septin MO and are noted by green asterisks in the grey scale image of Septin 2. (B) Side views showing cells where Septin 2 has been KD via MO (cells labeled in green) neighboring control cells. (C) Graph quantifying the relative intensity of Septin 2 in control cells and cells where Septin has been KD. n=2 experiments, 8 embryos, 5 bicellular junctions each/per embryo; 40 analyzed. p=0.0005 and error bars represent standard error of the mean (SEM).
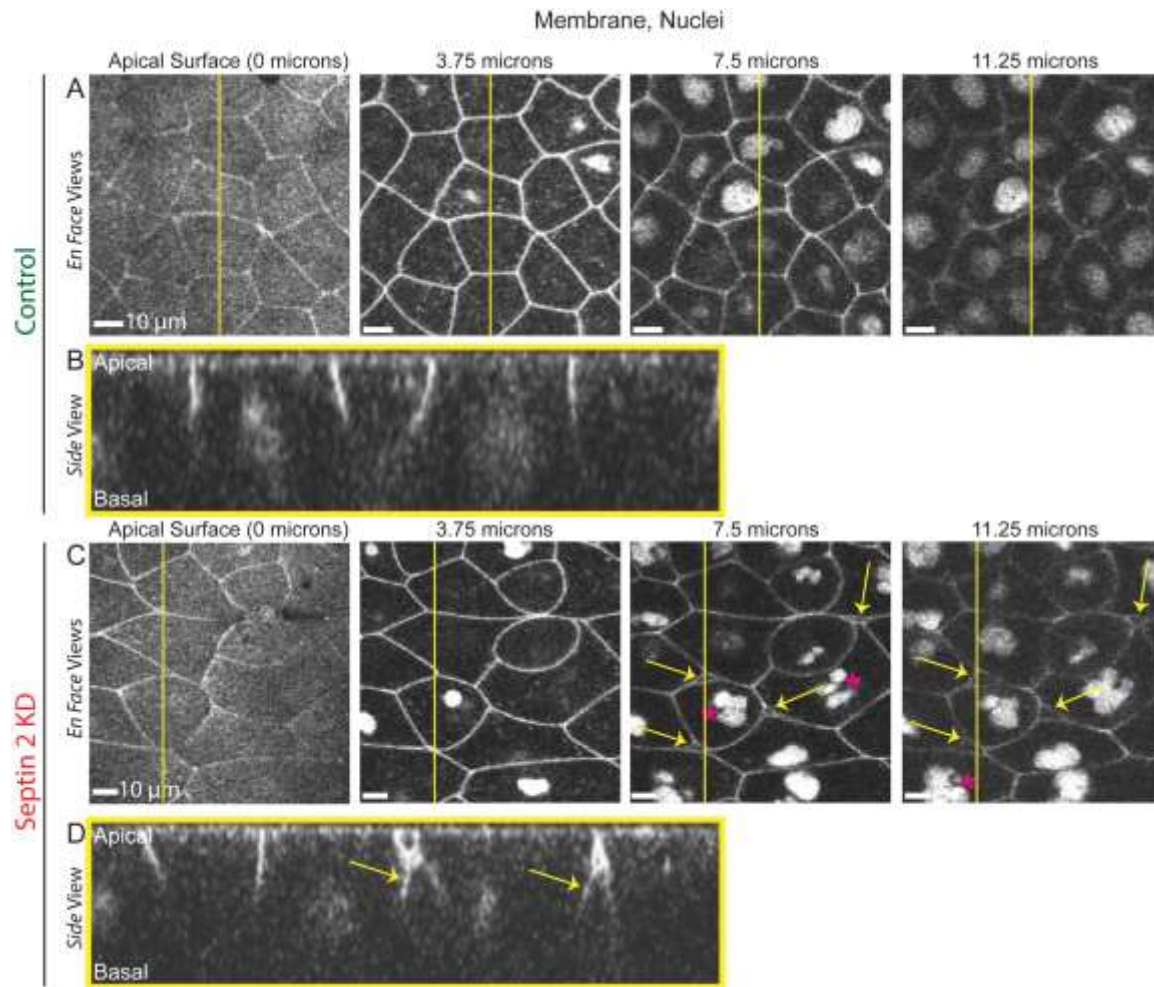
Figure 3.11 Septin 2 KD results in basolateral intercellular spaces. Control embryos were co-injected with a membrane marker (mCherry-farnesyl) and a DNA marker (mCherry-H2B), while Septin 2 KD embryos were additionally injected with Septin 2 MO. *En face* views of the apical membrane of control (A) and Septin KD (C) cells at varying depths within the epithelium ranging from 3.75-11.25 microns. Yellow lines indicate the YZ plane where side view regions were isolated and yellow arrows point to intercellular spaces. Side views of the tightly apposed membranes of control cells (B) and membranes of Septin 2 KD cells (D).
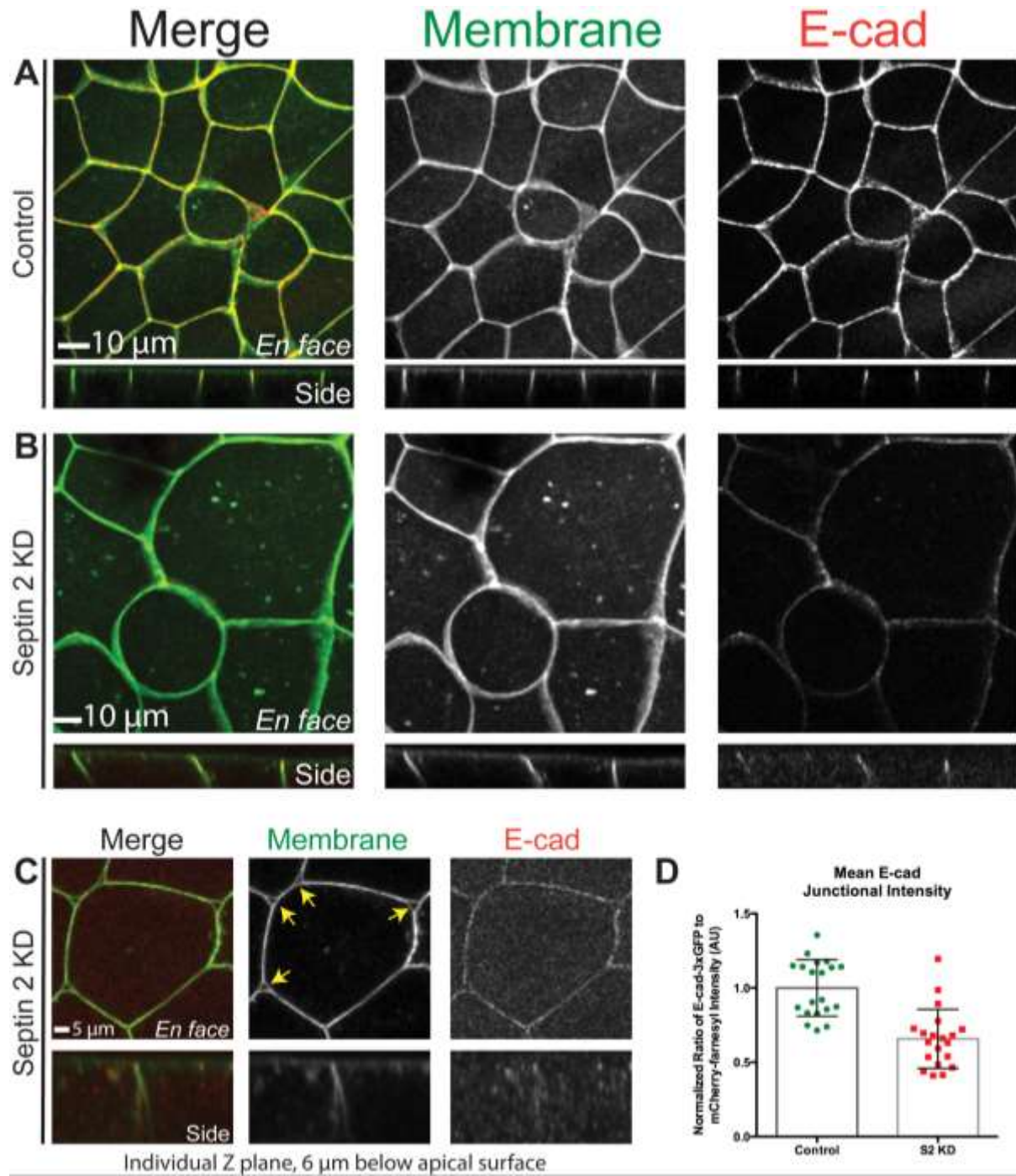
Figure 3.12 Septin 2 KD disrupts the adherens junction protein E-cadherin. Control embryos were co-injected with a membrane marker (mCherry-farnesyl pseudo-colored Green) and E-cadherin-3xGFP (pseudo-colored Red), while S2 KD embryos were additionally injected with Septin 2 MO. *En face* views and side views of Control (A) and S2 KD embryos (B). (C) Individual Z plane of *en face* and side views at 6 microns below the apical surface in a Septin 2 KD cell. (D) Quantification of the mean E-cadherin junctional intensity in Control and Septin 2 KD cells. n=1 experiment, 4 embryos, 5 bicellular junctions, p<0.001. Error bars represent standard error of the mean.

138
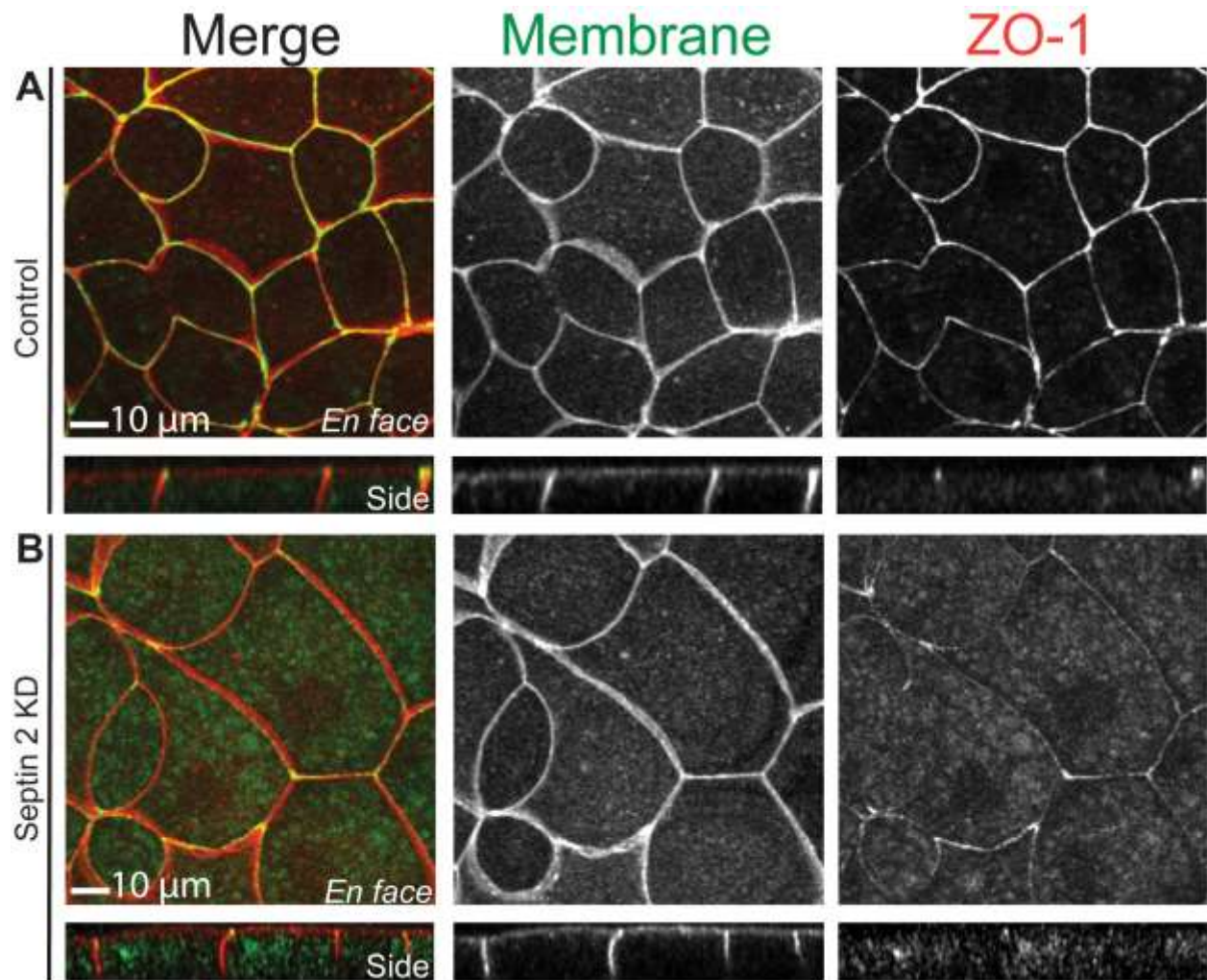
Figure 3.13 Knockdown of Septin 2 disrupts the tight junction protein ZO-1. Control embryos were co-injected with GFP-farnesyl and mRFP-ZO-1, while Septin 2 KD embryos were additionally injected with Septin 2 MO. *En face* and side views of Control (A) and Septin 2 KD (B) embryos. n=1 experiment.
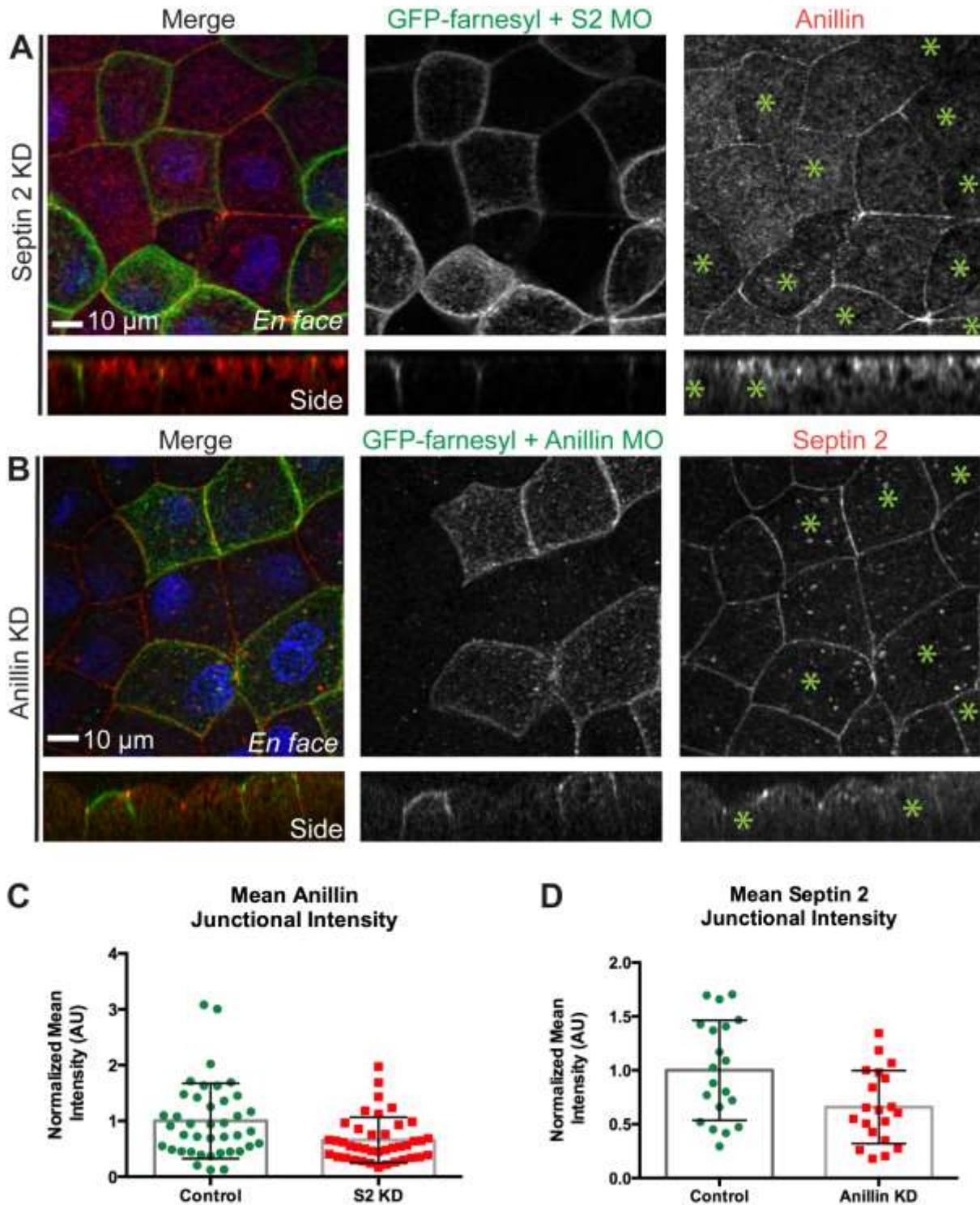
Figure 3.14 Characterization of the Anillin-Septin relationship at junctions. Embryos were mosaically injected 2 at the 4-cell stage with either Septin 2 MO or Anillin MO along with GFP-farnesyl. Cells that received MO are labeled in green. (A) *En face* and side views of Anillin staining to detect Anillin loclalization in control and Septin 2 KD cells. (B) *En face* and side views of Septin 2 staining to detect Septin 2 localization in control and Anillin KD cells. (C) Quantification of relative mean intensity of Anillin at

junctions in control and Septin 2 KD cells. n=2 experiments, 8 embryos, 5 bicellular junctions each; 40 analyzed; p=0.0075. (D) Quantification of relative mean intensity of Septin 2 at junctions in control and Anillin KD cells. n=1 experiment, 4 embryos, 5 bicellular junctions, p=0.012.

.

Materials & Methods:

DNA constructs and mRNA preparation. The following DNA constructs were used for the above experiments: pCS2+/mChe-UtrCH (F-actin probe; (Burkel, von Dassow, & Bement, 2007), and pCS2+/GFP-farnesyl (probe for membrane; (Reyes et al., 2014). mRNAs were transcribed using the mMessage mMachine SP6 kit (Ambion/Life Technologies, Grand Island, NY). 3XGFP-Anillin was generated using a GFP-*Xenopus* Anillin vector generously provided by Aaron Straight, Stanford University, as the template. Anillin was amplified by PCR and cloned into the pCS2+ or pCS2+/C-3XGFP vector using ClaI and XhoI restriction sites, as previously described.

Microinjections. Eggs were collected from ovulating *Xenopus laevis* females upon induction with HCG, fertilized in a dish and dejellied (A. L. Miller & Bement, 2009; Woolner et al., 2010). Eggs were stored in 1XMMR (Mark's modified Ringer solution 1X: 100 mM NaCl, 2 mM KCl, 2 mM CaCl2, 1 mM MgCl2, and 5 mM 4-(2-hydroxyethyl)-1-piperazineethanesulfonic acid, pH 7.4) and allowed to develop to the 2- or 4- cell stage when embryos were microinjected with mRNA. The following mRNA concentrations were used for microinjections: mCherry-membrane (10 µg/ml), GFP-membrane (10 µg/ml), mCherry-H2B (20 µg/ml), and mCherry-UtrCH (10 µg/ml).

Septin and Anillin Morpholinos.
Septin 2 and Septin 7 MOs targeted the following sequences (Kim et al., 2010):
Septin 2-MO: 5'TAAACTGAGCCTGTTGCTTTGACAT3'
Septin 7-MO: 5'TGCTGTAGAGTCAGTGCCTCGCCTT3'.

We previously characterized an Anillin antisense MO (Gene Tools) with the sequence: 5' –TGGCTAGTAACTCGATCCTCAGACT –3'. (Reyes et al., 2014)

Fixed staining and antibodies. All embryos were fixed and stained using 2% Tri-chloroacetic acid (TCA) fixation as previously reported (Reyes et al., 2014). Briefly, embryos were fixed in 2% TCA at the gastrula stage (10.5-11), bisected to isolate the

animal hemisphere of epithelial cells, permeabilized in PBS with 1% and 0.1% T-X-100, blocked O/N in PBST (0.1% T-X-100) supplemented with 5% FBS. Embryos were stained with respective primary antibodies and secondary antibodies O/N and in between were rinsed O/N. The day of imaging, embryos were DAPI stained and mounted.

Antibodies for fixed staining were used at the following concentrations: α-Septin 2 (Ab179436 [Abcam]) 1:40, α-Septin 2 (HPA018481 [Sigma]) 1:200, α-Septin 7 (NBP1-85730 [Novus biological]) 1:40, α-Anillin (PRIMM) 1:1000, α-mCherry (Ab125096 [Abcam]) 1:200, α-GFP (632381 [Clontech]) 1:200, α-β-Catenin (Ab2364 [Abcam]) 1:200, α-E-Cadherin (5D3-c [DSHB]) 1:200, α-ZO-1 (61-7300 [Invitrogen]) 1:200, α-ZO-1 (339100 [Life Technologies]) 1:1000, and Alexa Fluor 488 or Alexa 568 (anti-rabbit and anti-mouse Invitrogen) 1:200.

Quantification Methods:

All images and movies were acquired using an Olympus fluoview 1000 inverted confocal microscope with a 60x objective and at 1X zoom. Images were imported into the 3D image analysis software Volocity and analyzed in FIJI. Graphs were generated using PRISM.

Quantification to confirm S2 KD and to examine changes in relative intensity of S2 and Anillin upon KD of S2 or Anillin included the following methods: Volocity OIF files were imported into FIJI and Z-stacks flattened. For quantification of S2 KD, a 3 pixel wide line was drawn along 5 bicellular junctions per embryo in both control and Septin 2 KD cells, and the mean was calculated in FIJI. The mean intensity was then normalized to background by subtracting signal measured with the same dimensions in the cytoplasm. The average of control embryos was normalized to 1. This approach was also used to quantify Anillin when Septin 2 was KD and Septin 2 when Anillin was KD.

Quantification of E-cadherin in Septin 2 KD cells was performed by drawing a 3 pixel wide line in FIJI over 10 bicellular junctions per embryo for both controls and Septin 2

143

KD cells to measure the mean intensity of E-cadherin and the membrane channel. The mean intensity was measured at these bicellular junctions and the ratio of mean E-cadherin to mean membrane signal was plotted on a graph. 10 control measurements in 2 embryos and 10 Septin 2 KD measurements in 2 embryos were used in this analysis. n = 20 for control n = 20 for Septin 2 KD. The average of the control measurements was normalized to 1

Acknowledgments:

References:

Adam, J. C., Pringle, J. R., & Peifer, M. (2000). Evidence for Functional Differentiation amongDrosophila Septins in Cytokinesis and Cellularization. *Molecular Biology of the Cell*, *11*(9), 3123–3135. http://doi.org/10.1091/mbc.11.9.3123

Bertin, A., McMurray, M. A., Grob, P., Park, S.-S., Garcia, G., Patanwala, I., … Nogales, E. (2008). Saccharomyces cerevisiae septins: Supramolecular organization of heterooligomers and the mechanism of filament assembly. *Proceedings of the National Academy of Sciences*, *105*(24), 8274–8279. http://doi.org/10.1073/pnas.0803330105

Bertin, A., McMurray, M. A., Pierson, J., Thai, L., McDonald, K. L., Zehr, E. A., … Nogales, E. (2012). Three-dimensional ultrastructure of the septin filament network in Saccharomyces cerevisiae. *Molecular Biology of the Cell*, *23*(3), 423–432. http://doi.org/10.1091/mbc.E11-10-0850

Breznau, E. B., Semack, A. C., Higashi, T., & Miller, A. L. (2015). MgcRacGAP restricts active RhoA at the cytokinetic furrow and both RhoA and Rac1 at cell-cell junctions in epithelial cells. *Molecular Biology of the Cell*, *doi: 10.1091/mbc. E14-11-1553.*

Chuang, H. Y., & Ou, Y. H. (2014). Abstract 4068: Overexpression of anillin in colorectal cancer promotes the cell proliferation, cell mobility and cell invasion. *Cancer Research*, *74*(19 Supplement), 4068–4068. http://doi.org/10.1158/1538-7445.AM2014-4068

Field, C. M., al-Awar, O., Rosenblatt, J., Wong, M. L., Alberts, B., & Mitchison, T. J. (1996). A purified Drosophila septin complex forms filaments and exhibits GTPase activity. *The Journal of Cell Biology*, *133*(3), 605–616. http://doi.org/10.1083/jcb.133.3.605

Field, C. M., Coughlin, M., Doberstein, S., Marty, T., & Sullivan, W. (2005). Characterization of anillin mutants reveals essential roles in septin localization and plasma membrane integrity. *Development*, *132*(12), 2849–2860. http://doi.org/10.1242/dev.01843

Gilden, J., & Krummel, M. F. (2010). Control of cortical rigidity by the cytoskeleton: Emerging roles for septins. *Cytoskeleton*, *67*(8), 477–486. http://doi.org/10.1002/cm.20461

Guo, Z., Neilson, L. J., Zhong, H., Murray, P. S., Zanivan, S., & Zaidel-Bar, R. (2014). E-cadherin interactome complexity and robustness resolved by quantitative proteomics | Science Signaling. *Science Signaling*, *7*(354), rs7.

Hagiwara, A., Tanaka, Y., Hikawa, R., Morone, N., Kusumi, A., Kimura, H., & Kinoshita, M. (2011). Submembranous septins as relatively stable components of actin-based membrane skeleton. *Cytoskeleton (Hoboken, N.J.)*, *68*(9), 512–525. http://doi.org/10.1002/cm.20528

Hall, P. A., Todd, C. B., Hyland, P. L., McDade, S. S., Grabsch, H., Dattani, M., … Russell, S. E. H. (2005). The Septin-Binding Protein Anillin Is Overexpressed in Diverse Human Tumors. *Clinical Cancer Research*, *11*(19), 6780–6786. http://doi.org/10.1158/1078-0432.CCR-05-0997

John, C. M., Hite, R. K., Weirich, C. S., Fitzgerald, D. J., Jawhari, H., Faty, M., … Steinmetz, M. O. (2007). The Caenorhabditis elegans septin complex is nonpolar. *The EMBO Journal*, *26*(14), 3296–3307. http://doi.org/10.1038/sj.emboj.7601775

Kato, Y., Uzawa, K., Yamamoto, N., Kouzu, Y., Koike, H., Shiiba, M., … Tanzawa, H. (2007). Overexpression of Septin1: Possible contribution to the development of oral cancer. *International Journal of Oncology*, (31), 1021–1028.

Kim, S. K., Shindo, A., Park, T. J., Oh, E. C., Ghosh, S., Gray, R. S., … Wallingford, J. B. (2010). Planar Cell Polarity Acts Through Septins to Control Collective Cell Movement and Ciliogenesis. *Science*, *329*(5997), 1337–1340. http://doi.org/10.1126/science.1191184

Kinoshita, M., Field, C. M., Coughlin, M. L., Straight, A. F., & Mitchison, T. J. (2002). Self- and Actin-Templated Assembly of Mammalian Septins. *Developmental Cell*, *3*(6), 791–802. http://doi.org/10.1016/S1534-5807(02)00366-0

Kinoshita, M., Kumar, S., Mizoguchi, A., Ide, C., Kinoshita, A., Haraguchi, T., … Noda, M. (1997). Nedd5, a mammalian septin, is a novel cytoskeletal component interacting with actin-based structures. *Genes & Development*, *11*(12), 1535–1547. http://doi.org/10.1101/gad.11.12.1535

Kozubowski, L., Larson, J. R., & Tatchell, K. (2005). Role of the Septin Ring in the Asymmetric Localization of Proteins at the Mother-Bud Neck in Saccharomyces cerevisiae. *Molecular Biology of the Cell*, *16*(8), 3455–3466. http://doi.org/10.1091/mbc.E04-09-0764

Liu, J., Fairn, G. D., Ceccarelli, D. F., Sicheri, F., & Wilde, A. (2012). Cleavage Furrow Organization Requires PIP2-Mediated Recruitment of Anillin. *Current Biology*, *22*(1), 64–69. http://doi.org/10.1016/j.cub.2011.11.040

Liu, X.-F., Ishida, H., Raziuddin, R., & Miki, T. (2004). Nucleotide Exchange Factor ECT2 Interacts with the Polarity Protein Complex Par6/Par3/Protein Kinase Cζ (PKCζ) and Regulates PKCζ Activity. *Molecular and Cellular Biology*, *24*(15), 6665–6675. http://doi.org/10.1128/MCB.24.15.6665-6675.2004

Montagna, C., Lyu, M.-S., Hunter, K., Lukes, L., Lowther, W., Reppert, T., … Ried, T. (2003). The Septin 9 (MSF) Gene Is Amplified and Overexpressed in Mouse Mammary Gland Adenocarcinomas and Human Breast Cancer Cell Lines. *Cancer Research*, *63*(9), 2179–2187.

Mostowy, S., Bonazzi, M., Hamon, M. A., Tham, T. N., Mallet, A., Lelek, M., … Cossart, P. (2010). Entrapment of Intracytosolic Bacteria by Septin Cage-like Structures. *Cell Host & Microbe*, *8*(5), 433–444. http://doi.org/10.1016/j.chom.2010.10.009

Mostowy, S., & Cossart, P. (2012). Septins: the fourth component of the cytoskeleton. *Nature Reviews Molecular Cell Biology*, *13*(3), 183–194. http://doi.org/10.1038/nrm3284

Nagata, K., Kawajiri, A., Matsui, S., Takagishi, M., Shiromizu, T., Saitoh, N., … Inagaki, M. (2003). Filament Formation of MSF-A, a Mammalian Septin, in Human Mammary Epithelial Cells Depends on Interactions with Microtubules. *Journal of Biological Chemistry*, *278*(20), 18538–18543. http://doi.org/10.1074/jbc.M205246200

Oegema, K., Savoian, M. S., Mitchison, T. J., & Field, C. M. (2000). Functional Analysis of a Human Homologue of the Drosophila Actin Binding Protein Anillin Suggests a Role in Cytokinesis. *The Journal of Cell Biology*, *150*(3), 539–552. http://doi.org/10.1083/jcb.150.3.539

Olakowski, M., Tyszkiewicz, T., Jarzab, M., Król, R., Oczko-Wojciechowska, M., Kowalska, M., … Jarzab, B. (2009). NBL1 and anillin (ANLN) genes over-expression in pancreatic carcinoma. *Folia Histochemica Et Cytobiologica / Polish Academy of Sciences, Polish Histochemical and Cytochemical Society*, *47*(2), 249–255. http://doi.org/10.2478/v10042-009-0031-1

Park, T. J., Kim, S. K., & Wallingford, J. B. (2015). The planar cell polarity effector protein Wdpcp (Fritz) controls epithelial cell cortex dynamics via septins and actomyosin. *Biochemical and Biophysical Research Communications*, *456*(2), 562–566. http://doi.org/10.1016/j.bbrc.2014.11.078

Ratheesh, A., Gomez, G. A., Priya, R., Verma, S., Kovacs, E. M., Jiang, K., … Yap, A. S. (2012). Centralspindlin and α-catenin regulate Rho signalling at the epithelial zonula adherens. *Nature Cell Biology*, *14*(8), 818–828. http://doi.org/10.1038/ncb2532

Reyes, C. C., Jin, M., Breznau, E. B., Espino, R., Delgado-Gonzalo, R., Goryachev, A. B., & Miller, A. L. (2014). Anillin Regulates Cell-Cell Junction Integrity by Organizing Junctional Accumulation of Rho-GTP and Actomyosin. *Current Biology*, *24*(11), 1263–1270.

Rodal, A. A., Kozubowski, L., Goode, B. L., Drubin, D. G., & Hartwig, J. H. (2005). Actin and Septin Ultrastructures at the Budding Yeast Cell Cortex. *Molecular Biology of the Cell*, *16*(1), 372–384. http://doi.org/10.1091/mbc.E04-08-0734

Shindo, A., & Wallingford, J. B. (2014). PCP and Septins Compartmentalize Cortical Actomyosin to Direct Collective Cell Movement. *Science*, *343*(6171), 649–652. http://doi.org/10.1126/science.1243126

Sirajuddin, M., Farkasovsky, M., Hauer, F., Kühlmann, D., Macara, I. G., Weyand, M., … Wittinghofer, A. (2007). Structural insight into filament formation by mammalian septins. *Nature*, *449*(7160), 311–315. http://doi.org/10.1038/nature06052

Straight, A. F., Field, C. M., & Mitchison, T. J. (2005). Anillin Binds Nonmuscle Myosin II and Regulates the Contractile Ring. *Molecular Biology of the Cell*, *16*(1), 193–201. http://doi.org/10.1091/mbc.E04-08-0758

Surka, M. C., Tsang, C. W., & Trimble, W. S. (2002). The Mammalian Septin MSF Localizes with Microtubules and Is Required for Completion of Cytokinesis. *Molecular Biology of the Cell*, *13*(10), 3532–3545. http://doi.org/10.1091/mbc.E02-01-0042

Takizawa, P. A., DeRisi, J. L., Wilhelm, J. E., & Vale, R. D. (2000). Plasma Membrane Compartmentalization in Yeast by Messenger RNA Transport and a Septin Diffusion Barrier. *Science*, *290*(5490), 341–344. http://doi.org/10.1126/science.290.5490.341

Tanaka-Takiguchi, Y., Kinoshita, M., & Takiguchi, K. (2009). Septin-Mediated Uniform Bracing of Phospholipid Membranes. *Current Biology*, *19*(2), 140–145.

Tooley, A. J., Gilden, J., Jacobelli, J., Beemiller, P., Trimble, W. S., Kinoshita, M., & Krummel, M. F. (2009). Amoeboid T lymphocytes require the septin cytoskeleton for cortical integrity and persistent motility. *Nature Cell Biology*, *11*(1), 17–26. http://doi.org/10.1038/ncb1808

Versele, M., & Thorner, J. (2004). Septin collar formation in budding yeast requires GTP binding and direct phosphorylation by the PAK, Cla4. *The Journal of Cell Biology*, *164*(5), 701–715. http://doi.org/10.1083/jcb.200312070

Woolner, S., Miller, A., & Bement, W. (2010). Imaging the Cytoskeleton in Live Xenopus laevis Embryos. In R. H. Gavin (Ed.), *Cytoskeleton Methods and Protocols* (pp. 23–39). Humana Press. Retrieved from http://dx.doi.org/10.1007/978-1-60761-376-3_2

Conclusions

Prior to the work described in this dissertation, Anillin was thought to function primarily during cytokinesis to help organize and stabilize the cytokinetic contractile ring, which constricts like a belt to physically pinch one cell into two. Anillin is known to interact with major components of the contractile ring including F-actin, which provides the filamentous structural framework of the ring (Miller, Field, & Alberts, 1989; Oegema, Savoian, Mitchison, & Field, 2000), the motor protein Myosin-2, which generates contractility (Straight, Field, & Mitchison, 2005), and the small GTPase RhoA, which is the signal that promotes F-actin and Myosin-2's functional output at the division site in addition to recruiting Anillin there (Piekny & Glotzer, 2008). In previous studies in isolated cultured cells, Anillin was reported to be in the nucleus of non-dividing interphase cells and at the cleavage furrow of dividing cells (Field & Alberts, 1995; Oegema et al., 2000); however, in this dissertation we report that a population of Anillin is present at epithelial cell-cell junctions throughout the cell cycle, and that this population has an important role in maintaining TJ and AJ structure and function (Reyes et al., 2014). Further, we show that Anillin's C-terminal AHD and PH domains work cooperatively to target Anillin to junctions. While these findings have uncovered important roles for Anillin in epithelial cell biology, key questions remain about its direct mechanism of action and recruitment. The following pages discuss next steps and key questions of interest for future studies. Below is a brief outline of themes in this section.

Outline:

1.1 Elucidating the mechanism by which Anillin regulates epithelial cell-cell junctions.

1.2 Characterizing the role of Anillin at tricellular tight junctions (tTJs).

1.3 Roles for Anillin at junctions in other organisms and epithelial tissues.

1.4 Anillin overexpression and disease.

1.1. Elucidating the mechanism by which Anillin regulates epithelial cell-cell junctions.

In Chapter 2, we showed that when Anillin is knocked down (KD), the junctional accumulation of F-actin and Myosin-2 is reduced and that there are increased flares of active RhoA around the perimeter of cells, especially at or near tricellular junctions. As F-actin and Myosin-2 are downstream of the active RhoA pathway, this suggests that Anillin may function through RhoA to regulate the apical actomyosin belt, and therefore cell-cell junction integrity. Further work is necessary, however, to elucidate whether Anillin acts directly through RhoA to regulate junction integrity. In the cytokinesis literature, perturbation of Rho signaling by RNAi of its GEF (Ect2) (Hickson & O'Farrell, 2008), or deletion of the entire Anillin homology domain (AHD), which contains the Rho binding domain (RBD), underscored the importance of the Anillin-RhoA interaction in regulating the fidelity of cytokinesis (Piekny & Glotzer, 2008). RNAi of Ect2 abolished Anillin's recruitment to the furrow (Hickson & O'Farrell, 2008), and while cells expressing Anillin with the AHD deleted exhibited weak furrow recruitment, they failed cytokinesis (Piekny & Glotzer, 2008). Future studies where Anillin's RBD is disrupted by deletion or introduction of point mutations to disrupt Rho binding, or RNAi of Rho GEFs such as Ect2, will allow the direct assessment of the Anillin-RhoA interaction in regulating cell junctions. Examination of other effectors of the RhoA pathway when Anillin is KD such as the formin mDia or the kinases Citron and ROCK, which promote activation of Myosin-2, could also be informative here.

During cytokinesis, Rho activation is driven by the GEF Ect2, which interacts at the spindle midzone with the centralspindlin complex (heterotetrameric complex of MgcRacGAP and the plus-end-directed motor protein MKLP-1) (Mishima, Kaitna, & Glotzer, 2002; Somers & Saint, 2003; Yuce, Piekny, & Glotzer, 2005). Centralspindlin recruits Ect2 to the spindle midzone and equatorial cortex (Yuce et al., 2005) and promotes the local activation of RhoA, which recruits Anillin and promotes actomyosin ring formation. The centralspindlin complex (Ratheesh et al., 2012), Ect2 (X.-F. Liu, Ishida, Raziuddin, & Miki, 2004), and RhoA, are also present at cell-cell junctions and may be important for Anillin recruitment there. Interestingly, Anillin and Ect2 are known to form stable complexes in the absence of RhoA (Frenette et al., 2012), thus potentially providing a RhoA-independent mechanism by which Anillin could be recruited to junctions. It will be important to determine whether the mechanism of Anillin recruitment to junctions, in addition to its regulation of junctions is through Ect2-driven RhoA activation or other means.

RhoA signaling is a key regulator of both tight junctions (TJs) and adherens junctions (AJs) in epithelial cells. This is evidenced by the fact that when Rho is inhibited in MDCK cells, the TJ proteins ZO-1 and occludin are reduced at junctions, while when Rho is overexpressed ZO-1 and occludin are increased there (Gopalakrishnan et al., 1998). Further, AJ assembly is disrupted when Rho signaling is perturbed (Etienne-Manneville & Hall, 2002; Nusrat et al, 1995). This indicates that Rho activity must be properly balanced – too much or too little can disrupt junctions. Rho orchestrates junction assembly and the proper accumulation of junction proteins by regulating the apical actomyosin belt that links to junctions. Rho promotes dynamic reorganization of the apical actomyosin belt during tissue remodeling events such as cell migration - both in healthy cells that might migrate during a developmental processes like EMT, and cancer cells that dislodge themselves and invade other Tissues - or junction assembly (Balda & Matter, 2016). Rho activity at junctions is modulated by GEFs and GAPs. For example, the RhoGEF ARHGEF18/p114RhoGEF works with Myosin-2, cingulin and ROCK II to promote RhoA activation at junctions, which can promote local

reorganization of the actomyosin belt (Terry et al., 2011), and the RhoGEF ARHGEF11/PDZ-Rho-GEF is recruited to TJs by ZO-1 (Itoh et al., 2012). Given that Rho is a key regulator of both TJs and AJs, and that Anillin interacts with Rho, and also has an important role in TJ and AJ integrity, it will be important to further assess their relationship. One way to test this is to overexpress CA RhoA in a background depleted of Anillin to see if this rescues the reduction of junction proteins such as ZO-1 and E-cad as demonstrated in Chapter 1 of this thesis. This would suggest a direct mechanism between Anillin and RhoA in regulating junctions.

Recently, a paper showed that Anillin interacts with RhoG, also through its AHD region (Tian et al., 2015). RhoG is a small GTPase that is a member of the Rac subfamily of Rho GTPases (Bustelo, Sauzeau, & Berenjeno, 2007), but relatively little is known about it. It is involved in diverse cell processes including neurite outgrowth (Estrach et al., 2002), phagocytosis of apoptotic cells (deBakker et al., 2004), cell survival (Murga, Zohar, Teramoto, & Gutkind, 2002) and cell migration (Buul et al., 2007). As future studies continue to elucidate effectors of the RhoG pathway, such as Elmo (Katoh & Negishi, 2003), it will be important to closely examine their localization (whether they are junctional) and whether RhoG is present at and has a role in regulating epithelial cell-cell junctions. At present, RhoG has known roles in endothelial cell migration, a process, which involves reorganization of junctional components and cytoskeleton, but it has no known direct roles in the regulation of junctions (Buul et al., 2007; Pannekoek, Kooistra, Zwartkruis, & Bos, 2009). If indeed RhoG or its effectors are present at junctions, it will also be interesting to characterize the relationship between the RhoG pathway and Anillin at junctions.

1.2 Characterizing the role of Anillin at tricellular tight junctions.
Tricellular tight junctions (tTJs) are a distinct class of tight junction where three cells come together (Menco, 1988), and they have unique structural features and protein components. One feature is a network of strands that aligns along the apposing membranes of each cell, forming a central tube for the passage of macromolecules (Krug et al., 2009). Another feature is their unique enrichment of tTJ specific proteins including tricellulin and angulin family proteins, which are composed of three members:

angulin-1/LSR (lipolysis-stimulated lipoprotein receptor), angulin-2/ILDR1 (immunoglobulin-like (Ig-like) domain containing receptor 1), and angulin-3/ILDR2 (Higashi et al., 2013; Ikenouchi et al., 2005; R. Masuda, Semba, Mizuuchi, Yanagihara, & Yokozaki, 2010). Tricellulin is a tetraspan transmembrane protein that shares homology with occludin. While it is also present at bicellular TJs, it is particularly enriched at tTJs where it has an essential role in epithelial barrier function. Tricellulin KD is associated with reduced transepithelial resistance (indicative of epithelial barrier defect) and increased permeability to a 4,000 Da Dextran tracer molecule (Ikenouchi et al., 2005). Angulin family proteins are single pass transmembrane proteins that are also enriched at tTJs, where they are essential for barrier function and tricellulin recruitment (Higashi et al., 2013; S. Masuda et al., 2011).

When Anillin is KD, we have observed that increased flares of active RhoA often occur at or near tTJs, and when Anillin KD embryos are mounted in fluorescent dextran (3,000 Da), tTJs exhibit increased penetration compared to bicellular TJs (Reyes et al., 2014). While these data are intriguing and suggest a potential role for Anillin at tTJs, we have not observed a significant affect on tTJ structure upon Anillin KD in our system (Tomohito Highashi, unpublished). As the Anillin KD we achieve in our system is only partial, it will be important to explore other methods for more efficient KD, such as CRISPR/Cas and examine the effects on tTJs. The increased penetration of dextran at tTJs in Anillin KD embryos may suggest a loss of tension as tTJs are potentially sites of increased tension, as three cell membranes must tightly appose each other to maintain barrier integrity. Indeed, upon Anillin KD we observed apical doming of cells, which suggests a loss of tension. The fact that tTJs are composed of an intricate network of TJ strands, which form a central tube that regulates permeability, further implicates a potential relationship between Anillin and tTJs in regulating permeability (Mariano, Sasaki, Brites, & Brito, 2011). This tube has a diameter of about 10nm (Mariano et al., 2011) and is thought to serve two purposes: regulate the passage of macromolecules (Krug et al., 2009), and seal the tricellular contacts against viruses and antigens (Ohkuni et al., 2009). Because of its size, the central tube is thought to be a potential weak point for the epithelial barrier (Ikenouchi et al., 2005). However, not much is

known about how tTJs regulate this central tube to allow influx of macromolecules, while preventing the entry of potentially harmful pathogens and substances. As cells can regulate their permeability by dynamically rearranging their actin cytoskeleton (Madara, Moore, & Carlson, 1987), Anillin, a key scaffold for actomyosin contractile arrays, may also function in this context.

In septate junctions, the invertebrate equivalent of TJs, it is known that gliotactin, a cholinesterase-like molecule, acts as a 'tricellular plug' (TCP) for the central tube of tTJs (Schulte, Tepass, & Auld, 2003). Gliotactin is recruited to tTJs by the transmembrane protein Anakonda, which also has a significant role in regulating permeability (Byri et al., 2015). While a gliotactin or Anakonda homolog has not been identified in mammals, a similar protein may function in this capacity and/or a collection of proteins to provide stability for sealing, yet flexibility for regulation of macromolecule influx. Future work should examine the relationship between Anillin and tTJ specific proteins like tricellulin and the angulins. Indeed, tricellulin and angulin-1 have recently been detected at tTJs in the *Xenopus* epithelium (Higashi et al., 2016 accepted). Next steps may include examining changes in their localization or distribution when Anillin is KD.

1.3 Roles for Anillin at junctions in other organisms and epithelial tissues.

A recent study found Anillin's role in regulating the actomyosin belt and junctional integrity is conserved in human epithelial cells (Wang, Chadha, Feygin, & Ivanov, 2015). Perturbation of Anillin via RNAi resulted in discontinuous staining of the TJ proteins ZO-1, JAM-A and Occludin, in addition to disrupted localization of the AJ proteins E-cadherin, Cadherin-6 and β-catenin. The actomyosin belt became disorganized, as evidenced by a reduction of junctional F-actin and Myosin-2 and was also broader and loosely bundled. Trans-epithelial electrical resistance (TEER) was reduced, suggesting a loss of barrier integrity. Cell adhesion was also weakened as evidenced by increased cell dissociation upon mechanical perturbation with a pipette - control cells still formed clusters of three or more cells; however, cells depleted of Anillin displayed reduced cluster formation. This study confirms an emerging role for Anillin outside the context of

cytokinesis, in regulating cell-cell junctions. Further, it highlights a conserved role for Anillin in regulating junctions in amphibians and mammals.

It is intriguing, however, that Anillin was not detected at junctions in the Wang et al. study. Using DU145 Human prostate epithelial cells, A549 human lung epithelial cells and SK-CO15 human colonic epithelial cells, and three different anti-Anillin polycolonal antibodies, the authors only detected Anillin in the nucleus and weakly in the cytoplasm via immunofluoresence. The method of fixation used by Wang et al., however, was formaldehyde based (PFA), as opposed to acid-based (TCA; tri-chloroacetic acid) which is optimal to preserving membrane-bound or membrane associated proteins like Rho and Anillin (Kosako et al., 2000; Matsui, Yonemura, Tsukita, & Tsukita, 1999; Yonemura, Hirao-Minakuchi, & Nishimura, 2004). In the future, alternative anti-Anillin antibodies should be tested, in addition to other fixation conditions. Additionally, work investigating proliferating tissues, as opposed to mature monolayers of human epithelial cells and immunohistochemistry of intact human tissues may be necessary to address this. Interestingly, a study by Hall et al., examined Anillin's expression in human tumors and normal tissues using immunohistochemistry on sections of a range of human tissue samples (Hall et al., 2005). Using this approach, they detected expression of Anillin in oocytes, ovarian stroma, seminiferous tubules, fallopian tube, urothelium of the bladder, renal tubules, parathyroid, stomach, small intestine, brunners gland, colon, placenta, cerebral cortex, liver, myocardium, salivary gland and prostate. The authors noted that Anillin was detected in the nucleus and to varying degrees in the cytoplasm of all tissues; they only noted weak membrane association in skeletal muscle. It will be necessary to confirm whether the membrane associated population of Anillin in human skeletal muscle is indeed junctional by co-staining for TJ or AJ proteins, in addition to examining Anillin in other human tissues.

Anillin is known to be highly expressed in the testes, ovary and brain of both human and *Xenopus* tissues. Further, in *Xenopus*, Anillin has been detected as early as stage 1 (one cell stage) and as late as stage 60 (tadpole); thus, it will be an interesting future direction to examine whether Anillin is differentially expressed at junctions in different

tissues and/or during different stages of development. In Chapter 2, we did observe an enrichment of Anillin at the cortex in neurulating embryos (stage 14) compared to gastrulating embryos (stage 10.5). Work by Yanai et al. (2011) has laid a great foundation for this investigation with their comprehensive RNAseq analysis of *Xenopus* genes, in addition to the Gurdon Institute's growing EST database of *Xenopus tropicalis and laevis* gene expression, which includes Anillin and its expression in diverse tissues and at different developmental stages (Yanai, Peshkin, Jorgensen, & Kirschner, 2011).

While we recently reported detection of a population of Anillin at cell-cell junctions throughout the cell-cycle in actively proliferating epithelial tissue from gastrula stage *Xenopus* embryos we do not know what happens to Anillin in post-mitotic environments, especially given Anillin's important role in maintaining junction integrity. Anillin has distinct patterns of localization throughout the cell cycle. It is nuclear in non-dividing interphase cells, at the cortex during metaphase and at the cleavage furrow of dividing cells (Field & Alberts, 1995). After a cell completes division, Anillin is a substrate of the APC/C, which promotes its ubiquitination and degradation (Zhao & Fang, 2005). In intact mouse heart and brain tissues a decrease in Anillin is detected in post-mitotic cells (Hesse et al., 2012). It will be important to characterize whether the junctional localization of Anillin is present in both proliferating and non-proliferating cells.

1.4 **Anillin overexpression and disease.**
When Anillin was overexpressed in *Xenopus* embryos we observed bushy F-actin contractile rings in dividing cells, and increased junctional F-actin and P-MLC (Reyes et al., 2014). Cells were also domed, and the F-actin and Myosin-2 formed hypercontractile arrays around the cell, causing abnormal cell shapes (Reyes et al., 2014). These data suggest that a proper amount of Anillin expression must be maintained – either too much or too little Anillin causes junctional defects. Anillin expression must be tightly regulated in the cell to ensure just enough to preserve junction integrity and balance actomyosin mediated tension. This may be especially true for the case of having too much Anillin, as overexpression of Anillin is associated with diverse human cancers and its increased expression correlates with increased metastatic potential (Chuang & Ou, 2014; Hall et al., 2005; Olakowski et al., 2009).

Future work connecting the mechanisms behind the hypercontractile junctional actomyosin formation we observed upon Anillin overexpression with the increased motility observed in Anillin overexpression backgrounds (Chuang & Ou, 2014) may be of significant disease relevance.

A proper balance of RhoA is also essential in epithelial cells, as inhibition of Rho activity is associated with loss of cell adhesion as cells lose their polarity and become rounded (Winning, Ward, Scales, & Walker, 2002), and overexpression of RhoA promotes the invasion of tumor cells (Yoshioka, Nakamori, & Itoh, 1999). Anillin and RhoA have a well-established relationship in dividing cells, where active RhoA recruits Anillin to the cleavage furrow, and Anillin helps stabilize active RhoA in a positive feedback loop (Hickson & O'Farrell, 2008). Therefore, it will be important to understand their normal mechanism of co-regulation both in cytokinesis and at cell-cell junction in order to better understand what goes awry in human cancers. One way to begin to address this question is to overexpress the 3xGFP-tagged major domains of Anillin, and examine F-actin, Myosin-2, and RhoA-GTP to determine which domains are sufficient to recapitulate the Anillin overexpression phenotype: increased cortical F-actin, Myosin-2, apical doming and hypercontractile arrays. This would provide insight as to whether the mechanism is indeed Rho mediated - for example, if the AHD or combined AHDPH which consists of the Rho binding domain (RBD), is able to recapitulate the effect of full length Anillin. During optimization of expression for the AHDPH domain, we did observe examples of failed cytokinesis (data not shown), which may be indicative of it functioning as a dominant negative (DN) at high levels of expression. The AHDPH may function as a DN by being recruited to cell junctions, but because it lacks the actin and myosin biding domains, it cannot completely function to scaffold junctional actomyosin, however, we have not yet examined F-actin, Myosin-2 or RhoA-GTP in these cells. Apart from this, it will be interesting to examine how TJ and AJ proteins are affected when Anillin is overexpressed.

1.5 Anillin and cell-cell polarity.

We observed that upon Anillin KD, the polarity of the AJ protein β-catenin was perturbed. In control embryos β-catenin was enriched apically and present throughout the basolateral membrane; however, in Anillin KD embryos the apical enrichment was lost, and we observed examples of its redistribution in the cytoplasm (Reyes et al., 2014). Further, the TJ protein ZO-1 outlined the polygonal shape of control cells: however, when Anillin was KD, ZO-1 became wavy, and from side views we observed examples of more basal ZO-1 at sites of intercellular spaces (Reyes et al., 2014). Indeed, TJs are thought to function as both a barrier (keeping the inside in and the outside out) and fence (partitioning the apical and basal lateral membranes into distinct domains) (Aijaz, Balda, & Matter, 2006; Balda & Matter, 1998). Therefore, it is possible that disruption of the TJ protein ZO-1 when Anillin is KD may have impaired the TJ *fence* function, which is important for establishing apical/basal polarity. It will be necessary to examine whether the localization of key cell-polarity proteins such as aPKC, Crumbs, PALS and members of the PAR family are perturbed in a background where Anillin is depleted, to test if this is indeed the case.

Apical doming or rounding of cells occurred in Anillin KD embryos, which may be due to reduced tension and a loss of cell polarity. Epithelial cells that undergo epithelial to mesenchymal transitions (EMTs) during development or disease round up by down-regulating expression of junctional and polarity proteins (Moreno-Bueno, Portillo, & Cano, 2008; Vandewalle et al., 2005). As fixed staining for the TJ protein Claudin and AJ protein E-cadherin in Anillin KD embryos revealed a reduction in their relative intensity (Reyes et al., 2014), it will be of interest to perform western blots or a more quantitative approach like RT-PCR for junction and polarity proteins to more closely quantify and examine changes in expression at the protein and gene levels.

1.6 Identifying novel interactions between Anillin and junction proteins.

In Chapter 2, we found that Anillin co-localized with the TJ protein ZO-1 and partially overlapped with the AJ protein E-cadherin. Preliminary PLA data suggests that while Anillin may co-localize with ZO-1 and E-cadherin, it may interact with ZO-1, but not E-

cadherin. *Drosophila* Anillin also has SH3 binding domains upstream of the Actin binding domain (Field & Alberts, 1995). SH3 domains are known to mediate protein-protein interactions and are present in the PDZ domain of junctional proteins like ZO-1 (González-Mariscal, Betanzos, & Ávila-Flores, 2000), however, it is unknown how conserved Anillin's SH3 domains are across species, what protein-protein interactions they may mediate, and if Anillin has PDZ domains. If indeed, *Xenopus* has PDZ or SH3 domains, this may be a possible site of interaction between Anillin and ZO-1, but future biochemistry work is necessary to confirm which regions of Anillin directly interact with ZO-1 or other junctional proteins. Interestingly, a recent large-scale study using proteomics of proteins biotinylated by E-Cad-BirA detected Anillin in close proximity with the major AJ component E-cadherin – suggesting a possible interaction (Guo et al., 2014; Zaidel-Bar, 2013). Another genome wide screen in *Drosophila* S2 cells implicated Anillin as being important for cadherin-mediated cell adhesion, as KD of Anillin resulted in reduced protein levels of DE-cadherin and β-catenin (Toret, D'Ambrosio, Vale, Simon, & Nelson, 2014).

One approach to confirm Anillin's interaction with ZO-1 and more concretely determine if indeed Anillin may interact with AJ proteins like E-cadherin may include using the 3xGFP fragments of Anillin's major domains for immunoprecipitation (IP) and mass spectrometry (MS) analysis to identify novel junction proteins that interact with Anillin. Taking advantage of what we now know about the localization of the tagged Anillin fragments, we would aim to identify a protein (or proteins) that co-IP with the Anillin fragments that localize to apical junctions, but fails to co-IP with Anillin fragments that are not junctional. Candidate proteins should then be validated by testing whether they co-IP with Anillin (using antibodies specific for the candidate protein) and whether disrupting them affects Anillin's localization to cell-cell junctions.

1.7 Characterizing whether there are distinct populations of Anillin in the nucleus and at junctions.

While a population of Anillin is present at cell-cell junctions throughout the cell-cycle, another population is present in the nucleus during interphase, released from the

nucleus upon nuclear envelope breakdown, at the cortex during metaphase and at the cleavage furrow in dividing cells. It is unknown whether the junctional and nuclear pools are distinct populations in the cell or whether there is exchange between these pools of Anillin. We observed that of all the 3xGFP tagged fragments of Anillin binding domains, only the FBDMyo fragment exhibited nuclear localization. This is not surprising as this fragment contains Anillin's nuclear localization sequences (NLSs). Photobleaching all of the tagged Anillin at junctions or in the nucleus and looking for recovery using FRAP would be a good first step to begin to characterize the dynamics of the two Anillin pools. Another approach we are pursuing is to photoactivate one population of Anillin, junctional or nuclear, and test for exchange between the two populations.

Some organisms have more than one copy of Anillin and therefore different populations of Anillin with distinct localization patterns and functions in the cell. For example, *C. elegans* has three Anillin homologs: ANI-1, ANI-2 and ANI-3 (Maddox, Habermann, Desai, & Oegema, 2005). ANI-1 functions in cortical ruffling and pseudo cleavage during early embryo development, ANI-2 has important role in the adult gonad structure, while ANI-3 has no known function yet (Maddox et al., 2005). In *S. pombe* there are two Anillin-like proteins, Mid1 and Mid2, which are differentially phosphoregulated (Bahler et al., 1998; Sohrmann, Fankhauser, Brodbeck, & Simanis, 1996). *Drosophila* has three different splice forms of Anillin, one of which lacks the C-terminus of the protein, and humans may have as many as 8-14 splice variants (Piekny & Maddox, 2010). It has been posited that a splice variant of Anillin lacking the NLS could be constitutively expressed in the cytoplasm (Piekny & Maddox, 2010), however, the presence of alternate splice forms in humans has not been confirmed. While there is only one known isoform of Anillin in human and *Xenopus*, it is possible that there may be more (i.e. splice variants, alleles). If indeed there are distinct nuclear and junctional populations of Anillin, it will be important to determine if they are differentially regulated via phosphorylation or post-translational modification and if they are distinct isoforms.

1.8 Characterizing the mechanism of AHDPH cooperativity in Anillin's targeting to junctions.

To determine how Anillin is targeted to cell-cell junctions, in Chapter 2 we generated a series of fragments of Anillin's major functional domains tagged on the N-terminus with 3xGFP, expressed them in *Xenopus laevis* embryos, and quantified the extent of junctional co-localization with a membrane marker or tagged junctional protein. Analysis of the 3xGFP-tagged Anillin fragments revealed that, similar to full length Anillin, a combined AHDPH fragment exhibited narrow, apical localization at cell-cell junctions, indicating that these domains are sufficient for Anillin's recruitment to junctions. Neither the AHD nor the PH domain alone fully recapitulate full length Anillin's distribution. These findings suggest an important role for Anillin's AHD and PH domains together in its localization to cell-cell junctions, and indicate that proteins which bind Anillin via the AHD and PH may recruit Anillin to cell-cell junctions. Therefore, the AHD and PH domains may mediate important and yet unknown interactions between Anillin and cell-cell junction proteins.

Given that a combined AHDPH fragment of Anillin most closely recapitulates full length Anillin's junctional localization (narrow and apical junctional distribution), it will be important to determine how these domains work together to target Anillin to junctions. Many binding partners within Anillin's AHD and PH domains have overlapping binding sites, which may help explain the requirement for both domains, but it makes it especially challenging to introduce specific mutations to disrupt individual interactions. The AHD mediates several interactions with important proteins including the GEF Ect2, the GAPs **MgcRacGAP** and **p190RhoGAP** in addition to RhoA and **RhoG**, while the PH domain mediates interactions with **septins** and **lipids** (The binding partners that interact with both domains are highlighted in bold). To better tease apart the contributions of individual binding partners within these two domains, it will be necessary to disrupt Anillin's ability to interact with them individually via small deletion mutants or point mutantations and test for changes in Anillin's localization at junctions. Importantly, the approach used in this thesis to assess which domains of Anillin contribute to its localization at cell-cell junctions, demonstrates that the AHD and PH are

sufficient, but a complementary approach using deletion or point mutants would reveal which domains are *necessary*.

To assess the contribution of the Anillin-RhoA interaction to Anillin's targeting at cell junctions, we are currently pursing and considering several strategies. One in progress is to delete or make point mutants in Anillin's RBD domain. The crystal structure for the C-terminus of human Anillin and the *S. pombe* Anillin-like protein Mid1 bound to Rho was recently reported; this study also identified key residues within the RBD that bind Rho, which are informing our current work (Sun et al., 2015). If deletion or mutation of the RBD disrupted Anillin's ability to target to junctions (reduction or complete abolishment), this would indeed suggest an important role for Rho in Anillin targeting. While preliminary data from our lab suggests that deletion of Anillin's RBD or introducing point mutations within the RBD does not affect its ability to target to junctions, the extent of junctional localization has not been quantified to determine if there is a reduction or change in distribution compared to controls (Kayla Dinshaw, unpublished). Another complementary approach would be to mosaically overexpress constitutively active Rho. If this increased Anillin's localization at junctions, it would strengthen the case that active Rho is important for recruiting Anillin to junctions. Perturbation of RhoA in dividing cells with RNAi for the Rho GEF Ect2 or deletion of the AHD disrupts Anillin's ability to target to the furrow (Hickson & O'Farrell, 2008; Piekny & Glotzer, 2008); similar strategies could be used to test the effect on junctional Anillin recruitment. Recently, an optogenetic probe that can discretely activate RhoA in response to targeted laser light was generated (Wagner & Glotzer, 2016). The probe is modeled after the tunable light-inducible dimerization tags (TULIPs) technology, which uses the light inducible domain of *Avena sativ*a phototropin 1 (LOV2) and a PDZ domain to induce recruitment of proteins to the membrane using light activation (Strickland et al., 2012). The optogenetic probe for Rho activation uses a RhoGEF to locally activate RhoA at the membrane. Using this technology in intact epithelia like the *Xenopus* embryo to induce recruitment of active RhoA at junctions and examine whether Anillin is recruited could be a precise and effective way to characterize their relationship at junctions.

Unpublished work from our lab has shown that Anillin accumulates at transient sites of local RhoA activation at cell-cell junctions ("Rho flares"), in addition to regions of increased local tension – for example, we have observed Anillin accumulation at the junctions of a cell nearby the dividing cell, presumably in response to the increased local tension the dividing cell is exerting on its neighbor (Torey Arnold, unpublished). Further, at these sites, we have observed the GAP p190RhoGAP to co-accumulate with Anillin (Torey Arnold, unpublished), which is not surprising given that a recent study identified p190RhoGAP as a binding partner of Anillin and showed that the Anillin–p190RhoGAP interaction limits the activation of Rho in a tension-dependent manner (Manukyan, Ludwig, Sanchez-Manchinelly, Parsons, & Stukenberg, 2015). Other work in our lab has linked Rho flares to sites of junction repair, as local discontinuities or breaks in TJs (ZO-1, Occludin) are followed by a Rho flare and repair of the discontinuity (Rachel Stephenson, unpublished). In this dissertation we observed transient "flares" of active Rho to occur in control embryos, but more frequently and shorter lived in embryos where Anillin was KD via antisense morpholino (Reyes et al., 2014). These data and observations make the case for yet another mechanism of Anillin recruitment to cell junctions to be explored – discrete spatiotemporal regulation of RhoA and response to local tension.

Other Anillin binding partners of interest include septins and lipids (especially PIP_2). In dividing cells, PIP_2 is enriched at the cleavage furrow (citation), and Anillin is known to have increased affinity for PIP_2 relative to other lipid families (J. Liu, Fairn, Ceccarelli, Sicheri, & Wilde, 2012). Anillin interacts with PIP_2 via its PH domain (citation), and a recent paper also identified a C2 region (structural domain important for targeting to membranes) within Anillin's AHD domain (Sun et al., 2015). A paper by Liu et al. (2012) implicated the PH domain's interaction with lipids, specifically PIP_2, as important for Anillin's targeting to the cleavage furrow of dividing cells (J. Liu et al., 2012). When Anillin's PH domain was deleted or when point mutations were introduced into the PH domain that disrupted its ability to interact with lipids, Anillin was no longer recruited to the cleavage furrow. Further, when Anillin's interaction with Septin was abolished, but

its interaction with PIP_2 remained intact, Anillin was still able to localize at the cleavage furrow; however, the cells failed cytokinesis. The authors accomplished this by replacing Anillin's native PH domain, which binds septins and PIP_2, with the PH domain of PLCδ, which only binds PIP_2. This suggests that PIP_2, not septins, is important for Anillin's targeting at the furrow. Using a similar approach in the *Xenopus* epithelium could help us understand PIP_2 and Septin contributions to Anillin's targeting to junctions.

While Septins are dispensable for Anillin targeting to the cleavage furrow, it is possible that a different situation may exist at cell-cell junctions. Septins are a class of GTP-binding proteins that form rods and higher ordered structures (Mostowy & Cossart, 2012). Septins can act as diffusion barriers limiting the exchange of membrane inserted proteins and are thought to provide stability to the plasma membrane. Anillin and Septins have a well-characterized relationship during cytokinesis, as Anillin is required for recruitment of Septins to the cleavage furrow (Field & Alberts, 1995; Kinoshita, Field, Coughlin, Straight, & Mitchison, 2002; Oegema et al., 2000); however, potential roles of Septins at epithelial junctions are uncharacterized. Recently, a study published by Park et al. (2015) showed that when Septins are perturbed in the intact epithelium of *Xenopus* embryos this results in basal intercellular spaces (Park, Kim, & Wallingford, 2015). Further when GFP-tagged Septin was expressed in embryos it was present throughout the cortex (Park, Kim & Wallingford, 2015); however, the authors did not characterize whether this population specifically co-localized with junction proteins. It will be an important relationship to characterize for future studies. Some of the groundwork for this has been laid in Chapter 3 of this thesis.

1.9 Anillin and planar cell polarity.
When Anillin is KD in our system we have observed delays in blastopore closure, which is indicative of gastrulation defects; however, we have not yet characterized whether Anillin is specifically involved in regulating gastrulation. During gastrulation, embryos undergo the process of convergent extension (CE), where cells undergo elongation and compaction as the blastopore closes and the three major germ layers begin to be organized. KD of Septin in *Xenopus* embryos also leads to gastrulation defects (Kim et

al., 2010). When Septins are disrupted, CE is also disrupted and the blastopore remains enlarged (Kim et al., 2010). As Anillin binds Septins and is important for their recruitment during cytokinesis, it will be an interesting future direction to pursue. One technique that is often used to characterize defects in convergence and extension is a Keller explant, where a "microsurgery" is performed to isolate the cells that undergo CE to test if they elongate (Keller, Danilchik, Gimlich, & Shih, 1985). This can be performed on control embryos and embryos where Anillin has been KD or even in a background depleted of both Anillin and Septin, to compare the severity.

The planar cell polarity (PCP) pathway underlies the cell intercalation movements essential to the process of CE that happens during gastrulation, in addition to regulating other developmental processes like ciliogenesis. Septins have been linked to the PCP pathway through the PCP protein Fritz (also Wdpcp), which has a role in regulating proper cell elongation, and is required for Septin localization in the mesenchymal cells that undergo CE (Kim et al., 2010). While Anillin has no known interactions or relationships with proteins in the PCP pathway, it does not preclude the possibility of its involvement – especially given its well characterized relationship with Septins and the gastrulation defects we've observed in Anillin KD embryos. Further analysis may include examining proteins in the planar cell polarity pathway, such as Fritz, and whether they are perturbed in an Anillin KD environment.

1.10 Summary & Conclusions.
It is not surprising the important and widespread role Anillin has in the cell given its capacity to interact with several key cytoskeletal regulators such as GTPases, GEFs, GAPs, formins and cytoskeletal components themselves like Actin, MTs and Septins. Anillin is also ubiquitously expressed during development and is highly expressed in adult tissues such as the brain, heart, testes and ovary and is widely conserved and distributed in complex organisms. As highlighted above, however, key questions remain in understanding Anillin in the context of epithelia, which include determining its precise mechanism of regulating and recruitment to cell-cell junctions, whether it interacts with novel junction proteins, the extent to which junctional Anillin is conserved across

species, whether distinct populations/splice variants of Anillin exist in human/frog, characterizing Anillin overexpression and disease and investigating potential roles in developmental processes and pathways like gastrulation, the PCP pathway and cell polarity. As the answers to these questions are elucidated, Anillin will continue to emerge as a multi-tasking protein within epithelia, and possibly other cell types (mesenchymal, endothelial), even more so than at present.

References:

Aijaz, S., Balda, M. S., & Matter, K. (2006). Tight Junctions: Molecular Architecture and Function. In B.-I. R. of Cytology (Ed.) (Vol. 248, pp. 261–298). Academic Press. Retrieved from http://www.sciencedirect.com/science/article/pii/S0074769606480050

Bahler, J., Steever, A. B., Wheatley, S., Wang, Y., Pringle, J. R., Gould, K. L., & McCollum, D. (1998). Role of Polo Kinase and Mid1p in Determining the Site of Cell Division in Fission Yeast. *The Journal of Cell Biology*, *143*(6), 1603–1616. http://doi.org/10.1083/jcb.143.6.1603

Balda, M. S., & Matter, K. (1998). Tight junctions. *Journal of Cell Science*, *111*(5), 541–547.

Bustelo, X. R., Sauzeau, V., & Berenjeno, I. M. (2007). GTP-binding proteins of the Rho/Rac family: regulation, effectors and functions in vivo. *BioEssays*, *29*(4), 356–370. http://doi.org/10.1002/bies.20558

Buul, J. D. van, Allingham, M. J., Samson, T., Meller, J., Boulter, E., García-Mata, R., & Burridge, K. (2007). RhoG regulates endothelial apical cup assembly downstream from ICAM1 engagement and is involved in leukocyte trans-endothelial migration. *The Journal of Cell Biology*, *178*(7), 1279–1293. http://doi.org/10.1083/jcb.200612053

Byri, S., Misra, T., Syed, Z. A., Bätz, T., Shah, J., Boril, L., … Luschnig, S. (2015). The Triple-Repeat Protein Anakonda Controls Epithelial Tricellular Junction Formation in Drosophila. *Developmental Cell*, *33*(5), 535–548. http://doi.org/10.1016/j.devcel.2015.03.023

Chuang, H. Y., & Ou, Y. H. (2014). Abstract 4068: Overexpression of anillin in colorectal cancer promotes the cell proliferation, cell mobility and cell invasion. *Cancer Research*, *74*(19 Supplement), 4068–4068. http://doi.org/10.1158/1538-7445.AM2014-4068

deBakker, C. D., Haney, L. B., Kinchen, J. M., Grimsley, C., Lu, M., Klingele, D., … Ravichandran, K. S. (2004). Phagocytosis of Apoptotic Cells Is Regulated by a UNC-73/TRIO-MIG-2/RhoG Signaling Module and Armadillo Repeats of CED-12/ELMO. *Current Biology*, *14*(24), 2208–2216. http://doi.org/10.1016/j.cub.2004.12.029

Estrach, S., Schmidt, S., Diriong, S., Penna, A., Blangy, A., Forte, P., & Debant, A. (2002). The Human Rho-GEF Trio and Its Target GTPase RhoG Are Involved in the NGF Pathway, Leading to Neurite Outgrowth. Retrieved May 10, 2016, from http://www.sciencedirect.com/science/article/pii/S0960982202006589

Field, C. M., & Alberts, B. M. (1995). Anillin, a contractile ring protein that cycles from the nucleus to the cell cortex. *The Journal of Cell Biology*, *131*(1), 165–178. http://doi.org/10.1083/jcb.131.1.165

Frenette, P., Haines, E., Loloyan, M., Kinal, M., Pakarian, P., & Piekny, A. (2012). An Anillin-Ect2 Complex Stabilizes Central Spindle Microtubules at the Cortex during Cytokinesis. *PLoS ONE*, *7*(4), e34888. http://doi.org/10.1371/journal.pone.0034888

González-Mariscal, L., Betanzos, A., & Ávila-Flores, A. (2000). MAGUK proteins: structure and role in the tight junction. *Seminars in Cell & Developmental Biology*, *11*(4), 315–324. http://doi.org/10.1006/scdb.2000.0178

Guo, Z., Neilson, L. J., Zhong, H., Murray, P. S., Zanivan, S., & Zaidel-Bar, R. (2014). E-cadherin interactome complexity and robustness resolved by quantitative proteomics | Science Signaling. *Science Signaling*, *7*(354), rs7.

Hall, P. A., Todd, C. B., Hyland, P. L., McDade, S. S., Grabsch, H., Dattani, M., … Russell, S. E. H. (2005). The Septin-Binding Protein Anillin Is Overexpressed in Diverse Human Tumors. *Clinical Cancer Research*, *11*(19), 6780–6786. http://doi.org/10.1158/1078-0432.CCR-05-0997

Hesse, M., Raulf, A., Pilz, G.-A., Haberlandt, C., Klein, A. M., Jabs, R., … Fleischmann, B. K. (2012). Direct visualization of cell division using high-resolution imaging of M-phase of the cell cycle. *Nature Communications*, *3*, 1076. http://doi.org/10.1038/ncomms2089

Hickson, G. R. X., & O'Farrell, P. H. (2008). Rho-dependent control of anillin behavior during cytokinesis. *The Journal of Cell Biology*, *180*(2), 285–294. http://doi.org/10.1083/jcb.200709005

Higashi, T., Tokuda, S., Kitajiri, S., Masuda, S., Nakamura, H., Oda, Y., & Furuse, M. (2013). Analysis of the "angulin" proteins LSR, ILDR1 and ILDR2 – tricellulin recruitment, epithelial barrier function and implication in deafness pathogenesis. *J Cell Sci*, *126*(4), 966–977. http://doi.org/10.1242/jcs.116442

Ikenouchi, J., Furuse, M., Furuse, K., Sasaki, H., Tsukita, S., & Tsukita, S. (2005). Tricellulin constitutes a novel barrier at tricellular contacts of epithelial cells. *The Journal of Cell Biology*, *171*(6), 939–945. http://doi.org/10.1083/jcb.200510043

Katoh, H., & Negishi, M. (2003). RhoG activates Rac1 by direct interaction with the Dock180-binding protein Elmo. *Nature*, *424*(6947), 461–464. http://doi.org/10.1038/nature01817

Keller, R. E., Danilchik, M., Gimlich, R., & Shih, J. (1985). The function and mechanism of convergent extension during gastrulation of Xenopus laevis. *Development*, *89*(Supplement), 185–209.

Kim, S. K., Shindo, A., Park, T. J., Oh, E. C., Ghosh, S., Gray, R. S., … Wallingford, J. B. (2010). Planar Cell Polarity Acts Through Septins to Control Collective Cell Movement and Ciliogenesis. *Science*, *329*(5997), 1337–1340. http://doi.org/10.1126/science.1191184

Kinoshita, M., Field, C. M., Coughlin, M. L., Straight, A. F., & Mitchison, T. J. (2002). Self- and Actin-Templated Assembly of Mammalian Septins. *Developmental Cell*, *3*(6), 791–802. http://doi.org/10.1016/S1534-5807(02)00366-0

Kosako, H., Yoshida, T., Matsumura, F., Ishizaki, T., Narumiya, S., & Inagaki, M. (2000). Rho-kinase/ROCK is involved in cytokinesis through the phosphorylation of myosin light chain and not ezrin/radixin/moesin proteins at the cleavage furrow. *Oncogene*, *19*(52), 6059–6064.

Krug, S. M., Amasheh, S., Richter, J. F., Milatz, S., Günzel, D., Westphal, J. K., … Fromm, M. (2009). Tricellulin Forms a Barrier to Macromolecules in Tricellular Tight Junctions without Affecting Ion Permeability. *Molecular Biology of the Cell*, *20*(16), 3713–3724. http://doi.org/10.1091/mbc.E09-01-0080

Liu, J., Fairn, G. D., Ceccarelli, D. F., Sicheri, F., & Wilde, A. (2012). Cleavage Furrow Organization Requires PIP2-Mediated Recruitment of Anillin. *Current Biology*, *22*(1), 64–69. http://doi.org/10.1016/j.cub.2011.11.040

Liu, X.-F., Ishida, H., Raziuddin, R., & Miki, T. (2004). Nucleotide Exchange Factor ECT2 Interacts with the Polarity Protein Complex Par6/Par3/Protein Kinase Cζ (PKCζ) and Regulates PKCζ Activity. *Molecular and Cellular Biology*, *24*(15), 6665–6675. http://doi.org/10.1128/MCB.24.15.6665-6675.2004

Madara, J. L., Moore, R., & Carlson, S. (1987). Alteration of intestinal tight junction structure and permeability by cytoskeletal contraction. *American Journal of Physiology - Cell Physiology*, *253*(6), C854–C861.

Maddox, A. S., Habermann, B., Desai, A., & Oegema, K. (2005). Distinct roles for two C. elegans anillins in the gonad and early embryo. *Development*, *132*(12), 2837–2848. http://doi.org/10.1242/dev.01828

Manukyan, A., Ludwig, K., Sanchez-Manchinelly, S., Parsons, S. J., & Stukenberg, P. T. (2015). A complex of p190RhoGAP-A and anillin modulates RhoA-GTP and the cytokinetic furrow in human cells. *J Cell Sci*, *128*(1), 50–60. http://doi.org/10.1242/jcs.151647

Mariano, C., Sasaki, H., Brites, D., & Brito, M. A. (2011). A look at tricellulin and its role in tight junction formation and maintenance. *European Journal of Cell Biology*, *90*(10), 787–796. http://doi.org/10.1016/j.ejcb.2011.06.005

Masuda, R., Semba, S., Mizuuchi, E., Yanagihara, K., & Yokozaki, H. (2010). Negative Regulation of the Tight Junction Protein Tricellulin by Snail-Induced Epithelial-Mesenchymal Transition in Gastric Carcinoma Cells. *Pathobiology*, *77*(2), 106–113. http://doi.org/10.1159/000278293

Masuda, S., Oda, Y., Sasaki, H., Ikenouchi, J., Higashi, T., Akashi, M., … Furuse, M. (2011). LSR defines cell corners for tricellular tight junction formation in epithelial cells. *Journal of Cell Science*, *124*(4), 548–555. http://doi.org/10.1242/jcs.072058

Matsui, T., Yonemura, S., Tsukita, S., & Tsukita, S. (1999). Activation of ERM proteins in vivo by Rho involves phosphatidyl-inositol 4-phosphate 5-kinase and not ROCK kinases. *Current Biology*, *9*(21), 1259–S3. http://doi.org/10.1016/S0960-9822(99)80508-9

Menco, B. P. (1988). Tight-junctional strands first appear in regions where three cells meet in differentiating olfactory epithelium: a freeze-fracture study. *Journal of Cell Science*, *89*(4), 495–505.

Miller, K. G., Field, C. M., & Alberts, B. M. (1989). Actin-binding proteins from Drosophila embryos: a complex network of interacting proteins detected by F-actin affinity chromatography. *The Journal of Cell Biology*, *109*(6), 2963–2975. http://doi.org/10.1083/jcb.109.6.2963

Mishima, M., Kaitna, S., & Glotzer, M. (2002). Central Spindle Assembly and Cytokinesis Require a Kinesin-like Protein/RhoGAP Complex with Microtubule Bundling Activity. *Developmental Cell*, *2*(1), 41–54. http://doi.org/10.1016/S1534-5807(01)00110-1

Moreno-Bueno, G., Portillo, F., & Cano, A. (2008). Transcriptional regulation of cell polarity in EMT and cancer. *Oncogene*, *27*(55), 6958–6969. http://doi.org/10.1038/onc.2008.346

Mostowy, S., & Cossart, P. (2012). Septins: the fourth component of the cytoskeleton. *Nature Reviews Molecular Cell Biology*, *13*(3), 183–194. http://doi.org/10.1038/nrm3284

Murga, C., Zohar, M., Teramoto, H., & Gutkind, J. S. (2002). Rac1 and RhoG promote cell survival by the activation of PI3K and Akt, independently of their ability to stimulate JNK and NF-кB. *Oncogene*, *21*(2), 207–216. http://doi.org/10.1038/sj.onc.1205036

Nusrat, A., Giry, M., Turner, J.R., Colgan, S.P., Parkos, C.A., Carnes, D., Lemichez, E., Boquet, P., Madara, J.L. (1995). Rho protein regulates tight juncitons and perijunctional actin organization in polarized epithelia. *PNAS*, 92(23), 10629-33.

Oegema, K., Savoian, M. S., Mitchison, T. J., & Field, C. M. (2000). Functional Analysis of a Human Homologue of the Drosophila Actin Binding Protein Anillin Suggests a Role in Cytokinesis. *The Journal of Cell Biology*, *150*(3), 539–552. http://doi.org/10.1083/jcb.150.3.539

Ohkuni, T., Kojima, T., Ogasawara, N., Masaki, T., Ninomiya, T., Kikuchi, S., … Sawada, N. (2009). Expression and localization of tricellulin in human nasal epithelial cells in vivo and in vitro. *Medical Molecular Morphology*, *42*(4), 204–211. http://doi.org/10.1007/s00795-009-0470-y

Olakowski, M., Tyszkiewicz, T., Jarzab, M., Król, R., Oczko-Wojciechowska, M., Kowalska, M., … Jarzab, B. (2009). NBL1 and anillin (ANLN) genes over-expression in pancreatic carcinoma. *Folia Histochemica Et Cytobiologica / Polish Academy of Sciences, Polish Histochemical and Cytochemical Society*, *47*(2), 249–255. http://doi.org/10.2478/v10042-009-0031-1

Pannekoek, W.-J., Kooistra, M. R. H., Zwartkruis, F. J. T., & Bos, J. L. (2009). Cell-cell junction formation : The role of Rap1 and Rap1 guanine nucleotide exchange factors. *Biochimica et Biophysica Acta. Biomembranes*, *1788*(4), 790–796.

Park, T. J., Kim, S. K., & Wallingford, J. B. (2015). The planar cell polarity effector protein Wdpcp (Fritz) controls epithelial cell cortex dynamics via septins and actomyosin. *Biochemical and Biophysical Research Communications*, *456*(2), 562–566. http://doi.org/10.1016/j.bbrc.2014.11.078

Piekny, A. J., & Glotzer, M. (2008). Anillin Is a Scaffold Protein That Links RhoA, Actin, and Myosin during Cytokinesis. *Current Biology*, *18*(1), 30–36.

Piekny, A. J., & Maddox, A. S. (2010). The myriad roles of Anillin during cytokinesis. *Seminars in Cell & Developmental Biology*, *21*(9), 881–891. http://doi.org/10.1016/j.semcdb.2010.08.002

Ratheesh, A., Gomez, G. A., Priya, R., Verma, S., Kovacs, E. M., Jiang, K., … Yap, A. S. (2012). Centralspindlin and α-catenin regulate Rho signalling at the epithelial zonula adherens. *Nature Cell Biology*, *14*(8), 818–828. http://doi.org/10.1038/ncb2532

Reyes, C. C., Jin, M., Breznau, E. B., Espino, R., Delgado-Gonzalo, R., Goryachev, A. B., & Miller, A. L. (2014). Anillin Regulates Cell-Cell Junction Integrity by Organizing Junctional Accumulation of Rho-GTP and Actomyosin. *Current Biology*, *24*(11), 1263–1270.

Schulte, J., Tepass, U., & Auld, V. J. (2003). Gliotactin, a novel marker of tricellular junctions, is necessary for septate junction development in Drosophila. *The Journal of Cell Biology*, *161*(5), 991–1000.

Sohrmann, M., Fankhauser, C., Brodbeck, C., & Simanis, V. (1996). The dmf1/mid1 gene is essential for correct positioning of the division septum in fission yeast. *Genes & Development*, *10*(21), 2707–2719. http://doi.org/10.1101/gad.10.21.2707

Somers, W. G., & Saint, R. (2003). A RhoGEF and Rho Family GTPase-Activating Protein Complex Links the Contractile Ring to Cortical Microtubules at the Onset of Cytokinesis. *Developmental Cell*, *4*(1), 29–39. http://doi.org/10.1016/S1534-5807(02)00402-1

Straight, A. F., Field, C. M., & Mitchison, T. J. (2005). Anillin Binds Nonmuscle Myosin II and Regulates the Contractile Ring. *Molecular Biology of the Cell*, *16*(1), 193–201. http://doi.org/10.1091/mbc.E04-08-0758

Strickland, D., Lin, Y., Wagner, E., Hope, C. M., Zayner, J., Antoniou, C., … Glotzer, M. (2012). TULIPs: tunable, light-controlled interacting protein tags for cell biology. *Nature Methods*, *9*(4), 379–384. http://doi.org/10.1038/nmeth.1904

Sun, L., Guan, R., Lee, I.-J., Liu, Y., Chen, M., Wang, J., … Chen, Z. (2015). Mechanistic Insights into the Anchorage of the Contractile Ring by Anillin and Mid1. *Developmental Cell*, *33*(4), 413–426.

Tian, D., Diao, M., Jiang, Y., Sun, L., Zhang, Y., Chen, Z., … Ou, G. (2015). Anillin Regulates Neuronal Migration and Neurite Growth by Linking RhoG to the Actin Cytoskeleton. *Current Biology*, *25*(9), 1135–1145. http://doi.org/10.1016/j.cub.2015.02.072

Toret, C. P., D'Ambrosio, M. V., Vale, R. D., Simon, M. A., & Nelson, W. J. (2014). A genome-wide screen identifies conserved protein hubs required for cadherin-mediated cell–cell adhesion. *The Journal of Cell Biology*, *204*(2), 265–279. http://doi.org/10.1083/jcb.201306082

Vandewalle, C., Comijn, J., Craene, B. D., Vermassen, P., Bruyneel, E., Andersen, H., … Berx, G. (2005). SIP1/ZEB2 induces EMT by repressing genes of different epithelial cell–cell junctions. *Nucleic Acids Research*, *33*(20), 6566–6578. http://doi.org/10.1093/nar/gki965

Wagner, E., & Glotzer, M. (2016). Local RhoA Activation Induces Cytokinetic Furrows Independent of Spindle Position and Cell Cycle Stage. *bioRxiv*, 043836. http://doi.org/10.1101/043836

Wang, D., Chadha, G., Feygin, A., & Ivanov, A. (2015). F-actin binding protein, anillin, regulates integrity of intercellular junctions in human epithelial cells. - PubMed - NCBI. *Cell Mol Life Sci*, *72*(16), 3185–200.

Winning, R. S., Ward, E. K., Scales, J. B., & Walker, G. K. (2002). EphA4 catalytic activity causes inhibition of RhoA GTPase in Xenopus laevis embryos. *Differentiation*, *70*(1), 46–55. http://doi.org/10.1046/j.1432-0436.2002.700105.x

Yanai, I., Peshkin, L., Jorgensen, P., & Kirschner, M. W. (2011). Mapping Gene Expression in Two Xenopus Species: Evolutionary Constraints and Developmental Flexibility. *Developmental Cell*, *20*(4), 483–496. http://doi.org/10.1016/j.devcel.2011.03.015

Yonemura, S., Hirao-Minakuchi, K., & Nishimura, Y. (2004). Rho localization in cells and tissues. *Experimental Cell Research*, *295*(2), 300–314. http://doi.org/10.1016/j.yexcr.2004.01.005

Yoshioka, K., Nakamori, S., & Itoh, K. (1999). Overexpression of Small GTP-binding Protein RhoA Promotes Invasion of Tumor Cells. *Cancer Research*, *59*(8), 2004–2010.

Yuce, O., Piekny, A., & Glotzer, M. (2005). An ECT2–centralspindlin complex regulates the localization and function of RhoA. *The Journal of Cell Biology*, *170*(4), 571–582. http://doi.org/10.1083/jcb.200501097

Zaidel-Bar, R. (2013). Cadherin adhesome at a glance. *J Cell Sci*, *126*(2), 373–378. http://doi.org/10.1242/jcs.111559

Zhao, W., & Fang, G. (2005). Anillin Is a Substrate of Anaphase-promoting Complex/Cyclosome (APC/C) That Controls Spatial Contractility of Myosin during Late Cytokinesis. *Journal of Biological Chemistry*, *280*(39), 33516–33524. http://doi.org/10.1074/jbc.M504657200